The background of the slide is a dense, artistic collage of various planktonic organisms, including diatoms, radiolarians, and other marine microorganisms, rendered in a light blue/teal color against a dark blue background. The organisms are depicted in various orientations and sizes, creating a rich, textured pattern.

**Spatio-temporal dynamics of
North Sea plankton during low
productivity seasons and
implications for higher trophic
levels**

**Spatio-temporal dynamics of North Sea
plankton during low productivity
seasons and implications for higher
trophic levels**

Gregor Börner

Dissertation

with the aim of achieving a doctoral degree at

Faculty of Mathematics, Informatics and Natural Sciences

Department of Biology, University of Hamburg

Institute for Marine Ecosystem and Fisheries Science

Hamburg, 2023

Comission:

Prof. Christian Möllmann (supervisor), University of Hamburg

Dr. Marta Moyano (evaluator), University of Agder

Prof. Dr. Flemming Dahlke (chair), University of Hamburg

Prof. Dr. C-Elisa Schaum, University of Hamburg

Dr. Rolf Koppelman, University of Hamburg

Suggested date of defense: 15th of March 2023

*"You need to let the little things
that would ordinarily bore you
suddenly thrill you."*

— Andy Warhol

Acknowledgements

My first thank you goes to my supervisor, Marta Moyano for her guidance, expertise, and continuous supervision from anywhere, maternity leave, Norway, Spain and elsewhere throughout this PhD journey. In addition, I'd like to say thanks to my second supervisor, Christian Möllmann who adopted me when my working group went poof. Both of their supervision and constructive feedback have been instrumental in shaping my research and helping me develop as a scientist.

Collaboration is key in scientific research and I am grateful for the support and contribution of my colleagues and friends from GEOMAR, WMR, TI, NIOZ, IFREMER, and University of Bergen, who provided their valuable insights and expertise, and engaged in fruitful discussions during the different stages of this PhD rollercoaster. I would like to express my sincere gratitude to Anna Akimova for her invaluable statistical support throughout this thesis and her leadership in the final chapter. Her contributions have had a profound impact on the outcome of this work, and I am truly grateful for her input, without which this thesis would not have been as it is.

I also extend my sincere appreciation to my colleagues and friends at the IMF, whose support, contributions and insights have been invaluable. In no particular order, thanks to Silke, Rolf, Tina, Anne, Jasmin, Heike, Romain, Jana, Laurin, Felix, Dominik, Johanna, Helena, Elena, Frane, André, Rachel, Katharina and Franklin, Saskia, Claudia, Michael, Luisa, Elisa and all the others that crossed path with me throughout this journey. I would particularly like to thank Jan Conradt for your constant advice, support and expertise in all R and statistics related questions as well as all the break –time talks.

A shout-out goes to the Hamburger Berg-Party Peepz, Cami, Remy, Louise, Raquel and Marilisa. I will not forget all those crazy nights out, the “chilled” Friday-night aperitif, all those vodka shots, laughs, tears, sweat and everything else that is part of a party night on the Berg. Cami, also thanks for coaching me to swim like a fish. Ahuge Black-Mamba-Thank you goes out to Raquel, from colleagues, to friends to roommates, what a ride in this short amount of time. Without you, this thesis would not have been possible and I will never forget this. And last but not least, Marilisa, thanks for the entertainment!

Finally, I am deeply grateful to all of my Berlin friends and my family for their constant encouragement and support, whatever decision I make and which place I go. Their unwavering belief in my abilities and in me has been a source of strength and inspiration throughout this PhD, and I am forever thankful. A special thanks to Grit, who patiently dealt with the confusion regarding plans, deadlines, and everything else that, can be difficult to comprehend for someone outside of the PhD bubble. I could not have embarked on or completed this bumpy journey without your unwavering support and love. Thank you.

Summary

Plankton forms the foundation of the food webs and, therefore, to manage the ecosystem and fish stocks effectively, it is essential to understand the interactions between the different compartments of the plankton community and the associated environmental drivers. In the North Sea, winter is considered a low productivity season and it is a crucial time for the survival and growth of marine organisms, including early life stages of many fish species, such as the Atlantic herring (*Clupea harengus*). Nevertheless, despite the recognized importance of this season, our understanding of plankton dynamics is still very limited underlining the need for further investigations on the plankton standing stocks and community structure, which will constitute the prey fields for larger trophic levels.

In this thesis, I have evaluated the spatio-temporal dynamics of the North Sea plankton community during autumn and winter of different size fractions, the Protozoo- (PZP), the Microzoo- (MZP) and Mesozooplankton (MesoZP) community on a broad spatial scale across several years. The analysis of the PZP community revealed a homogenous community across the central North Sea with a general north-south gradient in terms of abundance of the two main groups, dinoflagellates and ciliates. We identified only marginal effects of environmental drivers that may affect PZP shifts in the taxonomic and size composition of the community. To accelerate the time-consuming plankton identification process, we developed an automated Dynamic Optimization Cycle (DOC) pipeline to frequently improve and adapt the accuracy of a plankton image classification model, which helped us to analyze the MZP and MesoZP community in the two main spawning grounds of herring in autumn and winter. By combining two different nets, we provided more accurate estimates of the MesoZP community and a novel dataset of MZP abundances and biomasses for autumn and winter. The application of two different analytical approaches, a taxonomic and a size-based approach identified distinct environmental drivers related to water masses affecting the community, such as salinity and temperature in the respective spawning ground. The generated slopes from the broad groups included in the size-based approach were then used to explore the feeding conditions of the herring larvae in the respective spawning ground and season via physiological modeling. The growth of small larvae in both areas was limited by food availability, even under favorable feeding conditions. In Downs, even larger larvae (>13 mm) were predicted to experience food limitation during winter, while in Buchan/Banks, they were able to approach their maximal growth capacity in autumn. However, in both areas the larvae showed generally better growth performance and survival when their prey fields were extended beyond the “traditional” prey items such as copepods and nauplii, including microplankters in their diet. These findings

highlight the importance of understanding the dynamics of the PZP, MZP and MesoZP communities, stressing the need for further monitoring within larval fish surveys in wintertime, especially given the ongoing low recruitment of North Sea herring.

The findings of this study contribute to a better understanding of the standing stock of plankton and its relationship with environmental drivers in temperate shelf seas. Therefore, this thesis offers additional knowledge for management of the North Sea ecosystem and fish stocks, and underscores the need for further investigation into the dynamics of plankton communities during low productivity periods.

Zusammenfassung

In der Nordsee ist der Winter eine entscheidende Zeit für das Überleben und Wachstum von Meeresorganismen, vom Phytoplankton bis zu den Fischen. Das Plankton bildet die Grundlage des Nahrungsnetzes, aber unser Verständnis seiner Dynamiken während dieser Zeiten der niedrigen biologischen Produktivität ist begrenzt. Für eine nachhaltige Bewirtschaftung des Ökosystems und der Fischbestände ist es unerlässlich, die Wechselwirkungen zwischen den verschiedenen Komponenten der Planktongemeinschaft und den Umweltfaktoren zu verstehen. Die Forschung am Atlantischen Hering und seinen Nahrungsfeldern kann wertvolle Aufschlüsse über die Nahrungsverhältnisse während dieser kritischen Periode liefern.

In meiner Doktorarbeit habe ich die räumlich-zeitliche Dynamik der Planktongemeinschaft der Nordsee während des Winters für verschiedene Größenfraktionen, und zwar die Protozoo- (PZP), die Mikrozoo- (MZP) und die Mesozooplanktongemeinschaft (MesoZP) auf einer breiten räumlichen Skala über mehrere Jahre hinweg untersucht. Die Analyse der PZP-Gemeinschaft ergab eine homogene Gemeinschaftsstruktur in der zentralen Nordsee mit einem allgemeinen Nord-Süd-Gefälle in Bezug auf die Abundanz der beiden Hauptgruppen, Dinoflagellaten und Ciliaten. Wir konnten nur marginale Auswirkungen von Umwelteinflüssen feststellen, die sich auf die Phänologie und die Zusammensetzung der Gemeinschaft von PZP auswirken könnten. Um den zeitaufwendigen Prozess der Planktonidentifizierung zu beschleunigen, entwickelten wir einen dynamischen Optimierungszyklus (DOC), um die Genauigkeit eines Modells zur Klassifizierung von Planktonbildern kontinuierlich zu verbessern und anzupassen, mit dessen Hilfe wir die Mikro- und MesoZP-Gemeinschaft in den beiden Hauptlaichgebieten des Atlantischen Herings im Herbst und Winter analysierten. Durch die Kombination von zwei verschiedenen Netzen konnten wir erstens, genauere Abundanz- und Biomasseschätzungen der MesoZP-Gemeinschaft und zweitens einen einzigartigen Datensatz von Mikrozooplankton-Abundanzen und -Biomassen für Herbst und Winter erstellen. Durch die Anwendung von zwei verschiedenen analytischen Ansätzen, einem taxonomischen und einem größenbasierten Ansatz, konnten eindeutige Umweltfaktoren identifiziert werden, die mit den Wassermassen aus dem Atlantik in Verbindung stehen, die sich auf die Gemeinschaft auswirken, wie z. B. der Salzgehalt und die Temperatur im jeweiligen Laichgebiet. Die aus dem größenbasierten Ansatz gewonnenen Steigungskurven wurden dann verwendet, um die Nahrungssituation der Heringslarven im jeweiligen Laichgebiet und in der jeweiligen Jahreszeit mittels larvenphysiologischer Modellierung zu untersuchen. Wir haben festgestellt, dass Heringslarven in Jahreszeiten mit geringer biologischer Produktivität besonders empfindlich auf Nahrungslimitierung reagieren, wobei die Mehrheit der Larven vor allem in den Wintermonaten von Nahrungslimitierung betroffen ist.

Die Heringslarven wuchsen jedoch im Allgemeinen besser und überlebten besser, wenn Mikroplankter in ihrer Nahrung enthalten waren. Diese Ergebnisse machen deutlich, wie wichtig die künftige Erfassung von MZP und MesoZP im Rahmen der Erhebung von Fischlarven im Winter ist, insbesondere angesichts der anhaltend geringen Rekrutierung von Nordseeheringen.

Diese Arbeit stellt eine umfassende Analyse der allgemeinen Planktodynamik auf einer breiten räumlichen und zeitlichen Skala dar. Wir haben Einblicke in die Dynamik von Planktongemeinschaften in der Nordsee während Zeiten geringer biologischer Produktivität gewonnen. Die Ergebnisse zeigen, wie wichtig es ist, die Wechselwirkungen zwischen MZP-/MesoZP-Gruppen und Umweltfaktoren während des Winters zu verstehen, und welche entscheidende Rolle das Plankton als Grundlage des marinen Ökosystems spielt. Wir haben auch die Vorteile automatisierter Routinen für die Klassifizierung von Plankton im Schnellverfahren und die Anpassung von Modellen aufgezeigt. Darüber hinaus unterstreicht die Studie die Vorteile einer gleichzeitigen Überwachung von MZP- und MesoZP im Rahmen von Fischlarvenerhebungen, insbesondere im Hinblick auf die anhaltend geringe Rekrutierung von Nordseeheringen. Die Ergebnisse dieser Studie tragen zu einem besseren Verständnis des Planktonbestandes und seiner Wechselwirkung mit Umweltfaktoren in gemäßigten Schelfgewässern bei. Insgesamt bietet diese Arbeit wichtige Anhaltspunkte für die Vorhersage und das Management des Nordsee-Ökosystems und der Fischbestände und unterstreicht die Notwendigkeit weiterer großräumiger Studien über die Dynamik von Planktongemeinschaften in Zeiten geringer biologischer Produktivität.

Contents

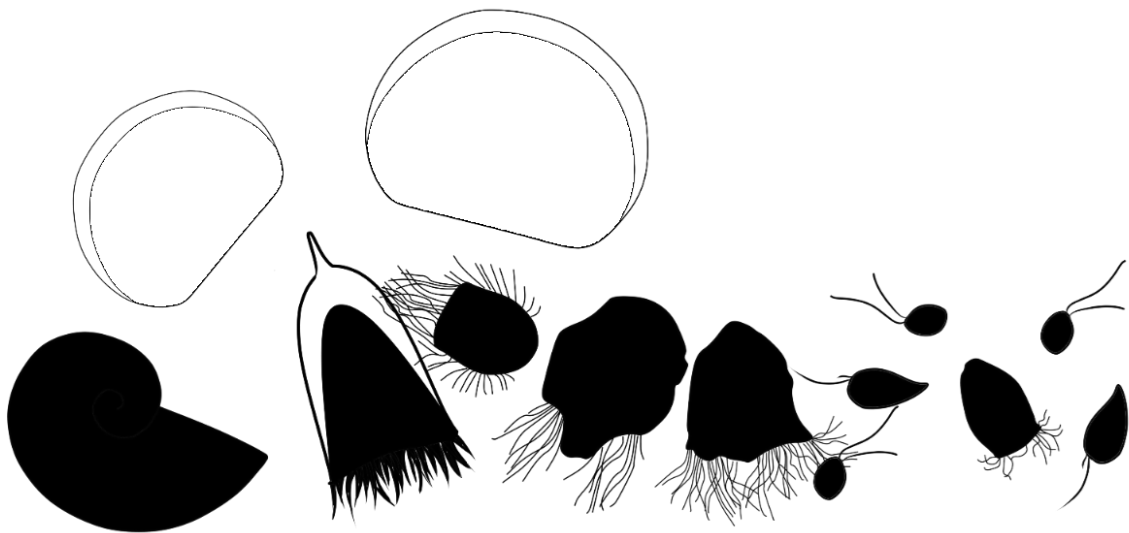
GENERAL INTRODUCTION	13
GENERAL DEFINITION	14
MICROPLANKTON.....	15
MESO(ZOO)PLANKTON	17
BIOGEOCHEMICAL CYCLE	18
ZOOPLANKTON: FOOD FOR ALL?.....	19
STANDING STOCK, BIOMASS AND SEASONAL DYNAMICS.....	21
SIZE STRUCTURE	23
BODY SIZE - WHAT DO WE NEED TO KNOW (AND WHY)?.....	23
THE SIZE-SPECTRA APPROACH.....	24
HOW DO WE STUDY PLANKTON?	26
PLANKTON SAMPLING	26
PRESERVATION AND ANALYSIS	28
PLANKTON TIME SERIES	30
THE NORTH SEA: A CASE STUDY	31
OBJECTIVES	35
CHAPTER 1 SPATIO-TEMPORAL DISTRIBUTION OF THE NORTH SEA WINTER PROTOZOOPLANKTON COMMUNITY BETWEEN 2014 AND 2021	45
INTRODUCTION	47
MATERIALS & METHODS	50
RESULTS.....	55
DISCUSSION.....	62
AUTHOR CONTRIBUTIONS	65
ACKNOWLEDGMENTS	65
REFERENCES.....	66
CHAPTER 2 AUTOMATED PLANKTON CLASSIFICATION WITH A DYNAMIC OPTIMIZATION AND ADAPTATION CYCLE.....	72
INTRODUCTION	74
MATERIALS & EQUIPMENT.....	78
METHODS.....	79
RESULTS.....	91
DISCUSSION.....	100
AUTHOR CONTRIBUTIONS	107
ACKNOWLEDGMENTS	107
REFERENCES.....	107
CHAPTER 3 PLANKTON COMMUNITY COMPOSITION AND SIZE STRUCTURE IN THE NORTH SEA IN AUTUMN AND WINTER FROM 2013-2019.....	113
INTRODUCTION	115
MATERIALS & METHODS	118
RESULTS.....	124
DISCUSSION.....	131
AUTHOR CONTRIBUTIONS	138
ACKNOWLEDGEMENTS	138
REFERENCES.....	138

CHAPTER 4 COMBINING MODELING WITH NOVEL FIELD OBSERVATIONS YIELDS NEW INSIGHTS INTO FOOD LIMITATION OF WINTERTIME LARVAL FISH.....	145
INTRODUCTION	147
DATA AND METHODS	149
METHODS.....	151
RESULTS.....	154
DISCUSSION.....	162
UNCERTAINTIES AND CRITICAL KNOWLEDGE GAPS.....	167
AUTHOR CONTRIBUTIONS	171
ACKNOWLEDGEMENTS	171
REFERENCES.....	171
GENERAL DISCUSSION.....	179
SUPPLEMENTS	197
SUPPLEMENTS: CHAPTER 1	198
SUPPLEMENTS CHAPTER 2	202
SUPPLEMENTS CHAPTER 3	226
SUPPLEMENTS CHAPTER 4	237
LIST OF PUBLICATIONS.....	246
EIDESSTATTLICHE VERSICHERUNG	247
FUNDING	248

Preface

A famous inspirational quote says 'It's always the little things that make the big things happen.' Similarly, in the ocean, the tiny plankton plays a crucial role in aquatic ecosystems. They affect the chemistry and climate of the planet; take carbon out of the atmosphere, locking it up for a time in their cells, in the animals that consume them, and in fecal pellets that they drop to the sea floor. Their timing of availability in the right size and the right place affects the survival of many other species, from fish up to the largest marine mammals. They are mediators of energy from bacterial- to higher trophic levels. Besides predation, they are one of the main controlling factors of year class strength of many commercial fish species. Yet, our knowledge on these tiny but essential organisms are limited in both, space and time and, therefore, it is important to expand our limited knowledge on standing plankton stocks and dynamics over different size fraction and large spatial and temporal spheres. As they are numerous in numbers, shapes and lifeforms, there is a need to merge different sampling methods and test different analytical approaches to understand their general dynamics, predict changes under ongoing climate change and, in order to do that, provide data for modelling approaches e.g. biogeochemical cycles, growth and survival models. In this thesis, I have analyzed the micro and mesozooplankton (MesoZP) community in the North Sea during winter, a time of the year which is rarely studied. Via the application of different sampling devices and analytical approaches, we show that there are unique patterns and drivers on both, at different temporal and spatial scales. Concurrently we present a unique 7-year dataset of zooplankton data from the central and southern North Sea, providing abundance, biomass and distribution of key plankton, from Protozoa- (PZP) to MesoZP groups (20-2000 μm). In the following introduction, I will briefly introduce the main plankton groups analyzed in this thesis, their importance for the ecosystem and the knowledge gaps, which I have addressed in this thesis.

General Introduction



Drawings by Justine Courboulès

Plankton

General definition

The word plankton stems from the Greek word “planao” which means, “to wander”. It encompasses all passively drifting organisms in the aquatic realm. Plankton is traditionally distinguished into phytoplankton (mainly autotrophs) and zooplankton (mainly phagotrophs). This distinction is simplified as the large diversity in plankton brought forth many different definitions of plankton organisms, distinguished based on their morphology, nutrition mode, life style, and size, among others (e.g. Castellani & Edwards 2017).

Zooplankton may be distinguished from phytoplankton on basis of morphology or nutrition mode. While phytoplankton is a primary producer, capable of performing photosynthesis, zooplankton is mainly considered heterotrophic, i.e., they consume organic particles with a variety of capturing techniques. This definition can be also tricky, though, as some zooplankton species can be, both autotroph and heterotroph, which is called mixotrophy. This nutrition mode is commonly found in flagellates and other protozoans, such as ciliates and foraminifera (Stoecker et al. 2017).

Plankton is also classified according to their life style. For instance, species that spend their whole lifetime in the pelagic realm are defined as holoplanktonic organisms, such as copepods and protozoans. In contrast, species that spend only part of their life cycle as a planktonic phase are termed meroplanktonic organisms. For example, some species switch from a planktonic larva to a benthic adult life stage (e.g. Decapods) or vice versa (e.g. hydrozoans), and although many fish species and cephalopods inhabit permanently the pelagic environment, their larvae are also considered meroplankton since they are drifting organisms, unable to swim against the currents.

Irrespectively of their classification, plankton forms the foundation of the aquatic food webs. When light and nutrient conditions allow it, phytoplankton can grow exponentially (Reid et al. 1990). As a result, a chain reaction is triggered with rapid growth of small zooplankton organism with fast generation times (e.g. protozoans) feeding on them (Aberle et al. 2007). Subsequently, larger and slow growing zooplankton taxa feed on them and are then a food source for higher trophic levels (van Beusekom & Diel-Christiansen 1993). This very brief and streamlined description is, in reality, much more complex, with many different pathways of energy as the above-described feeding modes and different life stages create more of a web than a chain like structure (Belgrano et al. 2005).

The term plankton comprises a large variety of different organisms with many different species, from nanoflagellates of two μm up to *Cyaneidae* species with more than 2 m of size (Fig. 1.1).

Body size is an important trait in the ocean as it can be used to characterize the capabilities and limitations of individual organisms (e.g. Litchman et al. 2013). Through power-law functions, organism size can be used to describe aspects of populations and organismal physiology across taxa (Peters & Wassenberg 1983) and can determine predator-prey relationships (Nakazawa et al. 2011). Schütt et al. (1892) did a first attempt of size classification, which underwent several modifications since. Almost 100 years later, Sieburth et al. (1978) revision was and still is widely accepted (Fig. 1.1), ranging from femto- to megaplankton, over eight orders of magnitude, among which this thesis focuses on two: micro- and mesoplankton.

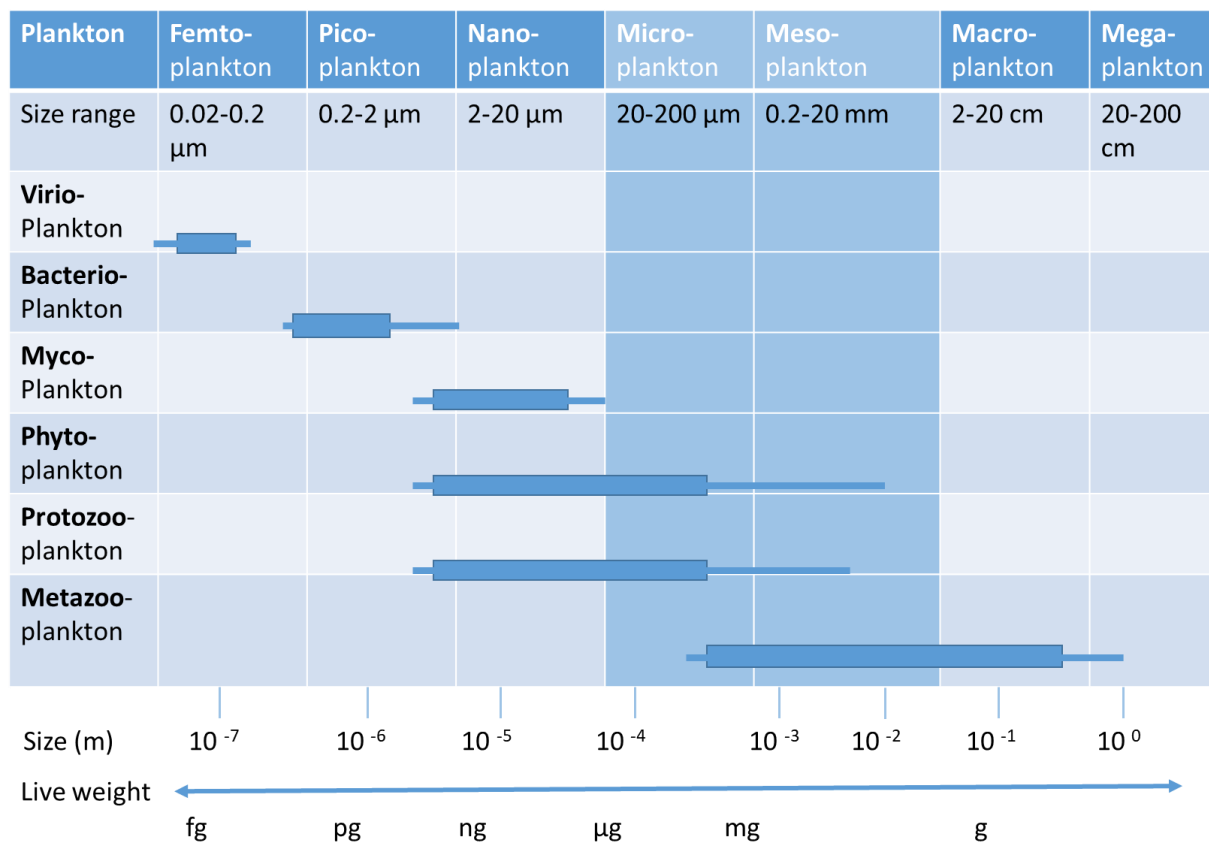


Figure 1.1 Classification of plankton in functional and size groups. The main plankton components of this study are highlighted in blue (redrawn from Sieburth et al. (1978)).

Microplankton

Microplankton is mainly defined by their size (20 – 200 μm (Fig. 1.1)); they are ubiquitous and highly abundant in all marine and limnic aquatic ecosystems. The microplankton is characterized by their trophic mode, into microphyto- and microzooplankton (MZP). The MZP fraction includes protozoans (Fig. 1.2 A, B, E), micrometazoa such as nauplii (Fig. 1.2 G), larval

stages of meroplankters and rotifers (Calbet & Alcaraz 2007). Ciliates and heterotrophic dinoflagellates usually dominate the microzooplankton community.

Ciliates are mostly free-living aquatic unicell organisms, characterized by an abundance of lash-like flagella (cilia) on their body surface (Paulin 1996). The cilia are used for locomotion and feeding by drawing in food particles. Ciliates are differentiated by either having a shell-like protection (lorica) or as “naked” ciliates without lorica (aloricata). For instance, in the order of *Tintinnida* (Fig. 1.2 B), the lorica is transparent and more like a shell, while ciliates of the genus *Strobilidium* sp. rely on their locomotion ability to avoid predators, with cilia that enables them to move faster (0.52 cm s^{-1}) than other protozoa (0.2 cm s^{-1}) (Jakobsen 2014). Some ciliates are mixotrophic using endosymbiotic algae or by sequestering chloroplasts from ingested algae that are kept functional in the ciliate cytoplasm (Esteban et al. 2010). However, most are holozoic and feed on bacteria, algae, particulate detritus, and other protozoans as big as their own size (Jonsson 1986). A few larger ciliate species are carnivorous and feed on small metazoans (Brown & Jenkins 1962). The division rate of ciliates is fast to keep pace with their phytoplanktonic prey, thus, they react immediately to algae growth and are usually the first grazers of phytoplankton blooms (Smetacek 1981, Aberle et al. 2007)

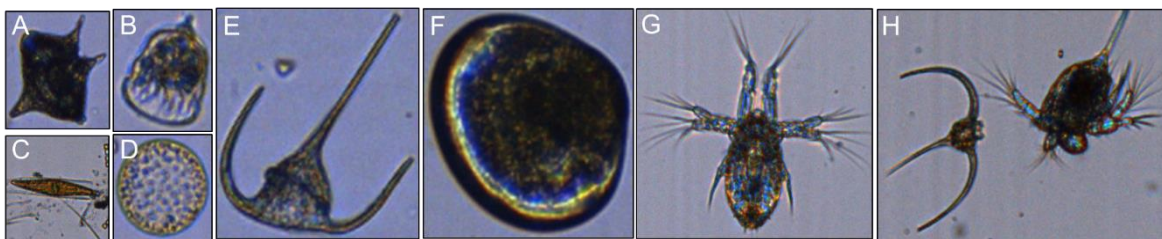


Fig. 1.2 Members of the Microplankton community of the winter North Sea derived with FlowCAM (4x) with *Protoperdinium* sp. (dinoflagellate) (A), *Tintinnida* (ciliate) (B), a pennate (C) and a discus diatom (D), *Tripos* sp. (dinoflagellate) (E), bivalve larvae (F), nauplii (G), a nauplii and *Tripos* sp. in size comparison (H).

Dinoflagellates are mainly unicellular organisms, with unique characteristics, such as flagellar insertion, among others. The name dinoflagellate is composed of the Greek word “dinos”, which translates as “whirling”, related to their distinctive swimming pattern, and the Latin “flagellum” which means, “whip”. They are widespread in marine and freshwater ecosystems with great diversity including autotrophic, heterotrophic, mixotrophic, parasitic, and symbiotic species (Riding et al. 2022); however, recent studies suggested that mixotrophy in dinoflagellates is more common than previously assumed (Flynn et al., 2013), bridging the gap between primary producers and consumers. Dinoflagellates are typically bi-flagellated with the two flagella perpendicular to each other, which is the cause for their characteristic spiral

motion pattern. They are distinguished into 'naked' or nonthecate species, possessing no tough cell walls, and 'armored' or thecate species, which are covered with a strong wall of interlocking cellulose plates. In some species, these plates have developed into spines, wings, or parachute-like extensions (e.g. *Triplos* sp., Fig. 1.2 E). Dinoflagellates are also important primary producers as many of them do photosynthesis, especially the thecate taxa. Many species are heterotrophic, like *Protoberidinium* sp. (Fig. 1.2 A), that engulf and digest their prey by surrounding it with a cytoplasmic sheet (pallium). Their prey includes other dinoflagellates, diatoms, microflagellates and bacteria. Various dinoflagellate species are large enough to consume copepod larvae as well as smaller phytoplankton. Dinoflagellates can form blooms, known as red tides, with densities of over one million cells per milliliter, when the conditions match. They then produce dinotoxins in enough amounts to be deadly to fish, seabirds and can also be dangerous for human consumption (shellfish poisoning) (e.g. Schantz 1975).

Meso(zoo)plankton

Planktonic organisms ranging in size 0.2–20 mm are referred to as mesozooplankton. Some of the main groups of mesozooplankton include copepods, euphausiids, chaetognaths, and gelatinous plankton but also compose many different development stages such as bivalve larvae, decapod zoea or fish larvae. Being regarded as the grazers of the sea, mesozooplankton functions as the central link between primary production, the microbial food web and higher trophic levels (Stoecker & Pierson 2019).

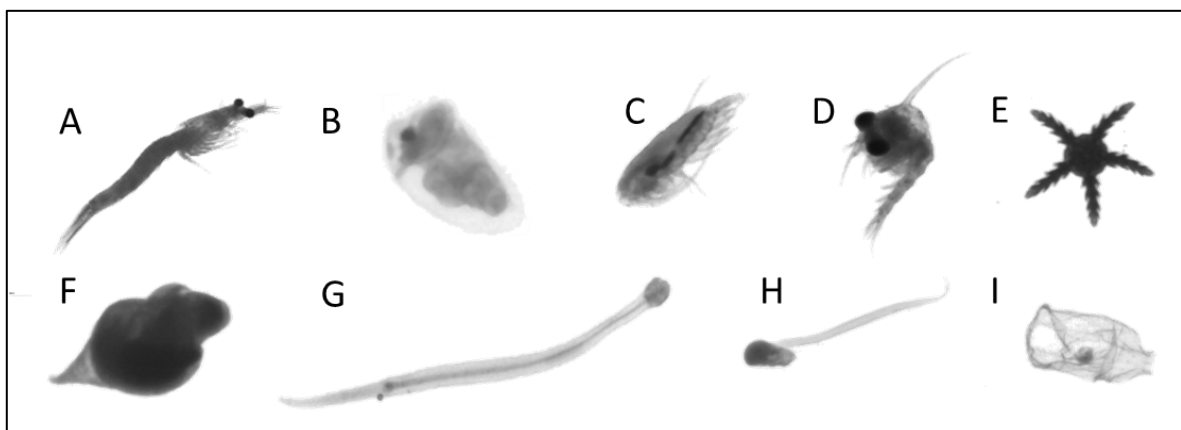


Fig. 1.3 Members of the Mesozooplankton community of the winter North Sea derived with ZooSCAN. Euphausiid (A), Cladocera (B), Copepod (adult) (C), Zoea larvae (D), Echinodermata larvae (E), veliger larvae (F), chaetognath (G), Appendicularia (H), hydrozoan medusae (I).

Copepods are the most abundant member of the mesoplankton community and are widespread in all aquatic ecosystems. Their life cycle is composed by several distinct life

stages (i.e., egg, multiple naupliar and copepodite stages and adults), making them members of the micro- and mesozooplankton community, throughout their development (Fig. 1.3 C and 1.2 H). They also support population fisheries of economically important species such as cod, herring, and salmon, by providing food for their larvae, and therefore, controlling their survival and, ultimately, the recruitment success of these species (Beaugrand et al. 2003).

Besides copepods, there is a diverse range of other zooplankton groups including euphausiids, mysids, chaetognaths, jellyfish, and ctenophores. Euphausiids are important prey for many fish species, including herring (Pearcy et al. 1979). Mysiids are omnivorous and opportunistic feeders, consuming a variety of prey including small crustaceans, detritus, and algae, and serving as an important prey item for many fish species (e.g. Eigaard et al. 2014). Chaetognaths are voracious predators, feeding mainly on other zooplankton and are considered one of the top predators in some marine ecosystems (Baier & Purcell 1997). Gelatinous zooplankton, including jellyfish and ctenophores, play important roles in marine ecosystems, consume a variety of prey, including copepods and fish larvae. Some species, however, can have negative impacts, such as forming blooms that can disrupt food webs and cause ecosystem shifts (see Purcell 2005). Copepods are by far the best studied group whereas the other groups are generally less abundant or less studied.

Biogeochemical cycle

Plankton, especially phytoplankton, are major contributors to oxygen production in the Earth's atmosphere. Through the process of photosynthesis, they use sunlight, carbon dioxide, and nutrients to produce organic matter and oxygen as a byproduct. In fact, it is estimated that up to 50% of the oxygen in the Earth's atmosphere comes from phytoplankton (Pörtner et al. 2014).

Plankton also play a critical role in the biological carbon pump (BCP), which is the process by which carbon is transferred from the surface ocean to the deep ocean (De La Rocha & Passow 2006) (Fig. 1.4). Phytoplankton's photosynthesis is the initial step in the cycle (Basu & Mackey 2018) and it has an effect on the environment via air-sea gas exchange (Raven 2007). When phytoplankton grows and reproduce, they take up carbon dioxide from the surface water and convert it into organic matter. This organic matter then sinks to deeper depths, either through the physical sinking of dead plankton or through the feeding activities of zooplankton and other organisms. This process effectively sequesters carbon in the deep ocean, helping to regulate the global carbon cycle and climate (Fig. 2).

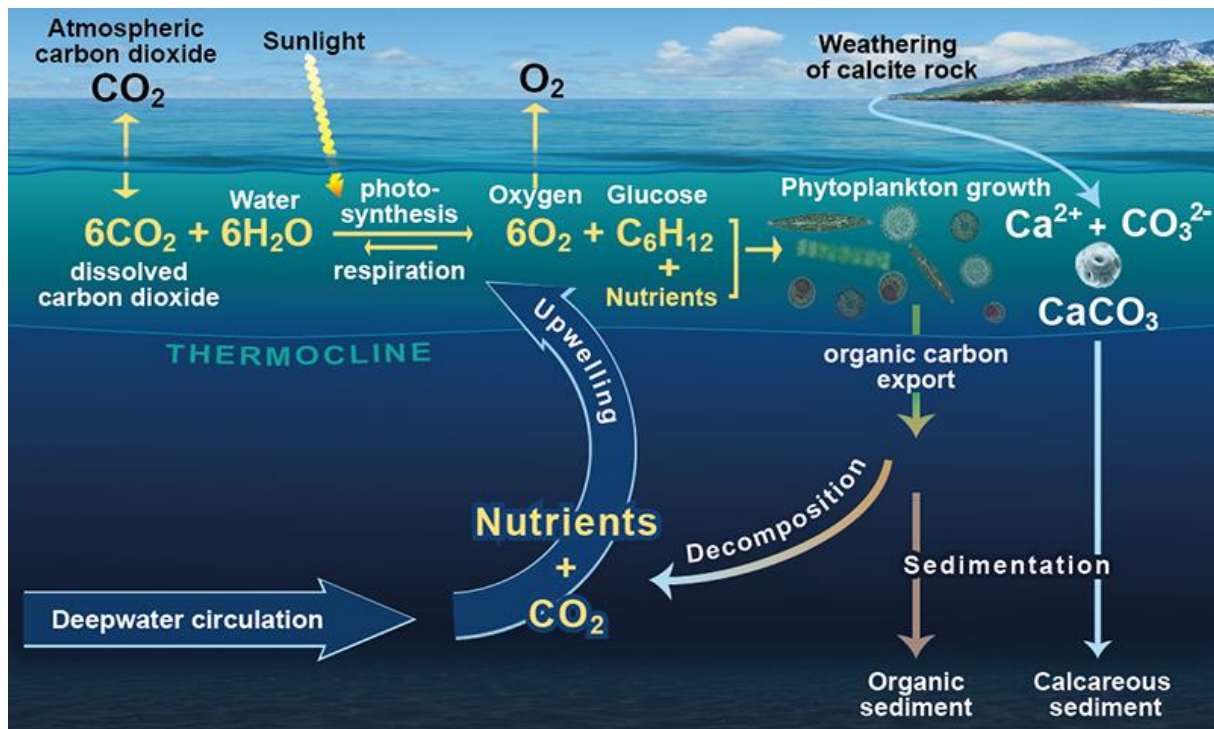


Figure 1.4. The biological carbon pump. Phytoplankton use energy from sunlight to convert carbon dioxide and water into glucose and oxygen, driving the marine food chain. The biological carbon pump, which involves the transformation of carbon dioxide and nutrients into organic carbon, sinking into the deep ocean and its decomposition at depth, contributes to the ocean's uptake and storage of carbon dioxide (From: NOC/V.Byfield).

Zooplankton have a crucial role in the efficiency of the BCP regulating the atmospheric carbon dioxide levels (Kwong & Pakhomov 2017). Cavan et al. (2017) underline the roles of zooplankton in improving the effectiveness of the BCP through the control of particles export by grazing, fractioning large and fast sinking particles in slower ones and moving particulate organic carbon (POC) to depth via diel vertical migration.

Zooplankton: Food for all?

Zooplankton plays an important role in the conservation of energy from primary producer (phytoplankton) to higher trophic levels (Aberle et al. 2007, Calbet 2008). The zooplankton occurrence and distribution influence pelagic fishery potentials. They are the initial prey for most fish larvae as well as for many planktivorous fish (e.g. herring). Zooplankton is so abundant in the world's oceans that it is the main food source of the oceans largest fish (Sims & Reid 2002) and whales (Gulland 2013). It has also a strong effect on biomass stocks of other planktonic groups, in fact zooplankton can alter the concentration of prey populations such as phytoplankton (by consumption, top-down control) and predator populations (by being consumed by higher trophic levels, bottom up), consequently having effects on fish biomass (Lomartire et al. 2021). First feeding larvae have a limited size of their mouth gape, which

constrains the size of prey they can capture. Throughout ontogeny, they need to switch to larger prey to meet their energy requirements (Fig. 1.5). This process is known as ontogenetic niche shift and is a common phenomenon in fish larvae (Werner & Gilliam 1984). This switch in prey often coincides with changes in habitat and behavior, and is a key factor in determining the distribution and survival of fish larvae in the ocean. Fish larval survival success is therefore dependent on its surrounding environmental conditions and plankton abundance and less by the quantity of parent stock (Pierre et al. 2018). After exhausting their yolk reserves and when switching from endogenous into exogenous feeding, fish larvae need to find suitable prey items (“critical period”; Hjort 1914). Based on this concept, Cushing (1990) developed the “match-mismatch” hypothesis, stating that the timing of larval production and their prey determines the strength of recruitment. The Match-Mismatch hypothesis has later been shown for herring larval survival, for instance, as low survival rates likely result from changes in prey availability, composition and quality (Payne et al. 2013, Lusseau et al. 2014, Alvarez-Fernandez et al. 2015). Later studies suggested a complex interplay of temperature, prey type and availability, with larval growth and survival in the North Sea (Hufnagl & Peck 2011, Hufnagl et al. 2015).

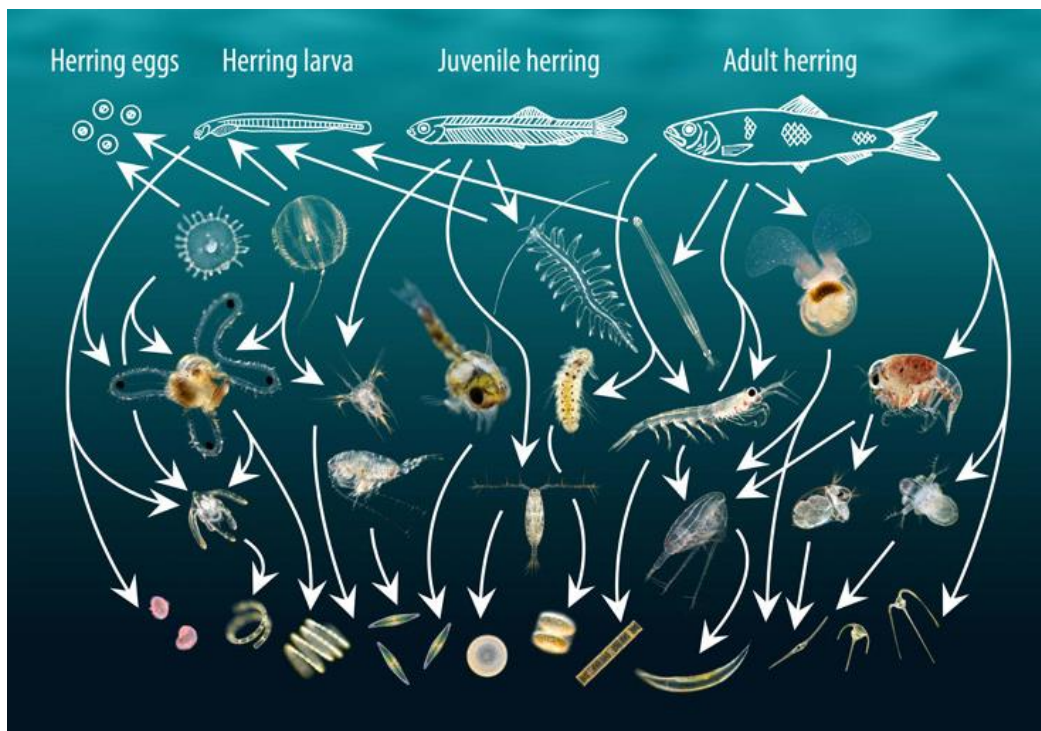


Figure 1.5: Example of the multi-branched plankton foodweb with respect to the different ontogenic stages of herring (From: [twitter.com/ @PlanktonPundit](https://twitter.com/PlanktonPundit) (Dr Richard Kirby))

In summary, Zooplankton is an essential component of marine food webs, as it transfers carbon to higher trophic levels, feeds on microorganisms (such as bacteria and PZP), and

provides a food source for fish and other invertebrates (Fig. 1.5) (Figueiredo et al. 2009, Bils et al. 2022).

Standing stock, biomass and seasonal dynamics

The assessment of phytoplankton standing stock and its seasonality is of critical importance. The seasonal cycle in temperate ecosystems is mainly controlled by the effect of light on phytoplankton growth and can be generally divided into three stages:

A spring bloom is initiated due to a combination of vertical stratification of the water column and increasing solar radiation after the replenishment of nutrients by convective mixing over the winter months (Lohmann & Wiltshire 2012). After that kick off, with some delay due to longer reaction times, spring blooms are controlled by the grazing pressure of the increasing zooplankton abundances and decreasing nutrient concentration within the upper mixed layer (Franks 2001). The strength of the grazing effect on the spring bloom depends on the size of the initial zooplankton population (Strom et al. 2001). Temperature is a critical factor in aquatic ecosystems as it governs the growth rate of planktonic organisms. In temperate ecosystems, zooplankton has to maintain a higher biomass since production, since the production rate is temperature driven and is altered during colder seasons. In warm water systems, the temperature, so the growth rate is generally higher and it is possible to build up large populations from lower standing stocks, once the energy to support growth is available (Harris et al. 2000).

During summer, when a strong thermocline prevents any mixing between surface and deeper waters and the available nutrients are efficiently recycled, phytoplankton growth is slowed down by nutrient limitation (Harrison et al. 1990). The summer period is controlled by grazing and the system is based on regenerated production.

With the decrease in day length and light intensity in autumn, the surface waters cool down and autumn winds re-mix the water column, resuspending nutrients into the water column. These resuspension coupled with still high light levels may induce an autumn bloom of phytoplankton (Richardson et al. 2000). In contrast to spring blooms, autumn blooms are less studied, although widely documented (Herring 2001, Raymont 2014) as a significant component of annual production in temperate areas (Findlay et al. 2006).

In late autumn/early winter the light levels decrease further, phytoplankton activity decreases and nutrient concentration increases. The particulate and dissolved organic matter from summer and autumn remains and sustains the growth of a microbial heterotrophic community, as profiteers from the absence of larger phytoplankton cells (Joint et al. 1986, Bils et al. 2019).

Here the concept of the microbial loop comes into play (Azam et al. 1983). Briefly, the microbial loop refers to the process by which small microorganisms (small phytoplankton and heterotrophic bacteria) use dissolved organic matter, converting it into biomass. These microorganisms are then consumed by small ciliates and dinoflagellates, which are then consumed by larger organisms, such as zooplankton, and ultimately passed up the food chain to higher trophic levels (Fig. 1.6) (Pomeroy et al. 2007). The strength of the microbial loop varies between seasons and can be enhanced during times of low phytoplankton productivity (Fileman et al. 2011).

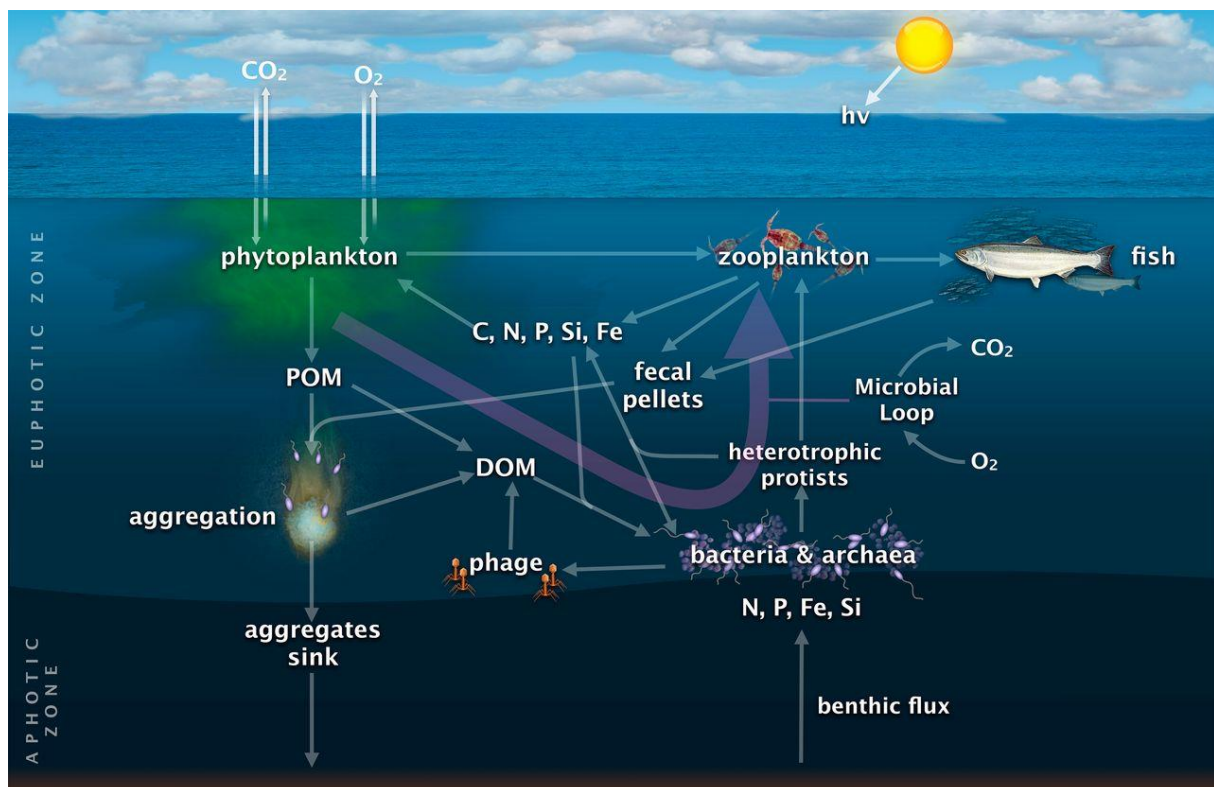


Fig. 1.6. Conceptual model of marine food web. Phytoplankton produce dissolved and particulate organic matter (DOM and POM, respectively) that bacteria and archaea use for respiration via the microbial loop (purple arrow), changing the expected carbon flow in traditional diatom-copepod-fish food chains. While food chain diagrams typically do not distinguish between different phytoplankton sizes, size can affect food web connections, and inorganic nutrients play a role in community composition. (From Worden et al. 2015)

In summary, relationship between the season depended standing plankton stocks and production of a population mainly relies on biotic conditions, such as food supply, and abiotic conditions such as temperature, light availability etc. In temperate seas such as the North Sea, these conditions vary greatly with seasons. Thus, the seasonal production rate and biomass of plankton is vital to understand its population dynamics and to detect any climate change or anthropogenic related changes. Changes in the population dynamics of plankton has the

potential to affect the population of all the species in the food web, and thus, the ecosystem (bottom-up control). The seasonal conditions may change under ongoing climate change and, thus, may dramatically affect the population dynamics. Zooplankton communities tend to rapidly respond to changes in environmental conditions, especially in coastal areas, where the combination of land and marine influences can lead to significant and abrupt changes in conditions (Richardson 2008, Dam & Baumann 2017). Therefore, zooplankton, especially the small fractions with short generation times are considered as useful bioindicators for accessing aquatic ecosystem health (Hays et al. 2005). It is therefore essential to understand and survey the standing stocks across the different seasons, but especially during times of low productivity, which is one of the main aspects of this thesis.

Size structure

Body size is a critical trait that influences various biological and biogeochemical processes, such as nutrient acquisition and particle export (Peters & Wassenberg 1983, Blanchard et al. 2017). The importance of body size has been acknowledged for almost 100 years (Elton 1927, Sheldon et al. 1972, Platt & Denman 1977). Size-based approaches have become increasingly popular in recent years as useful modeling tools for studying eutrophication and fishing effects (Trebilco et al. 2013, Sprules & Barth 2016, Blanchard et al. 2017). Despite variations in complexity and parameterizations (Mehner et al. 2018), all size-based models share the fundamental principle that the inefficiency of energy transfer and metabolism contributes to a decline in biomass at each level of the food chain (Kjørboe 2009).

Body Size - What do we need to know (and why)?

Body size is a critical functional trait to understand many ecological and evolutionary processes, since many of them are dependent on size (see Schmidt et al. 2006 and references therein). Many studies, including those focused on marine and limnic ecosystems, have demonstrated the correlation between various environmental factors and community size structure based on mean body size, size abundance, and biomass size spectra (e.g. Yvon-Durocher et al. 2011, García-Comas et al. 2014). Size spectra reflect well variations in ecosystem productivity as oligotrophic areas tend to have steeper slopes than eutrophic areas (Sprules & Munawar 1986). Size spectra reflect also predator-prey relationships in aquatic ecosystems as they show the distribution of biomass across different sizes of organisms (Kerr & Dickie 2001). Generally, the size of a predator determines the size range of its prey, and the abundance of each size class depends on the balance between predation and resource availability. The transfer of energy between trophic levels is also reflected in the size spectra, with larger organisms typically consuming smaller organisms and thus transferring energy up

the food chain (Kerr & Dickie 2001). Size index measurements can be used to understand and monitor the health of aquatic ecosystems (Sprules & Munawar 1986, Heneghan et al. 2019). Furthermore, intra-specific diversity in size is often related to the reproductive success of a population as larger organisms are in advantage (Schmidt et al. 2006).

The Size-spectra approach

The concept of size is not a new approach. In 1927, Elton introduced the “pyramid of numbers” to describe his observation that there is an inverse relationship between the number of organisms and their size (Elton 1927). In the early 1960, body size was reconsidered in ecological studies until Sheldon et al. (1972) fully revived this concept when they discovered broad regularities in the size structure of aquatic communities that is very similar to the pyramid of numbers from 1927. They introduced the concept of size spectra and the biomass spectrum, which displays equal biomass concentrations in logarithmically equal size categories (Fig. 1.7). The prevalence of size spectra slopes around -1.0 highlights the significant influence of size on marine predator-prey interactions, surpassing other traits like taxonomy or function (Sheldon et al. 1972, Quinones et al. 2003). Size spectra slopes have become a useful measure to evaluate bottom-up or top-down control in marine ecosystems (Silvert & Platt 1978, Zhou 2006), while the associated intercept can indicate productivity levels (Zhou 2006, Ye et al. 2013).

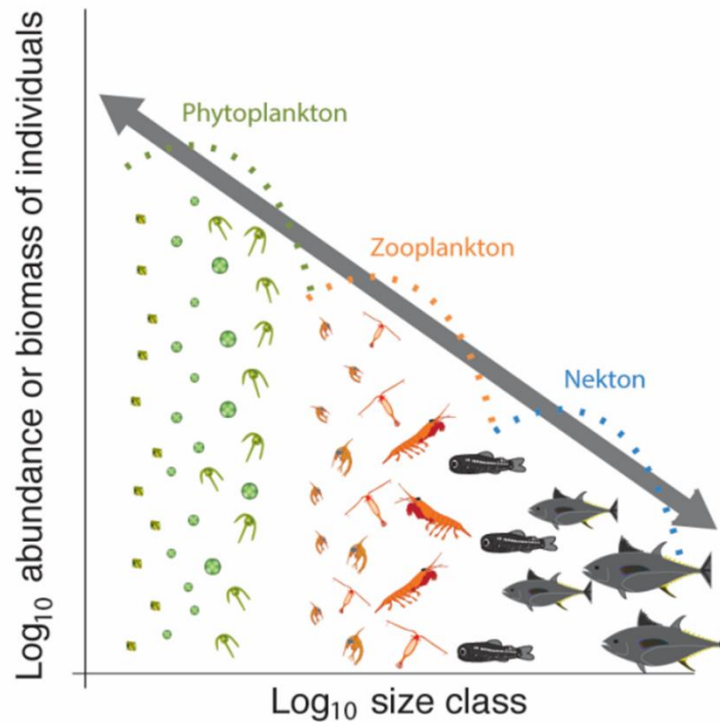


Fig. 1.7 Conceptual diagram of an aquatic biomass size spectra from phytoplankton (green), zooplankton (orange) to nekton (blue) and the theoretical slope of -1 (grey arrow) (From Kwong & Pakhomov 2017)

The size spectra approach was recently reconsidered due to a number of factors: First, the development of techniques to count and measure particles (e.g. FlowCAM, Coulter Counter) have helped to collect size data easy and fast (Dai et al. 2016). Second, size-based approaches help to simplify multiple, often poorly known processes for wide range of individuals in an aquatic assemblage (Ward et al. 2014). Third, thanks to advances in technology, assessing the size structure of a community has become simpler than evaluating other aspects, such as trophic transfer efficiency, predator–prey mass ratios, or production levels. Indeed, measuring the size structure of the community provides understanding into how the combined effects of these processes affect the food web (Jennings et al. 2002). While this approach has several advantages, such as providing insights into the structure and function of plankton communities, there are also some drawbacks to consider, such as the missing provision of the taxonomic identity of the organisms in each size class. This can limit the ability to accurately identify specific species and understand their roles in the ecosystem. Another point is plankton communities can be highly variable and complex, and it can be challenging to sample all size classes and accurately represent the entire community (Everett et al. 2017). This can lead to incomplete or biased data and limit the reliability and generalizability of the findings. Finally, the size spectra approach focuses primarily on the size distribution of plankton, which may not fully capture the complex ecological and environmental factors that

influence their abundance and distribution. This can limit the ability to understand the drivers of ecosystem dynamics and predict future changes. To ensure accuracy, plankton studies should incorporate a wide range of mass, ideally covering at least seven orders of magnitude to encompass small phytoplankton and zooplankton. Additionally, spatial and/or temporal integration should be incorporated to avoid potentially misleading short-term snapshots (Atkinson et al. 2021). These points will be tested and discussed in chapter 3 of this thesis.

How do we study plankton?

Knowledge on the plankton community, besides presence/absence, and its functioning, relies on answering the questions “how much”, “which”, “where” and “when”.

There are two main procedures to quantitatively measure plankton:

- 1) counting of organism and
- 2) biomass determination.

The most holistic approach involves both; however, counting of organisms, i.e., abundance, is the most commonly used metric. The biomass determination can be expressed as weight (wet mass, fresh mass, dry and ash mass) or as carbon content. The weight can be directly measured whereas carbon content is usually calculated using individual biomass conversion factors (e.g. Kiørboe 2013). For adequate biomass measures, size measurements are essential. However, size measurements from microscopy are time consuming and imprecise due to the vast spectrum of different shapes and measurement techniques. Often, mean sizes from literature are derived for biomass calculations (e.g. in Bils et al. 2019). For species that are consistent in size, like PZP, this approach could be appropriate. For taxa with different growth stages, however, literature values may not be precise enough and lead to miscalculations. Therefore, the instant provision of size by the image-based techniques (discussed below) is a feature that opened up new opportunities in plankton research.

Plankton sampling

Knowing the actual distribution of plankton in the ocean is a difficult task as they take place over enormous temporal and spatial scales. Most of the information about plankton comes from sampling either via scientific cruises or at fixed sampling stations (observational). In addition, laboratory experiments (experimental) provided species-specific insights and both data is complemented by modelling studies (theoretical). The combination of all three approaches (end-to-end studies) is the most promising approach, where modelling approaches provide information for a more specific sampling design for surveys or experiments, which again validate the modelling results.

Generally, the collection of plankton is yet a difficult task. The vast spectrum of different sizes, shapes and textures makes it very difficult to obtain a good overview of the entire plankton community. While phytoplankton biomass estimates nowadays can be derived from satellite imagery, most studies require abundance indices of specific taxa that can only be collected from in situ plankton sampling and determining its composition. Generally, Zooplankton has not received the same attention as the phytoplankton and fish communities within ecosystem studies in previous decades (Mitra et al. 2014). The most common sampling technique is using plankton nets, which has been established since the 20th century. These nets were specifically designed for different research objectives and species of interest with varying catch efficiencies and applications (Skjoldal et al. 2013). However, plankton nets have certain limitations that need to be taken into account, such as the avoidance of the sampling device by certain organisms, the clogging of the net meshes, the “slip through” of organisms due to their shape (e.g. elongated organisms such as appendicularia), and the general water pressure exerted on the organism through towing (see Skjoldal et al. 2013 for a comparison of different plankton nets). Another problem when sampling plankton is that plankton communities can be highly variable and patchy, with spatial and temporal differences in their distribution and abundance. This can make it challenging to accurately capture and represent the entire community and can lead to incomplete or biased data.

Additionally, some types of plankton, such as gelatinous organisms, may be difficult to capture with traditional nets or sampling methods, further limiting the ability to study these important organisms. For the more delicate members of the plankton community, the filtration through nets can cause damage and loss (e.g. up to 60% of MZP; Ref.). To avoid the damage of fragile organisms (e.g. PZP), a more gently sampling technique can be used, e.g. water samples by Niskin bottles, often mounted in a conventional rosette sampler. The Niskin bottles are deployed open and can be remotely closed to collect water samples at the desired discrete depths. However, water samples have the limitations that only a relatively small volume is taken and a single water sample may not be representative of the entire water column or the entire region of interest (Harris et al. 2000). To address all these challenges, researchers often use a combination of different sampling methods and approaches to gain a more complete and accurate understanding of plankton communities and their ecology (e.g. suggested by Calbet et al. 2001). In chapter 3 of this thesis, we apply two different nets to more efficiently sample the plankton community to get more accurate numbers of micro- and mesozooplankton abundance and biomass.

Preservation and Analysis

Irrespective of the net apparatus, when lifted off the water, samples are carefully washed with seawater into the cod-end and are usually preserved for further laboratory analysis. The type of preservation applied to fix the samples depends on the purpose for which the sample was taken. The range of preservation goes from freezing samples at different degrees, drying or storage in different preservation solutions. A common long-term preservation technique for taxonomical purposes is the fixation in a buffered 4% formalin-seawater solution, while ethanol is commonly used for molecular studies and fast freezing in liquid Nitrogen for stable isotopes and fatty acid analysis (Harris et al. 2000). Furthermore, the fixation methods must be adapted to the different planktonic groups of interest. For instance, Lugols Iodine fixation is commonly used as a fixative for microscopic analysis of phytoplankton, nanozooplankton, microzooplankton (Gifford & Caron 2000), and mesozooplankton samples (e.g. Jaspers & Carstensen 2009). This fixation technique is most delicately but preserved samples have a shelf-life of 6-12 months (Gifford & Caron 2000, Calbet et al. 2001). Despite the existing standard protocols, over the past decades, there are several in-depth discussions of the pros and cons of different sampling and preservation techniques for the different plankton groups (e.g. Steedman 1976, Heyman 1981, Wiackowski et al. 1994, Menden-Deuer et al. 2001). Once in the laboratory, preserved plankton samples are traditionally analyzed using microscopy. This approach offers a high taxonomic resolution, however, it is a labor intensive, time consuming and requires a certain level of expertise in plankton identification (Benfield et al. 2007, Culverhouse et al. 2014). These factors make it also biases and error sensitive due to different operators and fatigue (e.g., self-consistency can be < 80% in difficult identification tasks) (Culverhouse et al. 2014).

The complexity of the plankton community and the associated difficulties in sampling, preservation, sorting and identification of the samples, led to the development of techniques that simplify these processes and increase the applicability and, by extension, the survey plankton survey areas and times. One of the most successful and worldwide applied developments is the Continuous Plankton Recorder (CPR) by Sir Allister Hardy Foundation in 1964. The CPR was designed to be towed at top speeds up to 25 knots through the surface layers, which makes it easily applicable, even by non-scientific crews on ships of opportunity (see Warner & Hays 1994 for a detailed description). The plankton is sampled on a 270- μm mesh size gauze and identified through microscopy. Although the CPR provides a high frequency of plankton data with a large spatial coverage, the data quality is limited due the fact that it is towed at affixed depth and neglects the small size fractions below 270 μm .

To speed up the identification process of plankton net samples, reduce the costs and the associated errors of microscopy, automated image-based methods were developed, allowing the quick processing of higher number of samples. These methods (e.g. Flow Cytometer and Microscope, FlowCAM, or ZooSCAN) can provide instant information on abundance, biomass, seasonal variability of phyto- and zooplankton and the measures are comparable with microscope counts, especially for the most abundant classes (Álvarez et al. 2014, Naito et al. 2019). The recording of images enables the temporally unlimited storage of information even for samples that cannot withstand fixing agents for a long time (e.g. PZP)(Gifford & Caron 2000). These digital imaging techniques also have the advantage that they automatically provide estimates of the size of individual planktors, although at lower taxonomic resolution. On the other hand, these techniques/machines are very costly, bulky, not applicable at sea (ZooSCAN) and not suitable for large-scale sample analysis due to limitations by flowrate (FlowCAM) (Pitois et al. 2018).

A more recent approach is the development of *in situ* analyzing techniques using optical devices such as the Video Plankton recorder (VPR) which can provide insights into distributional and migration patterns of the larger plankton community (Davis et al. 1992, 2005). Since the VPR, several other devices for the *in-situ* imaging of plankton organisms were developed (e.g. SIPPER (Remsen et al. 2004), ISIS (Cowen & Guigand 2008) or the UVP (Picheral et al. 2010). The main limitation here is similar to the limitations with plankton nets: they cannot be deployed at all conditions at sea, their operation requires work force and is labor intensive (Pitois et al. 2018). That led to the development of all-in-one setups (e.g. Plankton Imager (PI) (Scott et al. 2021) or the PlanktoScope (Pollina et al. 2022), eliminating the limitations of gear applicability and involved labor and to provide autonomously acquired and analysis-ready-data without post-survey sample processing (e.g. (Culverhouse 2015).

While the number of tools for continuous collection of high resolved data are increasing, a major bottleneck is the processing and interpretation of this vast amount of plankton images and data gathered (Giering et al. 2022). Although the features of each pictured organism are measured and stored (e.g. size), the ecological interpretation of the images, i.e. the taxonomic classification mainly relies on human validation. The interplay of the aforementioned automatic image-based techniques with machine learning algorithms paved the way for the automatically recognition of the plankton up to species level (of certain distinct shaped organisms) and simultaneous size measuring.

The development of classification models developed in the 1980s (LeCun et al. 1989), first applied on plankton in 1998 (Tang et al. 1998) helped to drastically decrease the classification time by pre-sorting the images (e.g. supervised: EcoTaxa (Picheral et al. 2017) or unsupervised: Morphocluster (Schröder et al. 2020)) or entirely remove human interference

(e.g. Briseño-Avena et al. 2020). Today's classification models are able to achieve classification accuracy of over 95% on test data (e.g. Al-Barazanchi et al. 2018) with similar features than the training data. However, in the planktonic realm, high spatio-temporal dynamics of the community hinders the performance of those models (Moreno-Torres et al. 2012). The latest research trends are more directed away from fully unsupervised models and, towards a combination of AI as an application tool, helping to carry out tasks but not in autonomy (Giering et al. 2022).

In summary, plankton image classification systems can be used in a variety of applications, such as monitoring water quality (e.g. Budiarti et al. 2019) and tracking changes in plankton populations. Some challenges in building a plankton image classification system include the need for large amounts of labeled data, dealing with variations in lighting, plankton size ranges, and accounting for the complex shapes and textures of different plankton species. Overall, the development of plankton image classification systems has been an ongoing process, with researchers continually exploring new techniques and approaches to improve their accuracy and robustness. However, there are several limitations that remain challenging. One important issue is the availability of large datasets of "labelled" plankton images. Most of the available datasets are generated due to specific research questions and therefore, are not broadly applicable. Another issue are variations in plankton size and appearance: Plankton can vary greatly in size and appearance, making it difficult for image classification systems to accurately identify and classify different species. Additionally, variations in lighting conditions and image quality can also affect the performance of plankton image classification systems. Added to this, plankton can have complex shapes and textures, making it difficult for image classification systems to accurately extract features that are relevant for classification. Many deep learning-based plankton image classification systems are complex and difficult to adapt and interpret, making it hard to understand how they arrived at a particular classification decision and how the algorithm can be adapted. In chapter 2, we present an easy-to-apply, user-friendly pipeline for constant model adaptation to a changing plankton community.

Plankton Time Series

With ongoing climate change, the scientific interest showed an increasing focus on how this climate variability affects marine ecosystems. Hereby, multi-year time series are of special interest as they provide useful insights into interactions between the climate and the reaction of the planktonic community (e.g. Mackas et al. 2012a) as their changes can be mainly attributed to environmental causes due to the lack of human harvesting. The response of plankton changes through time series can be a key tool for effective management measures (Giering et al. 2022). Thanks to long term time series, it has been possible to identify a series

of changes in the North Sea (for a review see Sguotti et al. 2022) or to assess the status of biodiversity in the North Atlantic (McQuatters-Gollop et al. 2022). However, the main limitations of those time series mentioned are consistency in sampling method, spatial and temporal coverage (Mackas et al. 2012, Giering et al. 2022, McQuatters-Gollop et al. 2022). While phytoplankton measures can be interfered from satellites on broad spatial scales, zooplankton spatial coverage is yet scarce and highly inconsistent (Giering et al. 2022). Although the CPR data formed a base for many publications related to long-term monitoring (e.g. Beaugrand 2004, Leterme et al. 2005, Hinder et al. 2012, Bedford et al. 2020), the data derived, neglects taxa below 270 μm , is semi-quantitative and underestimates absolute numbers (Stevens et al. 2006, Dippner & Krause 2013). If we want to fully understand the possible effects of climate change on the plankton community and establish mitigation measures for its negative impacts, comprehensive studies including the smaller size fractions of the zooplankton are required. This stresses the need for further long-term studies at higher spatial scales, using traditional and new techniques that provide thorough information at the basis of the food webs. One of the main providers of time series data on various plankton groups are fixed monitoring stations where plankton is frequently sampled throughout the year at a specific location (e.g. L4 in the English Channel, (Widdicombe et al. 2010) or Helgoland Roads, Boersma et al. 2015). These stations enable long-term monitoring on a high taxonomic resolution with a focus on seasonal patterns and species composition. However, the stationary character, mainly in coastal areas, makes it difficult to extrapolate their findings across larger areas or to compare with other regions.

The North Sea: A case study

Hydrography

The North Sea (North Sea) is one of the most extensively studied but also exploited ecosystems in the world. Its location between Scandinavia, the European mainland and the British Isles makes it one of the most frequented shipping zones in the world. The North Sea covers 570,000 square km and is considered a shallow shelf ecosystem with a mean depth of roughly 100 m. The hydrology of the North Sea is strongly affected by the warm North Atlantic current, which enter the North Sea through the English Channel in the south and between the Shetland Islands and Norway from the north (Fig. 1.8) (Ducrotoy et al. 2000). On the eastside of the North Sea, colder and less saline Baltic seawater enters through the Skagerak, creating a counterclockwise circulation in the basin. Besides the Baltic waters, large amounts of fresh water enter through the Rhine, Elbe, Thames and other rivers, creating a salinity gradient between 33 and 35 between the German Bight in the south and the northern British Isles, respectively. The North Sea is also subject to strong seasonal fluctuations in terms of

temperature varying from ca. 6° C in January to 18° C in August (Ducrotoy et al. 2000). One of the most prominent features of the North Sea is its tidal motion with tidal differences of 4-12 m. The different physical conditions primarily define the different regions of the North Sea.



Fig. 1.8 The North Sea, the bordering countries and its Circulation system with the inflow of cold and salty Atlantic water (light blue) into the deeper northern central basin of the North Sea and along the Norwegian Trench up to the Skagerrak. Less salty coastal waters (dark blue) circulate in an anti-clockwise gyre in the southern North Sea basin (From OSPAR 2000).

The plankton community of the North Sea

The North Sea phytoplankton community is mainly composed of diatoms, dinoflagellates, and coccolithophores, which have distinct seasonal patterns (van Beusekom & Diel-Christiansen 1993). Diatoms dominate during the spring bloom, while dinoflagellates and coccolithophores are more abundant during summer and autumn. The annual average phytoplankton biomass in the North Sea is about 200 mg/m², with higher concentrations in the eastern and southern regions (Capuzzo et al. 2018). The species are mainly cosmopolitan in terms of temperature and salinity tolerances. Earlier studies revealed a general increase of diatoms and a simultaneous decrease of dinoflagellates in the southern as well as the northern North Sea (Hinder et al. 2012b, Beaugrand et al. 2014).

The phytoplankton in the North Sea shows two distinct blooming events, a spring bloom in late spring, early summer and a less pronounced autumn bloom triggered by high nutrient availability and sufficient solar irradiance (Irigoien et al. 2005). Blooms can be so extensive that they can be seen from space. The composition of phytoplankton in the North Sea is highly variable, with different species dominating in different areas and at different times of the year (van Beusekom & Diel-Christiansen 1993). Large blooms that can have significant ecological and economic impacts, both positive and negative. For example, blooms can support higher trophic levels by initiating secondary production in spring for instance but can also lead to oxygen depletion and harmful algal blooms (HAB) (Pitcher & Jacinto 2019). For instance, *Phaeocystis* spp. blooms have been associated with the formation of foam on beaches along the southwestern North Sea and Wadden Sea coasts, and the mortality of shellfish has been attributed to these blooms (Karlson et al. 2021).

Zooplankton in the North Sea are mainly composed of copepods, euphausiids, and appendicularians. The copepod *Calanus finmarchicus* and some species of the *Euphausiacea* as well as *Oikopleura* sp. characterize the zooplankton stock of the northern North Sea. Likewise, Euphausiids and appendicularians are also more common in the north. In the south, calanoid copepods like *Temora longicornis*, *Acartia* spp. and the *Pseudocalanus* group were typical inhabitants. The cyclopoid copepod *Oithona* spp. is also an abundant inhabitant of the central and northern North Sea (Krause & Martens 1990, van Beusekom & Diel-Christiansen 1993). The most common scyphozoans (jellyfish) of the North Sea are *Aurelia aurita*, *Chrysaora hysoscella*, and *Cyanea capillata*. Other species such as the *Cyanea lamarckii* and *Pelagia noctiluca* can also occur in the North Sea, but are less common. The *A. aurita* is the most widely distributed species and can be found throughout the North Sea, while *C. hysoscella* is more common in the southern and western parts of the North Sea. *C. capillata* is typically found in colder waters and is most common in the northern regions of the North Sea, but its distribution can also be influenced by currents and tides. The *C. lamarckii* and *P. noctiluca* are typically found in the southern and eastern parts of the North Sea, but their occurrence is generally more sporadic (Hay et al. 1990). However, due to the strong seasonality in the North Sea, the impact of the Atlantic inflow, and the relatively fast response of the zooplankton community to changes in hydrographic conditions and climate variability, their distribution and biomass patterns underlay strong inter-seasonal and inter-annual variability.

Atlantic Herring in the North Sea

The Atlantic Herring (*Clupea Harengus*) is the key ecological and economical fish species in the North Sea. Although decades of heavy exploitation, it is the most abundant planktivorous fish species with a wide distribution range from 40° to 60° N (ICES 2006). The different populations in the North Sea are roughly separated by their spawning seasons and areas (Fig. 1.9) in autumn (northern British Isles, Orkney, Buchan, Banks) and winter (English Channel, Downs) (ICES 2018). Due to its economic importance, the herring stocks in the North Sea are one of the best studied and observed stocks worldwide. The larvae of the autumn and winter spawners are annually investigated via the International Herring Larvae Survey (IHLS) and the International Bottom Trawl Survey (IBTS) (ICES 2022). Thanks to the thorough observation of these stocks, severe fluctuations in herring recruitment could be observed (Fässler et al. 2011). Here mainly the autumn spawning stock is on a constant low since the early 2000s, whereas SSB is stable and fishing pressure is relatively low (Schmidt et al. 2009).

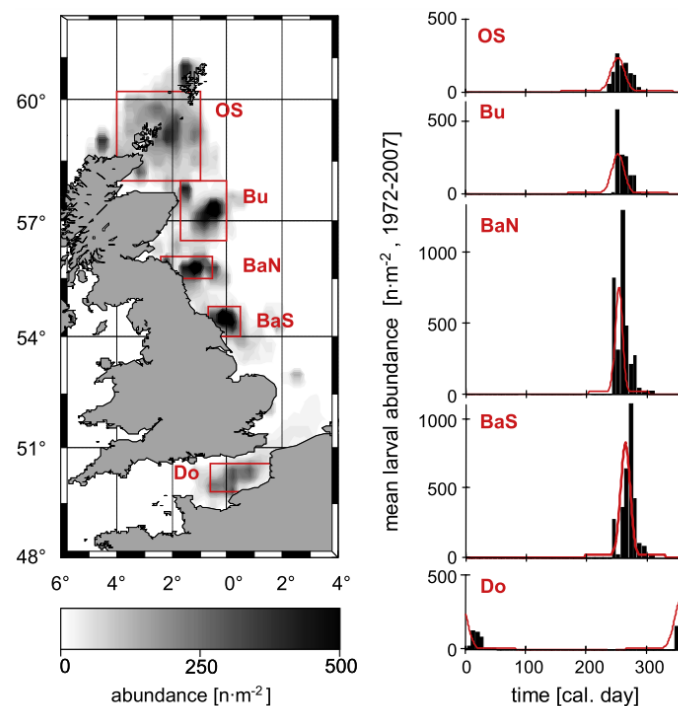


Fig. 1.9 Spawning areas (left) and times (right) of North Sea autumn spawning herring (*Clupea harengus*) between 1977 and 2006, as determined by the International Herring Larvae Survey. The spawning components include OS (Orkney/Shetland), BU (Buchan), BaN (Banks north), BaS (Banks south), and Do (Downs) (From Hufnagl et al. 2015).

During the respective spawning seasons, the herring gathers in shallow areas and spawn their sticky eggs over gravel beds. Due to the different spawning season, the newly hatched larvae experience completely different conditions (ICES 2006). While the spring spawned larvae hatch during the spring bloom and experience favorable condition for larval growth, the autumn and winter spawned larvae hatch into a period of low productivity. As soon as they have fully absorbed their yolk, the larvae need to find appropriate food in terms of size and energy. For many years, copepod nauplii were believed as the main energy source for these early life stages and the role of other, smaller planktonic prey was overseen. However, in the past 10 years, the role of smaller prey such as PZP was revived (e.g. Bils et al. 2017). Although, copepod eggs, nauplii and calanoid copepods were found to be the main prey types for clupeids (Checkley 1982, Kiørboe et al. 1985, Peck et al. 2012 and references therein), other studies showed that the larval diet is composed with up to 70% of protozooplankton (De Figueiredo et al. 2005) and prey smaller than 50 μm (Denis et al. 2016, Bils et al. 2022). Knowledge on prey fields and prey preferences, especially with reference to the conditions that autumn and winter spawned larvae experience and the increased role of PZP during periods of low productivity is of major importance to understand recruitment and prey field dynamics. Individual Based modelling (IBM) suggested that the interplay of temperature along with varying abundances of prey may have a severe effect on overwintering survival of those early life stages (Peck & Hufnagl 2012, Hufnagl et al. 2015). These results highlight the need to thoroughly study the dynamics of the lower trophic levels during these periods of low productivity, especially in temperate ecosystems like the North Sea. Therefore, in this thesis we investigate the dynamics of the lower trophic levels during periods of low productivity in the temperate ecosystems of the North Sea in order to gain a better understanding of the ecological processes that underpin these systems and to provide insights into the mechanisms that govern the recruitment dynamics of herring.

Objectives

The main aim of this thesis is to provide a comprehensive analysis of plankton dynamics during the low-productive seasons in the North Sea, which is one of the most extensively studied ecosystems in the world. We aimed to achieve this by utilizing a combination of sampling methods and analytical approaches to describe the long-term variability and interactions between micro/mesozooplankton groups and environmental drivers during winter. Furthermore, we used the observed plankton biomasses to generate prey fields and test the starvation potential of Atlantic herring larvae in their spawning grounds.

In Chapter 1, we provide essential information on the standing stock of PZP plankton, their spatial and temporal distribution and their environmental drivers during the low productivity

season in the North Sea. In Chapter 2, we implemented a pipeline for automatic classification of plankton images (dynamic optimization cycle, DOC), which is accessible by non-AI-experts and accelerates sample processing by reducing the time for manual validation. This classifier helped us to investigate the North Sea micro- and mesozooplankton community during autumn and wintertime between 2013 and 2019 (Chapter 3). Here we describe changes in plankton abundance, spatial distribution and size structure in Buchan/Banks and Downs, two of the main spawning grounds for Herring. We also identified environmental drivers applying a redundancy analysis that included the broad taxonomic and functional information obtained from FlowCAM and Zooscan, and examined environmental drivers using a size-spectra approach, focusing only on the size distribution. In Chapter 4, we used the size- and taxa-resolved zooplankton samples from the previous chapter to describe the available prey fields for early life stages of herring. We aimed to investigate the feeding conditions that young herring larvae experience in the spawning areas in the North Sea during the first month post-hatch and whether these conditions differ among autumn- and winter-spawning sites.

References

- Aberle N, Lengfellner K, Sommer U (2007) Spring bloom succession, grazing impact and herbivore selectivity of ciliate communities in response to winter warming. *Oecologia* 150:668–681.
- Al-Barazanchi H, Verma A, Wang SX (2018) Intelligent plankton image classification with deep learning. *Int J Comput Vis Robot* 8:561–571.
- Alvarez-Fernandez S, Licandro P, Van Damme CJG, Hufnagl M (2015) Original Article: Effect of zooplankton on fish larval abundance and distribution: A long-term study on North Sea herring (*Clupea harengus*). *ICES J Mar Sci* 72:2569–2577.
- Álvarez E, Moyano M, López-Urrutia Á, Nogueira E, Scharek R (2014) Routine determination of plankton community composition and size structure: A comparison between FlowCAM and light microscopy. *J Plankton Res* 36:170–184.
- Atkinson A, Lilley MKS, Hirst AG, McEvoy AJ, Tarran GA, Widdicombe C, Fileman ES, Woodward EMS, Schmidt K, Smyth TJ, Somerfield PJ (2021) Increasing nutrient stress reduces the efficiency of energy transfer through planktonic size spectra. *Limnol Oceanogr* 66:422–437.
- Azam F, Fenchel T, Field J, Gray J, Meyer-Reil L, Thingstad F (1983) The Ecological Role of Water-Column Microbes in the Sea. *Mar Ecol Prog Ser* 10:257–263.
- Baier CT, Purcell JE (1997) Trophic interactions of chaetognaths, larval fish, and zooplankton in the South Atlantic Bight. *Mar Ecol Prog Ser* 146:43–53.
- Basu S, Mackey KRM (2018) Phytoplankton as key mediators of the biological carbon pump: Their responses to a changing climate. *Sustain* 10.
- Beaugrand G (2004) The North Sea regime shift: Evidence, causes, mechanisms and consequences. *Prog Oceanogr* 60:245–262.

- Beaugrand G, Brander KM, Lindley JA, Souissi S, Reid PC (2003) Plankton effect on cod recruitment in the North Sea. *Nature* 426:661–664.
- Beaugrand G, Harlay X, Edwards M (2014) Detecting plankton shifts in the North Sea: A new abrupt ecosystem shift between 1996 and 2003. *Mar Ecol Prog Ser* 502:85–104.
- Bedford J, Ostle C, Johns DG, Atkinson A, Best M, Bresnan E, Machairopoulou M, Graves CA, Devlin M, Milligan A, Pitois S, Mellor A, Tett P, McQuatters-Gollop A (2020) Lifeform indicators reveal large-scale shifts in plankton across the North-West European shelf. *Glob Chang Biol* 26:3482–3497.
- Belgrano A, Scharler UM, Dunne J, Ulanowicz RE (2005) *Aquatic food webs: an ecosystem approach*. Oxford University Press.
- Benfield MC, Grosjean P, Culverhouse PF, Irigoien X, Sieracki ME, Lopez-Urrutia A, Dam HG, Hu Q, Davis CS, Hanson A, Pilskalns CH, Riseman EM, Schultz H, Utgoff PE, Gorsky G (2007) RAPID: Research on Automated Plankton Identification. *Oceanography* 20:172–218.
- van Beusekom J, Diel-Christiansen S (1993) A synthesis of phyto and zooplankton dynamics in the North Sea environment. *WWF Int Rep*:148.
- Bils F, Aberle N, van Damme CJG, Peck MA, Moyano M (2022) Role of protozooplankton in the diet of North Sea autumn spawning herring (*Clupea harengus*) larvae. *Mar Biol* 169:1–16.
- Bils F, Moyano M, Aberle N, van Damme CJG, Nash RDM, Kloppmann M, Loots C, Peck MA (2019) Broad-scale distribution of the winter protozooplankton community in the North Sea. *J Sea Res* 144:112–121.
- Bils F, Moyano M, Aberle N, Hufnagl M, Alvarez-Fernandez S, Peck MA (2017) Exploring the microzooplankton- ichthyoplankton link: A combined field and modeling study of atlantic herring (*clupea harengus*) in the irish sea. *J Plankton Res* 39:147–163.
- Blanchard JL, Heneghan RF, Everett JD, Trebilco R, Richardson AJ (2017) From Bacteria to Whales: Using Functional Size Spectra to Model Marine Ecosystems. *Trends Ecol Evol* 32:174–186.
- Boersma M, Wiltshire KH, Kong SM, Greve W, Renz J (2015) Long-term change in the copepod community in the southern German Bight. *J Sea Res* 101:41–50.
- Briseño-Avena C, Schmid MS, Swieca K, Sponaugle S, Brodeur RD, Cowen RK (2020) Three-dimensional cross-shelf zooplankton distributions off the Central Oregon Coast during anomalous oceanographic conditions. *Prog Oceanogr* 188:102436.
- Brown HP, Jenkins MM (1962) A protozoon (Dileptus; Ciliata) predatory upon metazoa. *Science* (80-) 136:710.
- Budiarti RPN, Tjahjono A, Hariadi M, Purnomo MH (2019) Development of IoT for automated water quality monitoring system. In: *2019 International Conference on Computer Science, Information Technology, and Electrical Engineering (ICOMITEE)*. IEEE, p 211–216
- Calbet A (2008) The trophic roles of microzooplankton in marine systems. In: *ICES Journal of Marine Science*. p 325–331
- Calbet A, Alcaraz M (2007) Microzooplankton, key organisms in the pelagic food web. *Fish Aquac* 5:227–242.
- Calbet A, Garrido S, Saiz E, Alcaraz M, Duarte CM (2001) Annual zooplankton succession in coastal NW Mediterranean waters: The importance of the smaller size fractions. *J Plankton Res* 23:319–331.

- Capuzzo E, Lynam CP, Barry J, Stephens D, Forster RM, Greenwood N, McQuatters-Gollop A, Silva T, van Leeuwen SM, Engelhard GH (2018) A decline in primary production in the North Sea over 25 years, associated with reductions in zooplankton abundance and fish stock recruitment. *Glob Chang Biol* 24:e352–e364.
- Cavan EL, Henson SA, Belcher A, Sanders R (2017) Role of zooplankton in determining the efficiency of the biological carbon pump. *Biogeosciences* 14:177–186.
- Checkley D (1982) Selective Feeding by Atlantic Herring (*Clupea harengus*) Larvae on Zooplankton in Natural Assemblages. *Mar Ecol Prog Ser* 9:245–253.
- Cowen RK, Guigand CM (2008) In situ ichthyoplankton imaging system (ISIIS): system design and preliminary results. *Limnol Oceanogr Methods* 6:126–132.
- Culverhouse PF (2015) Biological Oceanography Needs New Tools to Automate Sample Analysis. 1:14–15.
- Culverhouse PF, Macleod N, Williams R, Benfield MC, Lopes RM, Picheral M (2014) An empirical assessment of the consistency of taxonomic identifications. *Mar Biol Res* 10:73–84.
- Cushing DH (1990) Plankton production and year-class strength in fish populations: An update of the match/mismatch hypothesis.
- Dai L, Li C, Yang G, Sun X (2016) Zooplankton abundance, biovolume and size spectra at western boundary currents in the subtropical North Pacific during winter 2012. *J Mar Syst* 155:73–83.
- Dam HG, Baumann H (2017) Climate Change, Zooplankton and Fisheries. *Clim Chang Impacts Fish Aquac II*:851–874.
- Davis CS, Gallager SM, Berman MS, Haury LR, Strickler JR (1992) The video plankton recorder (VPR): design and initial results. *Arch Hydrobiol Beih* 36:67–81.
- Davis CS, Thwaites FT, Gallager SM, Hu Q (2005) A three-axis fast-tow digital Video Plankton Recorder for rapid surveys of plankton taxa and hydrography. *Limnol Oceanogr Methods* 3:59–74.
- Denis J, Vallet C, Courcot L, Lefebvre V, Caboche J, Antajan E, Marchal P, Loots C (2016) Feeding strategy of Downs herring larvae (*Clupea harengus* L.) in the English Channel and North Sea. *J Sea Res* 115:33–46.
- Dippner JW, Krause M (2013) Continuous plankton recorder underestimates zooplankton abundance. *J Mar Syst* 111–112:263–268.
- Ducrotoy J-P, Elliott M, de Jonge VN (2000) The North Sea. *Mar Pollut Bull* 41:5–23.
- Eigaard OR, Van Deurs M, Behrens JW, Bekkevold D, Brander K, Plambech M, Plet-Hansen KS, Mosegaard H (2014) Prey or predator - Expanding the food web role of sandeel *Ammodytes marinus*. *Mar Ecol Prog Ser* 516:267–273.
- Elton C (1927) *Animal Ecology*. Reprint, 2001.
- Esteban GF, Fenchel T, Finlay BJ (2010) Mixotrophy in Ciliates. *Protist* 161:621–641.
- Everett JD, Baird ME, Buchanan P, Bulman C, Davies C, Downie R, Griffiths C, Heneghan R, Kloser RJ, Laiolo L, Lara-Lopez A, Lozano-Montes H, Matear RJ, McEnnulty F, Robson B, Rochester W, Skerratt J, Smith JA, Strzelecki J, Suthers IM, Swadling KM, van Ruth P, Richardson AJ (2017) Modeling what we sample and sampling what we model: Challenges for zooplankton model assessment. *Front Mar Sci* 4:1–19.

- Fässler SMM, Payne MR, Brunel T, Dickey-Collas M (2011) Does larval mortality influence population dynamics? An analysis of North Sea herring (*Clupea harengus*) time series. *Fish Oceanogr* 20:530–543.
- De Figueiredo GM, Nash RDM, Montagnes DJS (2005) The role of the generally unrecognised microprey source as food for larval fish in the Irish Sea. *Mar Biol* 148:395–404.
- Figueiredo GM, Montagnes DJS, Nash RDM (2009) The importance of protozooplankton as prey for copepods in the coastal areas of the central Irish Sea. *Hydrobiologia* 628:227–239.
- Fileman ES, Fitzgeorge-Balfour T, Tarran GA, Harris RP (2011) Plankton community diversity from bacteria to copepods in bloom and non-bloom conditions in the Celtic Sea in spring. *Estuar Coast Shelf Sci* 93:403–414.
- Findlay HS, Yool A, Nodale M, Pitchford JW (2006) Modelling of autumn plankton bloom dynamics. *J Plankton Res* 28:209–220.
- Franks PJS (2001) Phytoplankton blooms in a fluctuating environment: The roles of plankton response time scales and grazing. *J Plankton Res* 23:1433–1441.
- García-Comas C, Chang CY, Ye L, Sastri AR, Lee YC, Gong GC, Hsieh C hao (2014) Mesozooplankton size structure in response to environmental conditions in the East China Sea: How much does size spectra theory fit empirical data of a dynamic coastal area? *Prog Oceanogr* 121:141–157.
- Giering SLC, Culverhouse PF, Johns DG, McQuatters-Gollop A, Pitois SG (2022) Are plankton nets a thing of the past? An assessment of in situ imaging of zooplankton for large-scale ecosystem assessment and policy decision-making. *Front Mar Sci* 9:1–16.
- Gifford DJ, Caron DA (2000) Sampling, preservation, enumeration and biomass of marine protozooplankton. *ICES Zooplankt Methodol Man*:193–221.
- Gulland JA (2013) Distribution and abundance of whales in relation to basic productivity. In: *The whale problem*. Harvard University Press, p 27–52
- Harris R, Wiebe P, Lenz J, Skjoldal H-R, Huntley M (2000) ICES zooplankton methodology manual. Elsevier.
- Harrison PJ, Thompson PA, Calderwood GS (1990) Effects of nutrient and light limitation on the biochemical composition of phytoplankton. *J Appl Phycol* 2:45–56.
- Hay SJ, Hislop JRG, Shanks AM (1990) North Sea Scyphomedusae; summer distribution, estimated biomass and significance particularly for 0-group Gadoid fish. *Netherlands J Sea Res* 25:113–130.
- Hays GC, Richardson AJ, Robinson C (2005) Climate change and marine plankton. *Trends Ecol Evol* 20:337–344.
- Heneghan RF, atton IA, Galbraith ED (2019) Climate change impacts on marine ecosystems through the lens of the size spectrum. *Emerg Top Life Sci* 3:233–243.
- Herring P (2001) *The biology of the deep ocean*. OUP Oxford.
- Heyman RP (1981) Narcotisation, fixation and preservation experiments with marine zooplankton. *Versl en Tech gegevens* 28:1–36.
- Hinder SL, Manning JE, Gravenor MB, Edwards M, Walne AW, Burkill PH, Hays GC (2012a) Long-term changes in abundance and distribution of microzooplankton in the NE Atlantic and North Sea. *J Plankton Res* 34:83–91.

- Hinder SL, Manning JE, Gravenor MB, Edwards M, Walne AW, Burkill PH, Hays GC (2012b) Long-term changes in abundance and distribution of microzooplankton in the NE Atlantic and North Sea. *J Plankton Res* 34:83–91.
- Hjort J (1914) Fluctuations in the great fisheries of Northern Europe. *Rapp Procés-Verbaux* 20:1–228.
- Hufnagl M, Peck MA (2011) Physiological individual-based modelling of larval Atlantic herring (*Clupea harengus*) foraging and growth: Insights on climate-driven life-history scheduling. *ICES J Mar Sci* 68:1170–1188.
- Hufnagl M, Peck MA, Nash RDM, Dickey-Collas M (2015) Unravelling the Gordian knot! Key processes impacting overwintering larval survival and growth: A North Sea herring case study. *Prog Oceanogr* 138:486–503.
- ICES (2022) Herring Assessment Working Group for the Area South of 62° N ACFM Subgroup Review of Herring Assessment Working Group (HAWG) Report. *ICES Sci Reports* 4:430.
- ICES (2006) ICES-Fishmap: Herring.
- ICES (2018) Report of the Herring Assessment Working Group for the Area South of 62° N (HAWG).
- Irigoien X, Flynn KJ, Harris RP (2005) Phytoplankton blooms: A ‘loophole’ in microzooplankton grazing impact? *J Plankton Res* 27:313–321.
- Jakobsen HH (2014) Escape response of planktonic protists to fluid mechanical signals.
- Jaspers C, Carstensen J (2009) Effect of acid Lugol solution as preservative on two representative chitinous and gelatinous zooplankton groups. *Limnol Oceanogr Methods* 7:430–435.
- Jennings S, Warr KJ, Mackinson S (2002) Use of size-based production and stable isotope analyses to predict trophic transfer efficiencies and predator-prey body mass ratios in food webs. *Mar Ecol Prog Ser* 240:11–20.
- Joint I, Owens N, Pomeroy A (1986) Seasonal production of photosynthetic picoplankton and nanoplankton in the Celtic Sea. *Mar Ecol Prog Ser* 28:251–258.
- Jonsson P (1986) Particle size selection, feeding rates and growth dynamics of marine planktonic oligotrichous ciliates (Ciliophora: Oligotrichina). *Mar Ecol Prog Ser* 33:265–277.
- Karlson B, Andersen P, Arneborg L, Cembella A, Eikrem W, John U, West JJ, Klemm K, Kobos J, Lehtinen S, Lundholm N, Mazur-Marzec H, Naustvoll L, Poelman M, Provoost P, De Rijcke M, Suikkanen S (2021) Harmful algal blooms and their effects in coastal seas of Northern Europe. *Harmful Algae* 102:101989.
- Kerr SR, Dickie LM (2001) *The biomass spectrum: a predator-prey theory of aquatic production*. Columbia University Press.
- Kjørboe T (2009) A mechanistic approach to plankton ecology. *ASLO Web Lect* 1:1–91.
- Kjørboe T (2013) Zooplankton body composition. *Limnol Oceanogr* 58:1843–1850.
- Kjørboe T, Munk P, Stottrup JG (1985) First feeding by larval herring.
- Krause M, Martens P (1990) Distribution patterns of mesozooplankton biomass in the North Sea.
- Kwong LE, Pakhomov EA (2017) Assessment of active vertical carbon transport: New methodology. *Uchenye Zap Kazan Univ Seriya Estestv Nauk* 159:492–509.

- De La Rocha CL, Passow U (2006) The biological pump. *Treatise on geochemistry* 6:83–111.
- LeCun Y, Boser B, Denker JS, Henderson D, Howard RE, Hubbard W, Jackel LD (1989) Backpropagation Applied to Handwritten Zip Code Recognition. *Neural Comput* 1:541–551.
- Leterme SC, Edwards M, Seuront L, Attrill MJ, Reid PC, John AWG (2005) Decadal basin-scale changes in diatoms, dinoflagellates, and phytoplankton color across the North Atlantic. *Limnol Oceanogr* 50:1244–1253.
- Litchman E, Ohman MD, Kiørboe T (2013) Trait-based approaches to zooplankton communities. *J Plankton Res* 35:473–484.
- Lohmann G, Wiltshire KH (2012) Winter atmospheric circulation signature for the timing of the spring bloom of diatoms in the North Sea. *Mar Biol* 159:2573–2581.
- Lomartire S, Marques JC, Gonçalves AMM (2021) The key role of zooplankton in ecosystem services: A perspective of interaction between zooplankton and fish recruitment. *Ecol Indic* 129.
- Lusseau SM, Gallego A, Rasmussen J, Hatfield EMC, Heath M (2014) North Sea herring (*Clupea harengus* L.) recruitment failure may be indicative of poor feeding success. *ICES J Mar Sci* 71:2026–2041.
- Mackas DL, Pepin P, Verheye H (2012) Interannual variability of marine zooplankton and their environments: Within- and between-region comparisons. *Prog Oceanogr* 97–100:1–14.
- McQuatters-Gollop A, Guérin L, Arroyo NL, Aubert A, Artigas LF, Bedford J, Corcoran E, Dierschke V, Elliott SAM, Geelhoed SCV, Gilles A, González-Irusta JM, Haelters J, Johansen M, Le Loc'h F, Lynam CP, Niquil N, Meakins B, Mitchell I, Padegimas B, Pesch R, Preciado I, Rombouts I, Safi G, Schmitt P, Schückel U, Serrano A, Stebbing P, De la Torre A, Vina-Herbon C (2022) Assessing the state of marine biodiversity in the Northeast Atlantic. *Ecol Indic* 141.
- Mehner T, Lischke B, Scharnweber K, Attermeyer K, Brothers S, Gaedke U, Hilt S, Brucet S (2018) Empirical correspondence between trophic transfer efficiency in freshwater food webs and the slope of their size spectra. *Ecology* 99:1463–1472.
- Menden-Deuer S, Lessard EJ, Satterberg J (2001) Effect of preservation on dinoflagellate and diatom cell volume and consequences for carbon biomass predictions. *Mar Ecol Prog Ser* 222:41–50.
- Mitra A, Castellani C, Gentleman WC, Jónasdóttir SH, Flynn KJ, Bode A, Halsband C, Kuhn P, Licandro P, Agersted MD, Calbet A, Lindeque PK, Koppelman R, Møller EF, Gislason A, Nielsen TG, St. John M (2014) Bridging the gap between marine biogeochemical and fisheries sciences; configuring the zooplankton link. *Prog Oceanogr* 129:176–199.
- Moreno-Torres JG, Raeder T, Alaiz-Rodríguez R, Chawla N V, Herrera F (2012) A unifying view on dataset shift in classification. *Pattern Recognit* 45:521–530.
- Naito A, Abe Y, Matsuno K, Nishizawa B, Kanna N, Sugiyama S, Yamaguchi A (2019) Surface zooplankton size and taxonomic composition in Bowdoin Fjord, north-western Greenland: A comparison of ZooScan, OPC and microscopic analyses. *Polar Sci* 19:120–129.
- Nakazawa T, Ushio M, Kondoh M (2011) *Scale Dependence of Predator-Prey Mass Ratio. Determinants and Applications*, 1st ed. Elsevier Ltd.
- Paulin JJ (1996) *Morphology and cytology of ciliates. Ciliates Cells as Org* Gustav Fischer, Stuttgart:1–40.

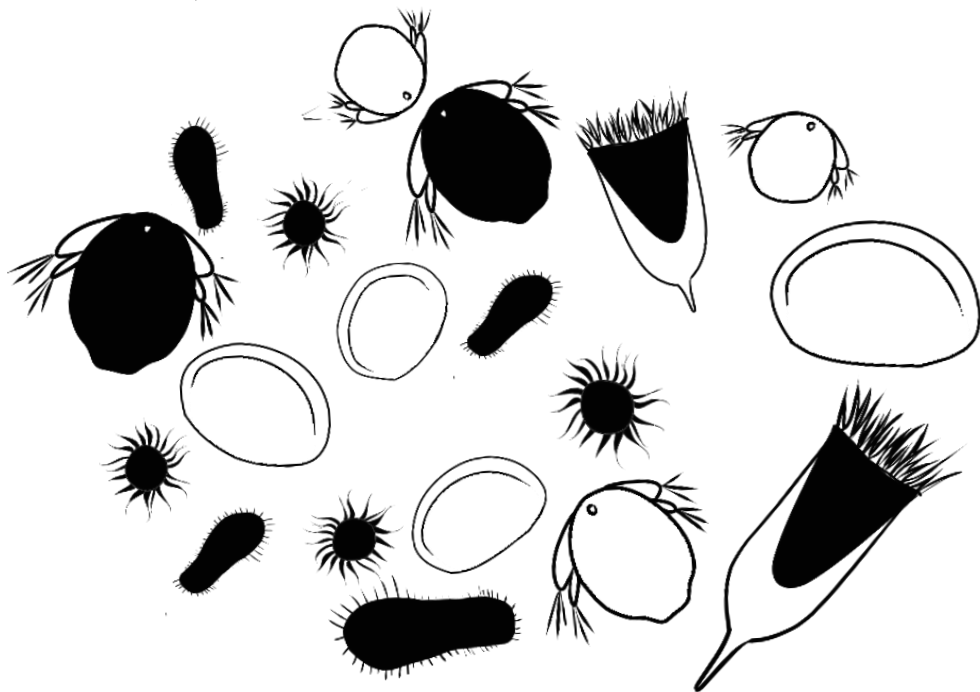
- Payne MR, Ross SD, Clausen LW, Munk P, Mosegaard H, Nash RDM (2013) Recruitment decline in North Sea herring is accompanied by reduced larval growth rates. *Mar Ecol Prog Ser* 489:197–211.
- Pearcy WG, Hopkins CCE, Grønvik S, Evans RA (1979) Feeding habits of cod, capelin, and herring in Balsfjorden, Northern Norway, July-August 1978: the importance of euphausiids. *Sarsia* 64:269–277.
- Peck MA, Huebert KB, Llopiz JK (2012) Intrinsic and Extrinsic Factors Driving Match-Mismatch Dynamics During the Early Life History of Marine Fishes. *Adv Ecol Res* 47:177–302.
- Peck MA, Hufnagl M (2012) Can IBMs tell us why most larvae die in the sea? Model sensitivities and scenarios reveal research needs. *J Mar Syst* 93:77–93.
- Peters RH, Wassenberg K (1983) The effect of body size on animal abundance. *Oecologia* 60:89–96.
- Picheral M, Colin S, Irisson JO (2017) EcoTaxa, a tool for the taxonomic classification of images.
- Picheral M, Guidi L, Stemmann L, Karl DM, Iddaoud G, Gorsky G (2010) The Underwater Vision Profiler 5: An advanced instrument for high spatial resolution studies of particle size spectra and zooplankton. *Limnol Oceanogr Methods* 8:462–473.
- Pierre M, Rouyer T, Bonhommeau S, Fromentin JM (2018) Assessing causal links in fish stock-recruitment relationships. *ICES J Mar Sci* 75:903–911.
- Pitcher GC, Jacinto GS (2019) 3.3 Ocean deoxygenation links to harmful algal blooms. In: *Ocean Deoxygenation: Everyone's problem-causes, impacts, consequences and solutions*. Gland Switzerland: IUCN, p 153–170
- Pitois SG, Tilbury J, Bouch P, Close H, Barnett S, Culverhouse PF (2018) Comparison of a cost-effective integrated plankton sampling and imaging instrument with traditional systems for mesozooplankton sampling in the Celtic Sea. *Front Mar Sci* 5:1–15.
- Platt T, Denman K (1977) Organisation in the pelagic ecosystem. *Helgoländer Wissenschaftliche Meeresuntersuchungen* 30:575–581.
- Pollina T, Larson AG, Lombard F, Li H, Le Guen D, Colin S, de Vargas C, Prakash M (2022) PlanktoScope: Affordable Modular Quantitative Imaging Platform for Citizen Oceanography. *Front Mar Sci* 9:1–15.
- Pomeroy LR, leB. WILLIAMS PJ, Azam F, Hobbie JE (2007) The microbial loop. *Oceanography* 20:28–33.
- Pörtner H-O, Karl DM, Boyd PW, Cheung W, Lluch-Cota SE, Nojiri Y, Schmidt DN, Zavialov PO, Alheit J, Aristegui J (2014) Ocean systems. In: *Climate change 2014: impacts, adaptation, and vulnerability. Part A: global and sectoral aspects. contribution of working group II to the fifth assessment report of the intergovernmental panel on climate change*. Cambridge University Press, p 411–484
- Purcell JE (2005) Climate effects on formation of jellyfish and ctenophore blooms: A review. *J Mar Biol Assoc United Kingdom* 85:461–476.
- Quinones RA, Platt T, Rodríguez J (2003) Patterns of biomass-size spectra from oligotrophic waters of the Northwest Atlantic. *Prog Oceanogr* 57:405–427.
- Raven JA (2007) *Aquatic photosynthesis*. Princeton University Press.
- Raymont JEG (2014) *Plankton & productivity in the oceans: Volume 1: Phytoplankton*. Elsevier.

- Reid PC, Lancelot C, Gieskes WWC, Hagmeier E, Weichart G (1990) Phytoplankton of the North Sea and its dynamics: A review.
- Remsen A, Hopkins TL, Samson S (2004) What you see is not what you catch: a comparison of concurrently collected net, Optical Plankton Counter, and Shadowed Image Particle Profiling Evaluation Recorder data from the northeast Gulf of Mexico. *Deep Sea Res Part I Oceanogr Res Pap* 51:129–151.
- Richardson AJ (2008) In hot water: Zooplankton and climate change. *ICES J Mar Sci* 65:279–295.
- Richardson K, Visser AW, Pedersen FB (2000) Subsurface phytoplankton blooms fuel pelagic production in the North Sea. *J Plankton Res* 22:1663–1671.
- Riding JB, Fensome RA, Soyer-Gobillard M-O, Medlin LK (2022) A Review of the Dinoflagellates and Their Evolution from Fossils to Modern. *J Mar Sci Eng* 11:1.
- Schantz EJ (1975) Poisonous red tide organisms. *Environ Lett* 9:225–237.
- Schmidt DN, Lazarus D, Young JR, Kucera M (2006) Biogeography and evolution of body size in marine plankton. *Earth-Science Rev* 78:239–266.
- Schmidt JO, Van Damme CJG, Röckmann C, Dickey-Collas M (2009) Recolonisation of spawning grounds in a recovering fish stock: recent changes in North Sea herring. *Sci Mar* 73:153–157.
- Schröder SM, Kiko R, Koch R (2020) Morphocluster: Efficient annotation of Plankton images by clustering. *Sensors (Switzerland)* 20.
- Schütt F (1892) Analytische Plankton-Studien: Ziele, Methoden und Anfangs-Resultate der quantitativ-analytischen Planktonforschung. Lipsius & Tischer.
- Scott J, Pitois S, Close H, Almeida N, Culverhouse P, Tilbury J, Malin G (2021) In situ automated imaging, using the Plankton Imager, captures temporal variations in mesozooplankton using the Celtic Sea as a case study. *J Plankton Res* 43:300–313.
- Sguotti C, Blöcker AM, Färber L, Blanz B, Cormier R, Diekmann R, Letschert J, Rambo H, Stollberg N, Stelzenmüller V, Stier AC, Möllmann C (2022) Irreversibility of regime shifts in the North Sea. *Front Mar Sci* 9:1–13.
- Sheldon RW, Prakash A, Sutcliffe WH (1972) The Size Distribution of Particles in the Ocean. *Limnol Oceanogr* 17:327–340.
- Sieburth JM, Smetacek V, Lenz J (1978) Pelagic ecosystem structure: Heterotrophic compartments of the plankton and their relationship to plankton size fractions 1. *Limnol Oceanogr* 23:1256–1263.
- Silvert W, Platt T (1978) Energy flux in the pelagic ecosystem: A time-dependent equation. *Limnol Oceanogr* 23:813–816.
- Sims DW, Reid PC (2002) Congruent trends in long-term zooplankton decline in the north-east Atlantic and basking shark (*Cetorhinus maximus*) fishery catches off west Ireland. *Fish Oceanogr* 11:59–63.
- Skjoldal HR, Wiebe PH, Postel L, Knutsen T, Kaartvedt S, Sameoto DD (2013) Intercomparison of zooplankton (net) sampling systems: Results from the ICES/GLOBEC sea-going workshop. *Prog Oceanogr* 108:1–42.
- Smetacek V (1981) The annual cycle of protozooplankton in the Kiel Bight.

- Sprules WG, Barth LE (2016) Surfing the biomass size spectrum: Some remarks on history, theory, and application. *Can J Fish Aquat Sci* 73:477–495.
- Sprules WG, Munawar M (1986) Plankton Size Spectra in Relation to Ecosystem Productivity, Size, and Perturbation. *Can J Fish Aquat Sci* 43:1789–1794.
- Steedman HR (1976) Zooplankton fixation and preservation. UNESCO Monogr Ocean Methodol 4:350.
- Stevens D, Richardson AJ, Reid PC (2006) Continuous Plankton Recorder database: Evolution, current uses and future directions. *Mar Ecol Prog Ser* 316:247–255.
- Stoecker D, Pierson J (2019) Predation on protozoa: Its importance to zooplankton revisited. *J Plankton Res* 41:367–373.
- Stoecker DK, Hansen PJ, Caron DA, Mitra A (2017) Mixotrophy in the Marine Plankton. *Ann Rev Mar Sci* 9:311–335.
- Strom SL, Brainard MA, Holmes JL, Olson MB (2001) Phytoplankton blooms are strongly impacted by microzooplankton grazing in coastal North Pacific waters. *Mar Biol* 138:355–368.
- Tang X, Stewart WK, Vincent L, Huang H, Marra M, Gallager SM, Davis CS (1998) Automatic Plankton Image Recognition. *Artif Intell Rev* 12:177–199.
- Trebilco R, Baum JK, Salomon AK, Dulvy NK (2013) Ecosystem ecology: Size-based constraints on the pyramids of life. *Trends Ecol Evol* 28:423–431.
- Ward BA, Dutkiewicz S, Follows MJ (2014) Modelling spatial and temporal patterns in size-structured marine plankton communities: Top-down and bottom-up controls. *J Plankton Res* 36:31–47.
- Warner AJ, Hays GC (1994) Sampling by the continuous plankton recorder survey. *Prog Oceanogr* 34:237–256.
- Werner EE, Gilliam JF (1984) The ontogenetic niche and species interactions in size-structured populations. *Annu Rev Ecol Syst* Vol 15:393–425.
- Wiackowski K, Doniec A, Fyda J (1994) An Empirical Study of the Effect of Fixation on Ciliate Cell Volume. *Mar Microb Food Webs*:59–69.
- Widdicombe CE, Eloire D, Harbour D, Harris RP, Somerfield PJ (2010) Long-term phytoplankton community dynamics in the Western English Channel. *J Plankton Res* 32:643–655.
- Worden AZ, Follows MJ, Giovannoni SJ, Wilken S, Zimmerman AE, Keeling PJ (2015) Rethinking the marine carbon cycle: Factoring in the multifarious lifestyles of microbes. *Science* (80-) 347.
- Ye L, Chang CY, García-Comas C, Gong GC, Hsieh C hao (2013) Increasing zooplankton size diversity enhances the strength of top-down control on phytoplankton through diet niche partitioning. *J Anim Ecol* 82:1052–1061.
- Yvon-Durocher G, Montoya JM, Trimmer M, Woodward G (2011) Warming alters the size spectrum and shifts the distribution of biomass in freshwater ecosystems. *Glob Chang Biol* 17:1681–1694.
- Zhou M (2006) What determines the slope of a plankton biomass spectrum? *J Plankton Res* 28:437–448.

Chapter 1

Spatio-temporal distribution of the North Sea winter protozooplankton community between 2014 and 2021



Drawings by Justine Courboulès

Spatio-temporal distribution of the North Sea winter protozooplankton community between 2014 and 2021

Gregor Börner^{1*}, Saskia Otto¹, Nicole Aberle¹, Rachel Harmer¹, Franziska Bils², Cindy J.G. van Damme³, Matthias Kloppmann⁴, Richard D.M. Nash^{5,6}, Christian Möllmann¹, Marta Moyano^{8,9}

Abstract

Microzooplankton are key players for trophic interactions and biogeochemical processes at the base of pelagic marine food webs. Taxonomic and ecological work on this group is extensive, but yet without many broad-scale studies. In this work, Protozooplankton, the rare yet important component of plankton communities in the size range $<200 \mu\text{m}$, was sampled during the annual North Sea International Bottom Trawl Survey (IBTS) in mid-winter (January-February). The study evaluated PZP abundance, biomass, community composition, and distribution between 2014 and 2021. The community composed of 22 subgroups of ciliates, dinoflagellates, and silicoflagellates. The most abundant were ciliates (others), dinoflagellates (others), and the dinoflagellate *Heterocapsa* spp. The PZP community mainly comprised of small taxa (mean size: $29 \mu\text{m}$) with low biomass and abundance ranging from 50-15470 Ind L⁻¹ and 0.001-1.57 $\mu\text{g C L}^{-1}$, respectively. Since 2014, a significant increase in PZP abundance was observed and a distinct spatial pattern with higher relative abundances of dinoflagellates and ciliates in the southern North Sea and the English Channel was found. Although nutrients appeared to affect certain taxa, a main environmental driver could not be detected. This study provides first insights on possible environmental drivers that affect PZP shifts in phenology and community composition; however, a longer time series and/or a higher taxonomic resolution is necessary to detect general trends, broadscale protozooplankton abundance and distribution in the North Sea and adds to our general understanding of microzooplankton dynamics during times of low productivity.

Keywords: protists, microzooplankton, community composition, time series, nutrients, low productivity

Authors' affiliation

1 Institute of Marine Ecosystem and Fishery Science, University of Hamburg, Große Elbstraße 133, Hamburg D-22767, Germany

2 OSPAR Commission, London, United Kingdom

3 Wageningen Marine Research, Haringkade 1, 1976 CP IJmuiden, the Netherlands

4 Thünen Institute of Sea Fisheries, Herwigstraße 31, Bremerhaven D-27572, Germany

5 Institute of Marine Research, PO Box 1870, Nordnes, 5817 Bergen, Norway

6 Centre for Environment, Fisheries and Aquaculture Science (Cefas), Pakefield Road, Lowestoft, Suffolk NR33 0HT, UK

7 IFREMER, Centre Manche Mer du Nord - 150, Quai Gambetta - 62200 Boulogne-sur-Mer

8 Norwegian Institute for Water Research (NIVA), Økernveien 94, 0579 Oslo, Norway

9 Center for Coastal Research, University of Agder, Universitetsveien 25, 4604 Kristiansand, Norway

Introduction

The concept of the microbial loop (Azam et al. 1983) brought protozooplankton (PZP) to attention and changed the concept of a “classical” marine food chain towards a food web, with PZP as an essential component (Montagnes et al. 2010a). Although the importance of PZP in trophic dynamics of pelagic systems and their critical contribution to marine biogeochemical processes are known, they are overlooked in monitoring programs (Stern et al. 2015, Bils et al., 2019). The PZP community is generally sampled at specific stations and/or during specific seasons in temperate shelf seas (Levinsen & Nielsen 2002, Figueiredo et al. 2009, Atkinson et al. 2021) or in specific areas such as the Arctic (Levinsen et al. 2000, Monti-Birkenmeier et al. 2021). An exception to this is the plankton monitoring program in Chesapeake Bay conducted from 1985 to 1987 (Dolan & Wayne Coats 1990) or a the broad-scale study of the PZP community across the North Sea during winter in 2014 (Bils et al. 2019) .

PZP can be classified as heterotrophic or mixotrophic and encompass many dinoflagellate and ciliate species. In most cases, they are grazers, able to consume more than twice as much biomass from primary production as mesozooplankton consumers (Buitenhuis et al. 2010, López-Abbate 2021). They also serve as prey items for copepods (Calbet & Saiz 2005) and higher trophic levels such as fish larvae (Montagnes et al. 2010b, Bils et al. 2022). The variety of feeding modes allows them to feed on prey from 1/10 of their size up to much bigger organisms (Jonsson 1986, Sherr & Sherr 1994) which allows them to consume bacteria and bacterivorous nanoflagellates, channeling the energy to higher trophic levels (Pomeroy 2001). However, the contribution of PZP to the microbial loop and the classical food web varies depending e.g. on oceanographic conditions and seasons. In oligotrophic systems, PZP serve as main mediators of energy from small cells to higher trophic levels (Fileman et al. 2011). In eutrophic systems, they replace phytoplankton when the conditions do not allow the development of larger cells during times of low productivity (Joint et al. 1986, Bils et al. 2019).

PZP are sensitive to most climate-related factors, and their responses can induce cascading effects in marine food webs (Caron & Hutchins 2013a). Although the thermal tolerance of protists is wide, even moderate temperature changes are known to cause direct effects on PZP community composition, abundances and feeding activities (Aberle et al. 2007, Caron & Hutchins 2013a). This might have important implications since previous studies showed that seasonality in phytoplankton growth is associated with shifts in PZP community composition, with temperature being identified as potential driver of grazing rates (Rose & Caron 2007, Lawrence & Menden-Deuer 2012). Higher temperatures are predicted to to directly affect heterotrophic processes (such as ingestion, growth rates (e.g., Regaudie-De-Gioux & Duarte 2012)). In general, warming is believed to strengthen top-down control of phytoplankton by PZP

(Rose & Caron 2007) as heterotrophic growth is more temperature-dependent than autotroph production (Aberle et al. 2012). Yet the relationship between temperature and PZP growth and survival is still unresolved (Anderson & Harvey 2019).

Because of their short life cycle, higher metabolic activity and growth rates, PZP are considered to be excellent bioindicators of environmental changes, as they respond quickly to shifts in the aquatic environment (Montagnes et al. 2003, Menden-Deuer et al. 2005, Aberle et al. 2012). Monitoring changes in abundance of key organisms and assigning them to a specific driver can function as an early warning system for ecosystem changes, such as those caused by changes in thermal regimes or due to localized pressures (such as anthropogenic nutrient loading)(Bedford et al. 2020a). However, the insufficient number of long-term monitoring programs at a high spatiotemporal resolution paired with a lack of microzooplankton field data has further hampered the identification of climate and human-driven effects on PZP communities. Therefore, there is a lack of understanding of the relationship between these small-sized planktonic groups and environmental variables (Liu et al. 2021). Moreover, the small number of observational data sets hinders the validation of the role of PZP in ecosystem functioning (e.g. ERSEM; Butenschön et al. 2016) or biogeochemical models (e.g. DGOM; Le Quéré et al. 2005).

The North Sea is arguably one of the most studied shelf seas around the world. The plankton community of this ecosystem has been well-monitored, either in coastal areas through a variety of single station-based surveys such as Helgoland Roads (Wiltshire & Manly 2004), Plymouth L4 (Harris 2010) or Stonehaven (Bresnan et al. 2015) or with the Continuous Plankton recorder (CPR) program (O'Brien et al. 2013), that monitors surface waters of the entire North Sea. The fixed coastal stations provide high temporal frequency data with high taxonomic resolution, but have shorter spatial and time-spans than for instance the CPR survey (Bedford et al. 2020b). At Helgoland Roads, for instance, although plankton data has been collected over the past 60 years (e.g. Franke et al. 2004), there are only a few periods where PZP was routinely analysed e.g. 2007-2009 (Löder et al. 2011) and 2010-2012 (Yang et al. 2014). Indeed, this is not a North Sea problem alone. Globally, PZP remains understudied and they are rarely monitor by routine oceanographic observations. In addition, the few studies monitoring PZP are usually done during spring and summer months but data during winter, when the importance of the microbial loop and subsequently PZP is elevated, are scarce (Bils et al. 2019).

The North Seas abiotic conditions (i.e. solar radiation, temperature, and storminess) can vary significantly by season, which yields distinct seasonal peaks in primary production, nutrient availability, and water mass stratification and mixing (e.g. Quante & Colijn 2016). Even though some recent studies offer opposing results (e.g. during polar night; Berge et al. 2015), the winter season in the northern hemisphere was broadly regarded as a period of minimal activity

and is just recently gaining more attention. Despite being a very well-studied ecosystem, knowledge on North Sea dynamics during winter is surprisingly limited. However, this knowledge is essential to grasp the recruitment dynamics of seasonally spawning fish like European herring (*Clupea harengus*) and European plaice (*Pleuronectes platessa*). Previous studies implicated PZP as a dietary source for larval fish (e.g. Illing et al. 2015, Bils et al. 2022). The microbial loop, transferring energy from phytoplankton to larger zooplankton via smaller picoplankton and nanoplankton, is particularly influential during times of low productivity. The conditions during winter favor pico- and nanoplankton and shifts the energy transfer to PZP, which affects energy transfer efficiency and ocean productivity (Fileman et al. 2011). In nutrient-rich temperate waters, larger diatoms usually dominate in spring, but during winter the microbial loop and with that the role of PZP can be enhanced (Fileman et al. 2011). As a consequence, copepods e.g. of the genus *Calanus*, have been found to switch their dietary choices when phytoplankton availability is low, opting for alternative prey sources like ciliates (Nejstgaard et al. 1997, Mayor et al. 2006) and heterotrophic protists (Levinsen & Nielsen 2002, Campbell et al. 2009). In situations where the ratio of microzooplankton to phytoplankton is in favour of the former, copepods in general demonstrate a greater preference for microzooplankton as a food source (Campbell et al., 2009).

As a unique attempt, Bils et al. (2019) implemented PZP sampling on the ICES-coordinated winter IBTS Q1 survey (International Bottom Trawl Survey, Quarter 1, ICES 2022) and presented the first broad-scale PZP study in mid-winter across the North Sea in 2014. Here, a homogenous community across the North Sea with the dominance of small sized taxa (<40 µm) was found with a generally low total biomass compared to other seasons. The lack of significant spatial patterns in PZP was assumed to be related to the unusual low temperature conditions during this specific year. It was stressed that a higher spatiotemporal sampling resolutions is needed to verify their results for the North Sea and to exclude limitations such as sampling within a patch. The study by Bils et al. (2019) offers an important contribution to the understanding of planktonic communities in the North Sea by providing an overview over the PZP community dynamics during winter. Although the results of the study were just a snapshot; they provide valuable insights into the complexity of this region. Furthermore, the authors' recognition of the need for additional sampling to understand the full range of planktonic biomass in the North Sea is a significant step forward in this field of research.

Here we present a follow-up study of PZP sampled during the IBTS Q1 to consolidate the knowledge on the PZP community composition and distribution during the winter season in the North Sea. We monitored the broad-scale distribution of PZP community composition and size-structure over seven consecutive years (2014-2021, with the data from Bils et al., 2019

included) thus aiming to link PZP community patterns with key abiotic variables such as temperature, salinity and nutrients.

Materials & Methods

Study Area

The North Sea is a large, semi-enclosed marginal sea with an area of 750 000 km² and a mean depth of 100 m. In the northern area, it is connected to the Atlantic Ocean, with a constant inflow of Atlantic waters into the North Sea, but it also receives low-salinity water from the Baltic in the East as well as from large rivers in the southern area. Warmer waters from the Atlantic enter the North Sea through the English Channel in the South, causing temperature amplitudes of approx. 8°C in the south versus about 2°C in the North (Becker & Pauly 1996). Salinity patterns in the North Sea display variation, from 35 in the open north North Sea and about 30 in the Wadden Sea due to river runoffs (Ducrotoy et al. 2000). These hydrographic patterns in combination with the topography of the North Sea produces a main cyclonic (anticlockwise) circulation current (Ducrotoy et al. 2000).

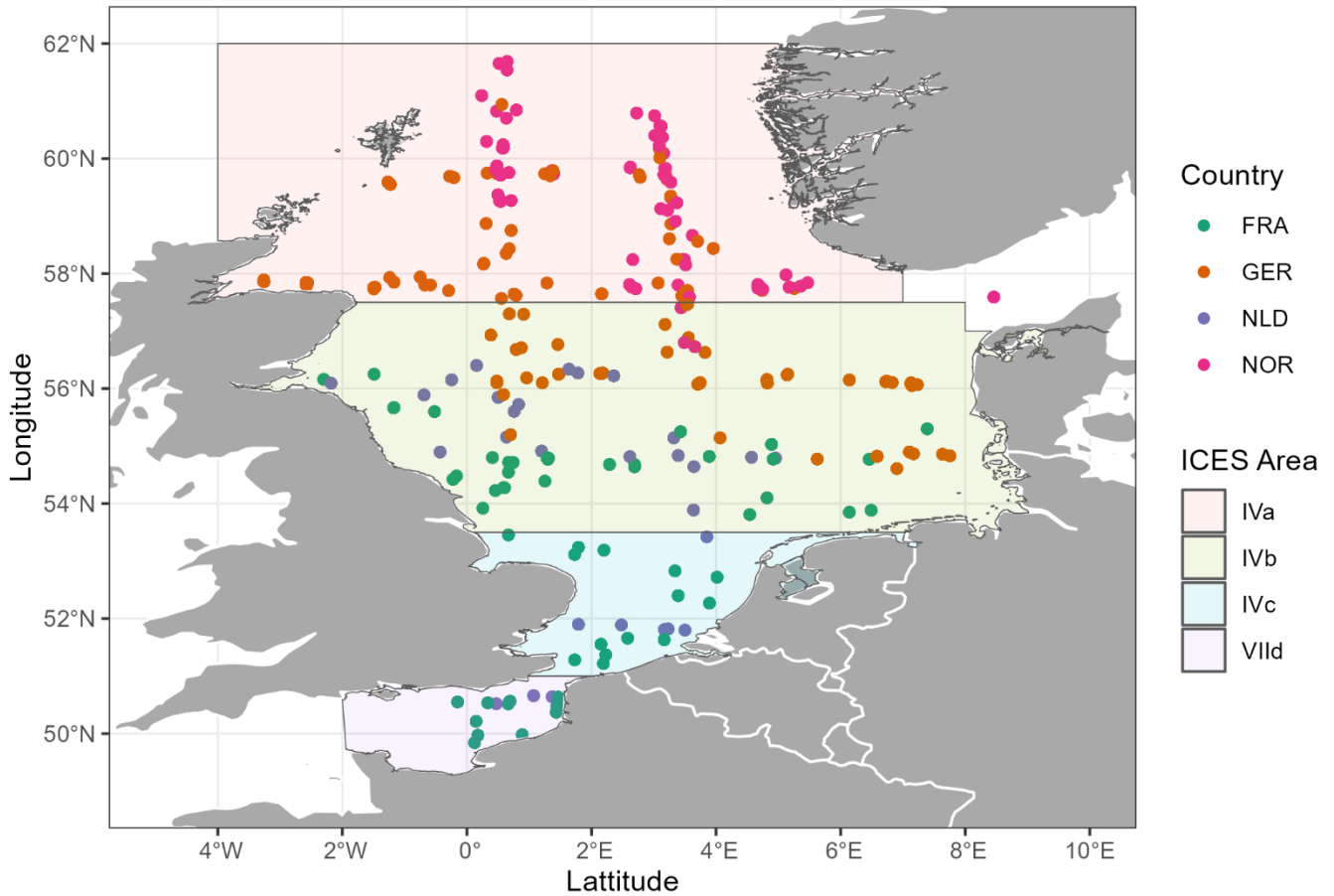


Figure 1. Protozooplankton sampling stations in the North Sea during the International Bottom Trawl Survey Q1 from 2014-2021. The ICES areas are depicted by the background color and the stations are colour-coded according to the IBTS leading country (FRA=France, GER=Germany, NLD=The Netherlands, NOR=Norway).

Sample collection and processing

PZP water samples were annually collected during the International Bottom-Trawl Quarter 1 Survey (IBTS Q1) between January and February from 2014 to 2021. This survey is coordinated by the International Council for the Exploration of the Sea (ICES). For this work, samples were collected in collaboration with institutes in the Netherlands, Norway, Germany, and France (Table 1, Fig. 1). Stations were selected along the north-south and east-west transects, pre-defined by Bils et al. (2019) (Fig. 1). On average, 25 to 40 stations were analyzed every year (Fig. S1) leading to a total of 267 stations analyzed (Table 1).

Sample collection and processing followed the methods in Bils et al. (2019). Water samples were collected at 10 m depth using a Niskin bottle attached to a CTD rosette. This depth was chosen to allow sampling in photic surface zone, even under rough sea conditions. Samples were immediately transferred to brown, 500 - mL glass bottles with acidified Lugol's iodine

solution (2% final concentration). They were stored cool, in darkness and analyzed within 12 months after collection.

Table 1. Summary of the number of protozooplankton samples collected in the North Sea during the International Bottom Trawl Survey Q1 per country and year. See Table S1 for a detailed list of the survey periods per country and year

Country	Samples (no. per year)								
	Sampling period (min. start – max. end)	2014	2015	2016	2017	2018	2019	2020	2021
France	11.1. – 13.2.	9	15	1	9	7	1	7	-
Germany	12.1. – 20.02.	14	12	14	24	16	6	10	13
Netherlands	21.01. – 08.02.	8	-	-	6	8	8	8	-
Norway	13.01. – 02.03.	8	7	11	3	12	12	8	8
Total	11.1. – 02.03.	39	34	26	42	43	27	33	21

Once in the laboratory, seawater samples were settled for 24- 48 h (HELCOM, 2014) in 20-100 mL sedimentation chambers (HydroBios), depending on the density of the sample, following the method proposed by Utermöhl (1958) and then counted using an inverted microscope (Leica DMI 3000, 200x). At stations with very low densities (total counts <100 organisms), to ensure accuracy and representative numbers of the community, the samples were concentrated before repeated counting via inverse filtration through a 5- μm mesh. To avoid any potential loss of organisms during the concentration process, the filtrate was periodically checked, but no loss was observed. Subsequently, all PZP organisms from each plate were counted, to avoid over-representation of less abundant groups. PZP organisms were classified into the two broad groups ciliates, dinoflagellates, and silicoflagellates. Note that due to the time and labor-intensive analysis of the water samples and the frequent change of analysts, silicoflagellates were only counted from 2018. For most years (2017-2021), organisms were identified to the lowest taxonomic level possible, following a combination of references and identification keys (Larink & Westheide 2006, Kraberg et al. 2010). The organisms were then pictured (Leica MC170HD). The size was measured using image analysis (Image J. 1.53e, Wayne Rasband, USA). Small organisms such as *Heterocapsa* spp. were counted but not photographed as they are uniform in size. Note that the following calculations were only applied on the years from 2017 onwards as previous years were based on mean size measures from literature (2014) or had no precise size measures (2015-2016).

Based on the size measures for the samples from 2017 onwards, biovolume (μm^3) was calculated using the formula for rotational ellipsoids provided by Olenina et al. (2006). Carbon

content ($\mu\text{g C L}^{-1}$) was calculated based on the carbon to volume relationship (C:Vol) for protists given by Mender-Deuer and Lessard (2000) (Table S1). Note that the size measures were not corrected for shrinkage as fixation effects have been found highly variable among different organism phylogenetic group, physiology or growth stage (JEROME et al. 1993, Wiackowski et al. 1994, Menden-Deuer et al. 2001).

Environmental data

To describe the habitat surface conditions during winter (i.e. January and February) we used a set of hydrographical and nutrient variables, i.e., temperature (TEMP), salinity (SAL), ammonium (NH_4), nitrate (NO_3), silicate (SI_4), total nitrogen (TN) and total phosphorus (TP). The data was retrieved from the ICES Data Portal (<https://data.ices.dk/view-map>) and, in the case of temperature and salinity, complemented with CTD measurements taken at the IBTS Q1 survey. For each sampling, we calculated mean values over the depth range of 0-10m. To match the environmental conditions with the PZP sampling locations, we applied for each year and variable an inverse distance weighted interpolation (Shepard 1968)

Statistical analysis

Temporal and spatial trends of main groups (univariate analysis)

To identify short-term trends in the total counts and the main groups ciliates and dinoflagellates between 2014 and 2021 as well as silicoflagellates between 2018 and 2021, we used generalized least squares (GLS), robust regression technique used to offset the effects of pseudo-replication or when the variances within groups are subject to variability (Pinheiro & Bates 2006). In addition, and even more important in this case, GLS is also able to estimate relationships between response and explanatory variables in the case of unbalanced sample numbers (see Table 1).

Specifically, we modelled the transformed abundances as a linear function of year while allowing variances to differ between the years or ICES areas.

$$y_{say} = \alpha + \beta * \text{year} + \epsilon_{say}, \text{ with } \epsilon_{say} \sim N(0, \sigma_z^2) \quad (1)$$

where y_{say} is the 4th-root transformed total or group abundance at sampling s , in ICES area a and year y . ϵ represents a random noise term assumed to be normally distributed with zero mean and a finite variance that is allowed to differ between areas a or years (indicated by the index z). The 4th-root transformation was applied to reduce the weighting of abundant data (Field et al. 1982) and intrinsic mean-variance relationships.

For each total and group-specific trend analysis we compared three models, one model including one variance term and one model including area or year-specific variance terms. As

model selection criterion we used the Akaike's Information Criterion (AIC) (MTW et al. 1998). The underlying statistical assumptions were verified through residual diagnostics of the optimal model.

Broad-scale spatial patterns were analyzed for each group individually using linear mixed effect (LME) models (Pinheiro & Bates 2006), in which the ICES areas were included as a fixed effect and year as a random effect,

$$y_{say} = \mu + a_a + \beta_y + \varepsilon_{say}, \varepsilon_{say} \sim N(0, \sigma^2) \quad (2)$$

where y_{say} is the 4th-root transformed total or group abundance at sampling s , in ICES area a and year y . μ represents the overall abundance mean, a_a the effect of the a^{th} area, β_y a random variable with a mean of zero and a variance of σ_β^2 , measuring the variance in mean values of the response variable across all the years included. ε represents a random variable assumed to be normally distributed with zero mean and finite variance.

To check for difference within the larger ICES areas, we applied the same modelling approach but divided IVa and IVb further into east and west. Again, underlying statistical assumptions were verified through residual diagnostics of the optimal model.

Compositional changes in space and time (multivariate analysis)

To investigate broad-scale spatio-temporal patterns in the community structure, we used distance-based permutational multivariate analysis of variance (PERMANOVA) (Anderson 2005) based on Bray–Curtis dissimilarities of the transformed abundances. The PERMANOVA model had two main terms, i.e. ICES area as fixed factor and year as random factor. Interaction terms between these factors were also tested.

Significant terms were then investigated using a posteriori pair-wise comparisons with the PERMANOVA t statistic and 1000 permutations. Based on these results, a similarity percentages (SIMPER; CLARKE 1993) analysis was applied on those pairs of ICES areas and/or years showing significant differences. The SIMPER procedure assessed the average percent contribution of PZP subgroups to the dissimilarity between ICES areas and/or years. This allows identifying the PZP subgroups that are likely to be the major contributors to any difference between pairs detected by the pairwise PERMANOVA. The subgroups with a consistent high impact on the dissimilarity between ICES areas or years serve as effective discriminatory subgroups (Clarke & Warwick 2001).

PZP and the environmental drivers

To identify ICES areas that share similar patterns of variability related to the similarity of environmental conditions, a hierarchical agglomerative cluster analysis (HCA) was applied.

The HCA with average linkage creates clusters and identifies areas and years with common environmental characteristics. To measure the distance between each pair of groups, the Euclidean distance was employed and displayed on a dendrogram (Krebs 1989). Differences in environmental conditions between areas and years were further visualized using non-metric multidimensional scaling (NMDS) on the basis of the Euclidean distances. In addition, correlation analysis was used to explore linkages between the total and group-specific PZP counts with the environmental variables (Murdoch & Chow 1996).

All analyses and graphical representations were performed using the R software (R Core Team, 2022). The GLS and LME analysis was performed using 'nmls' package (Pinheiro et al. 2017), the inverse weighted interpolation with the 'gstat' package (Pebesma 2004) and all multivariate analyses using the 'vegan' package (Oksanen et al. 2007).

Results

General composition, abundance and biomass of the PZP

We grouped the PZP community in three main groups, ciliates, dinoflagellates and silicoflagellates (from 2018). Within these three main groups, we identified 12 subgroups, of which three belonged to ciliates, eight to dinoflagellates and a single group as silicoflagellates. Overall, the total PZP community abundance measured across 267 stations ranged from 50 to 15470 Ind L⁻¹ with ciliates accounting for 35%, dinoflagellates for 64% and silicoflagellates for <2% of the total relative abundance across the analyzed time span (see Fig.2).

Overall, we found that small-sized organisms (<29±16 µm) dominated the community with only few subgroups >50 µm (e.g. Tintinnida spp., Tripos spp.) (Table 2). Ciliates other than *Mesodinium* spp. and Tintinnida (also called 'Ciliates (others)' hereafter) as well as dinoflagellates other than the subgroups listed in Table 1 (also termed 'Dinoflagellates (others)' hereafter) were present in all stations, with peak abundances of 4290 and 4500 Ind L⁻¹, respectively, and average contributions to the total abundances at around 30% (Table 2). *Heterocapsa* spp. represented another dominant group contributing on average 23% to the mean total abundances and appearing in 95% of the stations with maximum abundances up to 13,330 Ind L⁻¹ (Table 2).

In terms of biomass, the communities were generally dominated by Ciliates (others), Dinoflagellates (others) and *Tripos* spp., representing altogether an average of 55% to the mean total biomass. The average biomass of dinoflagellates was similar to that of ciliates (150 vs. 130 ng C L⁻¹, respectively) while silicoflagellates biomass was low (7.89 ng C L⁻¹) (Table 2). Due to the lack of significant spatio-temporal trends in biomass (except for silicoflagellates), this study focus on PZP abundance where significant patterns were observed.

Modelling the biomass showed no significant spatial and/or temporal trend for the PZP community, dinoflagellates and ciliates but silicoflagellates. Due to the lack of significant spatio-temporal trends in biomass (except for silicoflagellates), this study focus on PZP abundance where significant patterns were observed.

Table 2. Overview of the mean length (μm), standard deviation (sd), abundance (Ab, ind L⁻¹) and biomass (BM, ng C L⁻¹) of the North Sea winter PZP community, the main groups (groups) and subgroups (subgroups) for the available time span (years, * 2014-2021 ; ** 2014, 2017-2021 ; *** 2017 - 2021;**** 2018-2021). Minimum (min), maximum (max) and mean abundance and biomass estimates are reported.

	Length [μm]		Time	Abundance [N L ⁻¹]			Time	Biomass [ng C L ⁻¹]		
	Mean	Sd		MinAb	MaxAb	MeanAb		MinBM	MaxBM	MeanBM
PZP	28.95	16.6	*	50.00	15470.00	1591.42	***	1.29	1578.24	339.00
Groups										
Ciliates	27.9	19.4	*	6.00	4500.00	551.17	***	0.81	450.79	131.41
Dinoflagellates	29.9	14.4	*	30.00	14370.00	1018.88	***	1.38	1399.36	150.64
Silicoflagellates	24.6	4.5	****	2.00	230.00	21.37	****	0.71	35.86	7.89
Subgroups										
Ciliates										
<i>Ciliate spp.</i>	26.2	12.8	**	6.00	4290.00	540.14	***	0.81	375.20	98.85
<i>Mesodinium spp.</i>	17.6	3.6	**	4.00	590.00	42.10	***	0.24	17.25	1.62
<i>Tintinnina spp.</i>	88.2	51.4	**	2.00	450.00	28.36	***	1.42	256.39	18.77
Dinoflagellates										
<i>Tripos spp.</i>	68.2	15.3	**	2.00	1140.00	19.32	***	0.49	1209.77	33.48
<i>Dinoflagellate spp.</i>	24.13	8.1	**	14.00	2900.00	491.29	***	1.38	329.46	50.31
<i>Gyrodinium spp.</i>	48.0	17.8	**	3.33	850.00	46.55	***	0.37	86.06	2.7
<i>Heterocapsa spp.</i>	15.3	2.5	**	5.00	13330.00	503.07	***	0.37	137.51	17.18
<i>Katodinium spp.</i>	28.7	6.8	**	2.00	110.00	8.03	***	0.31	16.11	0.89
<i>Prorocentrum spp.</i>	49.1	4.9	**	5.00	130.00	5.98	***	2.22	68.75	2.19
<i>Protoperidinium spp.</i>	31.1	15.0	**	2.00	310.00	44.75	***	0.97	238.08	23.75
<i>Torodinium spp.</i>	32.7	9.1	**	2.00	1020.00	99.01	***	0.96	125.31	15.43
Silicoflagellates										
<i>Dictyochaceae spp.</i>	24.6	4.5	****	2.00	230.00	29.26	****	0.71	35.86	3.57

* 2014-2021 ; ** 2014, 2017-2021 ; *** 2017-2021; ****2018-2021

Temporal and spatial trends of PZP subgroups

Using the GLS modelling approach, we found a slight but significant increase in 4th root-transformed abundances of ciliates (slope = 0.15, $p = <0.001$) and dinoflagellate (slope = 0.12, $p = <0.001$) over the analyzed time span (Fig. S2A-C). Silicoflagellate abundances (2018-2021) showed in contrast a more steep increase in these last years (slope = 0.72, $p = <0.001$) (Fig. S2D).

The final LME models applied to test for differences between ICES areas included all year as a random effect and did not differentiate between eastern and western subareas within area

IVa and IVb. The model results show a clear latitudinal gradient in Ciliate abundances with highest predicted abundances in the English Channel (VIIId) (Fig. 3B). In contrast, abundances of Dinoflagellates and the general PZP community are highest in the central areas, i.e. IVb and particularly the southern Bight (IVc) (Fig. 3A/C), while Silicoflagellates are mainly present in the northern area IVc (>30 Ind L⁻¹) (Fig. 3D). Due to the dinoflagellate dominance in the community, they reflect the general PZP patterns (Fig. 3 A and C). Despite the significance of these spatial trends, please note their minor contribution to the overall variability as indicated by the marginal R² of 5 -15%. However, when including year as random factor, the model was able to explain over 60% of the variance (conditional R² of 52 -63%) suggesting stronger temporal than spatial dynamics.

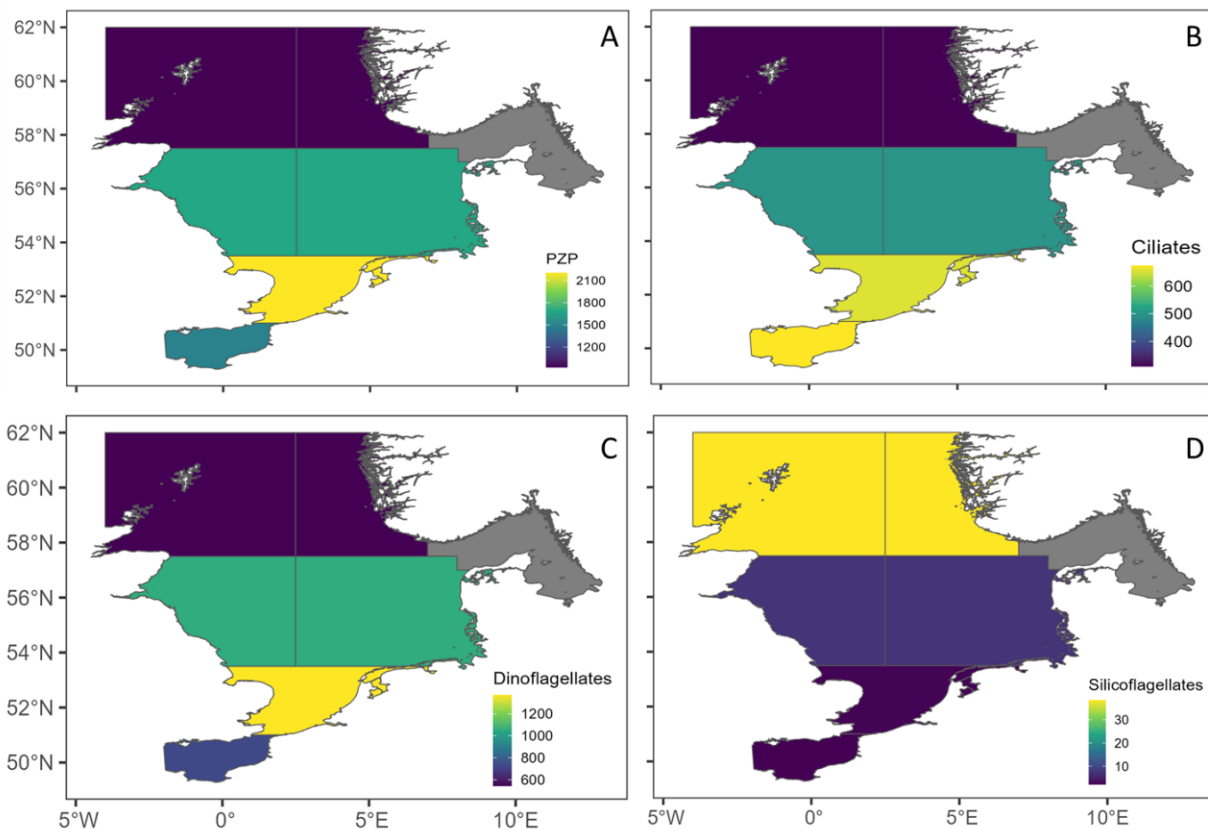


Figure 3. Predicted mean abundance (Ind L⁻¹) per North Sea ICES area for each of the broad PZP groups: (A) the whole PZP community, (B) ciliates, (C) dinoflagellates, and (D) silicoflagellates. Note that the scale differs between groups in order to maintain visual differences.

Compositional changes in space and time

PZP community structure showed substantial variation between ICES areas and years as indicated by the PERMANOVA ($p = <0.001$). The pairwise comparison showed that there are significant differences in taxon-specific abundances between IVa and all other ICES areas as well as between VIIa and both, IVb and IVc, verifying the north-south gradient and indicating a

significant shift in abundance in IVa. A SIMPER analysis revealed that the ICES areas differ by 37 to 41% among each other with seven taxa being mainly responsible for the dissimilarities (Table 3). Overall *Heterocapsa* spp. was the taxa contributing most to the dissimilarities between areas (prop. contrib >15%) (Table 3) with high abundances in the central North Sea (IVb and IVc) with a decrease towards the South (VIId) and North (IVa) (Fig. 4). *Torodinium* spp. contributed second most to dissimilarities between areas (>10%) with highest abundances also in IVa. *Gyrodinium* spp., *Protoperidinium* spp., *Mesodinium* spp. and Ciliates (others) were the other taxa responsible for the spatial difference contributing approx. 10% to the general dissimilarity per area (Table 2).

Table 3: Results of the SIMPER analysis (based on transformed abundance data) to identify taxa contributing most to dissimilarities among ICES areas (cumulative limit of 60%). The average abundance of area A (ava) and area B (avb), the difference in abundance between areas (diff), and the proportional overall contribution to the dissimilarity (prop.contrib) is shown.

pairs	subgroups	av. diss	ava	avb	diff	prop. contrib
IVb_IVa	37.9%					
	<i>Heterocapsa</i>	spp.	2.98	2.81	0.17	0.16
	<i>Torodinium</i>	spp.	2.13	1.71	0.43	0.11
	<i>Gyrodinium</i>	spp.	1.88	1.50	0.38	0.10
	<i>Protopteridinium</i>	spp.	1.68	1.53	0.14	0.09
	<i>Mesodinium</i>	spp.	1.28	0.89	0.38	0.09
	Ciliates (others)		4.52	4.16	0.36	0.08
IVc_IVa	40.6%					
	<i>Heterocapsa</i>	spp.	2.60	2.81	-0.21	0.16
	<i>Torodinium</i>	spp.	2.09	1.71	0.39	0.12
	<i>Protopteridinium</i>	spp.	1.60	1.53	0.07	0.10
	Ciliates (others)		4.47	4.16	0.32	0.09
	<i>Gyrodinium</i>	spp.	1.52	1.50	0.01	0.09
	<i>Tintinnida</i>		1.37	0.81	0.56	0.08
VIIId_IVa	38.7%					
	<i>Heterocapsa</i>	spp.	2.43	2.81	-0.37	0.15
	<i>Torodinium</i>	spp.	2.07	1.71	0.36	0.11
	<i>Protopteridinium</i>	spp.	1.84	1.53	0.31	0.09
	Ciliates (others)		4.62	4.16	0.47	0.09
	<i>Gyrodinium</i>	spp.	1.09	1.50	-0.41	0.09
	<i>Mesodinium</i>	spp.	1.14	0.89	0.25	0.09
VIIId_IVb	38.0%					
	<i>Heterocapsa</i>	spp.	2.43	2.98	-0.55	0.16
	<i>Torodinium</i>	spp.	2.07	2.13	-0.07	0.11
	<i>Gyrodinium</i>	spp.	1.09	1.88	-0.79	0.10
	<i>Protopteridinium</i>	spp.	1.84	1.68	0.17	0.09
	<i>Mesodinium</i>	spp.	1.14	1.28	-0.14	0.09
	<i>Tintinnida</i>		1.27	1.30	-0.03	0.09

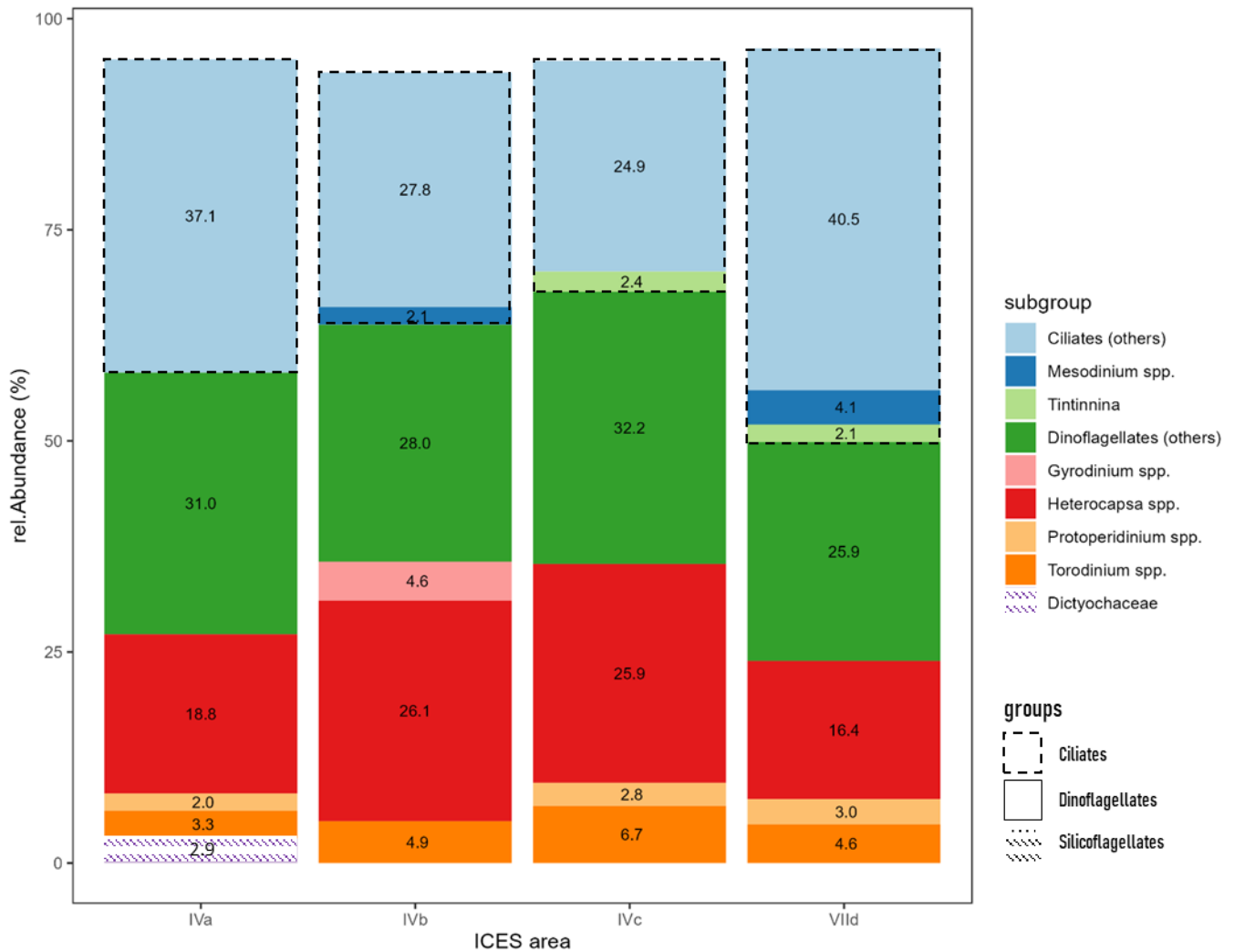


Figure 4. Relative contribution of the different North Sea PZP taxa in this study to the overall abundance per ICES area in %. Subgroups belonging to the ciliates main group are depicted in blue and framed with the dashed line, dinoflagellates are depicted in rainbow colors and silicoflagellates are grey. Note that subgroups <2% contribution are excluded for better representation.

Potential effects of environmental conditions

The cluster analysis of the environmental variables revealed a distinct separation into three clusters with one cluster presenting completely area VIId in all years (Fig. S2A). The second cluster represents the greater North Sea areas (IVa, IVb, IVc) in 2020 as well as IVa in 2018 and 2019 linked to a high nutrient regime (i.e. NO₃, Si₄, NH₄, and TP) (Fig. S2B). The third cluster comprises of the greater North Sea areas in the earlier years sharing similar characteristics in terms of salinity (SAL), temperature (TEMP), oxygen (DOXY), phosphorus (PH₄) and total nitrogen (TN) (Fig. S2B).

The results of the Pearson correlation analysis showed that the environmental variables had weak effects on the total PZP community ($r = \pm 0.3$) (Fig. 6A). Among the main groups, only nutrients (here NH₄, NO₃, Si₄ and tp) showed a moderate positive ($r = 0.6$) effect on

silicoflagellates (Fig. 6B). On subgroup level, again nutrients (NH₄, NO₃, SI₄ and tp) showed a moderate ($r=>0.4$) to strong positive correlation ($r=>0.6$) to some subgroups such as *Heterocapsa* spp., (NH₄, $r=>0.5$) or *Dictyocha* spp. spp. (tp, $r=>0.6$) (Fig. 6C). The results of the Pearson correlation analysis showed that the environmental variables had weak effects on the total PZP community ($r=<±0.3$) (Fig. 6A). Among the main groups, only nutrients (here NH₄, NO₃, SI₄ and tp) showed a moderate positive ($r=0.6$) effect on silicoflagellates (Fig. 6B). On subgroup level, again nutrients (NH₄, NO₃, SI₄ and tp) showed a moderate ($r=>0.4$) to strong positive correlation ($r=>0.6$) to some subgroups such as *Heterocapsa* spp., (NH₄, $r=>0.5$) or *Dictyocha* spp. spp. (tp, $r=>0.6$) (Fig. 6C).

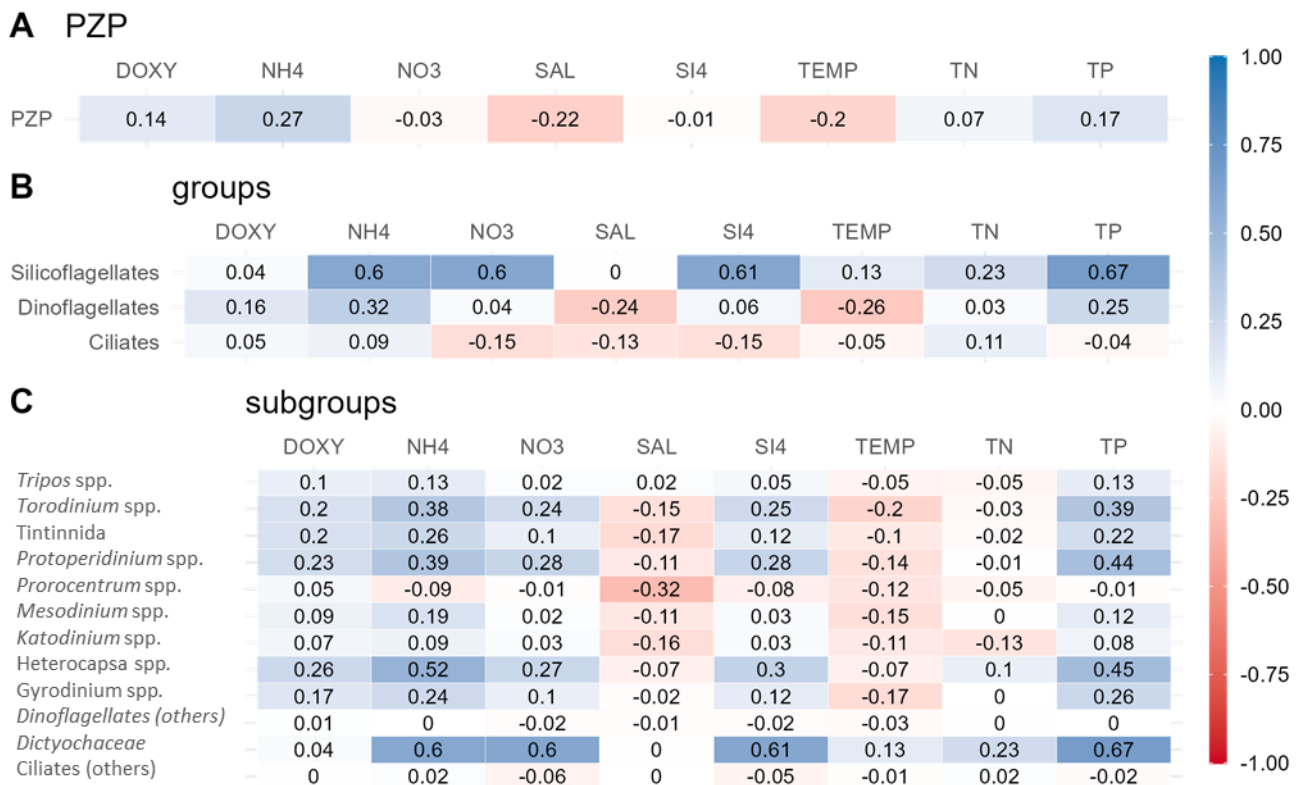


Figure 5: Visualization of correlation matrix of the environmental variables temperature (TEMP), salinity (SAL), oxygen (DOXY) and nutrients (NH₄ – Ammonia, NO₃ – Nitrogen, SI₄ – Silicates, TN – total Nitrogen, TP – total Phosphorus) related to the abundance of the total PZP (A) the groups (B) and the subgroups (C). The color intensity indicates positive (blue) correlation, negative correlation is shown in red and the numbers show effect strength.

Discussion

Studies of the plankton dynamics and community patterns during periods of low productivity in temperate marine ecosystems, such as late autumn and winter, are still scarce. Especially in terms of the small size fractions such as PZP which gain particular importance as energy mediators during these seasons (Calbet & Saiz 2005). In general, data with high spatiotemporal resolution of these groups is still limited although there is a great need to explore PZP dynamics, especially during times of low productivity of PZP, mesozooplankton and higher trophic levels (Bils et al. 2019). We found an overall homogenous PZP community in the North Sea, with an overall increase in abundance since 2014 and a distinct spatial north-south gradient. However, no direct environmental driver responsible for this gradient was identified.

General composition, abundance and biomass of the PZP

In the present study, the PZP community was composed of small organisms (on average 28.95 μm) with low abundances (average 1591 Ind L^{-1}) and biomass (339 ng C L^{-1}). These findings are consistent with the studies from autumn or winter in the North Sea (Löder et al. 2012, Bils et al. 2019) or in the Arctic (Levinsen & Nielsen 2002, Monti-Birkenmeier et al. 2021). In this study, the community in terms of abundances was dominated by dinoflagellates. Previous studies reported conflicting results, while some studies identify dinoflagellates as the primary group; others suggest ciliates (Burkill et al. 1993, Montagnes et al. 2010, Fileman et al. 2011), which makes it difficult to establish a correlation between a particular season and the increased presence of either group. It is likely that the contribution of ciliates and dinoflagellates varies depending on specific local conditions and processes (Bils et al. 2019). Across the different areas of the North Sea, the here reported results confirmed that the PZP community is homogeneously composed as reported by Bils et al. (2019). The results of the SIMPER analysis confirm these findings as differences in abundance of the main subgroups are contributing most to the dissimilarity between areas and not presence/absence of taxa. The only exception in this study are Silicoflagellates, being almost completely absent in southern areas. However, this group was not analyzed in previous studies but is generally linked to colder or temperate waters with peak appearance in late winter in the North Sea (Kraberg et al. 2010). Furthermore, the results show that across the study area, none of the ICES areas is dominated by certain taxa. There are variations in relative abundance between the main groups. However, these may be related to local effects as we found taxa-specific correlations, e.g. with nutrients, yet not strong enough to cause a dominance. In general, the community composition and size structure showed the typical characteristics of temperate regions during times of low productivity (Levinsen & Nielsen 2002, Löder et al. 2011).

Spatio-temporal trends of PZP abundance and composition

The observed increase in total abundance over the analyzed time span across all three main groups in the North Sea, is in line with previous reports, especially on dinoflagellates, which reflect the general PZP pattern reported in this study (e.g. Widdicombe et al. 2010, Beaugrand et al. 2014, Nohe et al. 2020). Leterme et al. (2005) observed a similar pattern in the Northeast Atlantic region, including the North Sea, with an increase in dinoflagellates during the same period. However, these long-term trends are widely based on continuous plankton recorder (CPR) data which doesn't sample the entire PZP size spectrum (incl. smaller planktonic size fractions <270 µm) and generally underestimates absolute abundances (John et al. 2001). The dataset used in this study differs from CPR datasets and more suited for PZP analyses due to appropriate sampling, preservation and counting procedures (Gifford & Caron 2000). More recently, Hernández-Fariñas et al. (2014) showed, that dinoflagellate abundance increased along the North Sea coast of France during the period 1992-2012. In this study, evidence for community shifts related to climate-driven changes in the coastal environment were provided. The discrepancies observed could be due to differences in sampling technique, as well as local characteristics, related to bathymetry, hydrography, anthropogenic activities, and effects of river run-offs and inflow from the Atlantic Ocean (Nohe et al. 2020). These contrasting findings highlight the need for a long-term PZP time series with a consistent sampling technique, to determine trends and to differentiate between environmental and local impacts to gain a better knowledge on the temporal trends of the PZP community.

The PZP community showed a distinct north-south gradient with low abundances in the north and high abundances in the southern Bight and the English Channel, verifying the pattern found in 2014 by Bils et al. (2019). Likewise, Widdicombe et al. (2010) reported an increasing trend in dinoflagellate abundance in the English Channel. In our study, *Heterocapsa* spp. was mainly responsible for differences between the northern and southern areas. We assume that the main *Heterocapsa* species found is *Heterocapsa cf. rotundata* as identified by Bils et al. (2019). *Heterocapsa cf. rotundata* is an ubiquitous species known to dominated ecosystems during wet and cold winters in other temperate seas such as Chesapeake Bay (Millette et al. 2015) or the Baltic Sea (Jaschinski et al. 2015). Note that the abundance of *H. cf. rotundata* increased since 2014 reported by Bils et al. (2019), however, this species was found to form winter blooms when the conditions are in favor (Millette et al. 2017). Moreover, *H. cf. rotundata* was found to increase its bacterial ingestion rate during times of low irradiation and thus, out-compete other taxa under low light conditions (Millette et al. 2015). *Torodinium* spp. was another species that was mainly responsible for the difference between the ICES areas, being most abundant in the central and southern North Sea, which was already the case in 2014

(Bils et al. 2019). However, over the analyzed time span, higher *Torodinium* spp. abundances in area VIIIId were also responsible for the dissimilarity to northern stations.

Within the transition areas to the Atlantic, slight changes in community composition, such as the increase of abundance of *Dictyocha* spp. (IVa) or *Mesodinium* spp. (VIIId) may indicate a gradual shift. These findings may indicate what has been hypothesized in previous studies, that water masses are more influential on ciliates for instance than biogeographic distribution patterns (Stoecker et al. 1994). In this regard, Yang et al. (2020) showed that the planktonic ciliate community structure, including the species number, abundance, biomass and diversity may be an ideal indicator of water masses without finding an unambiguous relation to environmental parameters itself.

Environmental drivers

PZP was found to be sensitive to most climate-related factors (Caron & Hutchins 2013b) and to shifts in the aquatic environment (Montagnes et al. 2003, Menden-Deuer et al. 2005, Aberle et al. 2012). Despite these previous findings, no distinct correlation between the environment and the PZP community in the North Sea was found. These results are in agreement with the weak effects detected by Bils et al. (2019) in 2014. In general, the environmental conditions in the North Sea are relatively stable over the analyzed time span, with distinct characteristics of the different ICES areas, as shown by the cluster analysis. In general, previous studies showed that heterotrophic dinoflagellates and ciliates may rather be affected by their prey and or predation by e.g. copepods than environmental drivers such as temperature (Riisgaard 2014). For the entire community, the spatial distribution patterns presented in this study may be more influenced by other local or physical factors. For instance, previous studies on ciliates assumed that spatial distribution patterns are more influenced by physical factors, such as freshwater intrusion and water currents, due to the comparatively limited motility of ciliates (Reid & Stewart 1989). Hinder et al. (2012) found that long-term changes of tintinnids in the UK shelf seas are mainly impacted by localized factors, which, however, could be partly attributed to larger climate patterns.

Conclusion

The analysis of this novel PZP dataset across several years allowed the identification of a specific spatial trends among a homogenous community across the North Sea. While the spatio-temporal analysis of the PZP revealed distinct patterning in the greater North Sea region, the correlation analysis of the subgroups in relation to the environmental variables and nutrients was less conclusive. In general, responses of PZP to the environment are induced by a complex interplay between local environmental conditions, global climatic phenomena, but also interspecific interactions (Caron & Hutchins 2013b). However, studying PZP means

also being faced with the fact that the oceanic environment is a highly dynamic environment with constant changes of the physical and chemical characteristics on both, small and large scales. The probability of working with the same PZP population is almost impossible due to currents and advections in combination with a rapid changing nutrient regime. The predominant PZP observations at fixed monitoring stations (e.g. L4 in the North Sea) allow a good overview of a sequence of community changes over different seasons but are hard to extrapolate over larger spatiotemporal scales. On the other hand, when analyzing broad scale data, it is difficult to archive a likewise high resolution. Therefore, broader groups are analyzed which makes it more difficult to detect patterns of change. Here we showed that there are constant spatial patterns in PZP distribution. However, due to the relatively constant environmental characteristics of the North Sea during winter, the effect of environmental drivers such as salinity and temperature remain low. Nutrients appear to have a stronger effect on certain taxa; however, the dominant groups appear unaffected. A fact that could hinder the direct linkage of PZP and the respective driving forces is the pooling of species into certain taxa, size classes or groups thus leading to biases related to a low taxonomic resolution. The PZP time series demonstrated general trends in the North Sea, but there are dynamic processes that cannot be directly linked with certain drivers, such as the general increase in abundance. Longer time series and/or higher taxonomic resolution would be necessary to more accurately identify long-term trends and the forces behind them.

Author Contributions

G.B. wrote the manuscript; G.B., N.A.M., M.M. conceived the study; F.B., C.V.D., M.K., R.D.M.N. did the sample collection, G.B., R.H. and F.B did the sample procession, G.B., S.O., did the statistical analyses; N.A.M., S.O., M.M., C.M. provided input and revisions to the manuscript.

Acknowledgments

We thank Ralf van Hal, Coline Lazard, Magnus Reeve and all other scientists from Wageningen Marine Research (IJmuiden, The Netherlands), IFREMER (L'Institut Français de Recherche pour l'Exploitation de la Mer, Boulogne-sur-mer, France), IMR (Institute of Marine Research, Bergen, Norway) and Thünen Institute of Sea Fisheries (Hamburg, Germany) who were involved in the IBTS survey and the sampling. Moreover, we would like to thank the entire crew of the RV Tridens, RV Thalassa, RV G.O. SARS, and the RV Walter Herwig. Furthermore, I would like to thank Nadja Gerull for the valuable help with the sorting and measuring process of the PZP pictures.

References

- Aberle N, Bauer B, Lewandowska A, Gaedke U, Sommer U (2012) Warming induces shifts in microzooplankton phenology and reduces time-lags between phytoplankton and protozoan production. *Mar Biol* 159:2441–2453.
- Aberle N, Lengfellner K, Sommer U (2007) Spring bloom succession, grazing impact and herbivore selectivity of ciliate communities in response to winter warming. *Oecologia* 150:668–681.
- Anderson MJ (2005) Permutational multivariate analysis of variance. *Dep Stat Univ Auckland, Auckl* 26:32–46.
- Anderson SR, Harvey EL (2019) Seasonal variability and drivers of microzooplankton grazing and phytoplankton growth in a subtropical estuary. *Front Mar Sci* 6:1–13.
- Atkinson A, Lilley MKS, Hirst AG, McEvoy AJ, Tarran GA, Widdicombe C, Fileman ES, Woodward EMS, Schmidt K, Smyth TJ, Somerfield PJ (2021) Increasing nutrient stress reduces the efficiency of energy transfer through planktonic size spectra. *Limnol Oceanogr* 66:422–437.
- Azam F, Fenchel T, Field J, Gray J, Meyer-Reil L, Thingstad F (1983) The Ecological Role of Water-Column Microbes in the Sea. *Mar Ecol Prog Ser* 10:257–263.
- Beaugrand G, Harlay X, Edwards M (2014) Detecting plankton shifts in the North Sea: A new abrupt ecosystem shift between 1996 and 2003. *Mar Ecol Prog Ser* 502:85–104.
- Becker GA, Pauly M (1996) Sea surface temperature changes in the North Sea and their causes. *ICES J Mar Sci* 53:887–898.
- Bedford J, Johns DG, McQuatters-Gollop A (2020a) Implications of taxon-level variation in climate change response for interpreting plankton lifeform biodiversity indicators. *ICES J Mar Sci* 77:3006–3015.
- Bedford J, Ostle C, Johns DG, Atkinson A, Best M, Bresnan E, Machairopoulou M, Graves CA, Devlin M, Milligan A, Pitois S, Mellor A, Tett P, McQuatters-Gollop A (2020b) Lifeform indicators reveal large-scale shifts in plankton across the North-West European shelf. *Glob Chang Biol* 26:3482–3497.
- Berge J, Daase M, Renaud PE, Ambrose WG, Darnis G, Last KS, Leu E, Cohen JH, Johnsen G, Moline MA, Cottier F, Varpe O, Shunatova N, Bałazy P, Morata N, Massabuau JC, Falk-Petersen S, Kosobokova K, Hoppe CJM, Węśławski JM, Kukliński P, Legeżyńska J, Nikishina D, Cusa M, Kędra M, Włodarska-Kowalczyk M, Vogedes D, Camus L, Tran D, Michaud E, Gabrielsen TM, Granovitch A, Gonchar A, Krapp R, Callesen TA (2015) Unexpected levels of biological activity during the polar night offer new perspectives on a warming arctic. *Curr Biol* 25:2555–2561.
- Bils F, Aberle N, van Damme CJG, Peck MA, Moyano M (2022) Role of protozooplankton in the diet of North Sea autumn spawning herring (*Clupea harengus*) larvae. *Mar Biol* 169:1–16.
- Bils F, Moyano M, Aberle N, van Damme CJG, Nash RDM, Kloppmann M, Loots C, Peck MA (2019) Broad-scale distribution of the winter protozooplankton community in the North Sea. *J Sea Res* 144:112–121.

- Bresnan E, Cook KB, Hughes SL, Hay SJ, Smith K, Walsham P, Webster L (2015) Seasonality of the plankton community at an east and west coast monitoring site in Scottish waters. *J Sea Res* 105:16–29.
- Buitenhuis ET, Rivkin RB, Séailley S, Le Quéré C (2010) Biogeochemical fluxes through microzooplankton. *Global Biogeochem Cycles* 24.
- Butenschön M, Clark J, Aldridge JN, Icarus Allen J, Artioli Y, Blackford J, Bruggeman J, Cazenave P, Ciavatta S, Kay S, Lessin G, Van Leeuwen S, Van Der Molen J, De Mora L, Polimene L, Sailley S, Stephens N, Torres R (2016) ERSEM 15.06: A generic model for marine biogeochemistry and the ecosystem dynamics of the lower trophic levels. *Geosci Model Dev* 9:1293–1339.
- Calbet A, Saiz E (2005) The ciliate-copepod link in marine ecosystems. *Aquat Microb Ecol* 38:157–167.
- Campbell RG, Sherr EB, Ashjian CJ, Plourde S, Sherr BF, Hill V, Stockwell DA (2009) Mesozooplankton prey preference and grazing impact in the western Arctic Ocean. *Deep Res Part II Top Stud Oceanogr* 56:1274–1289.
- Caron DA, Hutchins DA (2013a) The effects of changing climate on microzooplankton grazing and community structure: Drivers, predictions and knowledge gaps. *J Plankton Res* 35:235–252.
- Caron DA, Hutchins DA (2013b) The effects of changing climate on microzooplankton grazing and community structure: Drivers, predictions and knowledge gaps. *J Plankton Res* 35:235–252.
- CLARKE KR (1993) Non-parametric multivariate analyses of changes in community structure. *Aust J Ecol* 18:117–143.
- Clarke KR, Warwick RM (2001) Change in marine communities: an approach to statistical analysis and interpretation. 2nd edition. Primer-E, Plymouth. Plymouth, United Kingdom Prim:172.
- Dolan JR, Wayne Coats D (1990) Seasonal abundances of planktonic ciliates and microflagellates in mesohaline Chesapeake Bay waters. *Estuar Coast Shelf Sci* 31:157–175.
- Ducrotoy J-P, Elliott M, de Jonge VN (2000) The North Sea. *Mar Pollut Bull* 41:5–23.
- Field J, Clarke K, Warwick R (1982) A Practical Strategy for Analysing Multispecies Distribution Patterns. *Mar Ecol Prog Ser* 8:37–52.
- Figueiredo GM, Montagnes DJS, Nash RDM (2009) The importance of protozooplankton as prey for copepods in the coastal areas of the central Irish Sea. *Hydrobiologia* 628:227–239.
- Fileman ES, Fitzgeorge-Balfour T, Tarran GA, Harris RP (2011) Plankton community diversity from bacteria to copepods in bloom and non-bloom conditions in the Celtic Sea in spring. *Estuar Coast Shelf Sci* 93:403–414.
- Franke HD, Buchholz F, Wiltshire KH (2004) Ecological long-term research at Helgoland (German Bight, North Sea): Retrospect and prospect - An introduction. *Helgol Mar Res* 58:223–229.
- Gifford DJ, Caron DA (2000) Sampling, preservation, enumeration and biomass of marine protozooplankton. *ICES Zooplankt Methodol Man*:193–221.

- Harris R (2010) The L4 time-series: The first 20 years. *J Plankton Res* 32:577–583.
- Hernández-Fariñas T, Soudant D, Barillé L, Belin C, Lefebvre A, Bacher C (2014) Temporal changes in the phytoplankton community along the French coast of the eastern English Channel and the southern Bight of the North Sea. *ICES J Mar Sci* 71:821–833.
- Hinder SL, Manning JE, Gravenor MB, Edwards M, Walne AW, Burkill PH, Hays GC (2012) Long-term changes in abundance and distribution of microzooplankton in the NE Atlantic and North Sea. *J Plankton Res* 34:83–91.
- ICES (2022) IBTSWG (International Bottom Trawl Survey Working Group). 04:Expert Groups.
- Illing B, Moyano M, Niemax J, Peck MA (2015) Direct effects of microalgae and protists on herring (*Clupea harengus*) yolk sac larvae. *PLoS One* 10.
- Jaschinski S, Flöder S, Petenati T, Göbel J (2015) Effects of nitrogen concentration on the taxonomic and functional structure of phytoplankton communities in the Western Baltic Sea and implications for the European water framework directive. *Hydrobiologia* 745:201–210.
- JEROME CA, MONTAGNES DJS, TAYLOR FJR (1993) The Effect of the Quantitative Protargol Stain and Lugol's and Bouin's Fixatives On Cell Size: A More Accurate Estimate of Ciliate Species Biomass. *J Eukaryot Microbiol* 40:254–259.
- John EH, Batten SD, Harris RP, Hays GC (2001) Comparison between zooplankton data collected by the Continuous Plankton Recorder survey in the English Channel and by WP-2 nets at station L4, Plymouth (UK). *J Sea Res* 46:223–232.
- Joint I, Owens N, Pomeroy A (1986) Seasonal production of photosynthetic picoplankton and nanoplankton in the Celtic Sea. *Mar Ecol Prog Ser* 28:251–258.
- Jonsson P (1986) Particle size selection, feeding rates and growth dynamics of marine planktonic oligotrichous ciliates (Ciliophora: Oligotrichina). *Mar Ecol Prog Ser* 33:265–277.
- Kraberg A, Baumann M, Dürselen CD (2010) Coastal Phytoplankton: Photo Guide for Northern European Seas. Pfeil.
- Krebs CJ (1989) *Ecological Methodology*.—Harper and Row Publishers, New York, 654 pp.
- Larink O, Westheide W (2006) Coastal Plankton: Photo Guide for European Seas. F. Pfeil.
- Lawrence C, Menden-Deuer S (2012) Drivers of protistan grazing pressure: Seasonal signals of plankton community composition and environmental conditions. *Mar Ecol Prog Ser* 459:39–52.
- Leterme SC, Edwards M, Seuront L, Attrill MJ, Reid PC, John AWG (2005) Decadal basin-scale changes in diatoms, dinoflagellates, and phytoplankton color across the North Atlantic. *Limnol Oceanogr* 50:1244–1253.
- Levinsen H, Nielsen TG (2002) The trophic role of marine pelagic ciliates and heterotrophic dinoflagellates in arctic and temperate coastal ecosystems: A cross-latitude comparison. *Limnol Oceanogr* 47:427–439.
- Levinsen H, Turner JT, Nielsen TG, Hansen BW (2000) On the trophic coupling between protists and copepods in arctic marine ecosystems. *Mar Ecol Prog Ser* 204:65–77.
- Liu K, Chen B, Zheng L, Su S, Huang B, Chen M, Liu H (2021) What controls microzooplankton biomass and herbivory rate across marginal seas of China? *Limnol Oceanogr* 66:61–75.

- Löder MGJ, Kraberg AC, Aberle N, Peters S, Wiltshire KH (2012) Dinoflagellates and ciliates at Helgoland Roads, North Sea. *Helgol Mar Res* 66:11–23.
- Löder MGJ, Meunier C, Wiltshire KH, Boersma M, Aberle N (2011) The role of ciliates, heterotrophic dinoflagellates and copepods in structuring spring plankton communities at Helgoland Roads, North Sea. *Mar Biol* 158:1551–1580.
- López-Abbate MC (2021) Microzooplankton communities in a changing ocean: A risk assessment. *Diversity* 13:1.
- Mayor DJ, Anderson TR, Irigoien X, Harris R (2006) Feeding and reproduction of *Calanus finmarchicus* during non-bloom conditions in the Irminger Sea. *J Plankton Res* 28:1167–1179.
- Menden-Deuer S, Lessard EJ (2000) Carbon to volume relationships for dinoflagellates, diatoms, and other protist plankton. *Limnol Oceanogr* 45:569–579.
- Menden-Deuer S, Lessard EJ, Satterberg J (2001) Effect of preservation on dinoflagellate and diatom cell volume and consequences for carbon biomass predictions. *Mar Ecol Prog Ser* 222:41–50.
- Menden-Deuer S, Lessard EJ, Satterberg J, Grünbaum D (2005) Growth rates and starvation survival of three species of the pallium-feeding, thecate dinoflagellate genus *Protoperidinium*. *Aquat Microb Ecol* 41:145–152.
- Millette NC, Pierson JJ, Aceves A, Stoecker DK (2017) Mixotrophy in *Heterocapsa rotundata*: A mechanism for dominating the winter phytoplankton. *Limnol Oceanogr* 62:836–845.
- Millette NC, Stoecker DK, Pierson JJ (2015) Top-down control by micro- and mesozooplankton on winter dinoflagellate blooms of *Heterocapsa rotundata*. *Aquat Microb Ecol* 76:15–25.
- Montagnes DJS, Allen J, Brown L, Bulit C, Davidson R, Fielding S, Heath M, Holliday NP, Rasmussen J, Sanders R, Waniek JJ, Wilson D (2010a) Role of ciliates and other microzooplankton in the Irminger Sea (NW Atlantic Ocean). *Mar Ecol Prog Ser* 411:101–115.
- Montagnes DJS, Dower JF, Figueiredo GM (2010b) The protozooplankton-ichthyoplankton trophic link: An overlooked aspect of aquatic food webs. *J Eukaryot Microbiol* 57:223–228.
- Montagnes DJS, Kimman SA, Atkinson D (2003) Using Q10: Can growth rates increase linearly with temperature? *Aquat Microb Ecol* 32:307–313.
- Monti-Birkenmeier M, Diociaiuti T, Badewien TH, Schulz AC, Friedrichs A, Meyer B (2021) Spatial distribution of microzooplankton in different areas of the northern Antarctic Peninsula region, with an emphasis on tintinnids. *Polar Biol* 44:1749–1764.
- MTW, Parzen E, Tanabe K, Kitagawa G (1998) Selected Papers of Hirotugu Akaike.
- Nejstgaard JC, Gismervik I, Solberg PT (1997) Feeding and reproduction by *Calanus finmarchicus*, and microzooplankton grazing during mesocosm blooms of diatoms and the coccolithophore *Emiliana huxleyi*. *Mar Ecol Prog Ser* 147:197–217.
- Nohe A, Goffin A, Tyberghein L, Lagring R, De Cauwer K, Vyverman W, Sabbe K (2020) Marked changes in diatom and dinoflagellate biomass, composition and seasonality in the Belgian Part of the North Sea between the 1970s and 2000s. *Sci Total Environ* 716.

- O'Brien TD, Wiebe PH, Falkenhaus T (eds. (2013) ICES Zooplankton Status Report 2010/2011. ICES Cooperative Research Report No. 318.
- Oksanen J, Kindt R, Legendre P, O'Hara B, Stevens MHH, Oksanen MJ, Suggests M (2007) The vegan package. *Community Ecol Packag* 10:719.
- Olenina I (2006) Biovolumes and size-classes of phytoplankton in the Baltic Sea.
- Pebesma EJ (2004) Multivariable geostatistics in S: the gstat package. *Comput Geosci* 30:683–691.
- Pinheiro J, Bates D (2006) *Mixed-effects models in S and S-PLUS*. Springer science & business media.
- Pinheiro J, Bates D, DebRoy S, Sarkar D, Heisterkamp S, Van Willigen B, Maintainer R (2017) Package 'nlme'. *Linear nonlinear Mix Eff Model* version 3:274.
- Pomeroy LR (2001) Caught in the food web: Complexity made simple? *Sci Mar* 65:31–40.
- Quante M, Colijn F (2016) North Sea Region Climate Assessment (NOSCCA).
- Le Quéré C, Harrison SP, Prentice IC, Buitenhuis ET, Aumont O, Bopp L, Claustre H, Cotrim Da Cunha L, Geider R, Giraud X, Klaas C, Kohfeld KE, Legendre L, Manizza M, Platt T, Rivkin RB, Sathyendranath S, Uitz J, Watson AJ, Wolf-Gladrow D (2005) Ecosystem dynamics based on plankton functional types for global ocean biogeochemistry models. *Glob Chang Biol* 11:2016–2040.
- Regaudie-De-Gioux A, Duarte CM (2012) Temperature dependence of planktonic metabolism in the ocean. *Global Biogeochem Cycles* 26:1–10.
- Reid FMH, Stewart E (1989) Nearshore microplanktonic assemblages off southern California in February 1983 during the El Niño event. *Cont Shelf Res* 9:37–50.
- Riisgaard K (2014) Trophic role of Protozooplankton in northern marine ecosystems. PhD Thesis.
- Rose JM, Caron DA (2007) Does low temperature constrain the growth rates of heterotrophic protists? Evidence and implications for algal blooms in cold waters. *Limnol Oceanogr* 52:886–895.
- Shepard D (1968) A two-dimensional interpolation function for irregularly-spaced data. *Proc 1968 23rd ACM Natl Conf ACM* 1968:517–524.
- Sherr EB, Sherr BF (1994) Bacterivory and herbivory: Key roles of phagotrophic protists in pelagic food webs. *Microb Ecol* 28:223–235.
- Stoecker DK, Sieracki ME, Verity PG, Michaels AE, Haugen E, Burkill PH, Edwards ES (1994) Nanoplankton and protozoan microzooplankton during the JGOFS North Atlantic Bloom Experiment: 1989 and 1990. *J Mar Biol Assoc United Kingdom* 74:427–443.
- Utermöhl H (1958) Zur Vervollkommnung der quantitativen Phytoplankton-Methodik. *SIL Commun 1953-1996* 9:1–38.
- Wiackowski K, Doniec A, Fyda J (1994) An Empirical Study of the Effect of Fixation on Ciliate Cell Volume. *Mar Microb Food Webs*:59–69.
- Widdicombe CE, Eloire D, Harbour D, Harris RP, Somerfield PJ (2010) Long-term phytoplankton community dynamics in the Western English Channel. *J Plankton Res* 32:643–655.

- Wiltshire KH, Manly BFJ (2004) The warming trend at Helgoland Roads, North Sea: Phytoplankton response. *Helgol Mar Res* 58:269–273.
- Yang J, Huang S, Fan W, Warren A, Jiao N, Xu D (2020) Spatial distribution patterns of planktonic ciliate communities in the East China Sea: Potential indicators of water masses. *Mar Pollut Bull* 156:111253.
- Yang J, Löder MGJ, Wiltshire KH (2014) A survey of ciliates at the long-term sampling station 'Helgoland Roads', North Sea. *Helgol Mar Res* 68:313–327.

Chapter 2

Automated Plankton Classification with a Dynamic Optimization and Adaptation Cycle



Drawings adapted from Justine Courboulès

Automated Plankton Classification with a Dynamic Optimization and Adaptation Cycle

Jan Conradt^{1*}, Gregor Börner¹, Ángel Lopez-Urrutia², Christian Möllmann¹, Marta Moyano³

Abstract

With recent advances in Machine Learning techniques based on Deep Neural Networks (DNNs), automated plankton image classification is becoming increasingly popular within the marine ecological sciences. Yet, while the most advanced methods can achieve human-level performance on the classification of everyday images, plankton image data possess properties that frequently require a final manual validation step. On the one hand, this is due to morphological properties manifesting in high intra-class and low inter-class variability, and, on the other hand is due to spatial-temporal changes in the composition and structure of the plankton community. Composition changes enforce a frequent updating of the classifier model via training with new user-generated training datasets. Here, we present a Dynamic Optimization Cycle (DOC), a processing pipeline that systematizes and streamlines the model adaptation process via an automatic updating of the training dataset based on manual-validation results. We find that frequent adaptation using the DOC pipeline yields strong maintenance of performance with respect to precision, recall and prediction of community composition, compared to more limited adaptation schemes. The DOC is therefore particularly useful when analyzing plankton at novel locations or time periods, where community differences are likely to occur. In order to enable an easy implementation of the DOC pipeline, we provide an end-to-end application with graphical user interface, as well as an initial dataset of training images. The DOC pipeline thus allows for high-throughput plankton classification and quick and systematized model adaptation, thus providing the means for highly-accelerated plankton analysis.

Keywords: Machine Learning, Deep Neural Networks, plankton community, classification, model adaptation

Authors' affiliation

¹Institute of Marine Ecosystem and Fishery Science, Universität Hamburg, Hamburg, Germany,

²Centro Oceanográfico de Gijón, Instituto Español de Oceanografía, Gijón, Spain

³Department of Natural Sciences, Universitetet i Agder, Kristiansand, Norway

Introduction

Plankton is a diverse group of organisms with a key role in marine food-webs and biogeochemical cycles (e.g. Castellani & Edwards, 2017). It is furthermore responsible for about 50% of the global primary production, and they serve as prey for upper trophic levels and as recyclers of organic matter. Changes in their abundance, biogeography or size structure can thus lead to large changes at the ecosystem level (e.g. Capuzzo et al., 2017; Frederiksen et al., 2006). Climate change in particular can cause major changes in plankton community characteristics. The range of specific research on plankton in the ecological context is wide, covering issues such as the effect of ocean acidification on calcifying organisms (e.g. Stern et al., 2017), migrations of plankton taxa in response to ocean warming (Beaugrand, 2012), or the determination of available food biomass to larval fish at changing hatching times (Asch et al., 2019; Durant et al., 2019). Ultimately, however, many of these address – directly or indirectly – the effects of environmental change on the abundance of commercially exploited marine fish species, which are dependent on plankton either as food for their early life-stages, or as food of their prey. As plankton forms the base of any marine food web, climate effects are propagated to higher trophic levels via the response of the plankton community to climate change (Nagelkerken et al., 2017; Winder & Sommer, 2012). Monitoring its composition and abundance is hence of great importance to understanding the effects of climate change on the entire marine ecosystem and services it provides to humanity.

The study of plankton in an environmental context is both quantitative and qualitative in nature. While certain plankton estimates (e.g. phytoplankton biomass) can be inferred from analysis of satellite imagery, most studies require abundance indices of specific taxa that can only be derived from sampling plankton in situ and determining its composition. Depending on the research subject, the taxonomic, life-stage and size composition of plankton can e.g. indicate the presence of a community specific to a certain water mass / current (Russell, 1939; Beaugrand et al., 2002), an abundance shift of potentially climate-sensitive species, or the abundance of planktonic food suitable to a particular predator of interest (Dam & Baumann, 2017).

Traditionally, plankton samples have been analyzed by humans with optical devices like microscopes (Wiebe et al., 2017). The accuracy of taxonomic classification was usually high when done by experienced personnel, but it could decrease significantly in complex tasks, such as the differentiation between morphologically similar taxa (Culverhouse et al., 2003). Additionally, sample processing rate is limiting the total number of samples that could be processed using traditional microscopy. The introduction of plankton-image recorders for both in situ (e.g. Video Plankton Recorder, VPR, (Davis et al., 1992)) and/or fixed samples (e.g.

Flow Cytometer and Microscope (FlowCAM®; Sieracki et al., 1998)), together with the development of image-classification algorithms, has led to great advances in the processing of plankton samples over the last two-to-three decades (e.g. Kraberg et al., 2017; Lombard et al., 2019; Goodwin et al., 2022). Image recording enables the temporally unlimited storage of visual information even for samples that cannot withstand fixing agents for a long time. Furthermore, given that the photographs are stored on disk, all visual information is kept permanently, and is available for discussion, unlike the memories of an expert. However, one of the challenges of these plankton image-recording devices (like VPR or FlowCam) is the large number of images that need to be classified (e.g. > 52 million in Briseno-Avena et al. 2020). So far, classification models are intended to greatly increase classification speed, be it via an entire replacement of expert classification with model predictions (Briseno-Avena et al. 2020), or by yielding a rough pre-sorting that alleviates expert validation (Álvarez et al., 2014).

Image classification models were introduced in the late 1980s, first in the form of Neural Networks (NN), which were famously employed for the classification of handwritten digits by the US postal service (LeCun et al., 1989). In the mid-1990s, these were temporally superseded by Support-Vector Machines (SVMs), and for the first time applied for plankton classification in 1998 by Tang et al. (1998). Neural Networks were, at that time, relatively simple in design and could only be applied for simple classification tasks, e.g. discriminating between the clearly-shaped digits. While theory allowed the design of larger NNs for more complex targets like plankton images, constraints in computational power put a temporary constraint on this (e.g. Gu et al., 2018).

SVMs became the tool of choice for plankton classification in the 2000s and early 2010s due to relatively strong performance (e.g. Álvarez et al., 2012). However, they were limited in capability and convenience-of-use by the need for human-defined features for class-discrimination (a limitation not present in NNs). Such “feature-engineering” was required to reduce the enormous amount of information contained in an image (a data point in R^n -dimensional space, n being the number of pixels) to details required to automatically tell classes apart (Scholkopf & Smola, 2002). Many publications of that time concerned the engineering of new features for better class separation, and the problem of the redundancy of devised features (e.g. Tang et al., 1998; Tang et al., 2006; Li et al., 2014). Even then, unique difficulties posed by plankton images became apparent, including the transparent nature of many plankton taxa and morphological similarities between classes.

Computational power increased strongly in parallel to SVMs reaching their peak of popularity, and NNs eventually regained strong popularity (e.g. Chollet, 2017). In 2012, Krizhevsky et al. won the ImageNet contest with a so –called Deep Convolutional Neural Net (CNN), beating the peak performance achieved in the years prior by a before-unachieved margin. The

advances in classification accuracy led to massive investments into the design and application of Deep Neural Nets (the “parent class” of CNNs) in research and economy (Chollet, 2017).

Plankton classification eventually followed suite in this general trend (e.g. Orenstein et al., 2015; Al-Barazanchi et al., 2018), due to the capability of “deep” CNNs to devise and select features themselves; a process colloquially termed “Artificial Intelligence” (AI). CNNs are essentially a complex extension of multinomial regression, whereby the model input, the image, is an array of pixel values, and the output a quasi-“one-hot”-encoded class vector. The vector dimension with maximum value is taken as the predicted class index. Different from simple regression, several “layers” of neurons – essentially arrays or vectors, lie in-between the model input and output. These contain abstracted information from the image, with parameters between any element of two adjacent arrays or vectors determining the flow of information (i.e., the filtering-out of information) from lower- to higher-order input representation (LeCun et al., 2010). During model fitting, the backpropagation algorithm transmits classification loss to each parameter using differential calculus, allowing for gradient-based optimization of the complex NN (Rumelhart et al., 1986). Backpropagation essentially allows the model to “learn” to filter information “wisely” by optimizing its parameter values over multiple iterations of fitting (e.g. Goodfellow et al., 2016).

Today, CNN classification models can reach accuracies of well over 95 % (e.g. Al-Barazanchi et al., 2018), making automatic plankton classification appearing like a “solved task” at first sight. However, these accuracy values are usually derived from performance on test data originating from the same statistical population as the training data. Thus, these outcomes are only “snapshots” of the range of performances that will occur when a static model is applied to plankton samples that lie outside the “population”, where the training data originate from. More precisely, the plankton community tends to vary strongly in time and space, and this variability is precisely what most plankton researchers are interested in. As new taxa appear in a specific location or as formerly less-frequently encountered taxa increase in abundance, a classification model trained on a plankton community, or a pool of communities, from different geographic or temporal origin will likely perform poorly on the respective new samples. González et al. (2016) noted the variability in model performance on samples of different origins and recommended to focus the development of applications robust to various distances between training set and field samples. Also, the non-homogeneous distribution of plankton taxa in the field means that training datasets are often strongly non-homogeneous in distribution of images over classes, as well. This poses a constraint to the successful training of a CNN, since the resulting model will perform well on the dominating classes, but poorly on lower-abundant ones. Note that this is not necessarily reflected in the general accuracy metric, which only accounts for the total number of correctly classified images pooled over all classes.

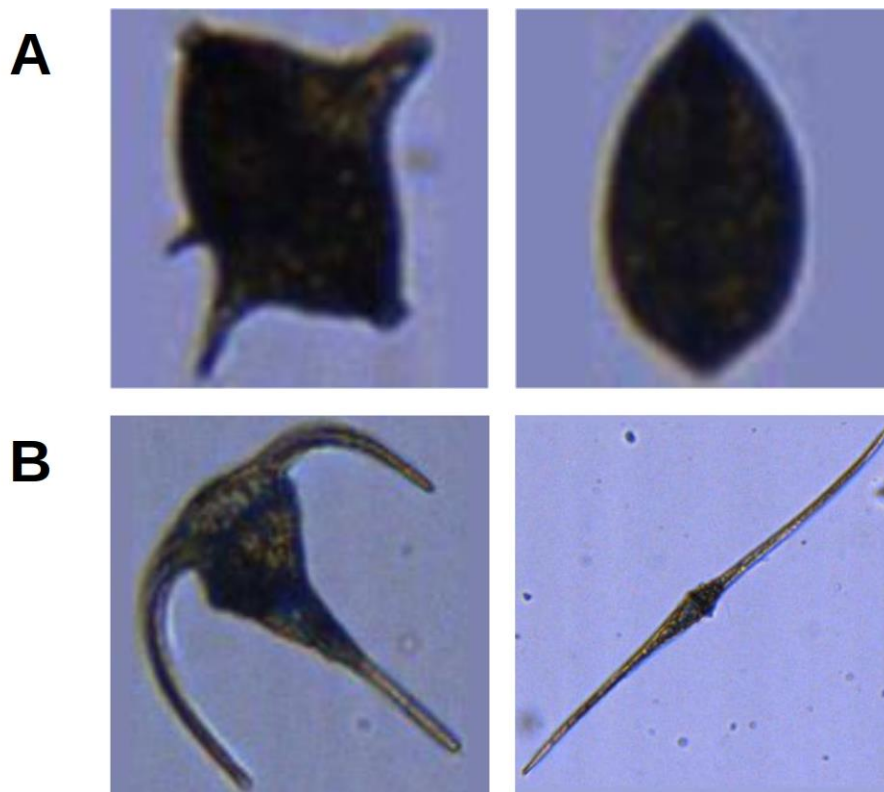


Fig. 1: Examples of strong inter-class similarity (A) and high intra-class similarity (B). (A) A dinoflagellate of the genus *Protoperidinium* (left), and a juvenile bivalve (right). (B) Two dinoflagellates: *Ceratium fusus* (left) and *Ceratium tripos* (right)

One further difficulty in automated plankton classification lies in the high intra-class variability in appearance (which is founded in the existence of sub-taxa, different life-stages or different appearances resulting from different imaging angles), and in sometimes high inter-class similarity (e.g. bivalves and some dinoflagellate taxa, fig. 1), of plankton organisms. Thus, if the intra-class variability is not homogeneously reflected in the training set, the ability of the CNN to discriminate between classes may be limited to only a fraction of the existing sub-classes.

In summary, the current constraints on successful training and application of models for automatic plankton classification are the often limited quality of training sets, and the high spatio-temporal dynamics of the plankton community. Under these circumstances, manual validation and correction of the model results is recommended (Gorsky et al., 2010), as is the adaptation of the model to avoid a decrease in classification performance. The latter usually requires the availability of machine-learning expertise, a commodity often lacking in the marine

sciences (Malde et al., 2020). Research and development should thus be focused on reducing the time required for the validation task and on improving operability of classifier models by non-AI-experts.

Here, we follow González et al.'s (2016) suggestion and propose a pipeline for alleviating the task of model adaptation to a changing plankton community, and thus for reducing the time for manual validation: A “dynamic optimization cycle” (DOC) for iterative use accessible by non-AI-experts. By making applied use of a trained model on field samples, correcting the classification and evaluating model performance through expert knowledge, and updating the model training set and the model itself (through training on the updated image set), the classifier model adapts to spatial and / or temporal changes in the plankton community. It thus maintains high classification performance, ensuring that validation workload remains relatively constant. The systematization of this procedure, and the implementation of the DOC as an end-to-end application with graphical user interface, removes the requirement for expertise in designing and coding CNNs. The DOC was designed for the classification of FlowCam images and the workflow related to studies using the FlowCam, but is likely applicable for other types of plankton images and different types of workflow, as well.

Materials & Equipment

Hardware and software requirements

Training of NNs was performed with a Nvidia® (Santa Clara / California / US) Quadro P2000 GPU with 4 GiB RAM (driver version 410.79) on a Dell® (Round Rock / Texas / US) Precision 5530 notebook with 32 GiB RAM. CUDA® (Nvidia, Santa Clara / California / US) version 10.0.130 was used for enabling the GPU to be used for general purpose processing. Programming was performed in Python 3.6.8 (van Rossum, 1995) using the Spyder Integrated Developer Environment (Raybaut, 2017) with lpython version 7.2.0 (Perez & Granger, 2007). Packages used for analyzing classification outputs included NumPy (Oliphant, 2006) and pandas (McKinney, 2010). Packages used for image pre-processing included Matplotlib (Hunter, 2007), PIL (Lundh & Ellis, 2019) and Scipy (Oliphant, 2007). Tensorflow 1.12.0 (Abadi et al., 2015) and Keras 2.2.4 (Chollet, 2015) (with Tensorflow backend) Advanced Programming Interfaces were used for building, training and application of the classifier models.

Methods

Model design and training

A convolutional neural net (CNN) was built based on the publicly available “VGG16” network architecture (Simonyan & Zisserman, 2015). This architecture consists of 13 convolutional layers, i.e. 13 intermediate data representations in the form of a stack of matrices that account for positional relationships between pixels of the input image. These layers are arranged in five “blocks” of two-to-three layers each, which are connected via non-parameterized information-pooling layers. The sixth block consisting of so-called “dense” layers was removed – as is usually done when applying a pre-defined architecture – and replaced with custom layers: one convolutional layer and two dense layers. The design of this custom “block” of layers - i.e. the number and type of layers, and the number of neurons (i.e. representation dimensions) of each – was the result of a try-and-error approach for achieving satisfying classification performance on training and validation images (Conradt, 2020). Details on the custom layers can be obtained from tab. SI V / 2.

Model parameters were initialized with the values provided together with the VGG16 architecture trained on ImageNet data (Deng et al., 2009.) for the respective part of the model, and with values drawn randomly from a Glorot uniform distribution for the custom layers, as per default in the Keras software. Model training (i.e. fitting) was started with the custom layers and the final block of convolutional layers of the VGG16 “base” set to trainable. Training was performed by feeding all training images in a sequence of batches of 20 randomly chosen images to the model. All other hyper-parameter settings (e.g. optimizer and learning rate for gradient-based fitting) can be obtained from Tab. SI IV / 1. The choice of hyper-parameter settings was based on a series of trial runs for different hyper-parameter set-ups (Conradt, 2020).

The entire set of training images was fed eight times (so-called “epochs”) to the model, with an increasing number of the layers of the VGG16 base being set to trainable (“unfrozen”) each epoch (Tab. SI V / 1). “Unfreezing” is a common procedure applied to ensure that learned features are gradually adapted towards our plankton dataset (VGG16 was originally trained on the ImageNet set of everyday-object images). The chosen number of epochs and the “unfreezing” schedule resulted from optimization through trial-and-error experimentation, as well (Conradt, 2020). They resulted in a steady increase of validation accuracy from approx. 88 % to approx. 94 % and a decrease of validation loss from approx. 0.34 to approx. 0.29 when trained on the baseline training set, though validation loss did increase slightly from a minimum value of approx. 0.26 at the third epoch (fig. SI VII / 1). Validation accuracy was surpassed by training accuracy by the second epoch, which is usually a sign of an onset of over-fitting (e.g.

Chollet, 2017); however, the fact that validation accuracy also still increased over the eight epochs was taken as a sign of a robust training schedule.

We did not utilize data augmentation, a technique in which artificial transformations are randomly applied to the training data to reduce model over-fitting and thus improve its generalizability (e.g. Chollet, 2017). While the approach is frequently applied in various image-classification tasks (e.g. Luo et al., 2018; Plonus et al., 2021), previous work had shown that data augmentation did not markedly improve the classification when applied to a partly identical data set of FlowCam images (Conradt, 2020). This observation has also been made in another instance on an independent plankton data set (Lumini & Nanni, 2019).

While both the set-up of the CNN and the training scheme may not represent an optimal configuration (for example, over-fitting occurred in our experiments), we found the configurations to yield consistently robust results that were sufficient to support research relying on the DOC pipeline (Börner et al., *in prep.*). Given the relatively high validation accuracy, our goal was not to further optimize model design or –training, but instead to maintain this satisfactory performance level over changes in the composition of plankton samples.

Image characteristics

Input image size was set to 120 x 120 x 3 pixels. A size of 256 x 256 x 3 pixels is more commonly used for plankton images (e.g. Al-Barazanchi et al., 2018; Orenstein & Beijbom, 2017; Cui et al., 2018), however preparatory work for the present study had shown that the chosen image size yielded better performance than a larger size, and leads to a faster processing due to the lower data dimensionality (Conradt, 2020). The use of a common square image shape leads to an altered visual appearance of plankton organisms if the original image had a height-length ratio very different from 1. This would increase intra-class variability, an undesirable trait as described above. Therefore, within the DOC pipeline, images are pre-processed via padding, i.e. by adding pixels in background color (the mode pixel value of the outermost pixel row for each color layer) to the sides or top and bottom to achieve square format, a common procedure in plankton-image classification (see e.g. Plonus et al., 2021).

Characteristics of the baseline training set

The baseline image dataset, which is updated as part of the adaptive procedures of the DOC pipeline, consists of 27900 RGB FlowCam images of plankton samples gathered from various North Sea surveys over several years. Images in the dataset were sorted into 15 classes, including 13 taxonomic groups as well as a detritus class and a “clumps” class that contains aggregates of plankton organisms and / or detritus. The distribution of images over classes was designed to reflect general, though not empirically determined, patterns of natural relative

abundance. However, the very abundant detritus class was reduced in relative proportion in order to avoid the learning of a quasi-binary classification scheme (detritus / non-detritus) by the classifier model. A random 80 % of images of each class were used as training images for the baseline model, while 10 % each were reserved for validation and testing purposes (see above). The characteristics of the baseline data set are given in Tab. SI VI / 1.

Classification thresholds

Within the DOC pipeline, the model classification is compared with expert validation. For each class, the relative amount of correct predictions is calculated and used as a threshold value against which the maximum probability value of the CNN output vector (the index of which is the class prediction) is compared. Probability values above the threshold lead to acceptance of the classification, as the model classification is deemed “certain”. Probability values below the threshold lead to rejection of the model classification, the image is then assigned to an “uncertain-classifications” category. Initially, thresholds were set to 60 % for all classes, as the difference between the properties of the baseline training set (on which the baseline model was trained) and the properties of the first station to be classified was deemed to be larger than that between subsequent modified training sets and stations.

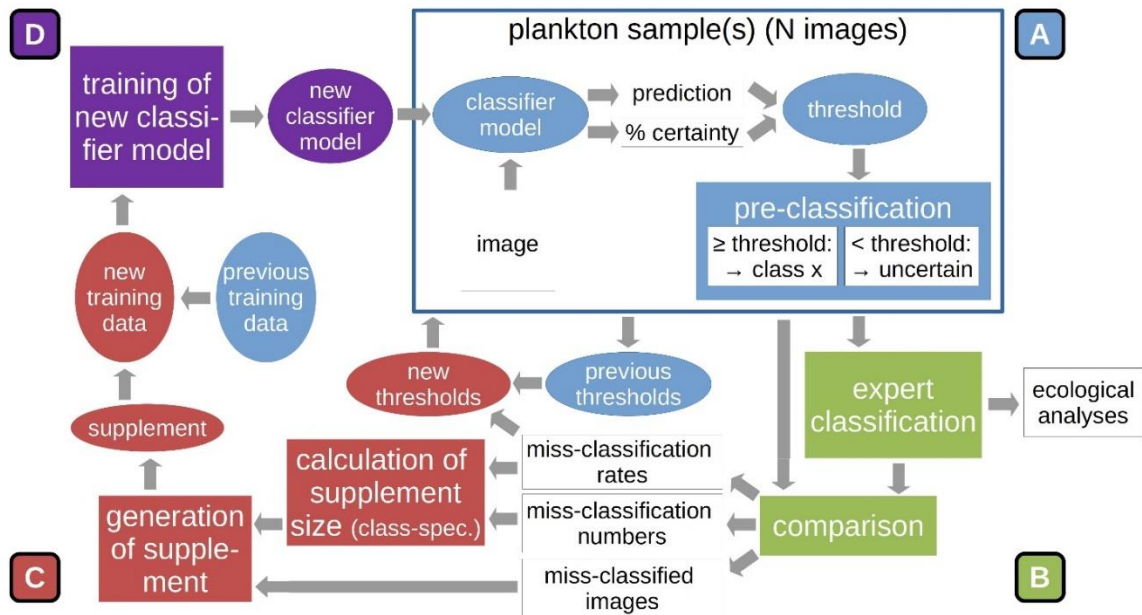


Fig. 2: Sequence of main procedures in the DOC pipeline: After the automatic classification and expert validation of a set of plankton samples (e.g. two), the original model training set is stocked up with a selection of miss-classified images, based on class-specific miss-classification rate. This constrained update reduces the dominance of naturally-abundant classes in the add-on set. A new classifier model is trained on this updated training set (also, not shown here, classification thresholds are reduced based on miss-classification rates). The new model is used to classify the next set of plankton samples.

This procedure was intended to speed up manual validation by implementing a sort out of images based on probability of miss-classification, which can then be checked more easily than if they were not separated from images with high probability of correct classification.

DOC pipeline procedures

The following describes the working steps for applying the DOC onto any given set of plankton samples (see also fig. 2). A more thorough user instruction with technical notes of importance is provided in the appendix.

1) Classification: The DOC pipeline is typically started by applying the provided classifier model directly on the classification of plankton samples, thus allowing for potentially large initial classification error. However, it is also possible to directly train a custom classifier model if the user has already generated a training set from manually labeled images. When creating a custom training set, it is important to limit the number of classes to 10-20. 700-1000 training images should be collected for classes deemed important for research.

The amount of training images for a "detritus" class can be higher (two-to-three-fold) if detritus is abundant, since this class is usually rather heterogeneous in shape and a high capacity for

differentiation between living and non-living particles is often desired (see tab. 3 for the properties of the initial training set used in the present study). The DOC was designed for research questions that primarily require quantitative measurements of major (i.e. abundant) plankton classes, not for qualitative analyses where the importance of taxa is not related to their abundance, e.g. biodiversity surveys. This should be considered when applying the DOC pipeline.

2) Validation: Following the classification of two to three plankton samples, the model classification is validated by a plankton expert. When using the DOC application, this involves moving wrongly-classified images into correct class folders, as the application automatically copies the plankton images into such newly-created folders. Note that expert validation is critical to the functioning of the DOC pipeline. While a full automatization of plankton image classification, i.e. the ability to work directly with model predictions, might be desirable in some applications, model adaptation to a changing plankton community does require expert involvement. The combination of automatic pre-classification with expert validation has been found to be effective for quantitative plankton studies, in particular when used to improve a model training set (Gorsky et al., 2010).

Performance of our baseline model was deemed insufficient to omit expert validation, as predicted relative abundances for certain classes were strongly different from the ground truth (fig. SI VIII / 1; Börner et al., *in prep.*). The DOC pipeline is designed to streamline and accelerate the validation process, as a full automatization of the classification is unlikely to be achievable with limited training data.

The number of samples to classify before continuing with the adaptation steps is likely case-specific and might require some initial trial-and-error experimentation. In our case studies, we classified two samples at a time.

3) Training-set update and threshold reduction: After expert validation, the original model training set is stocked up with images that were wrongly classified by the model, based on class-specific miss-classification rates. To this end, the classification performed by the model and the final validation by the expert are automatically compared. For each class, the correct-classification rate, i.e. the ratio of the number of correct model classifications to the total number of images assigned by the expert to that class, is calculated. The complement of these ratios is then normalized via division by the maximum miss-classification rate over all classes (eq. 1, top). These values are then multiplied by the number of wrongly-classified images of each class to determine the number of images to be added to the training set (eq. 1, bottom). Not selecting all wrongly-classified images reduces the over-proportionality of naturally-abundant, but relatively well-classified classes, e.g. detritus, in the image add-on, putting more emphasis on poorly-classified classes. The number of images added thus depends both on

the number of miss-classified images (and thus also on the size of the classified sample(s)) and on the relative class-specific performance of the model. The images added are selected randomly.

$$p_i = \frac{1 - \frac{C_i}{N_i}}{\max(1 - \frac{C_j}{N_j} \text{ for } j \in \{\text{class } 1 \dots \text{class } n\})}$$

$$A_i = F_i p_i$$

Eq. 1: Calculation of the proportion of miss-classified images to be added to the updated training dataset (top) and calculation of the number of images to be added to the training set (bottom). i = index for classes, p = proportion, C = number of correctly classified images in a given class, N = number of images assigned by expert to that class, A = number of images to be added to the training set, F = number of wrongly-classified images

Before training, 20 % of the images in the updated training set are set aside to serve as validation and test data (10 % each). While validation (during training, to check on model over-fitting) and testing (after training, to evaluate final model performance (e.g. Chollet, 2017)) are performed as part of the DOC application, the results are not of importance for the general usability of the DOC. These results are rather intended to provide users interested in modifying model architecture or training procedure with performance metrics. Note that training set updates are performed on the full 100 % of images of the previous training set (merging training, validation and test images of the back together), and that the setting-aside of 20 % of the images is done thereafter. In the present study, automatically generated validation and test results were not investigated. Instead, model performance was evaluated directly from the classification of survey samples (see below), which can therefore be considered our “test data sets”.

The training-set update constitutes one part of the adaptation procedure, as images are added to the training data based on class-specific miss-classification. A marked temporal or spatial increase in the abundance of a class that was underrepresented in the original training set will lead to that class being better represented in the adapted version of the training set. This also applies to classes and morphologically distinct sub-classes (sub-taxa) not contained in the original training set. It is up to the researcher implementing the DOC to decide whether a new class encountered in a sample should be included in the updated training set. If only very few individuals were encountered, it is not useful to set up a new class in the new training dataset, since with this low amount of training data, it would not be possible to train the model to reliably

recognize that class. In that case, it may make more sense to include the images in a taxonomically related class for the purpose of training-set adaptation.

Furthermore, the original threshold values for automatic culling of likely wrongly-classified images (see above) are multiplied with the aforementioned correct-classification rates. This reduces the threshold percentage value above which a classification will be deemed to be likely correct for classes that receive an increase in training images in the above adaptation step. It is assumed that large threshold values reduce classification performance by the assignment of many correctly-classified images to the “uncertain-classifications” category (images assigned to that category are treated as incorrect classifications). By decreasing the classification threshold, the number of correctly-classified images assigned to the predicted classes can theoretically be increased, leading to higher correct-classification rates. By decreasing classification thresholds more strongly for classes with relatively high miss-classification rate, the assignment of images to “true” class folders will increase for classes that have received an update of training images.

While classification thresholds may also be too low for some classes, with too many wrong classifications not assigned to the “uncertain-classifications” class, we found that the inter-play with the updating of the training set in response to correct-classification rates yielded a good trade-off between maintaining high precision and high recall. Performing only training-set updates or only threshold adaptation yielded higher precision or recall than the combined operations, though at the cost of the respective other metric (SI IX). We do, however, not exclude the possibility that classification performance may be limited at some point due to reduction of thresholds to values close to zero.

4) Model training: The model is then trained on the updated training set according to the training schedule described above. Again, implementing the same training schedule on different training sets can lead to performance loss; an individual experimental adaptation of the training schedule is avoided for the same reason as individual changes to model design (see above). It should be noted that it is not the existing baseline model that is re-trained on the new data; instead, a completely new model instance is generated, with model parameters initialized as described above. This was done to avoid an over-adaptation of the model on the training data, since re-training would have meant training the existing model for an *additional* set of epochs on an adapted but still similar training set (similarity referring to the fact that no original training images are dropped during alteration). Re-training the previous model in each iteration of the DOC was attempted but did not appear to improve results.

Not changing the model design, as is implemented in the DOC pipeline, can lead to lower-than-possible classification performance, since image sets of differing distributions of classes may be classified differently well with a given model design (data set shift; Moreno-Torres et

al., 2012). Still, the DOC concept is focused on streamlining the adaptation procedure; experimentation on model design in each adaptation step would slow down the overall adaptation process. Therefore, changing the model design is not a standard procedure in the DOC, but may be implemented if users find classification performance unsatisfactory in general. DOC users may opt to add the test data to the training set if they are not required for the above-mentioned check to increase the number of training images. In the case studies performed in the present work, this was not done, though, as performance was deemed satisfactory without adding the test images.

After training is completed, the new model can be applied on the next batch of plankton samples, and the cycle of adaptation continues anew. The DOC concept was devised based on the notion that plankton communities would change on a spatial and / or temporal gradient. In the authors' view, it therefore makes most sense to process the plankton samples in the same order as they were taken by the research vessel (or along hydrographical gradients).

User application

A user application with graphical user interface was designed to aid in the implementation of the DOC pipeline. For practical purposes, it is intended that the DOC pipeline be implemented by a broad user group not necessarily familiar in the use of programming languages and / or Machine-Learning techniques. The DOC application was therefore designed to enable an end-to-end implementation of all pipeline steps described above. It consists of a series of executable, partially nested, Python scripts, one executable Bash (GNU, 2007) script that accesses the Python scripts and a comprehensive instruction guide describing the implementation of all DOC-pipeline steps in the application context (SI 1). None of the scripts is protected, which allows users familiar with the Python programming language to edit and change scripts in order to make custom changes to the pipeline processes, if desired.

The DOC application was written in the Python programming language, making extensive use of the *TkInter* package for graphical-user-interface design (Lundh, 2019) and of the *os* package for file-system access. One script utilized to start the application was written in the Bash command language.

The DOC application was designed for use on Linux (The Linux Foundation, San Francisco / CA) operating systems (tested on Ubuntu 18 and Linux Mint 19). It requires hardware and drivers enabling the training and application of Deep Neural Networks for image classification. For the application development and for conducting the case studies, a Nvidia® Quadro P2000 graphics-processing unit (GPU) was utilized. Further system details are given in SI II. The DOC application requires the installation of Python 3 (was tested under Python 3.6) via the Anaconda (Anaconda Software Distribution, 2020) distribution, and the creation of a dedicated

Python environment containing i.a. the packages Tensorflow (Abadi et al., 2015) and Keras (Chollet, 2015). Full details on the environment setup are given in SI III.

The DOC application is started via the Bash script, whereupon each of the DOC processes can be started. The single processes can be executed in the order described above and suggested in the instruction manual, but can also be executed singularly, e.g. when only image classification, but not the implementation of the full DOC pipeline is desired.

The DOC user application will be made available on github.com/JanCo93 upon publication. The baseline training set is planned for a release on zenodo.org at the time of publication.

Case studies – North Sea surveys

The DOC pipeline was applied to samples taken on two plankton surveys in order to test the performance of the approach.

The surveys were conducted in autumn and winter 2019 in the Western North Sea (Fig. 3). The first survey, undertaken in September 2019, started offshore the East Coast of Scotland at approx. 57.5 °N / 0 °E, and moved gradually closer to the British coast in a zig-zag trajectory between approx. 56.2 °N and 57.5 °N. Samples were taken at these two latitudes and at approx. 57.9 °N. The second survey was conducted in December 2019 in the English Channel, starting at the eastern entrance of the Channel at approx. 51.6 °N / 2 °E, continuing south-westwards until approx. 50.25 °N / -1 °E, and changing direction north-east-wards, for a route parallel to but closer to the French coast than the initial trajectory (fig. 3). Plankton samples were taken with a PUP net (mesh size: 55 µm) attached to a GULF VII sampler (HYDRO-BIOS Apparatebau GmbH), which was towed in double-oblique hauls.

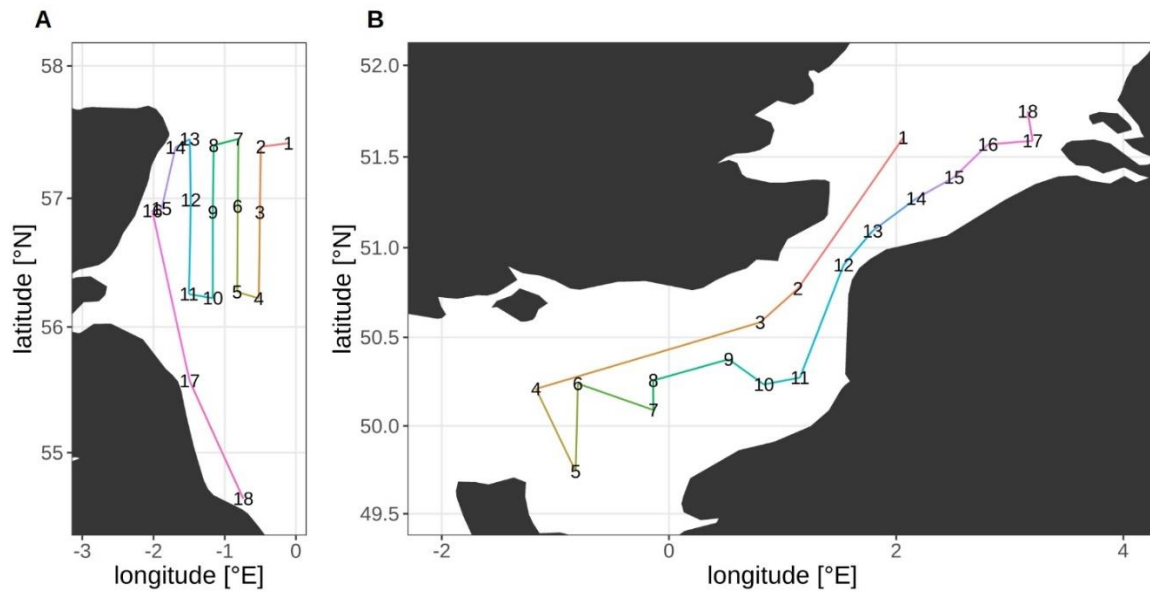


Fig. 3: Survey transects and location of the sampling stations from the September (A) and December (B) surveys.

Plankton samples were stored in 4%-formaldehyde-seawater solution. Once in the laboratory, samples were processed using a FlowCam, following the FlowCam® Manual V 3.0 (Fluid Imaging Technologies, 2011), as described in Börner et al. (*in prep*). The FlowCam flow chamber had a depth of 300 μm , which was also the maximum size of plankton particles processed by the apparatus (the minimum particle size was determined by the PUP net mesh size of 55 μm). Flow rate was set to 1.7 mL min^{-1} , in order to achieve high image quality at an acceptable processing speed. Using the AutoImage mode of the FlowCam's Visual Spreadsheet software, images were saved for later processing.

For both surveys, the DOC pipeline was implemented for the classification of 18 samples, with the samples being processed in the sequence they were taken at sea (one sample was taken at each station). The processing sequence equals a spatial and temporal trajectory through plankton habitat. The adaptation procedure was implemented every second station, pooling the images for both stations in order to calculate the misclassification rate and to supply the information for the update of the training set. Classification performance was then calculated for each pair of stations (see below), which in the end yielded a performance trajectory over the survey samples and adaptation steps. Each mark on the trajectory thus constituted the performance of one specific model (trained on one specific version of the training set) applied to one specific set of images. In the Machine-Learning context, this information yielded the *test performance* of the models at the different adaptation steps, i.e. and indicator of their performance on non-training images under constant field conditions (e.g. Chollet, 2017).

In order to assess the importance of the continuous adaptation, a set of reference runs was performed: After each adaptation step, the current model was saved, and all subsequent samples were classified with this model (previous samples were not classified, as images contained in these were introduced into the training set during previous adaptation cycles). This way, we generated a set of reference classification trajectories in which adaptation is stopped after various numbers of samples processed (and thus on different points of the survey trajectory). This set was used to assess the value of continuous adaptation of the training set and the training of new models thereon: By comparing the performance of an adapted model to a non-adapted or less-adapted model at a specific mark on the classification trajectory, the value of adaptation could be determined for a specific sample or point on the survey trajectory. Integrated over all samples, this allowed evaluating the performance of DOC-based adaptation over the survey- / adaptation trajectory, with respect to overall advantage and potential temporal dynamics in the magnitude of adaptation advantage.

With eight adaptation steps, nine different classification trajectories resulted in total: The fully-adaptive pathway (with one adaptation cycle and the usage of a new model every second station), and eight pathways in which adaptation was stopped at a specific station (fig. 4).

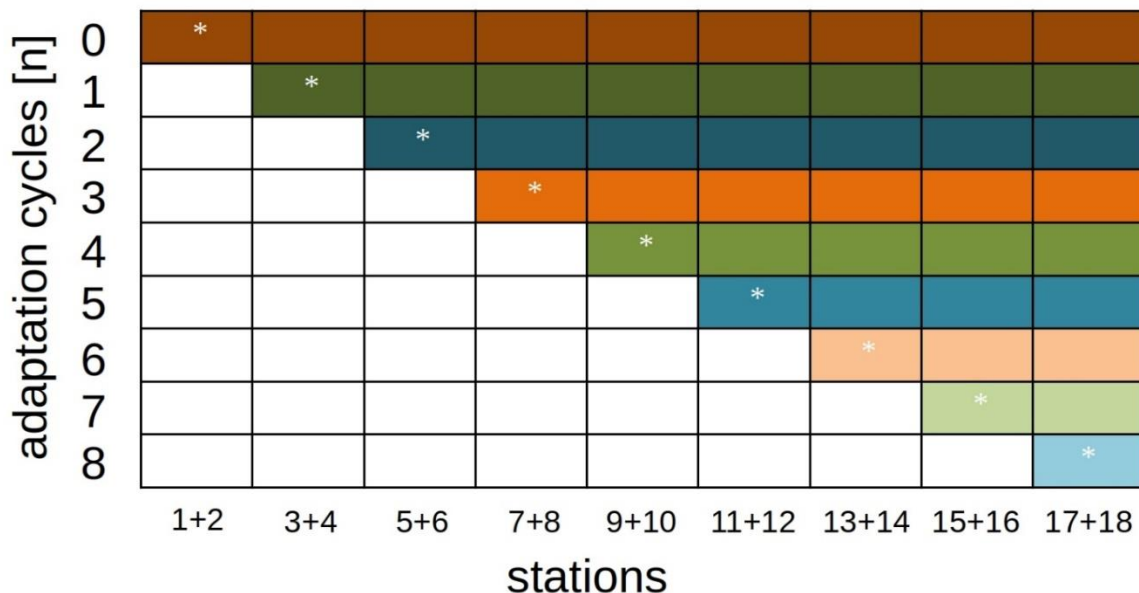


Fig. 4: Model-adaptation / station-classification schedule for performance analyses. The diagonal row (marked with stars) represents the fully-adaptive implementation of the DOC pipeline, where an adaptation is implemented every second station. All other colored rows shows reference runs where samples are classified with an existing model and without further adaptation.

We implemented the adaptation pathway twice for each survey to account for random effects in the adaptation procedure. These primarily include the parameter initialization before training of every models (i.e., at every adaptation step) except the base model (which was always identical) and the selection of miss-classified images for the updating of the training dataset.

Analysis of classification performance

Three performance metrics were calculated for comparison of the model classification and the expert classification (the result of the validation step):

I) Recall is the class-specific ratio of correctly-classified images (true positive classifications) to the total number of images (true positive plus false negative classifications), where the total number is defined by the expert classification (eq. 2). This metric indicates the expert effort required to find miss-classified images in all other class folders.

II) Precision is the class-specific ratio of correctly-classified images (true positive classifications) to the sum of correctly-classified images (true positive classifications) and wrongly-classified images (false positive classifications), where the total number is defined by the expert classification (eq. 2). This metric indicates the expert effort required to find all images that were mistakenly assigned to a specific class folder.

$$recall = \frac{n(true\ positive)}{n(true\ positive) + n(false\ negative)}$$

$$precision = \frac{n(true\ positive)}{n(true\ positive) + n(false\ positive)}$$

Eq. 2: Definitions of recall and precision (class-specific metrics)

Of these two metrics, means and standard deviations weighted by class abundance (number of images assigned by expert to a specific class) were calculated for each pair of stations and each adaptation trajectory. Recall and precision values for “detritus”, “clumps” and “uncertain predictions” classes were not included in the mean calculations in order to focus on the living components of the plankton (which are the target of plankton research). More specifically, they were excluded from the calculation of average recall, since miss-classification of detritus is of little concern in research focusing on living biomass, and clumps are miss-classifications per se, since a researcher would need to analyze clumps compositions manually anyway. The three classes were excluded from calculation of average precision, since the direct aim of achieving high precision is to reduce the effort of removing miss-classified images from a given class folder. Since detritus, clumps and uncertain classifications are not directly of interest in plankton research, the desire to achieve “clean” folders for these classes is comparatively low.

III) Categorical cross entropy (hereafter referred to simply as “cross-entropy”) measures the loss between a true and a predicted distribution (eq. 3). We calculated this metric for the true (derived from expert classification) relative class abundances with the predicted (derived from model classification) relative class abundances. In our application, cross-entropy measures the goodness of predicting the quantitative plankton-community composition. Again, the “detritus”, “clumps” and “uncertain predictions” classes were not included in the cross-entropy calculation. For classes with a predicted relative number of zero, this value was set to one divided by the total number of images at a given station (the cross-entropy is not defined for data including zero-values; hence, we artificially introduce one correct classification, which we assume to be a plausible stochastic error given numbers of images per station of usually more than ten-thousand). We compared cross-entropy with class-specific differences between true and predicted relative abundance to analyze the driving factors behind changes in cross-entropy, i.e. in the goodness of prediction of the plankton-community composition.

$$\gamma_i = - \sum_{i=1}^{N_c} a_i \log \hat{a}_i$$

Eq. 3: Categorical cross entropy (γ). a = true relative abundance, \hat{a} = predicted relative abundance, N_c = number of classes

Cross-entropy represents information loss between true and predicted distributions, which makes it difficult to interpret single values. Therefore, we used the metric exclusively for comparative purposes (e.g. comparing the cross-entropy between different adaptation modes).

Analyses and visualization were performed in R version 3.6.3 (R Core Team, 2020), partially using the packages “tidyverse” (Wickham et al., 2019), “viridis” (Garnier, 2018) and “radiant.data” (Nijs, 2020).

Results

Overall performance in the fully-adaptive mode of the DOC was relatively high with regard to recall, with weighted means ranging between approx. 82 and 92 % over all survey-station pairs. Precision was lower, with weighted means ranging between approx. 50-75 % for the September survey, and approx. 60-80 % (with one very low value of 30 % at start) for December. Performance was sufficiently large to enable successful usage of the DOC application in the context of experimental research work, which benefitted from the time-savings through semi-automatic classification and model adaptation (Börner et al., *in prep.*).

Altogether, a fully-adaptive implementation (adaptation cycle implemented every second station) of the DOC frequently achieved comparatively high or top level mean performance in recall and precision metrics, though absolute and comparative performance varied between both survey month, and, more strongly, between classes (for details see below). Performance gains were often largest in the first one to two adaptation cycles, i.e. after the first adaptation of the baseline training set.

Recall

Overall, there were no clear trends in mean recall development over stations for the larger part of the classification trajectory, neither in the fully-adaptive nor in the less-adaptive implementations (fig. 5): In the September trajectory, mean recall for the fully-adaptive mode decreased from approx. 90 % by approx. 10 % after the third station pair (stations 5 and 6), and increased again somewhat after stations 11 and 12. Mean recall at stations 17 / 18 was approx. 91 %. In the December trajectory, mean recall for the same mode increased strongly between stations 3 / 4 and stations 5 / 6, from approx. 20 % to slightly over 90 %. Recall remained at a relatively high, though slightly decreasing level, having a final value of approx. 85 % at stations 17 / 18.

Relative performance to less adaptive DOC implementations differed initially strongly between the two surveys, but became more similar thereafter. While in the September samples no large performance difference was visible between the adapted and the baseline model at stations 2 / 3, recall for the more adaptive model strongly outperformed that of the less adaptive one in the December samples, as a value of over 90 % was achieved with the former, while no marked performance difference to the first station (approx. 20 % mean recall) was detected in the latter. With the exception of the baseline model used for the December samples, which remained at low-level performance of approx. 40 % mean over the trajectory, recall of the fully-adaptive mode was not markedly superior or even somewhat inferior (in the December samples) to that of less adaptive approaches, depending on the replicate. Performance of all adaptive modes converged to a relatively similar value (approx. 91 %) in the final September sample (see also fig. SI X / 1). Convergence was not present in the December samples.

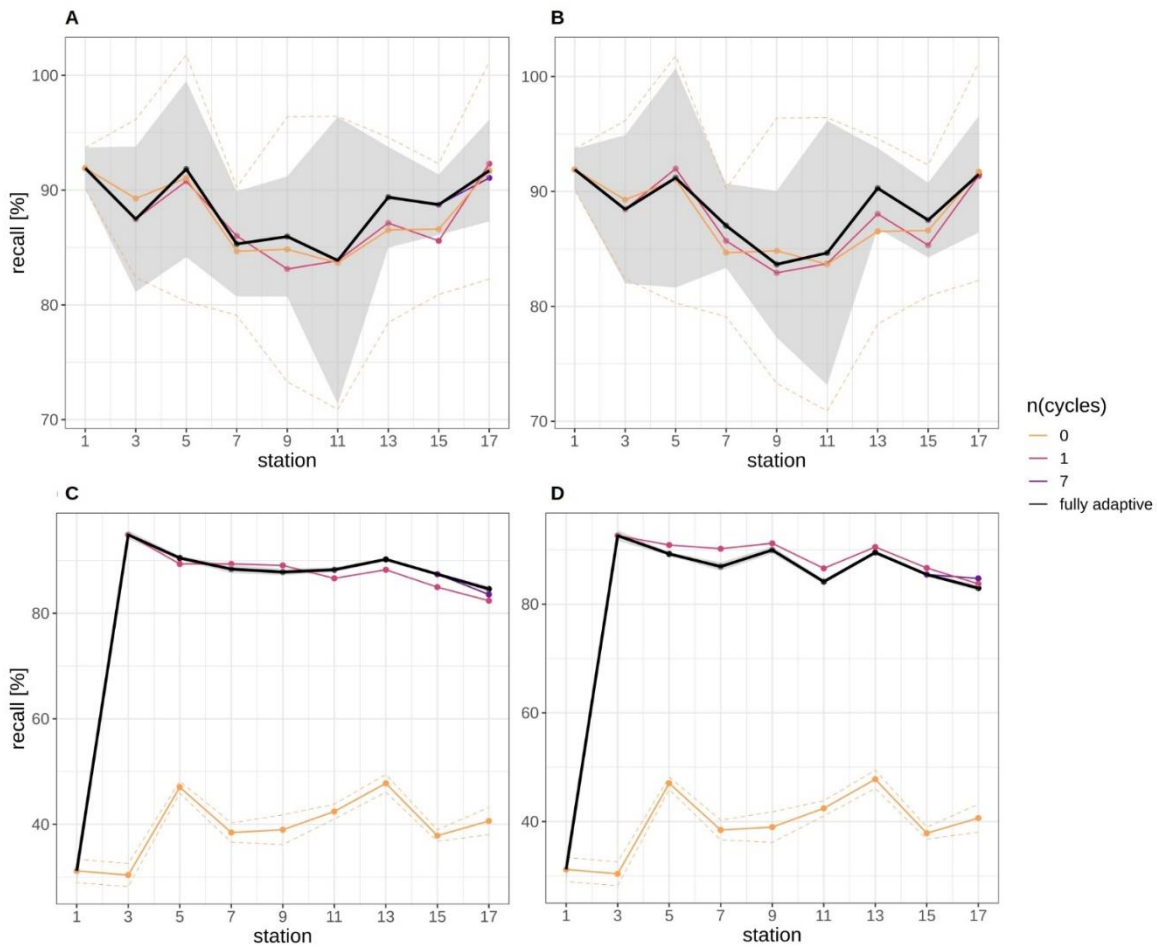


Fig. 5: Recall trajectories for different modes of adaptation using the DOC. Solid black line represents weighted mean of the fully-adaptive implementation, grey area denotes the corresponding weighted standard deviation. Colored solid and dashed lines represent weighted mean and weighted standard deviation of less-adaptive implementations (denoted by the number of adaptation cycles). (A), (B): September survey; (C), (D): December survey. Results for two replicates are shown for each survey. Note that weighted standard deviation for the fully-adaptive implementation in the December survey was not omitted, but is very small compared to that in the September survey. Trajectories for all nine adaptation modes are shown in fig. SI X / 1.

Recall trajectories differed strongly between classes, and showed stronger fluctuations between station pairs than the weighted mean trajectory over all classes, with values of zero and 100 % being reached occasionally (figs. 6, SI X / 2). Trajectories for the fully-adaptive implementation of the DOC were relatively similar between replicates, though. For many classes, a recall of markedly over 90 % was achieved at least occasionally in fully adaptive mode, although the identity of these classes differed between September and December surveys. Classes for which a relatively high recall was frequently achieved (though not necessarily consistently over all stations) included *Ceratium* spp., *Protoperdinium* spp. (September survey only), copepods, detritus and diatoms. All other classes showed relatively high performance at least once in the recall trajectory; thus it is not possible to name classes for which recall was particularly poor. The comparative performance of the fully-adaptive

implementation of the DOC varied strongly between classes, as well. Furthermore, performance also varied between surveys, and to a smaller extent between replicates. For some classes, such as bivalves (September), detritus (both surveys), diatoms (both surveys), dinoflagellates (September), foraminiferans (September), unknown taxa A, B and C (only present in September), as well as copepods (December), the fully-adaptive implementation yielded near- or top-level performance over the larger part of the stations trajectory. For other classes, including copepods (September) and *Dinophysis* spp. (September), comparative performance was relatively constantly poor. It should be noted that performance differences between different modes of adaptation were of various magnitudes between classes. In most classes, the recall trajectory of the fully-adaptive implementation followed the general trend shown by all modes of adaptation.

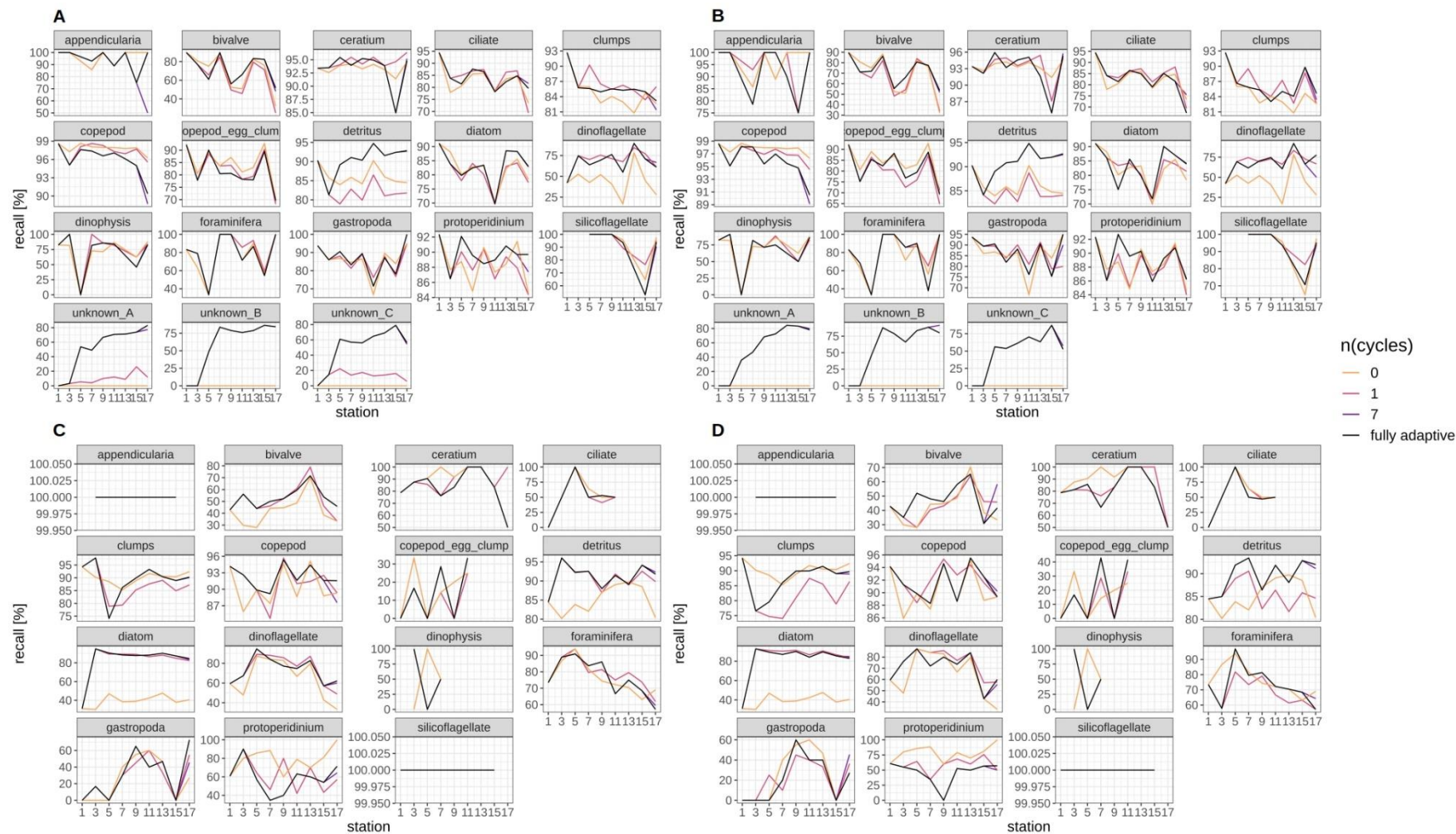


Fig. 6: Class-specific recall for the September (**A**, **B**) and December (**C**, **D**) surveys. Results for two replicates are shown for each survey. Black line represents fully adaptive DOC implementation (training-set update every second station); colored lines represent less-adaptive implementations (denoted by the number of adaptation cycles). Trajectories for all nine adaptation modes are shown in fig. SI X / 2.

Precision

In general, mean precision increased in both survey trajectories slightly, in all but the two least adaptive implementations of the DOC after a more variable initial phase (first two station pairs) (fig. 7). Mean precision increased from approx. 60 % at stations 5 / 6 to approx. 75 % at stations 15 / 16 in the September survey, and from approx. 65 % to approx. 80 % in the December survey. Mean precision then decreased again from stations 15 / 16 to station 17 / 18, from the mentioned values to approx. 63 % in the September survey, and to approx. 70 % in the December survey. Altogether, the trajectory of mean precision was smoother for the December survey, i.e. there was little fluctuation between adjacent station pairs.

Different from the recall trajectories, mean precision of the fully-adaptive mode of the DOC was frequently at top level compared to less-adaptive modes, in both the September and the December survey (for almost every station in the latter) (see also fig. SI X / 3). The zero-adaptive implementation (use of the baseline model for all classifications) showed markedly lower performance than all other implementations over the full trajectory in the December samples, while lowest performance was achieved by the one-time-adapted model in the September samples. In the latter case, the performance difference was not as pronounced as in the September samples, though. While mean precision for the weakest-performing mode was relatively constant to slightly decreasing in the September survey (approx. 55 % at stations 5 / 6 to approx. 50 % at stations 17 / 18), it did temporarily increase from stations 7 / 8 to a peak at stations 13 / 14 (from approx. 20 % to approx. 75 % to approx. 25 % at stations 17 / 18) in the December survey.

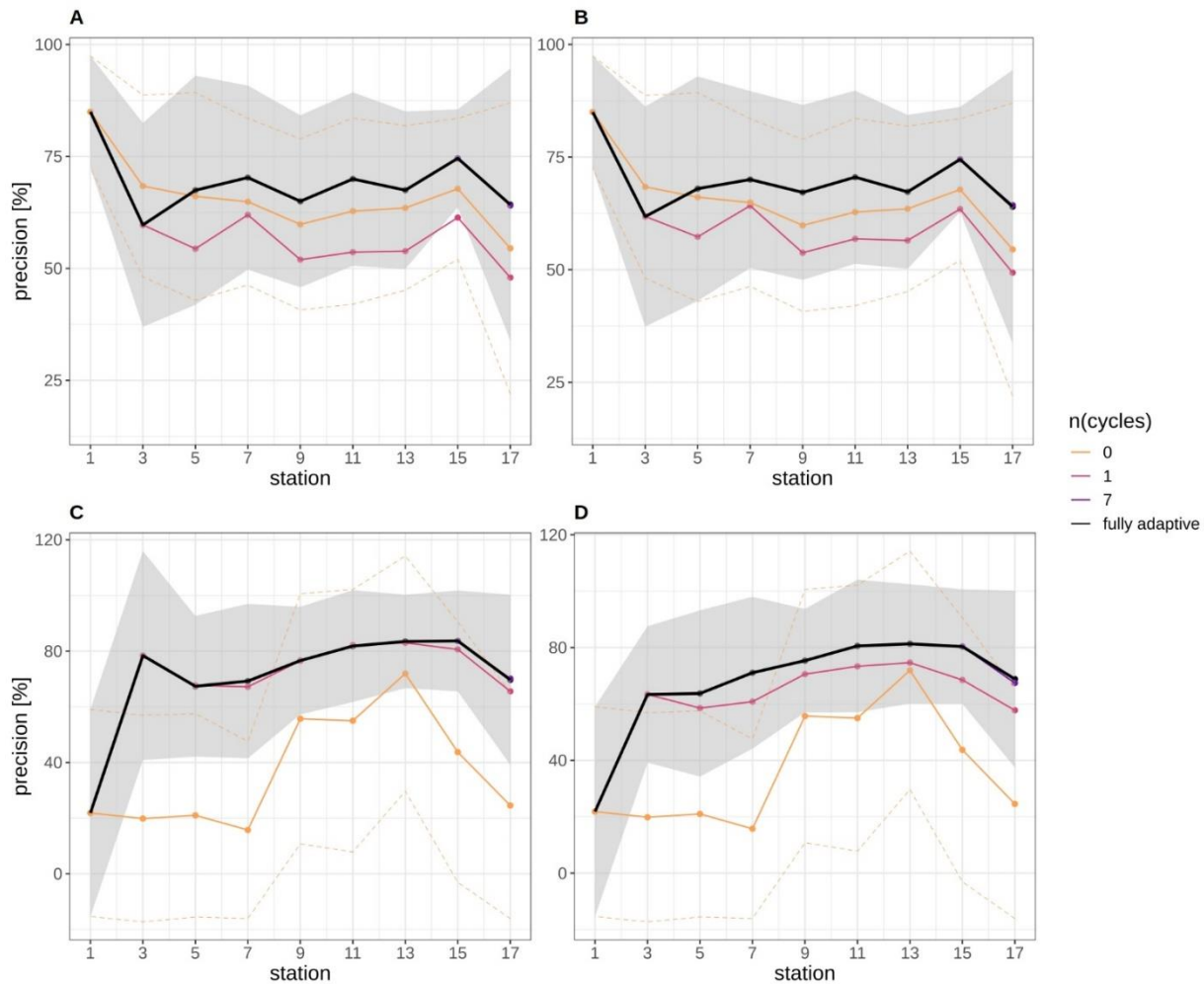


Fig. 7: Precision trajectories for different modes of adaptation using the DOC. Solid black line represents weighted mean of the fully-adaptive implementation, grey area denotes the corresponding weighted standard deviation. Colored solid and dashed lines represent weighted mean and weighted standard deviation of less-adaptive implementations (denoted by the number of adaptation cycles). (A, B): September survey; (C, D): December survey. Results for two replicates are shown for each survey. Trajectories for all nine adaptation modes are shown in fig. SI X / 3.

Precision trajectories differed strongly between classes and surveys, but were mostly consistent between replicates, both with regard to the fully-adaptive implementation of the DOC and to its comparison with less-adaptive implementations (figs. 8, SI X / 4). For most classes, precision varied strongly between adjacent stations, and did not bear a clearly increasing or decreasing trend. For many classes in the September survey, the fully-adaptive implementation achieved near- or top-level performance over the larger part of samples; exceptions include the “clumps” class, copepod egg clumps, detritus, dinoflagellates and the two unknown taxa “A” and “B”. However, unlike in the case of class-specific recall, a comparatively poor or very poor performance was observed for none of these exceptions. In the December survey, the fully-adaptive implementation achieved average performance for the larger number of classes. Exceptions with near- or top-level performance over

the larger part of the trajectory include bivalves, *Dinophysis* spp., foraminiferans and *Protoberidinium* spp.; for few additional classes, top-level performance was achieved in only one of the two replicates. Very poor performance was also noted for a few classes (appendicularians, copepod egg clumps, gastropods), but again only in one of the two replicates. As with class-specific recall, performance differences between differently-adaptive modes were of different magnitudes for different classes, and the precision trajectories of the fully-adaptive mode in general followed the trend of all other modes of adaptation.

Cross-entropy

Cross-entropy in general decreased over the stations trajectory, representing an increasing similarity between true (as defined by classification expert) and predicted distributions of relative abundances of plankton classes (fig. 9). By the end of the trajectory (stations 17 / 18), cross-entropy of the fully-adaptive implementation was decreased to approx. 90 % and 40 % of its value at the start of the trajectory for the September and December surveys, respectively. The cross-entropy trajectories were markedly smoother for the December survey than that for the September survey, which featured an oscillatory pattern from stations five / six onwards. In the September survey, the deviation between true and predicted distributions was driven by a variety of classes, including the constantly strongly abundant diatoms and *Protoberidinium* spp. classes, as well as the occasionally strongly abundant *Ceratium* spp. class and the little-abundant unknown taxa “B” and “C” (fig. 10). The cross-entropy decrease was primarily driven by lowered differences between predicted and true relative abundances of the diatoms class and of the two unknown taxa. Differences were not lowered by a large amount; however, the magnitude of absolute differences was not large ($\ll 10$ % at maximum). In the December survey, the deviation was almost exclusively driven by the strongly-abundant diatoms class and the little-abundant *Protoberidinium* spp. class. Cross-entropy decrease was notably driven by a decrease in the difference between predicted and true relative abundance for both classes. Differences decreased by a large magnitude, from more than 50 % absolute to markedly less than 20 %.

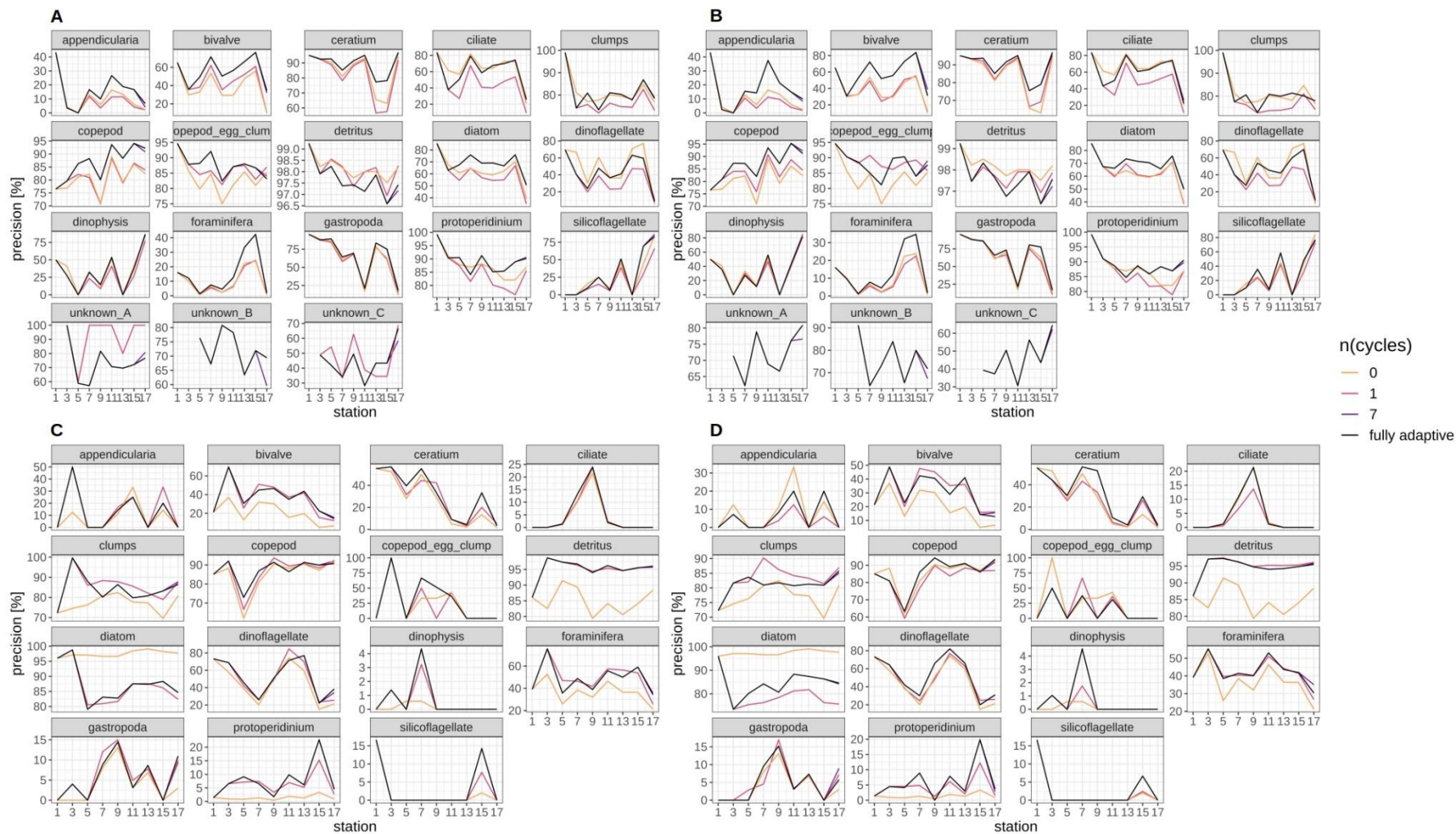


Fig. 8: Class-specific precision for the September (**A, B**) and December (**C, D**) surveys. Results for two replicates are shown for each survey. Black line represents fully adaptive DOC implementation (training-set update every second station); colored lines represent less-adaptive implementations (denoted by the number of adaptation cycles). Results for two replicates are shown for each survey. Trajectories for all nine adaptation modes are shown in fig. S1 X / 4.

Cross-entropy was lowest over all stations compared to all other adaptation modes, in the fully-adaptive implementation of the DOC (see also fig. SI X / 5). It was markedly higher in the two least-adaptive implementations in the September survey, and in the none-adaptive implementation in the December survey, compared to all other implementations. Relative cross-entropy dynamics over time were similar among all adaptation modes.

Discussion

Our results show that adapting a classifier model to changes in the plankton community is vital for ensuring continuously high classification performance. As the comparison between the fully-adaptive and less-adaptive performance trajectories demonstrates, the standardized procedure implemented in the DOC pipeline generates suitable adaptation steps via training-set stock-up and reduction of classification thresholds, making the DOC an appropriate tool for implementing model adaptation.

Our results confirm that continuous adaptation via the DOC pipeline clearly improves classification performance compared to more limited or no adaptation. The fact that performance of the classifier model improved over adaptation steps – primarily in comparison to less-adaptive scenarios, but to some extent also over survey stations, with regard to precision and cross-entropy – shows that the DOC is indeed able to cope with and actively learn from a difficult classification task. However, it is worth noting that improvement was not existing or continuous for all metrics and taxa, with e.g. mean recall not showing clear signs of improvement over stations. Given that neural networks generally require large amounts of data for training (Goodfellow, 2016), a larger initial training set and processing of larger samples might have yielded a clearer, more universal performance improvement. Still, in the context of field research, where image data from a new region and / or time period may initially be sparse, the DOC pipeline makes effective use of the incoming data such that best possible performance is frequently achieved.

With regard to precision and cross-entropy metrics, the highest possible performance is achieved for almost every sample by the fully-adaptive implementation of the DOC, while recall performance is often at very high comparative levels. The same is true for a number of single taxa that are of strong importance in the study of the ecological function of marine plankton, e.g. in the determination of planktonic biomass available as food to commercially-harvested fish (e.g. Peck et al., 2012). Thus, fully continuous adaptation yields the best performance possible per sample when integrating over all three performance metrics.

It should be noted that the DOC was not designed with the intention of advancing classification performance in terms of improving accuracy on artificially created validation datasets. Rather, the aim was to design a procedure that achieves acceptably good performance for applied research work that

focuses on abundant and broad taxonomic plankton groups, and in particular maintains that level of performance even as the classifier model is confronted with changes in the plankton community. Still, with weighted mean recall ranging from 80 to over 90 %, the classification performance of our model is comparable to the current state of the art, which ranges approximately between 80 and 95 % (Dai et al., 2016; Luo et al., 2018, Briseno-Avena et al., 2021). Although some studies have reported very high accuracies of over 95 % (Al-Barazanchi et al., 2018; Cui et al., 2018), this performance metric appears to depend strongly on the diversity of samples and on the classes chosen to report accuracy on (Briseno-Avena et al., 2021; Luo et al., 2018), which makes model comparisons difficult. Compared to recall, precision of our approach is somewhat low at 60 to 80 %, but still similar to the 84 % reported by Luo et al. (2018).

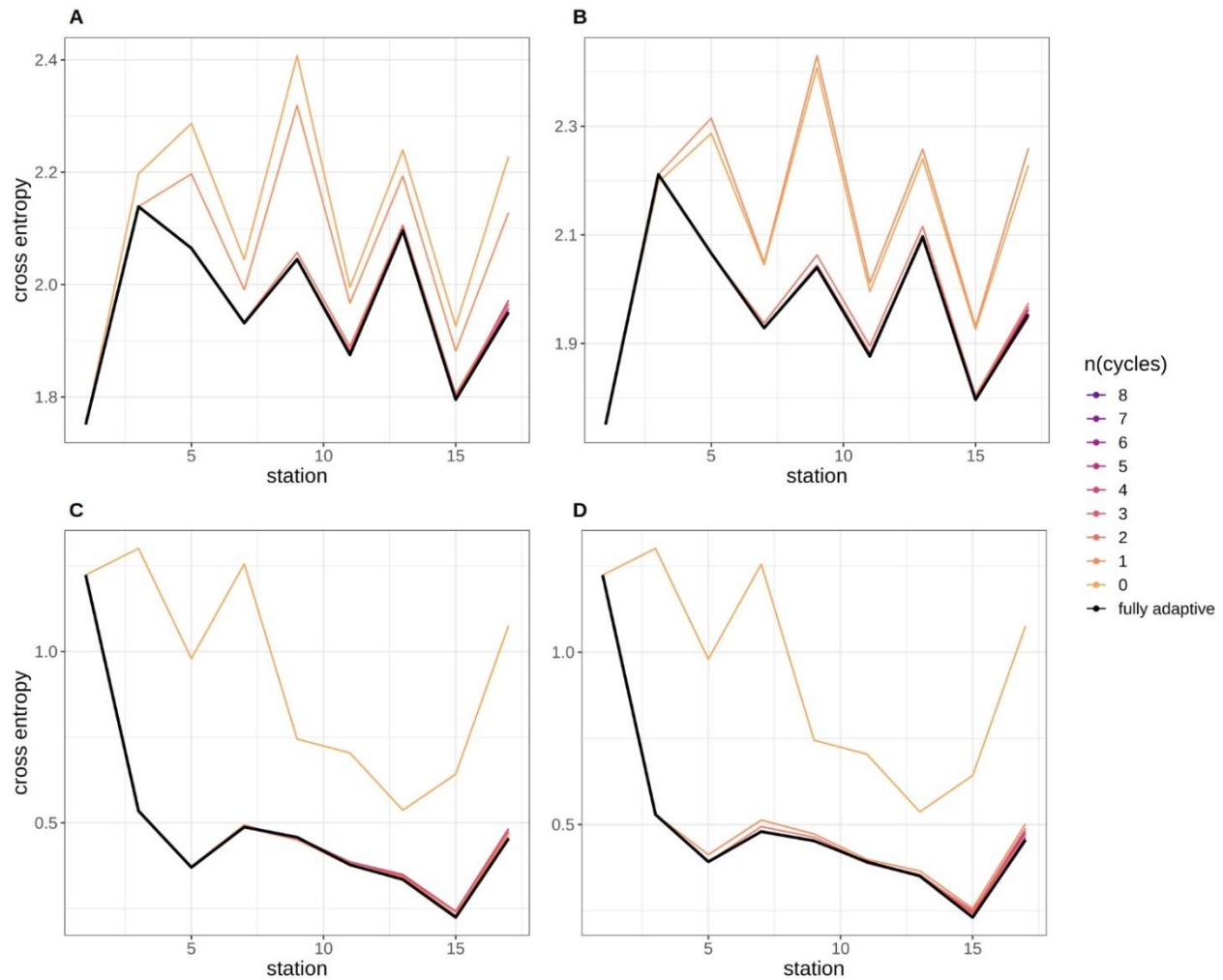


Fig. 9: Cross-entropy trajectories for different modes of adaptation using the DOC. Solid black line represents weighted mean of the fully-adaptive implementation, grey area denotes the corresponding weighted standard deviation. Colored solid and dashed lines represent weighted mean and weighted standard deviation of less-adaptive implementations (denoted by the number of adaptation cycles). (A, B): September survey; (C, D): December survey. Results for two replicates are shown for each survey. Trajectories for all nine adaptation modes are shown in fig. SI X / 5.

Given that speed and easiness of adaptation was also deemed critical for applied usage of the model, the DOC omits a thorough sample-specific model optimization (by means of re-designing the architecture of the Deep Neural Network or changing the training scheme), which might have yielded stronger performance. However, trading in performance optimization for performance reliability and easiness of adaptation did not affect the usefulness of the procedure in applied research, as shown by Börner et al. (*in prep.*).

Performance trajectories varied strongly between the two surveys, but to a lesser extent between replicates, both with regard to weighted-mean and to class-specific performance in most classes. This demonstrates that the DOC is affected by natural variability in the plankton community rather than by

technical random factors (e.g. the sampling of additional training images during the adaptation procedure). In particular, performance appears to be affected by the complexity of the plankton community, as expressed via the degree of homogeneity of relative abundances of the plankton taxa: In the September survey, taxa that made up a very minor part of the total number of plankton organisms of the December samples (e.g. *Ceratium* spp.) were comparatively increased in relative abundance, yielding a more heterogeneous plankton community. Furthermore, the increase varied between survey stations, creating an additional spatial level of heterogeneity. Consequently, the capacity to correctly predict the distribution pattern over classes, as measured by cross-entropy, became lower, as did the capacity to improve that performance by applying the DOC over several stations. As a result, mean precision was also lower for the September samples, as the increased abundance of non-major classes (for which fewer training images were available) likely led to more miss-classifications that reduced the purity of the model-generated class folders. Given that precision for the September samples increased slightly over stations, and markedly over the number of adaptation steps employed, it becomes visible that the DOC still led to adaptation even in this more difficult classification situation.

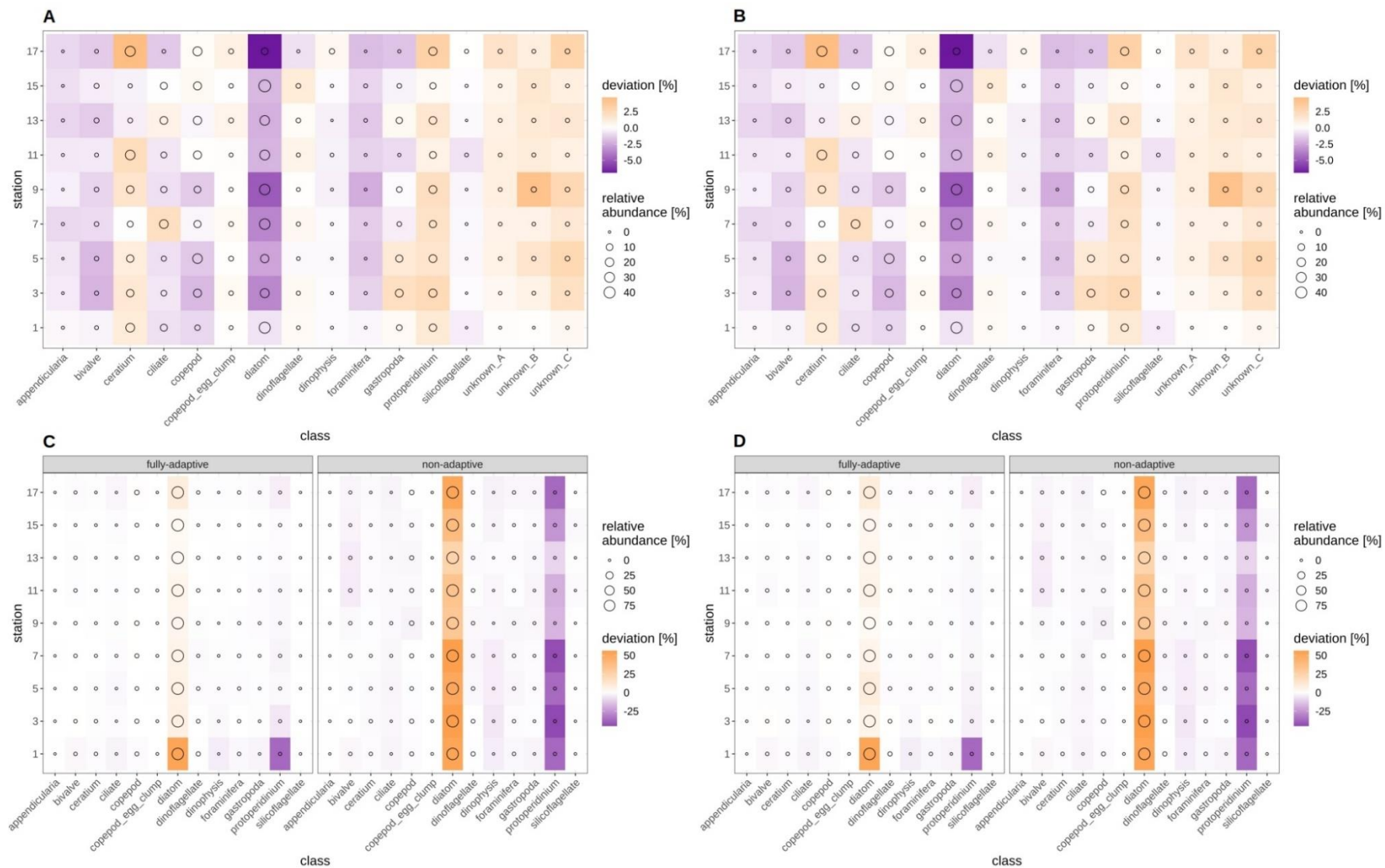


Fig. 10: Deviation between true and predicted (via non-validated automatic classification) relative class abundances for the September (**A**, **B**) and December (**C**, **D**) surveys, for the fully-adaptive DOC implementation and for classification of all samples with the baseline model (no adaptation). Results for two replicates are shown for each survey. Circle size indicates true relative abundance.

The fact that high recall was achieved for the diatom, copepod and some dinoflagellate classes, and that poor precision only occurred in some rather minor classes, makes the DOC useful for research questions addressing abundant plankton taxa. These can include analyses on the amount of potential plankton food available to larval fish, which combine classification with length measurements on the plankton items to calculate taxon-specific biomass estimates (e.g. Kiørboe, 2013; Menden-Deuer & Lessard, 2000). A high classification success on abundant classes thus enables a rapid estimation of the larger part of planktonic biomass, while low classification success on more rare classes does not influence biomass estimation particularly strongly. The distribution of classification performance over classes thus also shows that the DOC is particularly useful for broad quantitative analyses on the plankton community. It is not particularly well suited for qualitative surveys e.g. intended to assess the biodiversity of a certain marine area, which naturally require a classification with higher taxonomic resolution. Still, the DOC can in theory also facilitate expert-based high-level classification, as a performance improvement on a broad taxonomic scale will help the expert to better focus on the finer-scale classification of the taxon of interest. However, this would require the usage of different imaging devices, since FlowCam image resolution only allows for broad taxonomic classification even by experts (sensu Álvarez et al., 2014).

It should be pointed out that the viability of our DOC over longer series of survey samples might not necessarily follow the trends observed on the classification trajectories presented here. While the fact that performance improvements were observed in both the September and December transects indicates stability of the DOC pipeline under various ecological conditions, it remains to be seen how its performance behaves beyond the 18 stations per survey covered here. It is possible that at some point, a manual re-design of the training set might be necessary due to very drastic changes in the plankton community (note that the DOC approach does not discard training images during adaptation, leading to an increase in complexity of the training dataset over samples). Also, the continued decreasing of classification thresholds might at some point prove detrimental to classification precision due to many wrong classifications appearing in class folders instead of the “uncertain-classifications” folder. Some indications of deteriorating performance in the final survey samples (precision in September samples, recall in December samples) were observed in our case study, which might be an indication of the effects mentioned. For applied usage, we suggest to monitor the performance trajectory of the DOC in order to determine whether manual adjustments are advisable. Additionally, depending on the performance level found acceptable and the perceived chance of strong community changes, it may not be necessary to implement the DOC adaptation scheme after each processed sampled. It is up to the user to decide on a good trade-off between the performance improvement achieved through model adaptation and the time saved by not implementing the DOC adaptation steps.

The DOC pipeline proposed by us is not the first attempt at continually maintaining or improving model performance as new plankton samples are classified and validated in applied use: Gorsky et al. (2010) initially made use of a plankton training set not specifically built for their study, and obtained improved classification results once adding validated images from their samples and training a model on this. They continued this procedure until further improvements became marginal. Li et al. (2022) systematized a scheme of human-model interaction, where validated images are added to the training set during applied usage of the classifier. However, neither study has explicitly quantified performance decay nor the effect of training-set updates over a spatial trajectory as presented here. Also, both used expert validation to grow the training set in a rather non-systematized manner, and classification thresholds (to accept or discard a model classification as “uncertain”) were not adapted. While a non-systematized growing of the training set achieved marked performance improvements in both studies, our work shows that careful systematized training-set updates and adaptation of classification thresholds initially improve and then maintain classification performance without the need for continuously adding all validated images, which would lead to increased training durations.

Our DOC application joins a growing number of pipelines and applications designed to facilitate the embedding of machine-learning models into the workflow of plankton classification. These include the Prince William Sound Plankton Camera (Campbell et al., 2020), the Scripps Plankton Camera system (Orenstein et al., 2020) and the MorphoCluster clustering workflow (Schröder et al., 2020). All of these applications incorporate a step of manual validation in the workflow; however, none of them incorporate a dedicated standardized scheme for dynamic adaptation, as proposed by our study. The MorphoCluster is an exception to the supervised classification schemes presented in most other applications, since it makes use of an unsupervised clustering algorithm that groups the plankton images in a data-driven manner. It therefore appears not to require a dedicated dynamic adaptation; however, the interpretation of the resulting clusters may be less straight-forward than the expert check of a machine classification. While the MorphoCluster appears particularly useful for in-situ monitoring studies that focus on fine-resolution taxon recognition, we assume that our DOC may be of more convenient use in quantitative studies that primarily address a fixed set of broad taxonomic groups.

Compared to other applications that often present an end-to-end system from field sampling to classification, and related hardware, our DOC covers a relatively small part of the overall workflow. Future extensions of our application would primarily address a more direct coupling to size measurements on the plankton images (used, together with a class-specific conversion factor, to calculate the biomass of every plankton item (e.g. Kiørboe, 2013; Menden-Deuer & Lessard, 2000)), as well as to the preceding photography in the FlowCam. Further extensions

could include the incorporation of automatic performance monitoring in order to give advice to the user of when a manual re-design of the training set or a manual adaptation of classification thresholds might be necessary.

Conclusions

Our DOC proves to be a capable tool for adapting a classifier model on a plankton community changing over the spatial and temporal dimension. Our method continually delivers high or highest performance compared to non- or less-adaptive approaches, especially for abundant classes, though is subject to sample-specific variability in the difficulty of classification. Combined with the streamlining of the adaptation process and the availability of an easy-to-operate user interface, the DOC serves as an aide for quantitative plankton analysis on a broad taxonomic level that performs reliably under changing community patterns.

Author Contributions

J.C. wrote the manuscript; J.C., G.B., M.M. conceived the study; G.B., J.C. did the classification experiments and analyses; J.C. did the programming of the DOC application; A.L., M.M., C.M. provided input and revisions to the manuscript.

Acknowledgments

The authors wish to like Jens Floeter and Rene Plonus for helpful comments, as well as André Harmer for initial guidance in the programming with Python and Rachel Harmer for help with manual annotation of the baseline training set. Parts of the intellectual content of this manuscript were included, in very preliminary form, in the master's thesis (Conradt, 2020).

References

- Abadi, M., Agarwal, A., Barham, P., Brevdo, E., Chen, Z., Citro, C. et al. (2015). TensorFlow: Largescale machine learning on heterogeneous systems. Preliminary White Paper. 19 pp.
- AlBarazanchi, H., Verma, A. and Wang, S. X. (2018). Intelligent plankton image classification with Deep Learning. In: *Int. J. Comput. Vis. Robot.* 8, 561571. <https://dx.doi.org/10.1504/IJCVR.2018.095584>
- Álvarez, E., LópezUrrutia, Á. and Nogueira, E. (2012). Improvement of plankton biovolume estimates derived from imagebased automatic sampling devices: application to FlowCam. *J. Plankton Res.* 34, 454469. <https://doi.org/10.1093/plankt/fbs017>
- Álvarez, E., Moyano, M., LópezUrrutia, Á., Nogueira, E. and Scharek, R. (2014). Routine determination of plankton community composition and size structure: a comparison between FlowCAM and light microscopy. *J. Plankton Res.* 36, 170184. <https://doi.org/10.1093/plankt/fbt069>

- Anaconda Software Distribution (2020). Anaconda Documentation. Anaconda Inc. <https://docs.anaconda.com/>. Last access on 5th July, 2020
- Asch, R. G., Stock, C. A. and Sarmiento, J. L. (2019). Climate change impacts on mismatches between phytoplankton blooms and fish spawning phenology. *Glob. Chang. Biol.* 25, 25442559. <https://doi.org/10.1111/gcb.14650>
- Beaugrand, G., Ibañez, F., Lindley, A. & Reid, P. C. (2002). Diversity of calanoid copepods in the North Atlantic and adjacent seas: species associations and biogeography. *Mar. Ecol. Prog. Ser.* 232, 179195. <http://dx.doi.org/10.3354/meps232179>
- Beaugrand, G. (2012). Unanticipated biological changes and global warming. *Mar. Ecol. Prog. Ser.* 445, 293301. <http://dx.doi.org/10.3354/meps09493>
- Börner, G., Frelat, R., Akimova, A., van Damme, C., Peck, M. A. and Moyano, M. (*in prep.*). Interannual variability in the plankton community composition and size structure in the North Sea in fall and winter from 20132019
- BriseñoAvena, C., Schmid, M. S., Swieca, K., Sponaugle, S., Brodeur, R. D. and Cowen, R., K. (2020). Threedimensional crossshelf zooplankton distributions off the Central Oregon Coast during anomalous oceanographic conditions. In: *Prog. in Oceanogr.* 188, 102436. <https://doi.org/10.1016/j.pocean.2020.102436>
- Campbell, R., Roberts, P. and Jaffe, J. (2020). The Prince William Sound Plankton Camera: a profiling in situ observatory of plankton and particulates. *ICES J. Mar. Sci.* 77: 14401455. <https://doi.org/10.1093/icesjms/fsaa029>
- Capuzzo, E., Lynam, C. P., Barry, J., Stephens, D., Forster, R. M., Greenwood, N. et al. (2017). A decline in primary production in the North Sea over 25 years, associated with reductions in zooplankton abundance and fish stock recruitment. *Glob. Chang. Biol.* 24, e352e364. <https://doi.org/10.1111/gcb.13916>
- Castellani, C. and Edwards, M. (2017). *Marine Plankton*. Oxford, UK: Oxford University Press
- Chollet, F. (2015). *Keras*. <https://www.keras.io>. [Accessed 5th July, 2020]
- Chollet, F. (2017). *Deep Learning with Python*. New York, NY: Manning Publications Company
- Conradt, J. (2020). Automated plankton image classification with a Capsule Neural Network. [master's thesis]. [Hamburg (DE)] Universität Hamburg
- Cui, J., Wei, B., Wang, C., Yu, Z., Zheng, H., Zheng, B. and Yang, H. (2018). Texture and shape information fusion of Convolutional Neural Network for plankton image classification. In: 2018 OCEANS MTS/IEEE Kobe TechnoOceans (OTO), 15. <https://doi.org/10.1109/OCEANSKOB.2018.8559156>
- Culverhouse, P. F., Williams, R., Reguera, B., Herry, V. and GonzálezGil, S. (2003). Do experts make mistakes? A comparison of human and machine identification of dinoflagellates. *Mar. Ecol. Prog. Ser.* 247, 1725. <http://dx.doi.org/10.3354/meps247017>
- Dai, J., Yu, Z., Zheng, H., Zheng, B. and Wang, N. (2016). "A hybrid Convolutional Neural Network for plankton classification", in *Computer Vision – ACCV 2016 Workshops*, eds. C. S. Chen, J. Lu & K. K. Ma (Cham, CH: Springer), 102114. http://dx.doi.org/10.1007/9783319545264_8
- Dam, H. G. and Baumann, H. (2017). "Climate change, zooplankton and fisheries", in *Climate change impacts on fisheries and aquaculture*, eds. B. F. Phillips & M. PérezRamírez, (Hoboken, NJ: WileyBlackwell), 851874

- Davis, C. S., Gallager, S. M., Berman, S. M., Haury, L. R. and Strickler, J. R. (1992). The Video Plankton Recorder (VPR): Design and initial results. *Arch. Hydrobiol. Beih. Ergebn. Limnol.* 36, 6781
- Deng, J., Dong, W., Socher, R., Li, L.J., Li, K. and FeiFei, L. (2009). Imagenet: A largescale hierarchical image database. 2009 IEEE conference on computer vision and pattern recognition, 248255. <https://doi.org/10.1109/CVPR.2009.5206848>
- Durant, J. M., Molinero, J.C., Ottersen, G., Reygondeau, G., Stige, L. C. and Langangen, Ø. (2019). Contrasting effects of rising temperatures on trophic interactions in marine ecosystems. *Sci. Rep.* 9, 15213. <https://doi.org/10.1038/s4159801951607w>
- Frederiksen, M., Edwards, M., Richardson, A. J., Halliday, N. C. and Wanless, S. (2006). From plankton to top predators: bottomup control of a marine food web across four trophic levels. *J. of Anim. Ecol.* 75, 12591268. <https://doi.org/10.1111/j.13652656.2006.01148.x>
- Garnier, S. (2018). viridis: Default color maps from 'matplotlib'. R package version 0.5.1. <https://CRAN.Rproject.org/package=viridis>
- Glorot, X. and Bengio, J. (2010). Understanding the difficulty of training deep forward neural networks. *Proceedings of the 13th International Conference on Artificial Intelligence and Statistics* 9, 249256
- GNU, P. (2007). Free Software Foundation. Bash [Unix shell program]
- González, P., Álvarez, E., Díez, J., LópezUrrutia, Á. and Coz, J. J. del (2016). Validation methods for plankton image classification systems. *Limnol. Oceanogr. Methods* 15, 221237. <https://doi.org/10.1002/lom3.10151>
- Goodfellow, I. J., Bengio, Y. and Courville, A. (2016). *Deep Learning*. Cambridge, MS: The MIT Press
- Goodwin, M., Halvorsen, K. T., Jiao, L., Knausgård, K. M., Martin, A. H., Moyano, M., Oomen, R. et al. (2022). Unlocking the potential of deep learning for marine ecology: A review exemplified through seven established and emerging applications. *ICES J. Mar. Sci.* fsab255. <https://doi.org/10.1093/icesjms/fsab255>
- Gorsky, G., Ohman, M. D., Picheral, M., Gasparini, S., Stemmann, L., Romagnan, J.B. et al. (2010). Digital zooplankton image analysis using the ZooScan integrated system. *J. Plankton Res.* 32, 285303. <https://doi.org/10.1093/plankt/fbp124>
- Gu, J., Wang, Z., Kuen, J., Ma, L., Shahroudy, A., Shuai, B. et al. (2018). Recent advances in convolutional neural networks. *Pattern Recognit.* 77, 354377. <https://doi.org/10.1016/j.patcog.2017.10.013>
- Hunter, J. D. (2007). Matplotlib: a 2D graphics environment. *Comput. Sci. Eng.* 9, 9095
- Kingma, D. and Ba, J. (2014): Adam: A method for stochastic optimization. *arXiv [Preprint]*. Available at: [arXiv:1412.6980](https://arxiv.org/abs/1412.6980) (Accessed 5th July, 2020)
- Kjørboe, T. (2013). Zooplankton body composition. *Limnol. Oceanogr.* 58, 18431850. <http://dx.doi.org/10.4319/lo.2013.58.5.1843>
- Kraberg, A., Metfies, K. and Stern, R. (2017). „Sampling, preservation and counting of samples I: phytoplankton”, in *Marine Plankton*, eds. C. Castellani & M. Edwards (Oxford, UK: Oxford University Press), 91103

- Krizhevsky, A., Sutskever, I. and Hinton, G. E. (2012). ImageNet classification with Deep Convolutional Neural Networks. *Adv. Neural Inf. Process. Syst.* 1, 10971105. <https://doi.org/10.1145/3065386>
- LeCun, Y., Boser, B., Denker, J. S., Henderson, D, Howard, R. E., Hubbard, W. and Jackel, L. D. (1989). Backpropagation applied to handwritten zip code recognition. *Neural Comput.* 1, 541551. <https://doi.org/10.1162/neco.1989.1.4.541>
- LeCun, Y., Kavukcuoglu, K. and Farabet, C. (2010). Convolutional networks and applications in vision. *Proceedings of 2010 IEEE International Symposium on Circuits and Systems*, 253256. <https://doi.org/10.1109/ISCAS.2010.5537907>
- Li, J., Chen, T., Yang, Z., Chen, L., Liu, P., Zhang, Y. et al. (2022). Development of a buoyborne underwater imaging system for *in situ* mesoplankton monitoring of coastal waters. *IEEE J. Ocean. Eng.* 47, 88110. <https://doi.org/10.1109/JOE.2021.3106122>
- Li, Z., Zhao, F., Liu, J. and Qiao, Y. (2014). Pairwise nonparametric discriminant analysis for binary plankton image recognition. *IEEE J. Ocean. Eng.* 39, 695701. <https://doi.org/10.1109/JOE.2013.2280035>
- Lombard, F., Boss, E., Waite, A. M., Vogt, M., Uitz, J. et al. (2019). Globally consistent quantitative observations of planktonic ecosystems. *Front. Mar. Sci.* 6, 196. <https://doi.org/10.3389/fmars.2019.00196>
- Lumini, A. and Nanni, L. (2019). Deep learning and transfer learning features for plankton classification. *Ecol. Inform.* 51, 3343. <https://doi.org/10.1016/j.ecoinf.2019.02.007>
- Lundh, F. (2019). An introduction to TkInter. <http://www.pythonware.com/library/tkinter/introduction/index.htm>. [Accessed 5th July, 2020]
- Lundh, F. and Ellis, M. (2019). Python Imaging Library (PIL). <http://www.pythonware.com/products/pil/> [Accessed 5th July, 2020]
- Luo, J. Y., Irsson, J.O., Graham, B., Guigand, C., Sarafraz, A., Mader, C. and Cowen, R. K. (2018). Automated plankton image analysis using convolutional neural networks. *Limnol. Oceanogr. Methods* 16, 814827. <https://doi.org/10.1002/lom3.10285>
- Malde, K., Handegard, N. O., Eikvil, L. and Salberg, A.B. (2020). Machine intelligence and the datadriven future of marine science. *ICES J. Mar. Sci.* 77, 12741285. <https://doi.org/10.1093/icesjms/fsz057>
- McKinney, W. (2010). Data structures for statistical computing in Python. *Proceedings of the 9th Python in Science Conference (SciPy)*, Austin / TX, USA, 5156. <http://dx.doi.org/10.25080/Majora92bf192200a>
- MendenDeuer, S. and Lessard, E. J. (2000). Carbon to volume relationships for dinoflagellates, diatoms, and other protist plankton. In: *Limnol. Oceanogr.* 45, 569579. <https://doi.org/10.4319/lo.2000.45.3.0569>
- MorenoTorres, J. G., Raeder, T., AlaizRodríguez, R., Chawla, N. V. and Herrerra, F. (2012). A unifying view on dataset shift in classification. *Pattern Recogn.* 45, 521530. <https://doi.org/10.1016/j.patcog.2011.06.019>
- Nagelkerken, I., Goldenberg, S. U., Ferreira, C. M., Russell, B. D. and Connell, S. D. (2017). Species interactions drive fish biodiversity loss in a highCO₂ world. *Curr. Biol.* 27, 21772184. <https://doi.org/10.1016/j.cub.2017.06.023>

- Nijs, V. (2020). radiant.data: Data menu for Radiant: business analytics using R and Shiny. R package version 1.3.12. <https://CRAN.Rproject.org/package=radiant.data>
- Oliphant, T. E. (2006). A guide to NumPy. US: Trelgol Publishing
- Oliphant, T. E. (2007). Python for scientific computing. *Comput. in Sci. Eng.* 9, 1020. <http://dx.doi.org/10.1109/MCSE.2007.58>
- Orenstein, E. C., Beijbom, O., Peacock, E. E. and Sosik, H. (2015). WHOIPlankton – A large scale fine grained visual recognition benchmark dataset for plankton classification. *arXiv [Preprint]*. Available at: [arXiv:1510.00745](https://arxiv.org/abs/1510.00745) (Accessed 5th July, 2020)
- Orenstein, E. C. and Beijbom, O. (2017). Transfer learning and Deep feature extraction for planktonic image data sets. 2017 IEEE Winter Conference on Applications of Computer Vision (WACV), 10821088. <https://doi.org/10.1109/WACV.2017.125>
- Orenstein, E. C., Ratelle, D., BrieseñoAvena, C., Carter, M. L., Franks, P. J. S., Jaffe, J. S. and Roberts, P. L. D. (2020). The Scripps Plankton Camera system: A framework and platform for in situ microscopy. *Limnol. Oceanogr. Methods* 18, 681695. <https://doi.org/10.1002/lom3.10394>
- Peck, M. A., Huebert, K. B. & Llopiz, J. K. (2012). Intrinsic and extrinsic factors driving matchmismatch dynamics during the early life history of marine fishes. *Adv. Ecol. Res.* 47, 177302. <https://doi.org/10.1016/B9780123983152.00003X>
- Perez, F. and Granger, B. E. (2007). IPython: a system for interactive scientific computing. *Comput. Sci. Eng.* 9, 2129. <https://doi.org/10.1109/MCSE.2007.53>
- Plonus, R.M., Conradt, J., Harmer, A., Janßen, S. and Floeter, J. (2021). Automatic plankton image classification – Can capsules and filters help cope with data set shift? *Limnol. Oceanogr. Methods* 19, 176195. <https://doi.org/10.1002/lom3.10413>
- R Core Team (2020). R: An language and environment for statistical computing. R Foundation for Statistical Computing, Vienna, Austria. URL <https://www.Rproject.org/>
- Raybaut, P. (2017). Spyder Documentation – Release 3. Available online at: [pythonhosted.org](https://pythonhosted.org/spyder/)
- van Rossum, G. (1995). Python tutorial. Technical Report CSR9526. Centrum voor Wiskunde en Informatica (CWI), Amsterdam, NL
- Rumelhart, D. E., Hinton, G. E. and Williams, R. J. (1986). Learning representations by backpropagating errors. *Nature* 323, 533536. <https://doi.org/10.1038/323533a0>
- Russell, F. S. (1939). Hydrographical and biological conditions in the North Sea as indicated by plankton organisms. *ICES J. Mar. Sci.* 14, 171192. <https://doi.org/10.1093/icesjms/14.2.171>
- Scholkopf, B. and Smola, A. (2002). Learning with kernels: Support vector machines, regularization, optimization and beyond. Cambridge, MS: The MIT Press
- Schröder, S.M., Kiko, R. and Koch, R. (2020): MorphoCluster: Efficient annotation of plankton images by clustering. *Sensors* 20, 3060. <http://dx.doi.org/10.3390/s20113060>
- Sieracki, C. K., Sieracki, M. E. and Yentsch, C. S. (1998). An imaginginflow system for automated analysis of microplankton. *Mar. Ecol. Prog. Ser.* 168, 285296
- Simonyan, K. and Zisserman, A. (2015). Very Deep Convolutional Networks for largescale image recognition. *arXiv [Preprint]*. Available at: <https://arxiv.org/abs/1409.1556> (Accessed on 5th July, 2020)

- Stern, R., Taylor, C. and Sadri, S. (2017): "Protozooplankton: Foraminifera", in *Marine Plankton*, eds. C. Castellani and M. Edwards (Oxford, UK: Oxford University Press), 194197
- Tang, X., Stewart, W. K., Huang, H., Gallager, S. M., Davis, C. S., Vincent, L. and Marra, M. (1998). Automatic plankton image recognition. *Artif. Intell. Rev.* 12, 177199. <https://doi.org/10.1023/A:1006517211724>
- Tang, X., Lin, F., Samson, S. and Remsen, A. (2006). Binary plankton image classification. *IEEE J. Ocean. Eng.* 31, 728735. <http://dx.doi.org/10.1109/JOE.2004.836995>
- Wickham, H., Averick, M., Bryan, J., Chang, W., D'Agostino McGowan, L., Francois, R. et al. (2019). Welcome to the tidyverse. *J. Open Source Softw.* 4, 1686. <http://dx.doi.org/10.21105/joss.01686>
- Wiebe, P. H., Bucklin, A. and Benfield, M. (2017). „Sampling, preservation and counting of samples II: zooplankton”, in *Marine Plankton*, eds. C. Castellani & M. Edwards (Oxford, UK: Oxford University Press), 104135
- Winder, M. and Sommer, U. (2012): Phytoplankton response to a changing climate. *Hydrobiologia* 698, 516. <https://doi.org/10.1007/s10750012114>

Chapter 3

Plankton community composition and size structure in the North Sea in autumn and winter from 2013- 2019



Drawings by Justine Courboulès

Plankton community composition and size structure in the North Sea in autumn and winter from 2013-2019

Gregor Börner ¹, Romain Frelat ², Anna Akimova ³, Cindy van Damme ⁴, Myron A. Peck⁵, Marta Moyano ^{6,7}

Abstract

Plankton dynamics in temperate ecosystems are mainly studied during the productive seasons, whereas less is known for winter, particularly for microplankton. Using image-based techniques, we investigated the North Sea micro- and mesozooplankton community composition, abundance and size structure (55-2000 μm) during autumn- (Buchan/Banks area) and wintertime (Downs area) between 2013 and 2019. Community diversity (broad taxa) was similar across years and areas, but abundance was lower in Downs compared to Buchan/Banks for most microplankters (e.g. *Tripos* spp. and ciliates) and, to a lower degree, for mesozooplankton (e.g. copepods). Average slopes of normalized abundance size spectra (NASS) reflected these spatial differences with steeper slopes (i.e. lower contribution of large organisms) in Downs (-1.67) compared to Buchan/Banks (-1.45). Spatiotemporal changes in the planktonic community and their potential environmental drivers were examined using a redundancy analysis (including taxonomy and size) and a correlation analysis using NASS slopes (size only). Both approaches highlighted the importance of water mass properties (e.g. salinity, temperature, turbidity) in shaping the spatiotemporal variability of the plankton, although the amount of explained variance differed between approaches (11 vs. 46%). Our results contribute to a better understanding of standing stock of plankton and its relationship with environmental drivers during winter in a temperate shelf sea, highlighting how novel solutions to plankton monitoring (i.e. automated routines implemented in fisheries surveys) can provide much-needed information for models of lower trophic levels or plankton consumers.

Keywords: plankton dynamics, microplankton, mesozooplankton, size spectra, image-based analysis, FlowCAM, Zooscan

Authors' affiliation

1 Institute of Marine Ecosystem and Fishery Science, University of Hamburg, Große Elbstraße 133, Hamburg D-22767, Germany

2 International Livestock Research Institute, Nairobi, Kenya

3 Thünen Institute of Sea Fisheries, Herwigstraße 31, Bremerhaven D-27572, Germany

4 Wageningen Marine Research, Haringkade 1, 1976 CP IJmuiden, the Netherlands

5 Royal Netherlands Institute for Sea Research (NIOZ), Department of Coastal Systems (COS), PO Box 59, 1790 AB Den Burg (Texel), the Netherlands

6 Norwegian Institute for Water Research (NIVA), Økernveien 94, 0579 Oslo, Norway

7 Center for Coastal Research, University of Agder, Universitetsveien 25, 4604 Kristiansand, Norway

Introduction

Plankton is the foundation of the marine food webs including the productivity of all higher trophic levels (Ryther 1969). Besides being the main energy source for higher trophic levels, some planktonic organisms can serve as bioindicators of ecosystem state, while others can pose a threat to other marine organisms (e.g., red tides) (McQuatters-Gollop et al. 2009, Bedford et al. 2018, 2020b). Climate-related changes in plankton communities can result in cascading effects on the entire ecosystem (Murphy et al. 2020, Sguotti et al. 2022). While extensive research is available on plankton phenology, abundance and community composition during relatively productive seasons in temperate marine ecosystems, much less is known about their dynamics during seasons of low productivity (e.g. wintertime). This accounts especially for the microzooplankton, including both protists (ciliates and dinoflagellates) and small metazoans (e.g. copepod nauplii, meroplanktonic larvae) between 20 to 200 μm in size. This small size fraction of plankton plays a significant role in the ecosystem as key consumers of primary production, important players in the microbial loop, and as potentially abundant prey resource for mesozooplankton and fish larvae (e.g. Calbet 2008, Montagnes et al. 2010). During periods of low light intensity and nutrient limitation, conditions that are not favorable for the growth and productivity of large phytoplankton cells, metazoan abundance can be low (Montagnes et al. 2010) and the trophodynamic importance of protists and other players in the microbial loop can be enhanced (Fileman et al. 2011). Thus, monitoring comprehensive plankton dynamics during periods of low productivity can be critical to understanding the factors shaping seasonal changes in marine ecosystems.

The majority of the broad-scale zooplankton monitoring focuses on mesozooplankton (the size fraction between 200 and 2000 μm) (e.g. Doray et al. 2018, Yebra et al. 2022), but overlooks the microzooplankton (20-200 μm). For example, the Continuous Plankton Recorder (CPR), one of the longest ongoing plankton sampling programs starting in the 1930s in the eastern North Atlantic and now conducted in many regions worldwide (e.g. western North Atlantic, Australia), provides large-scale coverage on the abundance (semi-quantitative) and distribution of zooplankton (>270 μm) in surface waters (Richardson et al. 2006, Dippner & Krause 2013). In contrast, microzooplankton is sampled either with limited spatially extend, for instance at fixed monitoring stations (e.g. Eloire et al. 2010, Löder et al. 2011), or constrained to single cruises mainly during the productive season (e.g. Dolan et al. 2021, Yang et al. 2021). The reason behind the lack of long-term, large-scale microzooplankton data is likely due to logistical challenges in sampling (i.e. size range between water samples and regular plankton nets) and sample preservation (i.e. lugol-preserved samples have a shelf-life of 6-12 months; Gifford & Caron 2000, Calbet et al. 2001). Therefore, there is a need to further develop easy-to-use, time-effective routines for microzooplankton sampling and processing in order to better

understand general plankton dynamics, food webs and build more robust ecosystem models (Calbet 2008, Lombard et al. 2019, Lehtiniemi et al. 2022). In this sense, implementing advanced methods (e.g., image analysis, metabarcoding) to track temporal and spatial changes in the entire planktonic community composition and abundance is now the goal of many monitoring programs embracing an ecosystem-based approach for fisheries and management (Lombard et al. 2019, Vazquez et al. 2021).

Over the past decades, the automatic processing of plankton organisms using image analysis technologies and machine learning algorithms has exploded (Goodwin et al. 2022). While traditional identification of preserved samples via microscopy offers a high taxonomic resolution, it is a labor intensive, time consuming and costly process (Benfield et al. 2007). It is also error-prone due to operator fatigue or human bias (e.g., self-consistency can be < 80% in difficult identification tasks) (Culverhouse et al. 2014). Automated image-based methods can alleviate some of these issues, allowing the processing of higher number of samples, albeit at a lower taxonomic resolution (i.e. rarely to species level). The outcomes of these methods (e.g. Flow Cytometer and Microscope (FlowCAM) or ZooSCAN) in terms of abundance, biomass and seasonal variability of phyto- and zooplankton are comparable with microscope counts, especially for the most abundant classes (Álvarez et al. 2014, Naito et al. 2019). These digital imaging techniques also have the advantage that they automatically provide estimates of the size of individual planktons.

Given the functional complexity of the zooplankton community and methodological difficulties to estimate its diversity, alternative metrics based on size have been used to represent this diversity in the food-web studies and ecosystem models. A size-spectra approach, introduced by Sheldon (1972), is a widely used approach to investigate the spatiotemporal variability of zooplankton, predator-prey interactions, and to model the productivity of the higher trophic levels feeding on zooplankton (e.g. Serra-Pompei et al. 2022). The zooplankton size-spectra is often reported in terms of the Normalized Abundance Size Spectra (NASS) or Normalized Biomass Size Spectra (NBSS) (Sprules & Barth 2016). The slope of NASS is generally close to -2.0 (-1.0 for NBSS) and can indicate bottom-up or top-down control of the marine ecosystem (Silvert & Platt 1978, Zhou 2006a). The intercept of these size spectra reflects ecosystem productivity and varies substantially between oligotrophic and highly productive ecosystems (Zhou 2006a, Ye et al. 2013).

The North Sea is a temperate shelf ecosystem with pronounced seasonal changes in primary and secondary productivity (Krause et al. 2003). Long-term time-series are available for many species and groups of plankton, fishes and marine mammals that serve as a basis for a regular assessment of the North Sea environmental status (ICES, 2022). In terms of plankton, weekly time series spanning several decades are available for phyto-, micro- and zooplankton at some

fixed stations, such as Plymouth L4 (Eloire et al. 2010, Lehtiniemi et al. 2022) or Helgoland Roads (e.g. Pitois et al. 2009, Widdicombe et al. 2010). Additionally, time series with a broader spatial scale, such as the CPR, are available for mesozooplankton groups, such as copepods, euphausiids and meroplankton (e.g. Richardson et al. 2006, Dippner & Krause 2013).

Thanks to these time series, it has been possible to identify long-term changes in the North Sea, such as regime shifts (e.g. in 1988), a general decrease in primary productivity and holoplankton, and poleward range shift in cold-water copepod species (e.g. *Calanus finmarchicus*) leading to an increased relative contribution of small-sized, warm-water species (e.g. *Calanus helgolandicus*) (for a review see Sguotti et al. 2022). Despite being a well-studied ecosystem, there is a general lack of knowledge on plankton dynamics during wintertime for most temperate seas. Besides providing a better understanding of the dynamics of lower trophic levels, this knowledge is essential to assess potential food limitation in higher trophic levels, e.g. early life stages of commercially important winter-spawning fishes such as Atlantic herring (*Clupea harengus*) and European plaice (*Pleuronectes platessa*). This is especially relevant because of the relatively low recruitment success that, for example herring experienced during the most recent decade (ICES, 2022), which has been related to warming and changes in prey type and abundance (see Alvarez-Fernandez et al. 2015 and references therein).

In this study, we investigated the North Sea micro- and mesozooplankton community during autumn and wintertime between 2013 and 2019. Samples were obtained during a routine fisheries survey, which covered the traditional spawning grounds of Atlantic herring in the western (Buchan/Banks in September, autumn) and southern North Sea (Downs in late December, winter). Our objectives were i) to describe spatiotemporal changes in the plankton community composition, abundance, and size structure in both sampling areas, ii) to identify environmental drivers of changes in the size composition of plankton, and iii) to identify environmental drivers of changes in plankton diversity that included the broad taxonomic and functional information obtained from image-based analysis (FlowCAM and ZooSCAN). Our results provide essential information on the standing stock of plankton and their environmental drivers during the low productivity season in the North Sea. We discuss the benefits and drawbacks of the sampling methods and statistical approaches, as well as provide recommendations for future zooplankton monitoring in the North Sea and other temperate coastal systems.

Materials & Methods

Sample collection

The plankton samples were taken on board the Dutch research vessel *Tridens* within the framework of the International Herring Larval Survey (IHLS), coordinated by the International Council for the Exploration of the Sea (ICES). The Dutch surveys cover the three spawning grounds of the North Sea Autumn Spawning herring: Buchan and Banks in September and Downs in late December (Fig. 1). On each station, ichthyo- and mesozooplankton were sampled using a modified GULF VII net (280 μm mesh size; Nash et al. 1998), which had attached a PUP-net (55 μm mesh size) for micro(zoo)plankton sampling (Fig. 2). The double-net was towed in double oblique hauls at 5 knots down to 5 m above sea floor to cover the whole water column. Once onboard, samples from both nets were preserved in 4% formaldehyde. Out of the sampling grid, six transects in Buchan/Banks and three transects in Downs were chosen for plankton analysis in this study (Fig.1), representing the onshore-offshore and north-south gradients. Typically, 25-35 samples per IHLS survey were available, although in three Downs surveys <10 samples along the predefined transects were sampled (Fig. S1).

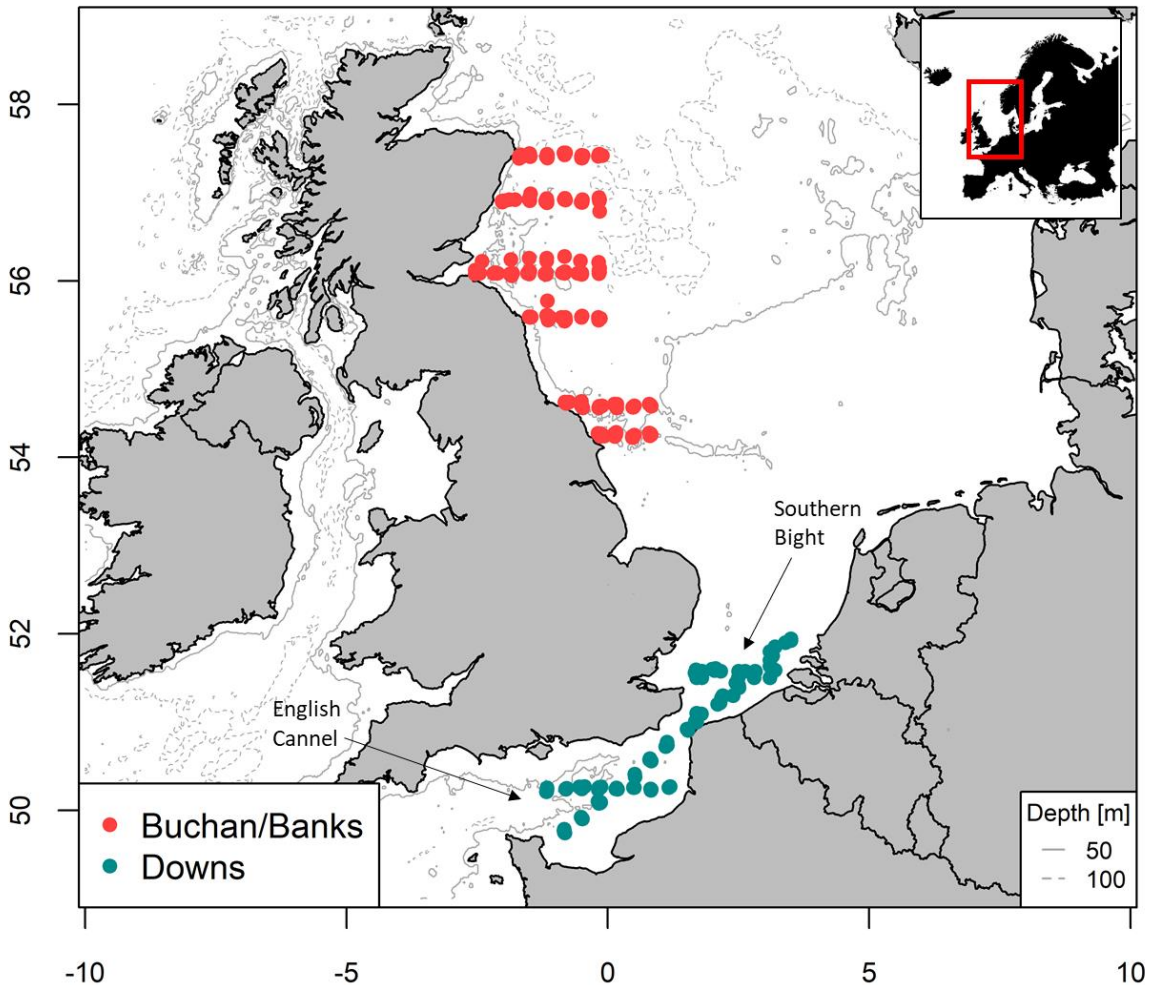


Fig. 1. Selected transects from the International Herring Larval Survey in the Buchan/Banks (September / autumn; red dots) and Downs spawning grounds (December / winter; cyan dots) analyzed in this study. Arrows indicate the two subareas in the Downs spawning grounds (English Channel and Southern Bight). See sampling stations per year for each specific year in Fig. S1.

Sample analysis

Microplankton samples - FlowCAM

Once in the laboratory, the microplankton samples from the PUP net were rinsed and sieved through a 300- μm mesh. The fraction below 300 μm was retained and diluted (approx. 4000 particles mL^{-1} ; 50-500 mL, depending on the density of each sample).

Subsequently the samples were analyzed using the FlowCAM (Yokagawa Fluid Imaging, USA; Sieracki et al., 1998) with a 300 μm flow chamber (i.e. upper size limit for the particles analyzed). The amount of sample to process was set according to the particle concentration, aiming at approx. 10,000 pictures per sample containing a minimum of 10% living organisms (generally >30%). Subsequently, images were classified using the workflow principle of the dynamic optimization cycle (Conradt et al. 2022). Pictures from living organisms were grouped

into 11 taxa sets: bivalve, tripos, ciliate, copepod, diatom, dinoflagellate, dinophysis, foraminifera, gastropoda, protopteridium, and silicoflagellate, which included species, genus or families, with class as the lowest taxonomic resolution (Fig. S2). Note that the metazoan groups from the PUP net samples (bivalves, gastropods, and copepods) refer to their larval stages (e.g. nauplii in the case of copepods). Due to the distinct differences in shapes, some specific genera were separated from the general class, e.g. tripos, dinophysis and protopteridium were considered separately from the general dinoflagellate class. Appendicularia from the PUP net samples were excluded from the analysis due size measurement issues related to their transparency. Likewise, pictures of unknown organisms and non-living particles (such as detritus, sand, fibers etc.) were excluded from further analysis. Note that the relative amount of detritus within each sample was calculated per station and used as an index of turbidity (in %).

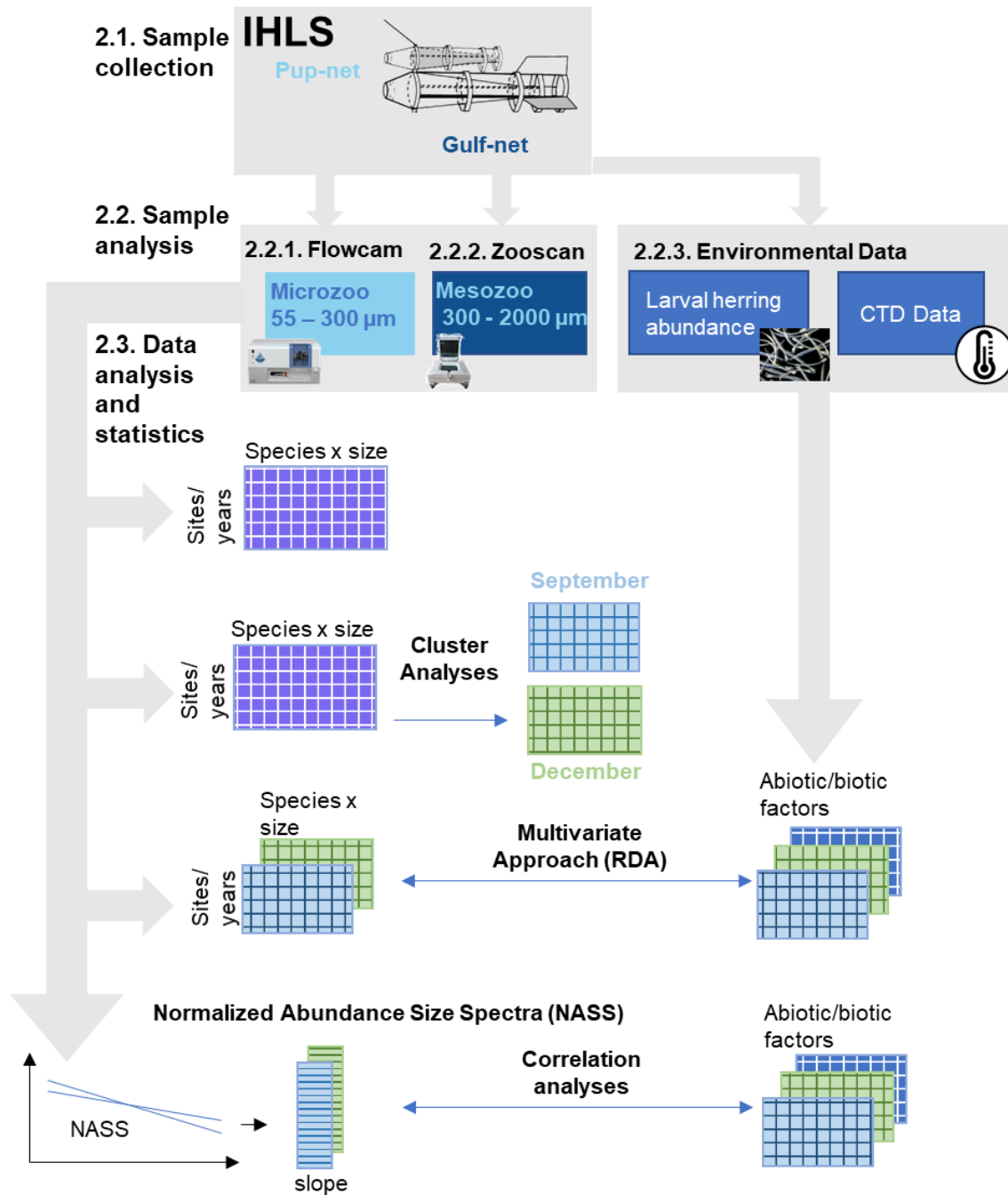


Fig. 2. Flowchart of the methodology encompassing field sampling and data analyses in this study. Numbers indicate section numbers in the text.

Mesozooplankton samples - ZooSCAN

Mesozooplankton samples were subsampled using 1/16 to 1/1024 of the original sample following Motoda (1967) and one subsample per station was placed into the ZooSCAN v.2 (Gorsky et al. 2010). The images captured by the ZooSCAN were classified automatically using ImageJ software (v. 1.41o) with ZooProcess (v.7.19) and the Plankton Identifier software (v.1.3.4), followed by a final manual validation step. Organisms were grouped into 10 taxa sets:

appendicularia, chaetognatha, cladocera, copepods, diatoms, echinodermata, gastropods, jellies, malacostraca, and polychaeta (Fig. S2). The metazoan groups echinoderms, malacostraca, and gastropods, refer to their larval stages. As for microplankton, we treated classes that were easily distinguishable due to their shape as separate taxa sets. For instance, we pooled all gelatinous zooplankton except chaetognatha and appendicularians in the jellies taxa (mainly ctenophores).

Environmental data & larval fish

Environmental variables (water temperature, salinity) were recorded by a CTD (conductivity, temperature, depth) profiler (Seabird SBE 911) attached to the Gulf VII net. For further analysis, salinity and temperature were averaged over the upper 20 m of the water column. Turbidity was calculated, based on the amount of detritus contained in each sample (see 2.2.1). Herring larvae in the GULF VII net were counted and measured to the nearest millimeter. Further technical and methodological details for the larval handling and the survey can be found at Schmidt et al. (2009) and references therein.

Data analysis and statistics

Micro- and mesozooplankton datasets were combined to analyze the planktonic community between 55 and 2000 μm . Classes that were present in both methods (copepods, gastropods and diatoms) were merged together (Fig. S2). To avoid overlapping in size classes and double counts, taxa $<300 \mu\text{m}$ were excluded from the mesozooplankton dataset.

The biovolume (BV, μm^3) of each planktonic organism was calculated using a modified version of the formula proposed by Saccà (2016)

$$\text{BV} (\mu\text{m}^3) = \frac{4}{3} * \sqrt{\pi^{-1} * \text{AR} * \text{A}^3} \quad (1)$$

where AR is the aspect ratio (ratio between the width and the length) and A is the area (μm^2) of each organism. Both values were determined by the FlowCAM and ZooSCAN. The BV was then used to calculate the carbon biomass for the different plankton taxa using taxa-specific equations (Table S1; Menden-Deuer et al. 2001, Kjørboe 2013). Note that sizes (width and length) were not corrected by the potential effect of fixation. We are aware of the fact that the fixation can cause swelling, shrinking or even the loss of certain organisms (e.g. Calbet and Saiz 2005), and discuss this topic below (see section 4.1).

Hierarchical cluster analysis (HCA) was applied to detect changes in the plankton community across seasons/areas. Abundance data was scaled using the triple-square-root transformation to reduce the data skewness (Legendre & Gallagher 2001). The Euclidean Distance and the

Ward linkage was calculated on the transformed abundance data per species and survey (Buttigieg & Ramette 2014, Murtagh & Legendre 2014). Additionally, we conducted a SIMilarity PERcentages (SIMPER) analysis (Clarke, 1993) to determine the taxonomic groups that contributed most to the dissimilarities between the two spawning grounds.

To investigate the changes in the plankton size-structure of the plankton community, NASS were constructed for each station. All zooplankton organisms were grouped into size classes based on their BV (irrespective of taxa), using a doubling or octave scale (Sheldon et al. 1972, Blanco et al. 1994). Size classes with low counts (0.01% of all records) were excluded, leading to classes ranging between size 14 (BV $\sim 1.6 \times 10^5 \mu\text{m}^3$) and 33 (BV $\sim 8.5 \times 10^9 \mu\text{m}^3$). The total abundance of each size class was divided by its width (in terms of BV) in order to normalize the size-spectra. A linear weighted regression was fitted to the obtained NASS:

$$\log_2\beta(\text{BV}) = a \log_2 \text{BV} + b \quad (2)$$

where a and b were the slope and the intercept of the NASS β (BV), respectively. Weights of the regression were proportional to the zooplankton abundance in the corresponding BV classes.

The influence of environmental drivers on the plankton community was explored using two approaches: a correlation analysis on the size-resolved dataset (NASS slopes) and a redundancy analysis (RDA) which used the taxa- and size- resolved plankton community structure (Legendre 2001). Prior the RDA approach, the abundance data was transformed after Hellinger (Legendre & Gallagher 2001). The environmental variables used in both approaches included water temperature and salinity averaged over the upper 20 m, distance to shore (m), depth (m) and turbidity (%). Moreover, we used the larval herring abundance (ind m^{-3}) for each station as an additional explanatory variable. In the size only approach, Pearson correlation (Pearson 1896) was used to identify the relations between the potential environmental drivers and NASS variability. An ANalysis Of VARiance (ANOVA) was used to test the significance of the explanatory variables on the Principle Components (RDA-PC) of the abundance data.

All analyses and graphical representations were performed using the R software (R core Team, 2022). The RDA analysis was performed using 'ade4' package (Bougeard & Dray 2018) and the HCA with the 'gplots' package (Warnes et al., 2022).

Results

Plankton community composition

In total, 18 taxonomic groups of plankton were identified across both areas. Most taxa were present in all surveys, except two Downs surveys in 2013 and 2018 with reduced spatial coverage (Fig. 3). The hierarchical cluster analysis clearly separated the planktonic communities in Buchan/Banks and Downs (Fig. 3). The SIMPER analysis revealed that the areas were 22.7% different from each other with most taxonomic groups being significantly more abundant ($p < 0.05$) in Buchan/Banks than Downs (Table S2). *Triplos*, *dinophysis*, *silicoflagellates*, *ciliates*, *protopteridinium* and gastropod larvae had higher abundances in Buchan/Banks, being responsible for >62% of the dissimilarity between the areas/seasons (in bold in Fig. 3, Table S2). Diatoms, bivalves and dinoflagellates had similar abundances in both areas, and only foraminifera were more abundant in Downs.

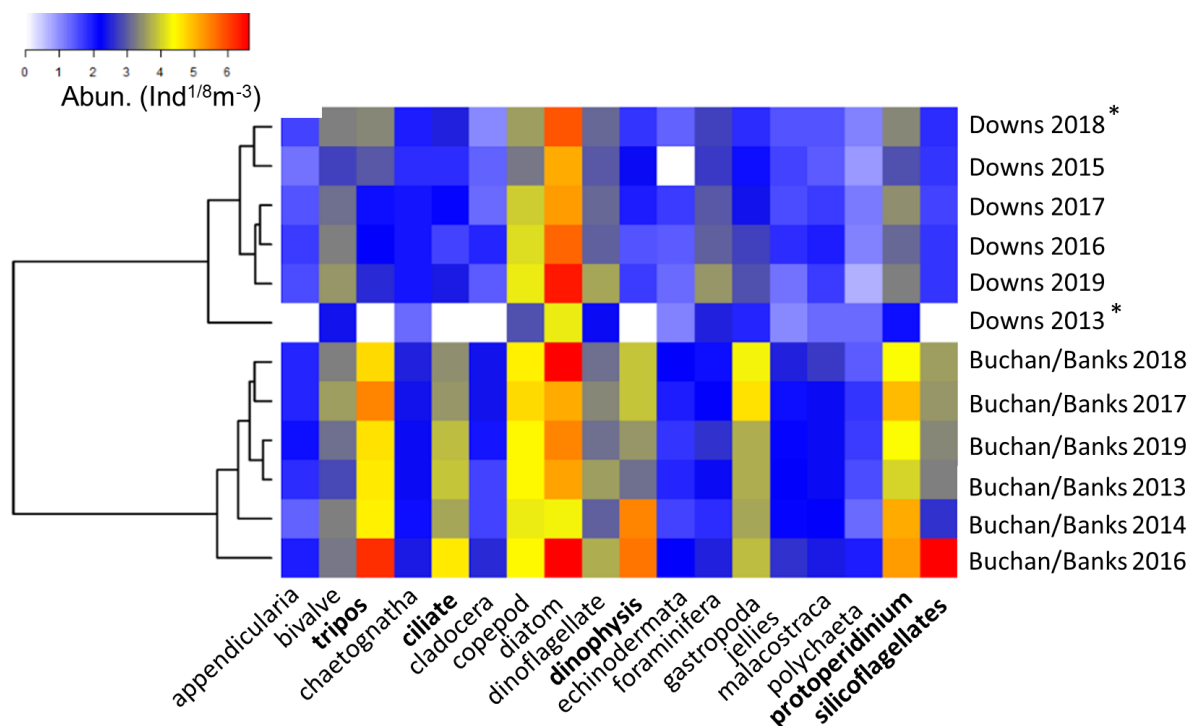


Fig. 3. Clustering and associated heatmap of the abundance of different micro- and mesozooplankton taxa (x-axis) for each of the analyzed North Sea cruises (y-axis indicating location, Downs or Buchan/Banks, and year). In the heatmap the colors blue (low abundance) to red (high abundance) indicate the strength of association by showing the frequency of triple-square-root transformed abundance ($\text{ind}^{1/8} \text{m}^{-3}$) per taxa in each year and area. White color indicates the missing taxa. The dendrogram clusters together cruises from each area. Note the asterisk (*) indicate years with the reduced spatial coverage (see Fig S1). Taxa sets mainly responsible for dissimilarities between spawning grounds are written in bold.

Overall, microplankton taxa (including nauplii) contributed >98% to the total plankton abundance of which diatoms and tripos dominated (>50% in Buchan/Banks and 90% in Downs) (Table S3, S4). Copepod nauplii were less abundant (approx. 4-5% of the total microplankton abundance, Table S3, S4), but they dominated in terms of biomass (27% of the total microplankton biomass in Buchan/Banks vs 41% in Downs, Table S5, S6). For the mesozooplankton, gastropods and larger copepods dominated the community in terms of both abundance and biomass, contributing on average 10 % (30 %) of total mesozooplankton abundance and 38% (43%) of total biomass in Buchan/Banks (Downs). The average abundance ratio of microplankton to mesozooplankton was 90:1 for Buchan/Banks and 235:1 for Downs (Table S3, S4). Due to the differences in the planktonic community shown with the HCA, we further analyzed both sampled areas/seasons separately.

Environmental drivers of plankton abundance and distribution

Environmental conditions were distinct and showed clear spatial patterns in both studied areas/seasons. We provide more details on the environmental conditions in supplementary materials (Fig. S3), and focus here only on their relations with the planktonic community.

In the Buchan/Banks area, the six explanatory variables used in the RDA explained 11.4% of the total variation in plankton abundance, whereby the half of this covariation (6%) was summarized in the first Principal Component of the abundance data (RDA-PC1, Fig. 4A). Middle sized gastropods, ciliates and chaetognatha (size classes 18-22) had the highest positive scores in RDA-PC1 and small silicoflagellates, dinophysis and jellies (size class 14-17) had the highest negative scores (Fig. 4A, 4B). Larger size classes (26-33) did not show any distinct pattern and their RDA-PC1 scores ranged between -0.1 and 0.1 (Fig. 4B). The observed spatial pattern in the Buchan/Banks area (Fig. 4C) was consistent over the sampled years, except for 2016, which appeared to have exceptionally low salinity, resulting in negative scores for most stations, associated with higher abundance of silicoflagellates, dinophysis and jellies (Fig. 4D). All six explanatory variables were significant (ANOVA, $p < 0.001$), but salinity, turbidity, and bottom depth had the highest positive scores, mainly in northern stations (Fig. 4C, 4E).

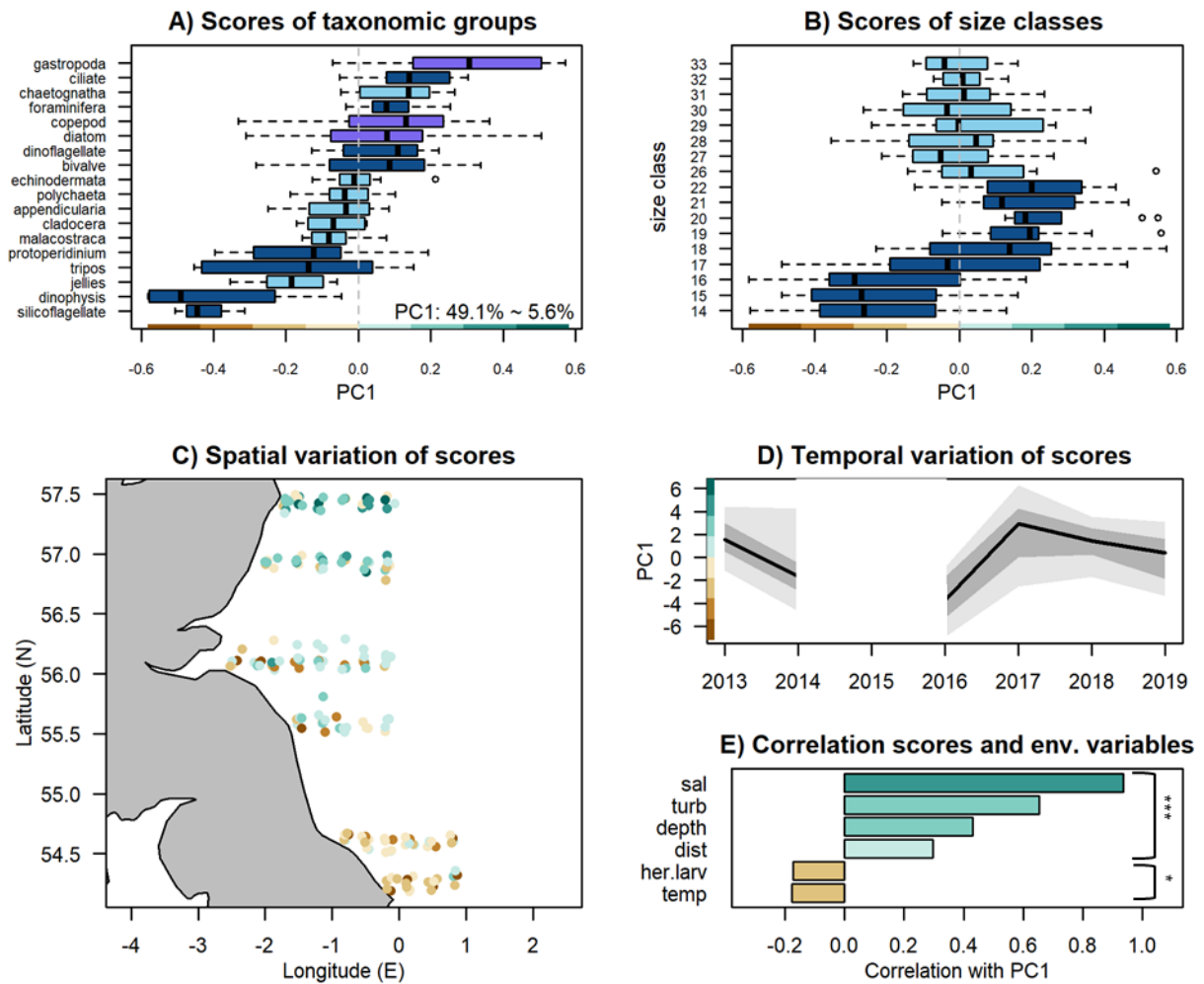


Fig. 4. Results of the redundancy analysis (RDA) analyzing the effect of five environmental drivers (distance to shore (dist), turbidity (turb), salinity (sal), temperature (temp), and bottom depth (depth)) and herring larvae abundance (her.larv) on the zooplankton community composition and distribution during the Buchan/Banks surveys (September/autumn). Each subpanel displays the scores of the Principal Component 1 (PC1) among taxonomic groups and the explained variability (A), the size classes with the different types indicated in dark blue (FlowCAM), light blue (ZooSCAN) and purple (both) (B), The map of the stations' score shows its spatial variation, with the stations coordinates being jittered to avoid overlap among years (C). The temporal variation of stations' score is represented with a bold black line for the median, dark grey area for the inter quartile range, and light grey area for the 95% quantiles (D). Pearson correlation coefficient between the PC1 and the six explanatory variables: herring larvae abundance (her.larv), distance to shore (dist), salinity (sal), temperature (temp), turbidity (turb) and bottom depth (depth) including the significance lines (***) $p < 0.001$, * $p < 0.05$). Color intensity is proportional to the correlation coefficients (brown – negative, cyan – positive) and shows the impact on the respective station (E).

In the Downs area, the RDA explained in total 10.6% of the variability in plankton abundance within the analyzed period, of which 33.5% (3.6% of total variation) was framed within the RDA-PC1 (Fig. 5A). Large chaetognatha (size class 30-31), tripos and dinoflagellates were more abundant in the English Channel, while medium to large sized copepods (size class 26-28), polychaeta and jellies were more abundant in the Southern Bight stations and had the highest positive scores (Fig. 5A, 5B). Most distribution of scores per size classes crosses zero (except

classes 14, 15, 19 and 22) and the absolute value of the median score per size class is between -0.2 and 0.2; hence, there was no pronounced effect of most size classes on RDA-PC1 (Fig.5B). The described west-east pattern was detected in all years with full spatial coverage (2016, 2017 and 2019) (Fig. 5C and 5D). Four of the six explanatory variables (i.e temperature, salinity, depth and turbidity) had a significant effect on RDA-PC1 (ANOVA, $p < 0.001$, Fig. 5E). Overall, temperature, salinity and depth had the highest negative scores, generally towards the southwestern stations (Fig. 5E).

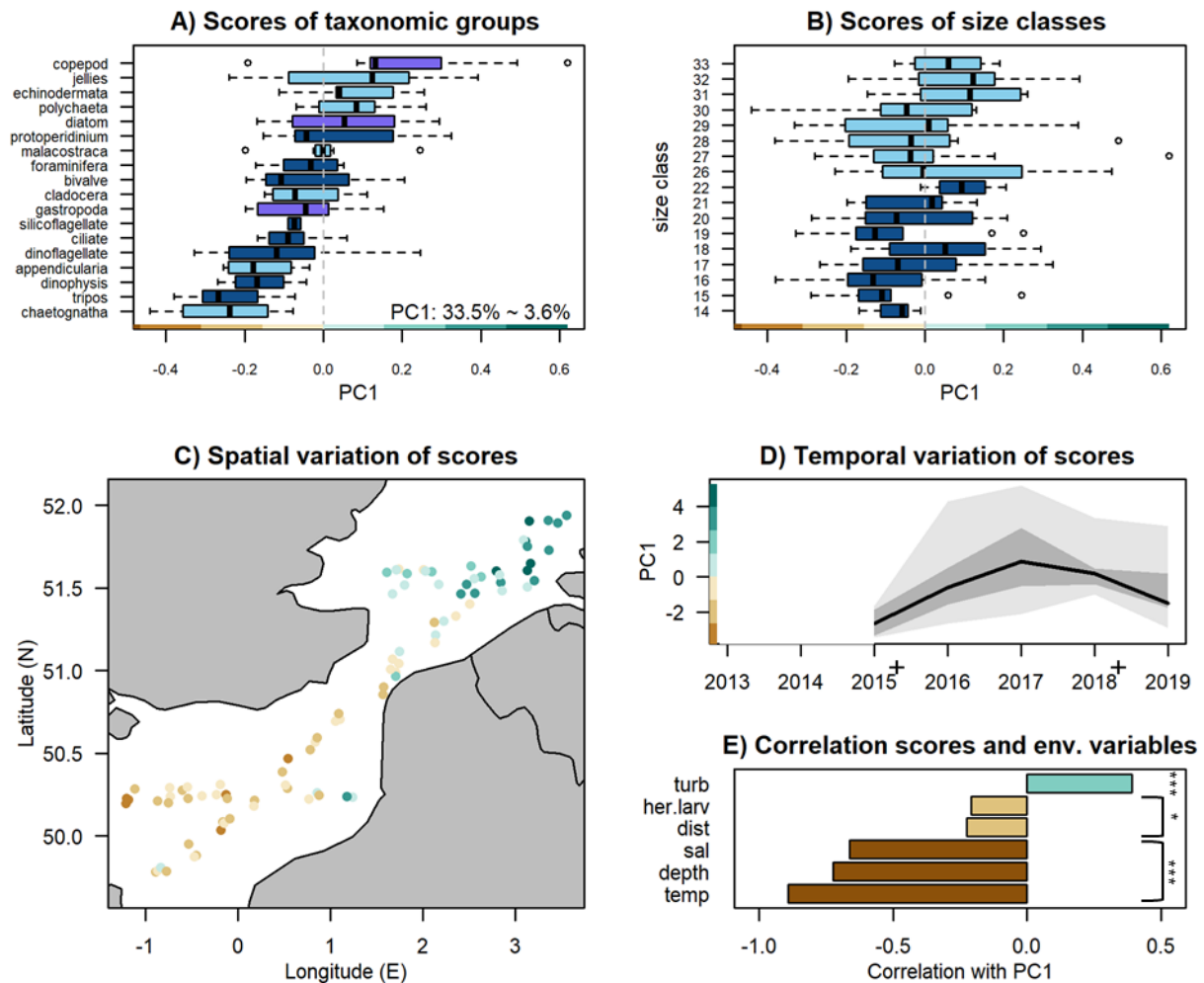


Fig. 5 Results of the redundancy analysis (RDA) analyzing the effect of five environmental drivers (distance to shore (dist), turbidity (turb), salinity (sal), temperature (temp), and bottom depth (depth)) and herring larvae abundance (her.larv) on the zooplankton community composition and distribution during the Downs surveys (December/winter). Each subpanel displays the scores of the Principal Component 1 (PC1) among taxonomic groups and the explained variability (A), the size classes with the different types indicated in dark blue (FlowCAM), light blue (ZooSCAN) and purple (both) (B), The map of the stations' score shows its spatial variation, with the stations coordinates being jittered to avoid overlap among years (C). The temporal variation of stations' score is represented with a bold black line for the median, dark grey area for the inter quartile range, and light grey area for the 95% quantiles. Years with + indicate incomplete sampling (D). Pearson correlation coefficient between the PC1 and the six explanatory variables: herring larvae abundance (her.larv), distance to shore (dist), salinity (sal), temperature (temp), turbidity (turb) and bottom depth (depth) including the significance lines (** $p < 0.001$, * $p < 0.05$). Color intensity is proportional to the correlation coefficients (brown – negative, cyan – positive) and shows the impact on the respective station (E).

Larval herring abundance, used as a predation index, had a significant effect on the RDA-PC1 in Buchan/Banks (ANOVA, $p < 0.001$) but not in the RDA-PC1 Downs (ANOVA, $p > 0.05$). In all cases, it had a lower score than other environmental variables tested, and, therefore, the lowest effect on the plankton community (Pearson correlation coefficient, $r = > -0.2$).

Plankton size structure and environmental drivers

The total mean NASS slope for Buchan/Banks was -1.45 (Fig. 6A), with the highest frequencies between -1.2 and -1.6 (Fig. 6B). The range of NASS intercepts was between 5 and 30 (Supplements 2). The correlation analysis using the NASS slopes in Buchan/Banks showed only slight tendency to flatter slopes (> -1.4 , light to dark-orange dots in Fig. 6C) at the northern stations (indicating a higher abundance of larger organisms). Mean NASS slope was steeper in 2014 and 2016 (< -1.6) than in 2017, 2018 and 2019 (> -1.4) (Fig. 6D). The NASS slopes in Buchan/Banks showed the strongest correlations with salinity and turbidity ($r = 0.57$ and $r = 0.58$, respectively, $p < 0.001$), but all other environmental variables, except herring larval abundance, were significant as well at $p < 0.05$ (Fig. 6E). The temporal distribution of the NASS slopes in Buchan/Banks reflected well the patterns captured in the RDA-PC1 scores. The amount of variability in the NASS slopes explained by the environmental variables in Buchan/Banks was 46% (adj. R^2).

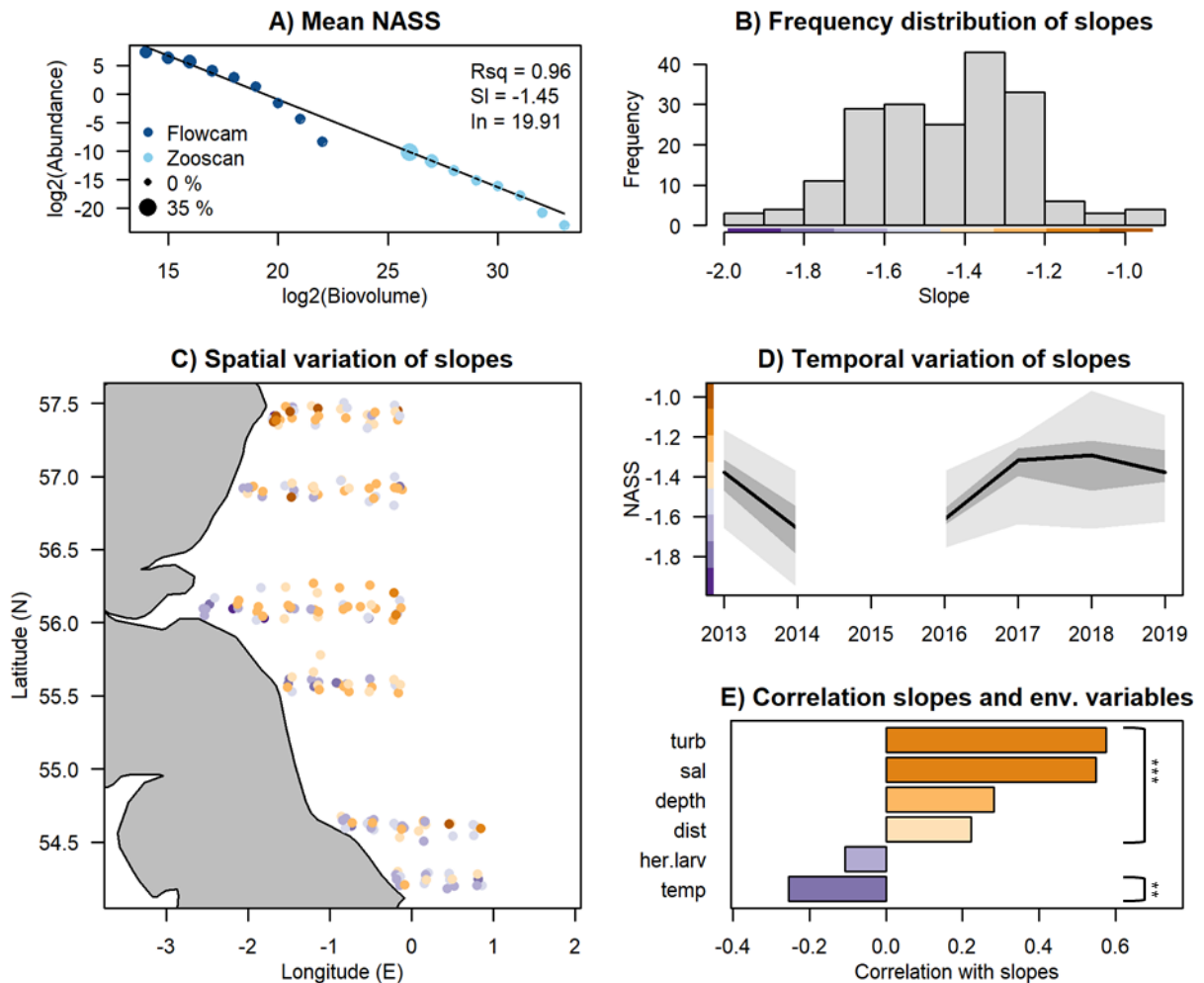


Fig. 6 Mean normalized abundance size spectra (NASS) calculated for all stations in Buchan/Banks survey in September/autumn (A). The dots in light blue represents size classes sampled by FlowCAM, in dark blue by ZooSCAN. The size of the dots represents the relative abundance of the size class, used in the weight linear regression to derive the slope of the size spectra. Information on the goodness of fit ($R^2 = 0.96$), slope ($SI = -1.45$) and intercept ($ln = 19.91$) are detailed. (B) Histograms showing the distribution of individual slopes. (C) The map of the NASS slope depicted in color shows its spatial variation, with the stations coordinates being jittered to avoid overlap. (D) The temporal variation of NASS slope is represented with a bold black line for the median, dark grey area for the inter quartile range, and light grey area for the 95% quantiles. (E) Pearson correlation coefficient between the slope and the six explanatory variables: herring larvae abundance (her.larv), distance to shore (dist), salinity (sal), temperature (temp), turbidity (turb) and bottom depth (depth) including the significance lines (** $p < 0.01$, *** $p < 0.001$). Color intensity is proportional to the correlation coefficients (purple – negative, orange – positive).

In Downs, the mean NASS slope was -1.67 (Fig. 7A), with highest frequencies between -1.9 and -1.6 (Fig. 7B). The range of NASS intercepts was between 15 and 30 (Supplements 2). In years with full spatial coverage (2016, 2017, 2019), the NASS slopes in Downs showed a gradient with flatter size spectra (> -1.4) in the northeastern stations and steeper slopes (< -1.6) in the southwestern stations (Fig. 7C and 7D). The NASS slopes in this area showed a high negative correlation with temperature, salinity and depth ($r = -0.52$, $r = -0.49$, and $r = -0.34$ respectively, $p < 0.05$) (Fig. 7E), while turbidity showed the highest correlation (positive) with the NASS slopes ($r = 0.58$, $p < 0.05$) (Fig. 7E). Similar to Buchan/Banks, the temporal

distribution of the NASS slopes in Downs followed a similar pattern to that observed in the RDA-PC1 scores. Note that the amount of variability in the NASS slopes explained by the environmental variables in this area was 55% (adj. R^2).

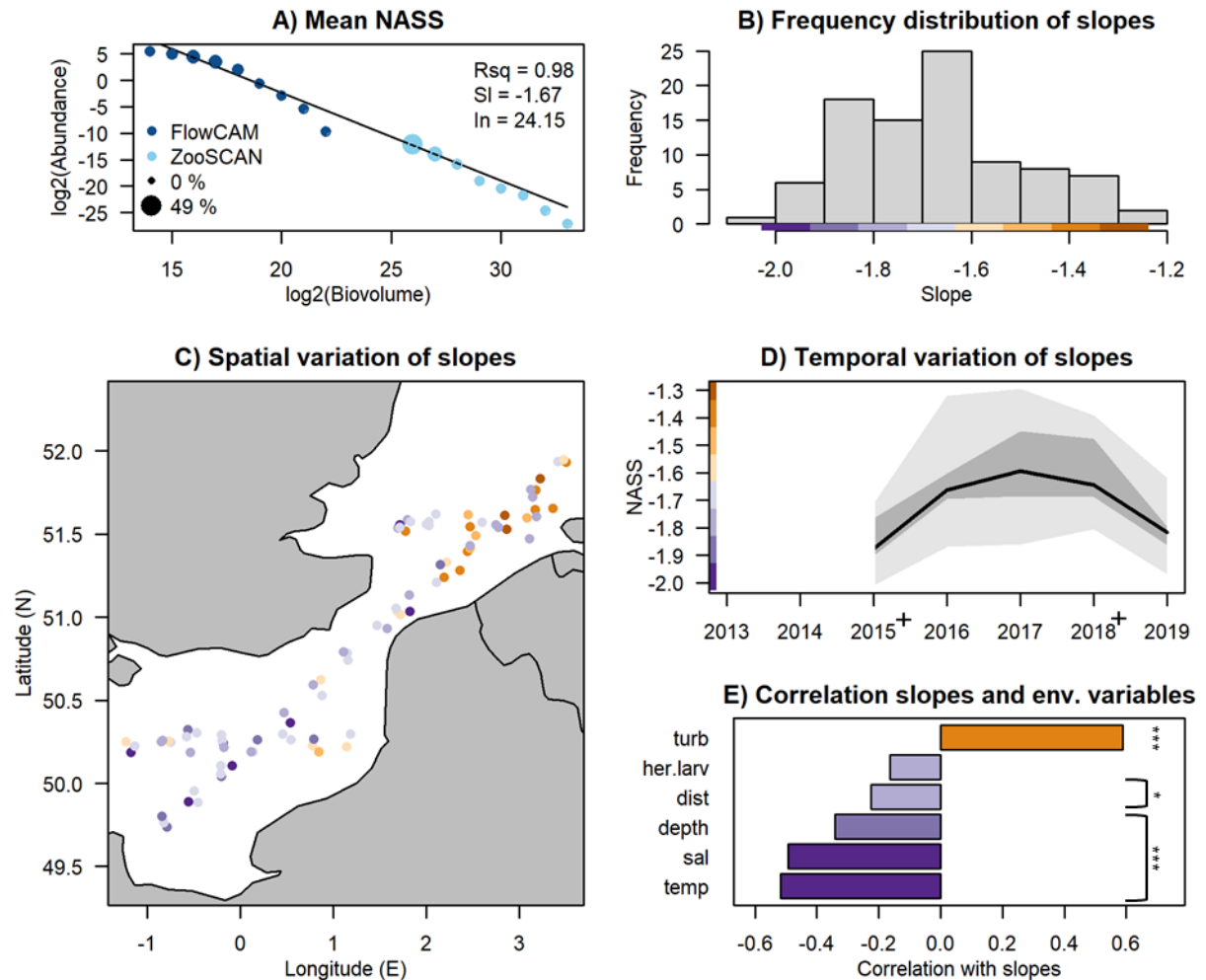


Fig. 7 Normalized abundance size spectra (NASS) calculated for the complete dataset for Downs survey in December/ winter (A). Information on the goodness of fit ($Rsq = 0.98$), slope ($SI = -1.67$) and intercept ($ln = 24.15$) are detailed. The size of the dots represents the relative abundance of the size class, used in the weight linear regression to derive the slope of the size spectra. The dots in light blue represents size classes sampled by FlowCAM, in dark blue by ZooSCAN. (B) Histograms with the distribution of slopes. (C) The map of the stations' slope depicted in color shows its spatial variation, with the stations coordinates being jittered to avoid overlap. (D) The temporal variation of stations' slope is represented with a bold black line for the median, dark grey area for the inter quartile range, and light grey area for the 95% quantiles. Years with + indicate incomplete sampling. (E) The Pearson correlation coefficient between the slope and the five explanatory variables: herring larvae abundance (her.larv), distance to shore (dist), salinity (sal), turbidity (turb) and bottom depth (depth) including the significance lines (** $p < 0.001$, * $p < 0.05$). Color intensity is proportional to the correlation coefficients (purple – negative, orange - positive).

Discussion

Spatio-temporal variability in plankton community composition

Periods of low productivity in temperate marine ecosystems, such as late autumn and winter, have received less attention in plankton ecology studies as the more productive seasons (i.e. spring and summer). During those periods, the role of microzooplankton as an energy mediator is expected to be enhanced (Calbet & Saiz 2005), but there is still limited broad-scale data available to explore the variability and the trophodynamic role of this group, even in well-studied marine ecosystems (Bils et al. 2019). The present study provides broad-scale survey results of the autumn and winter standing stocks of micro- and mesozooplankton in the western and southern North Sea during seven years.

Within the studied areas and years, the planktonic community was homogeneous in terms of the relative contribution of different taxa during autumn and winter, but the absolute abundance of organisms in almost all taxa (except diatoms, dinoflagellates and bivalves) was lower during winter. The observed broad range in abundances was consistent with other studies (mean range 182.9 – 3825.4 ind m⁻³, Table S7). For example, the observed total plankton abundance in the English Channel during winter was within the range of previously reported values (354.9 vs 266.6 ind m⁻³ in Dudeck et al. 2021, and 1500.0 ind m⁻³ in Eloire et al. 2010, Table S6). The same applies to specific taxonomic groups. For example, the mean abundance of copepod nauplii in autumn and winter (55 and 38.1 ind L⁻¹, respectively) was similar to values reported at the Dove station (4.0 to 20.0 ind L⁻¹ in autumn, 15.0 to 43.0 ind L⁻¹ in winter ; Pitois et al. 2009). It is important to note that the overall abundance in Buchan/Banks was slightly lower than reported from other studies in the North Sea (4172.9 ind m⁻³, Eloire et al. 2010) and other temperate seas (1239.0 ind m⁻³ in Georges Bank, Morse et al. 2017), despite using a similar sampling method. This is mainly largely attributed to two years of particularly low plankton abundance (see e.g. 2013 and 2019, Table S3). This is a good example of the potential pitfalls of short time series, where unusual years can have a great effect on the overall results (e.g. Widdicombe et al. 2010). Although total abundances may differ, the relative abundance of various groups such as copepods (60 to 80%) agrees with other studies (e.g. Morse et al. 2017, Tab. S7).

The sampling method presented here, using two plankton nets simultaneously (mesh size 55 and 280 µm), has been already proposed as the most adequate approach to capture the entire mesozooplankton assemblage, including small copepods (e.g. *Oithona* spp.) and other small metazoans (Calbet et al. 2001).

On average, 11% more of the copepodites and adult copepods (>200 μm) were captured in the 55- μm plankton net compared to the 280- μm GULF VII alone. The abundance of mesozooplankton caught in the GULF net alone was 7.2 times lower when using only a traditional 200- μm net versus a combination with a 55 μm net, similar to a previous study (8.1 times lower, Calbet et al. 2001).

This finding advocates for the combined use of different mesh-sized nets in large-scale routine monitoring programs to gain a more realistic estimate of large microzooplankton and the entire mesozooplankton community.

The average abundance of protists (dinoflagellates and ciliates) obtained in this study was between two and six orders of magnitude lower than previously reported for the North Sea (Bresnan et al. 2015, Bils et al. 2019; Table S7). This discrepancy is likely due to differences in sampling and preservation methods. Those studies sampled protists using Niskin bottles and preserved the samples in lugol, whereas a PUP net was used here and the samples were fixed in formaldehyde. Mesh filtering of a plankton net can lead up to 60% loss of protists (Gifford & Caron 2000), and formaldehyde fixation causes soft-bodied dinoflagellates and ciliates to dissolve (Calbet & Saiz 2005). Therefore, it is important to interpret our results for protozoa with caution, as our method most probably underestimates their abundance. Among the ciliates, tintinnids are the only group able to better withstand various types of preservation and filtration (Modigh & Castaldo 2005). For this group, abundances reported here were comparable with a previous study in the North Sea (Bils et al. 2019, Table S7).

Spatio-temporal variability in the plankton size structure

Body size is an important ecological trait, which is relatively easy to measure in plankton samples, especially via automatic image analysis. These body sizes can be used to build zooplankton size spectra (either NASS or NBSS), which can serve as indicators of ecosystem status (Blanchard et al. 2017, Atkinson et al. 2021) and are helpful tools identifying alterations in the food-web structure (Gorokhova et al. 2016). While NBSS are arguably more common in plankton ecology studies (e.g. Sprules & Munawar 1986, San Martin et al. 2006), here we chose to calculate NASS over NBSS because i) the biovolume was based on linear measures of organisms directly provided by FlowCAM and ZooSCAN, ii) species or genus specific conversion formulas between individual biovolume and biomass had to be applied on “broad” taxa sets, which might lead to biomass miscalculations; and iii) the calculated NASS and associated linear model (Eq. 2) resulted in a higher coefficient of determination ($R^2= 0.98 \pm 0.02$) than for the NBSS ($R^2= 0.83 \pm 0.11$).

In this study, the average NASS slopes were -1.45 (± 0.20 SD) in Buchan/Banks and -1.67 (± 0.18 SD) in Downs. The steeper slopes in Downs during winter indicate lower abundances

of larger organisms compared to Buchan/Banks, which were reflected well in the microzooplankton:mesozooplankton abundance ratio for both areas. NASS intercepts were similar in both sampling areas, although Buchan/Banks showed a wider range (5 to 30) compared to Downs (15 to 30). If we consider the intercept as a reflection of the primary production (Ye et al. 2013), it appears that the production levels are on a comparable levels despite the different seasons.

The NASS slopes reported in this study were below the theoretical value of -2.0 for NASS (which translates into -1.0 for NBSS) (Blanco et al. 1994). This theoretical value is based on analysis of the whole pelagic community (from picoplankton to fish), and therefore a direct comparison is not possible when analyzing a limited size range (Kerr & Dickie 2001). Furthermore, comparison with previously reported slopes must be done with care due to various variables, units and axis scaling used within size-spectra approaches (Blanco et al., 1994; Sprules & Barth 2016). Sampling, counting or preservation methodologies used for small-sized organisms here can potentially affect the NASS as well. For instance, NASS slopes of phytoplankton samples (3 to 100 μm ESD) from the Cantabrian Sea differed based on the preservation and analysis method: -1.77 for samples preserved in lugol and analyzed with microscopy vs -1.99 and -2.11 for fresh samples analyzed using the FlowCAM with two different imaging modes (in \log_{10} -biovolume; Álvarez et al. 2014). These accuracies need to be taken into account when exploring differences across ecosystems or among years and/or season (e.g. Zhang et al. 2019), although trends within studies can always be compared. For example, steeper NBSS slopes were observed offshore compared to nearshore for nano- and microplankton in the southern China Sea (Liu et al. 2021), while mesozooplankton NBSS slopes flattened offshore in the subarctic North Pacific (Kwong et al. 2022). In this latter work and others in temperate seas (e.g. Atkinson et al. 2021), NBSS showed a significant seasonality, with steep slopes (and lower intercepts in some cases) during the winter. These results agree with the steeper slopes reported in our study, although no difference in the intercepts was found here. In this sense, it is important to note that there are significant differences between both studied areas in terms of seasonality, water mass properties, and bathymetric characteristics, among others.

Environmental drivers of the plankton taxonomic composition and size structure

Salinity, turbidity, depth and distance to the coast were found to be the main drivers of the plankton community and size composition in Buchan/Banks in autumn (Figs 4E and 6E), while temperature, salinity, depth and turbidity were the main factors in Downs in winter (Figs 5E and 7E). Temperature and salinity are known to be related to the water masses and their

dynamics, whereas turbidity (defined here as percentage of detritus) is mainly driven by processes like river runoff, dust deposition and resuspension of seabed sediments. Both studied areas are strongly influenced by the inflow of highly saline Atlantic water and river runoff (Lee 1980). In the Buchan/Banks area, Atlantic water flows southward and mixes gradually with the less saline North Sea coastal waters influenced by the freshwater discharge from Tyne, Tees and Humber rivers (Emeis et al. 2015). No clear temperature gradient was observed between the two water masses in autumn (Fig S3) and, therefore, temperature appeared to be a less pronounced explanatory variable in both RDA and correlation analysis applied to the zooplankton data in this region (Figs 4E, 6E).

Gastropod larvae and chaetognaths were found in higher abundances at the northern stations of Buchan/Banks, in the area strongly influenced by the Atlantic inflow. This agrees well with previous findings of the gastropods *Spiratella retroversa*, *Clione limancina*, and the chaetognath *Sagitta elegans* being characteristic taxa in the northwestern North Sea (Vane 1961, Bone et al. 1987). Tintinnids (the major group in the ciliate taxa set in this study) were found to be abundant at the northern stations in Buchan/Banks as well, whereas they have been previously reported to be more abundant in the southern North Sea during wintertime (Bils et al. 2019). This discrepancy may be related to the different environmental preferences of different tintinnid species (e.g. salinity, Cordeiro et al. 1997), which were not accounted for in our broad taxa sets. Silicoflagellates, dinoflagellates (such as *Dinophysis spp.*) and gelatinous plankton (pooled as “jellies” here) were more abundant in the fresher and shallower waters in the south. Although nutrients were not measured, we speculate that those taxa sets were more abundant there due to an elevated nutrient concentration associated with the river runoff as suggested by Jochem & Babenerd (1989) and Purcell et al (2001).

Turbidity was identified as one of the factors affecting the variability of the zooplankton community and its size structure in the Buchan/Banks area. Turbidity was positively correlated with salinity; therefore, high turbidity cannot be ascribed to the river inflow there. We assume that elevated turbidity at the northern stations was linked to the vertical water mixing and sediment resuspension. Wilson & Heath (2019) showed that in September the water column is well-mixed in the Buchan area (north), whereas it is predominantly stratified in the Banks area (south). Since the effects of turbidity were weaker than the effects of salinity, we assume that the former had just an ancillary effect on the plankton community.

Changes in the NASS slope in Buchan/Banks were consistent with the observed community composition and the distribution of the water masses. Since large zooplankton taxa such as gastropoda and chaetognatha were more abundant in the north and small-sized taxa such as silicoflagellates and dinophysis in the south, the NASS slope was relatively flat in the northern stations (>-1.6) compared to the southern ones (<-1.6 , Fig. 6C). The temporal distribution of

the NASS slope reflected well the patterns captured in the RDA PC1 scores for Buchan/Banks, as the curve-shape over the analyzed time span was equivalent (Figs 4D and 6D).

Our observations on the environmental variables in Downs in December showed a prominent southwest-northeast gradient from warmer, more saline and less turbid waters of Atlantic origin in the English Channel to colder, fresher and more turbid coastal waters in the Southern Bight (Fig S3). Chaetognaths, dinoflagellates, and tripos were dominant taxa sets in the central English Channel, whereas large copepods, jellies and echinoderm larvae were more abundant in the Southern Bight. These results are consistent with reported higher winter abundances of copepods near the Belgium and Dutch coasts compared to the English Channel (Dudeck et al. 2021). As for the jellies, although they are generally known to thrive in warmer waters, high abundances of gelatinous plankton have been previously observed under cold conditions across the North Sea and in the Celtic Sea (Purcell 2005, Haberlin et al. 2019). Similarly to the Buchan and Banks area, we presume that a nutrient flux from the Rhine-Meuse-Scheldt delta can potentially explain the elevated jellyfish abundance in the Southern Bight (Purcell et al. 2001). Furthermore, since the shallow English Channel and Southern Bight are well-mixed in winter (Wilson & Heath 2019), we assume that the elevated turbidity associated with low saline waters in the Southern Bight was linked to the river discharge.

The influence of temperature and salinity on the slope of the NASS was consistent with the results of the RDA: flatter NASS slope (>-1.6) in the Southern Bight dominated by larger organisms, and steeper slopes (-1.7) in the English Channel with a higher contribution of smaller organisms. Note that we found a stronger influence of turbidity on the NASS slope than on the community structure (Figs 5E and 7E). In fact, among all tested variables, turbidity appeared to have the strongest correlation with NASS slope (Fig 5E). This can be related to the accumulation of larger size classes (zooplankton) but not smaller ones (phytoplankton and protists) near turbidity maxima, as observed in some estuarine systems like Chesapeake Bay (Roman et al. 2001, Keller et al. 2014).

Previous studies have reported the impacts of the water masses dynamics and Atlantic inflow on the planktonic community and its spatiotemporal variability in the North Sea (e.g. Krause et al. 2003, Taylor et al. 2021). Our results confirm that the water mass structure, zooplankton community and size structure are strongly related during the low productive season in the North Sea. However, beside environmental effects, biological interactions (predation, grazing, competition) are known to modify zooplankton community and size spectra to a large extent (Zhou 2006b, Zhou et al. 2009). Our approach of combining planktonic organisms into broad taxonomic groups did not allow elaborating on the complex food-web dynamics within the zooplankton community. Only the external predation pressure of herring larvae was tested here. We found a weak (not significant for Downs) relationship between zooplankton

community and size structure and herring abundance. These results are in line with Pepin & Penney (2000), who found no significant effects of larval predation on zooplankton biomass in the Newfoundland coastal waters.

Taxonomic information vs size spectra

Plankton time-series are increasingly used to inform marine policy and management about the state and productivity of ecosystems (McQuatters-Gollop et al. 2015, Bedford et al. 2018, 2020b). In particular, fisheries management is interested in zooplankton data since fish early-life stages and recruitment success depends on zooplankton stock and productivity. In this regard, it is important to generate data at an adequate spatial and temporal resolution that can reveal changes in ecosystem functioning. The development of easy and time-cost-effective tools to provide key data on plankton groups, their abundance or biomass is thus gaining increased attention (e.g. Pollina et al. 2022). The state-of-the-art automated image processing, although being time-effective, allows to identify zooplankton organisms to rather broad taxonomical groups (e.g. copepods, chaetognaths, dinoflagellates) and barely to the species level. Such analysis seems to be adequate to provide abundances and biomasses of certain zooplankton groups, which have been used to detect large-scale, long-term changes in the planktonic community in response to climate-related processes (e.g. Bedford et al. 2020a) and to create prey fields for studying foraging in early life stages of fish (Akimova et al., submitted). However, this broad taxonomical resolution precludes studying the environmental drivers affecting the community composition. In our study, the environmental variables explained a small percentage (11%) of the total spatiotemporal variability of the planktonic community (see section 3.5). This was probably due to the use of broad taxa sets, as different genera and taxa can have different habitat preferences. For instance, the copepod taxa set is likely partially composed of four common North Sea species (*Calanus finmarchicus*, *Calanus helgolandicus*, *Oithona atlantica*, and *Oithona similis*), which have very distinct affinities for temperature and salinity (Lindegren et al. 2020).

Once the taxonomic information was disregarded and a size-based approach was used, the identified environmental drivers remained similar but the proportion of the explained variance increased to 46% (see section 4.3). These results agree with previous studies suggesting that size spectra are particularly useful as they provide a simple metric of the ecosystem status that can be linked to general changes in food-web structure and ecosystem productivity (Sprules & Munawar 1986, Petchey & Belgrano 2010). The size spectra approach is often used to simplify energy fluxes from lower to higher trophic levels, in size-structured ecosystem models (e.g. Blanchard et al. 2017). In particular, this approach has been widely applied in larval fish

modelling given a limited ability of fish larvae to consume certain size fractions of their planktonic prey field (e.g. Huebert & Peck 2014).

The results from our study highlight the benefits and limitations of using taxonomically- and size-resolved vs. solely size-resolved plankton datasets. However, one needs to be careful with the choice of resolution as recent studies showed how it can drastically change the picture of the correlation between plankton and associated variables, such as patterns being emphasized or small scale changes being lost (Scott et al. 2023). The choice of a suitable methodology needs to consider the level of community discrimination required for a particular research question and additional factors such as data resolution, the available working time and local expertise. Ideally, both approaches would be used in combination to explore different aspects of the planktonic community. A third alternative approach would be the functional trait-based approach, where taxa are grouped into classes defined by their functional roles (e.g. feeding mode) rather than their size or taxonomic identity (Venello et al. 2021). This change to a functional approach would also reduce the complexity from the higher taxonomic resolution, providing a different view on the plankton community composition. In this regard, Venello et al. (2021) suggested that a combination of species/region specific and functional group-based analysis may lead to a more comprehensive view on zooplankton community dynamics.

Conclusion and Outlook

The present study provides a thorough examination of the plankton standing stocks and spatio-temporal changes in abundance of the micro- and mesozooplankton community in a temperate marine ecosystem during low productivity seasons. The planktonic community was shaped along environmental gradients, primarily salinity, temperature and turbidity, which are related to inflows of North Atlantic waters in the western and southern North Sea. These gradients became apparent when analyzing the community structure as broad taxa and size spectra slopes, suggesting that the size spectra approach can be a useful tool to track the variability in the plankton community related to environmental drivers.

Routine larvae surveys, such as the IHLS, offer a unique and low-cost opportunity for additional micro- and mesozooplankton sampling. So far, the IHLS only accounted for herring larvae in the Gulf VII plankton samples, and other planktonic organisms that have been analyzed only for targeted studies (e.g. Dudeck et al. 2021). However, this ecosystem-based approach to fisheries surveys is the way forward and has already been implemented elsewhere such as the PELGAS survey in the Bay of Biscay (Doray et al. 2018). The combination of automated survey instruments (e.g. PlanktoScope; Pollina et al. 2022) with automated plankton classification tools (Conradt et al. 2022) can greatly reduce the work effort, thus allowing for high frequency sampling in space and time. Ultimately, the combination of both traditional and

novel instruments and procedures will help to optimize survey design and resolution (Scott et al. 2023) to get a more holistic understanding of ecosystem processes. Plankton datasets stemming from this kind of surveys will support the goal of designing public and global datasets of plankton, which can be used i) as early-warning indicators of hydro-climatic changes (Bedford et al. 2018; Taylor et al, 2021), ii) for model validation, e.g. Nutrient Phytoplankton Zooplankton Detritus (NPZD) models (D’Alelio et al. 2016) or iii) to help identifying the top-down control of planktivorous fish and the strengths of bottom-up drivers of fish recruitment (Akimova et al. submitted), supporting the stock assessment and management process.

Author Contributions

G.B, M.M. and M.A.P. conceived the study; G.B. and C.v.D. performed the sampling; G.B., R.F., A.K. and M.M. did the data analysis; G.B. wrote the first draft of the manuscript and the co-authors provided comments.

Acknowledgements

This research was funded by the German Research Foundation (DFG) under project THRESHOLDS (Disentangling the effects of climate-driven processes on North Sea herring recruitment through physiological thresholds, MO 2873-3-1). We sincerely thank the crew, the students and the cruise leaders of the IHLS aboard of the RV Tridens. Furthermore, we thank Rachel Harmer, Silke Janßen and Sophie Lanners, which helped scanning and sorting plankton pictures and Jan Conradt for the help with the statistics.

References

- Akimova A, Börner G, Peck MA, van Damme C, Moyano M (2022). Combining modeling with novel field observations yields new insights into food limitation of wintertime larval fish [Manuscript submitted for publication].
- Alvarez-Fernandez S, Licandro P, Van Damme CJG, Hufnagl M (2015) Effect of zooplankton on fish larval abundance and distribution: A long-term study on North Sea herring (*Clupea harengus*). *ICES J Mar Sci* 72:2569–2577.
- Álvarez E, Moyano M, López-Urrutia Á, Nogueira E, Scharek R (2014) Routine determination of plankton community composition and size structure: A comparison between FlowCAM and light microscopy. *J Plankton Res* 36:170–184.
- Atkinson A, Lilley MKS, Hirst AG, McEvoy AJ, Tarran GA, Widdicombe C, Fileman ES, Woodward EMS, Schmidt K, Smyth TJ, Somerfield PJ (2021) Increasing nutrient stress reduces the efficiency of energy transfer through planktonic size spectra. *Limnol Oceanogr* 66:422–437.

- Bedford J, Johns D, Greenstreet S, McQuatters-Gollop A (2018) Plankton as prevailing conditions: A surveillance role for plankton indicators within the Marine Strategy Framework Directive. *Mar Policy* 89:109–115.
- Bedford J, Johns DG, McQuatters-Gollop A (2020a) Implications of taxon-level variation in climate change response for interpreting plankton lifeform biodiversity indicators. *ICES J Mar Sci* 77:3006–3015.
- Bedford J, Ostle C, Johns DG, Atkinson A, Best M, Bresnan E, Machairopoulou M, Graves CA, Devlin M, Milligan A, Pitois S, Mellor A, Tett P, McQuatters-Gollop A (2020b) Lifeform indicators reveal large-scale shifts in plankton across the North-West European shelf. *Glob Chang Biol* 26:3482–3497.
- Benfield MC, Grosjean P, Culverhouse PF, Irigoien X, Sieracki ME, Lopez-Urrutia A, Dam HG, Hu Q, Davis CS, Hanson A, Pilskałn CH, Riseman EM, Schultz H, Utgoff PE, Gorsky G (2007) RAPID: Research on Automated Plankton Identification. *Oceanography* 20:172–218.
- Bils F, Moyano M, Aberle N, van Damme CJG, Nash RDM, Kloppmann M, Loots C, Peck MA (2019) Broad-scale distribution of the winter protozooplankton community in the North Sea. *J Sea Res* 144:112–121.
- Blanchard JL, Heneghan RF, Everett JD, Trebilco R, Richardson AJ (2017) From Bacteria to Whales: Using Functional Size Spectra to Model Marine Ecosystems. *Trends Ecol Evol* 32:174–186.
- Blanco J, Echevarria F, Garcia CM (1994) Dealing with size-spectra: Some conceptual and mathematical problems. *Sci Mar Vol* 58:1–48.
- Bone Q, Brownlee C, Bryan GW, Burt GR, Dando PR, Liddicoat MI, Pulsford AL, Ryan KP (1987) On the differences between the two ‘indicator’ species of chaetognath, *Sagitta setosa* and *S. elegans*. *J Mar Biol Assoc United Kingdom* 67:545–560.
- Bougeard S, Dray S (2018) Supervised Multiblock Analysis in R with the ade4 Package. *J Stat Softw* 86:1–17.
- Bresnan E, Cook KB, Hughes SL, Hay SJ, Smith K, Walsham P, Webster L (2015) Seasonality of the plankton community at an east and west coast monitoring site in Scottish waters. *J Sea Res* 105:16–29.
- Buttigieg PL, Ramette A (2014) A guide to statistical analysis in microbial ecology: A community-focused, living review of multivariate data analyses. *FEMS Microbiol Ecol* 90:543–550.
- Calbet A (2008) The trophic roles of microzooplankton in marine systems. *ICES J Mar Sci* 65:325–331.
- Calbet A, Garrido S, Saiz E, Alcaraz M, Duarte CM (2001) Annual zooplankton succession in coastal NW Mediterranean waters: The importance of the smaller size fractions. *J Plankton Res* 23:319–331.
- Calbet A, Saiz E (2005) The ciliate-copepod link in marine ecosystems. *Aquat Microb Ecol* 38:157–167.
- Campos CC, Garcia TM, Neumann-Leitão S, Soares MO (2017) Ecological indicators and functional groups of copepod assemblages. *Ecol Indic* 83:416–426.

- Clarke KR (1993) Non-parametric multivariate analyses of changes in community structure. *Aust J Ecol* 18:117–143.
- Conradt J, Börner G, López-Urrutia Á, Möllmann C, Moyano M (2022) Automated Plankton Classification With a Dynamic Optimization and Adaptation Cycle. *Front Mar Sci* 9:1–19.
- Cordeiro TA, Brandini FP, Martens P (1997) Spatial distribution of the Tintinnina (Ciliophora, Protista) in the North Sea, spring of 1986. *J Plankton Res* 19:1371–1383.
- Culverhouse PF, Macleod N, Williams R, Benfield MC, Lopes RM, Picheral M (2014) An empirical assessment of the consistency of taxonomic identifications. *Mar Biol Res* 10:73–84.
- D'Alelio D, Libralato S, Wyatt T, Ribera D'Alcalà M (2016) Ecological-network models link diversity, structure and function in the plankton food-web. *Sci Rep* 6:1–13.
- Daly KL, Smith Jnr WO (1993) Physical-biological interactions influencing marine plankton production. *Annu Rev Ecol Syst* 24:555–585.
- Dippner JW, Krause M (2013) Continuous plankton recorder underestimates zooplankton abundance. *J Mar Syst* 111–112:263–268.
- Dolan JR, Moon JK, Yang EJ (2021) Notes on the occurrence of tintinnid ciliates, and the nasselarian radiolarian amphimelissa setosa of the marine microzooplankton, in the chukchi sea (Arctic ocean) sampled each august from 2011 to 2020. *Acta Protozool* 60.
- Doray M, Petitgas P, Romagnan JB, Huret M, Duhamel E, Dupuy C, Spitz J, Authier M, Sanchez F, Berger L, Dorémus G, Bourriau P, Grellier P, Massé J (2018) The PELGAS survey: Ship-based integrated monitoring of the Bay of Biscay pelagic ecosystem. *Prog Oceanogr* 166:15–29.
- Dudeck T, Rohlf N, Möllmann C, Hufnagl M (2021) Winter zooplankton dynamics in the English Channel and southern North Sea: Trends and drivers from 1991 to 2013. *J Plankton Res* 43:244–256.
- Eloire D, Somerfield PJ, Conway DVP, Halsband-Lenk C, Harris R, Bonnet D (2010) Temporal variability and community composition of zooplankton at station L4 in the Western Channel: 20 years of sampling. *J Plankton Res* 32:657–679.
- Emeis KC, van Beusekom J, Callies U, Ebinghaus R, Kannen A, Kraus G, Kröncke I, Lenhart H, Lorkowski I, Matthias V, Möllmann C, Pätsch J, Scharfe M, Thomas H, Weisse R, Zorita E (2015) The North Sea - A shelf sea in the Anthropocene. *J Mar Syst* 141:18–33.
- Fasham MJR (1978) The Application of Some Stochastic Processes to the Study of Plankton Patchiness. In: *Spatial Pattern in Plankton Communities*. Springer, p 131–156
- Fileman ES, Fitzgeorge-Balfour T, Tarran GA, Harris RP (2011) Plankton community diversity from bacteria to copepods in bloom and non-bloom conditions in the Celtic Sea in spring. *Estuar Coast Shelf Sci* 93:403–414.
- Gifford DJ, Caron DA (2000) Sampling, preservation, enumeration and biomass of marine protozooplankton. *ICES Zooplankt Methodol Man*:193–221.
- Goodwin M, Halvorsen KT, Jiao L, Knausgård KM, Martin AH, Moyano M, Oomen RA, Rasmussen JH, Sørtdalen TK, Thorbjørnsen SH (2022) Unlocking the potential of deep learning for marine ecology: overview, applications, and outlook. *ICES J Mar Sci* 79:319–336.

- Gorokhova E, Lehtiniemi M, Postel L, Rubene G, Amid C, Lesutiene J, Uusitalo L, Strake S, Demereckiene N (2016) Indicator properties of baltic zooplankton for classification of environmental status within marine strategy framework directive. *PLoS One* 11:1–26.
- Gorsky G, Ohman MD, Picheral M, Gasparini S, Stemmann L, Romagnan JB, Cawood A, Pesant S, García-Comas C, Prejger F (2010) Digital zooplankton image analysis using the ZooScan integrated system. *J Plankton Res* 32:285–303.
- Haberlin D, Raine R, McAllen R, Doyle TK (2019) Distinct gelatinous zooplankton communities across a dynamic shelf sea. *Limnol Oceanogr* 64:1802–1818.
- Huebert KB, Peck MA (2014) A day in the life of fish larvae: Modeling foraging and growth using quirks. *PLoS One* 9.
- ICES (2022): ICES Advice 2022. ICES Advice Publications. Collection. <https://doi.org/10.17895/ices.pub.c.5796935.v82>
- Jochem F, Babenerd B (1989) Naked *Dictyocha speculum* - a new type of phytoplankton bloom in the Western Baltic. *Mar Biol* 103:373–379.
- Keller DP, Lee DY, Hood RR (2014) Turbidity Maximum Entrapment of Phytoplankton in the Chesapeake Bay. *Estuaries and Coasts* 37:279–298.
- Kerr SR, Dickie LM (2001) *The biomass spectrum: a predator-prey theory of aquatic production*. Columbia University Press.
- Kjørboe T (2013) Zooplankton body composition. *Limnol Oceanogr* 58:1843–1850.
- Krause M, Fock H, Greve W, Winkler G (2003) North Sea zooplankton: A review. *Senckenbergiana Maritima* 33:71–204.
- Kwong LE, Ross T, Luskow F, Florke KRN, Pakhomov EA (2022) Spatial, seasonal, and climatic variability in mesozooplankton size spectra along a coastal-to-open ocean transect in the subarctic Northeast Pacific. *Prog Oceanogr* 201:102728.
- Legendre P (2001) Model II regression - User's guide. *R Vignette* 4:1–14.
- Legendre P, Gallagher ED (2001) Ecologically meaningful transformations for ordination of species data. *Oecologia* 129:271–280.
- Lehtiniemi M, Fileman E, Hällfors H, Kuosa H, Lehtinen S, Lips I, Setälä O, Suikkanen S, Tuimala J, Widdicombe C (2022) Optimising sampling frequency for monitoring heterotrophic protists in a marine ecosystem. *ICES J Mar Sci* 79:925–936.
- Lindegren M, Thomas MK, Jónasdóttir SH, Nielsen TG, Munk P (2020) Environmental niche separation promotes coexistence among ecologically similar zooplankton species—North Sea copepods as a case study. *Limnol Oceanogr* 65:545–556.
- Liu Z, Li QP, Ge Z, Shuai Y (2021) Variability of plankton size distribution and controlling factors across a coastal frontal zone. *Prog Oceanogr* 197:102665.
- Löder MGJ, Meunier C, Wiltshire KH, Boersma M, Aberle N (2011) The role of ciliates, heterotrophic dinoflagellates and copepods in structuring spring plankton communities at Helgoland Roads, North Sea. *Mar Biol* 158:1551–1580.

- Lombard F, Boss E, Waite AM, Uitz J, Stemmann L, Sosik HM, Schulz J, Romagnan JB, Picheral M, Pearlman J, Ohman MD, Niehoff B, Möller KO, Miloslavich P, Lara-Lopez A, Kudela RM, Lopes RM, Karp-Boss L, Kiko R, Jaffe JS, Iversen MH, Irisson JO, Hauss H, Guidi L, Gorsky G, Giering SLC, Gaube P, Gallager S, Dubelaar G, Cowen RK, Carlotti F, Briseño-Avena C, Berline L, Benoit-Bird KJ, Bax NJ, Batten SD, Ayata SD, Appeltans W (2019) Globally consistent quantitative observations of planktonic ecosystems. *Front Mar Sci* 6.
- Mackas DL, Boyd CM (1979) Spectral analysis of zooplankton spatial heterogeneity. *Science* (80-) 204:62–64.
- McQuatters-Gollop A, Edwards M, Helaouët P, Johns DG, Owens NJP, Raitsos DE, Schroeder D, Skinner J, Stern RF (2015) The Continuous Plankton Recorder survey: How can long-term phytoplankton datasets contribute to the assessment of Good Environmental Status? *Estuar Coast Shelf Sci* 162:88–97.
- McQuatters-Gollop A, Gilbert AJ, Mee LD, Vermaat JE, Artioli Y, Humborg C, Wulff F (2009) How well do ecosystem indicators communicate the effects of anthropogenic eutrophication? *Estuar Coast Shelf Sci* 82:583–596.
- Menden-Deuer S, Lessard EJ, Satterberg J (2001) Effect of preservation on dinoflagellate and diatom cell volume and consequences for carbon biomass predictions. *Mar Ecol Prog Ser* 222:41–50.
- Modigh M, Castaldo S (2005) Effects of fixatives on ciliates as related to cell size. *J Plankton Res* 27:845–849.
- Montagnes DJS, Dower JF, Figueiredo GM (2010) The protozooplankton-ichthyoplankton trophic link: An overlooked aspect of aquatic food webs. *J Eukaryot Microbiol* 57:223–228.
- Morse RE, Friedland KD, Tommasi D, Stock C, Nye J (2017) Distinct zooplankton regime shift patterns across ecoregions of the U.S. Northeast continental shelf Large Marine Ecosystem. *J Mar Syst* 165:77–91.
- Motoda S (1967) Devices of Simple Plankton Apparatus III. 北海道大學水産學部研究彙報 18:3–8.
- Murphy GEP, Romanuk TN, Worm B (2020) Cascading effects of climate change on plankton community structure. *Ecol Evol*:2170–2181.
- Murtagh F, Legendre P (2014) Ward's Hierarchical Agglomerative Clustering Method: Which Algorithms Implement Ward's Criterion? *J Classif* 31:274–295.
- Naito A, Abe Y, Matsuno K, Nishizawa B, Kanna N, Sugiyama S, Yamaguchi A (2019) Surface zooplankton size and taxonomic composition in Bowdoin Fjord, north-western Greenland: A comparison of ZooScan, OPC and microscopic analyses. *Polar Sci* 19:120–129.
- Nash RDM, Dickey-Collas M, Milligan SP (1998) Descriptions of the gulf VII/PRO-NET and MAFF/guildline unencased high-speed plankton samplers. *J Plankton Res* 20:1915–1926.
- Pearson K (1896) VII. Mathematical contributions to the theory of evolution.—III. Regression, heredity, and panmixia. *Philos Trans R Soc London Ser A, Contain Pap a Math or Phys Character* 187:253–318.
- Pepin P, Penney R (2000) Feeding by a larval fish community: Impact on zooplankton. *Mar Ecol Prog Ser* 204:199–212.

- Petchey OL, Belgrano A (2010) Body-size distributions and size-spectra: Universal indicators of ecological status? *Biol Lett* 6:434–437.
- Pitois SG, Shaw M, Fox CJ, Frid CLJ (2009) A new fine-mesh zooplankton time series from the Dove sampling station (North Sea). *J Plankton Res* 31:337–343.
- Pollina T, Larson AG, Lombard F, Li H, Le Guen D, Colin S, de Vargas C, Prakash M (2022) PlanktoScope: Affordable Modular Quantitative Imaging Platform for Citizen Oceanography. *Front Mar Sci* 9:1–15.
- Purcell JE (2005) Climate effects on formation of jellyfish and ctenophore blooms: A review. *J Mar Biol Assoc United Kingdom* 85:461–476.
- Purcell JE, Breitbart DL, Decker MB, Graham WM, Youngbluth MJ, Raskoff KA (2001) Pelagic cnidarians and ctenophores in low dissolved oxygen environments: A review. p 77–100
- R Core Team (2022). R: A language and environment for statistical computing. R Foundation for Statistical Computing, Vienna, Austria. URL <https://www.R-project.org/>.
- Richardson AJ, Walne AW, John AWG, Jonas TD, Lindley JA, Sims DW, Stevens D, Witt M (2006) Using continuous plankton recorder data. *Prog Oceanogr* 68:27–74.
- Roman MR, Holliday D V., Sanford LP (2001) Temporal and spatial patterns of zooplankton in the Chesapeake Bay turbidity maximum. *Mar Ecol Prog Ser* 213:215–227.
- Ryther JH (1969) Photosynthesis and fish production in the sea. *Science* (80-) 166:72–76.
- Saccà A (2016) A simple yet accurate method for the estimation of the biovolume of planktonic microorganisms. *PLoS One* 11.
- San Martin E, Harris RP, Irigoien X (2006) Latitudinal variation in plankton size spectra in the Atlantic Ocean. *Deep Res Part II Top Stud Oceanogr* 53:1560–1572.
- Schmidt, J. O., Van Damme, C. J., Röckmann, C., & Dickey-Collas, M. (2009). Recolonisation of spawning grounds in a recovering fish stock: recent changes in North Sea herring. *Scientia Marina*, 73(S1), 153-157.
- Serra-Pompei C, Ward BA, Pinti J, Visser AW, Kiørboe T, Andersen KH (2022) Linking Plankton Size Spectra and Community Composition to Carbon Export and Its Efficiency. *Global Biogeochem Cycles* 36:1–19.
- Sguotti C, Blöcker AM, Färber L, Blanz B, Cormier R, Diekmann R, Letschert J, Rambo H, Stollberg N, Stelzenmüller V, Stier AC, Möllmann C (2022) Irreversibility of regime shifts in the North Sea. *Front Mar Sci* 9:1–13.
- Sheldon RW, Prakash A, Sutcliffe WH (1972) The Size Distribution of Particles in the Ocean. *Limnol Oceanogr* 17:327–340.
- Sieracki CK, Sieracki ME, Yentsch CS (1998) An imaging-in-flow system for automated analysis of marine microplankton.
- Sprules WG, Barth LE (2016) Surfing the biomass size spectrum: Some remarks on history, theory, and application. *Can J Fish Aquat Sci* 73:477–495.
- Sprules WG, Munawar M (1986) Plankton Size Spectra in Relation to Ecosystem Productivity, Size, and Perturbation. *Can J Fish Aquat Sci* 43:1789–1794.

- Suthers I, Rissik D, Richardson A (2019) *Plankton: A guide to their ecology and monitoring for water quality*. CSIRO publishing.
- Taylor MH, Akimova A, Bracher A, Kempf A, Kühn B, Hélaouët P (2021) Using Dynamic Ocean Color Provinces to Elucidate Drivers of North Sea Hydrography and Ecology. *J Geophys Res Ocean* 126.
- Vane FR (1961) Continuous plankton records: contribution towards a plankton atlas of the north-eastern Atlantic and the North Sea. Part III: Gastropoda. *Bull Mar Ecol* 5:98–101.
- Vazquez EG, Georges O, Fernandez S, Ardura A (2021) EDNA metabarcoding of small plankton samples to detect fish larvae and their preys from Atlantic and Pacific waters. *Sci Rep*:1–13.
- Venello TA, Sastri AR, Galbraith MD, Dower JF (2021) Zooplankton functional group responses to environmental drivers off the west coast of Vancouver Island, Canada. *Prog Oceanogr* 190:102482.
- Warnes G, Bolker B, Bonebakker L, Gentleman R, Huber W, Liaw A, Lumley T, Maechler M, Magnusson A, Moeller S, Schwartz M, Venables B (2022). *gplots: Various R Programming, Tools for Plotting Data*. R package version 3.1.3
- Widdicombe CE, Eloire D, Harbour D, Harris RP, Somerfield PJ (2010) Long-term phytoplankton community dynamics in the Western English Channel. *J Plankton Res* 32:643–655.
- Wilson RJ, Heath MR (2019) Increasing turbidity in the North Sea during the 20th century due to changing wave climate. *Ocean Sci* 15:1615–1625.
- Yang J, Chen Z, Chen D, Xu D (2021) Spatial distribution of the microzooplankton communities in the northern South China Sea: Insights into their function in microbial food webs. *Mar Pollut Bull* 162:111898.
- Ye L, Chang CY, García-Comas C, Gong GC, Hsieh C hao (2013) Increasing zooplankton size diversity enhances the strength of top-down control on phytoplankton through diet niche partitioning. *J Anim Ecol* 82:1052–1061.
- Yebra L, Puerto M, Valcárcel-Pérez N, Putzeys S, Gómez-Jakobsen F, García-Gómez C, Mercado JM (2022) Spatio-temporal variability of the zooplankton community in the SW Mediterranean 1992–2020: Linkages with environmental drivers. *Prog Oceanogr* 203.
- Zhang W, Sun X, Zheng S, Zhu M, Liang J, Du J, Yang C (2019) Plankton abundance, biovolume, and normalized biovolume size spectra in the northern slope of the South China Sea in autumn 2014 and summer 2015. *Deep Sea Res Part II Top Stud Oceanogr* 167:79–92.
- Zhou M (2006) What determines the slope of a plankton biomass spectrum? *J Plankton Res* 28:437–448.
- Zhou, M., Tande, K. S., Zhu, Y., & Basedow, S. (2009). Productivity, trophic levels and size spectra of zooplankton in northern Norwegian shelf regions. *Deep Sea Research Part II: Topical Studies in Oceanography*, 56(21-22), 1934-1944.

Chapter 4

Combining modeling with novel field observations yields new insights into food limitation of wintertime larval fish



Drawings adapted from

Justine Courboulès

Combining modeling with novel field observations yields new insights into food limitation of wintertime larval fish

Anna Akimova¹, Gregor Börner², Myron A. Peck³, Cindy van Damme⁴ and Marta Moyano^{5,6}

Abstract

Recruitment success of marine fishes is generally considered to be highly dependent on larval growth and survival. In temperate ecosystems, fish larvae can be particularly sensitive to food limitation during the low productivity seasons, especially as the frequency of warmer winter increases. We combined seven years of in situ sampling of larval fish, novel observations on zooplankton via automated image analyses, and larval physiological modelling to explore feeding conditions of Atlantic herring larvae (*Clupea harengus*) in the North Sea. The observed plankton size-structure was close to the theoretical optimum for larval foraging, but not the biomass. Our results for autumn larvae supported Hjort's critical period hypothesis: small first-feeding larvae were predicted to have a high probability of starvation, whereas larvae >13 mm were able to reach their maximal growth capacity. In winter, the majority of herring larvae of all tested sizes (5 to 27 cm) experienced food-limitation with over 35% probability of starvation. Sensitivity analysis suggested that young herring larvae improve their growth performance and probability of survival if feed not only on copepods and their life-stages but include other microplankters in their diet. Given projected warming of the North Sea, our model predicts that herring larvae would require 28% (35%) more prey biomass in autumn (winter) to sustain their growth and survival in the future. This finding together with the ongoing low recruitment of North Sea herring underscore the importance of future micro- and mesoplankton monitoring within a scope of wintertime larval fish surveys.

Keywords: larval fish, bioenergetic model, herring, North Sea, zooplankton size-spectra, foraging, starvation, physiology

Authors' affiliation

1Thünen-Institute of Sea Fisheries, Bremerhaven, Germany.

2 Institute of Marine Ecosystem and Fishery Science, Hamburg University, Germany,

3 Royal Netherlands Institute for Sea Research, Department of Coastal Systems, Texel, The Netherlands,

4 Wageningen Marine Research, IJmuiden, The Netherlands,

5 Norwegian Institute for Water Research (NIVA), Oslo, Norway

6 Center for Coastal Research, University of Agder, Kristiansand, Norway

Introduction

Fish early life is widely acknowledged as a critical period determining variation in fish recruitment and, to a large extent, the population size of various fish species (e.g. Chambers and Trippel, 1997; Fuiman and Werner, 2002). The larval stage is often considered the main bottleneck due to high starvation and predation mortality (Bailey and Houde, 1989; Pepin et al., 2015). Both mortality agents are not fully independent and may interact with each other at various spatial and temporal scales (e.g. Petrik et al., 2014; Akimova et al., 2019). Several prominent recruitment hypotheses linking larval foraging success, growth and survival have emerged in the of 20th century, starting with the “critical period” hypothesis of Hjort (1914) and moving towards more complex concepts of “growth-survival”, “stage duration”, and “bigger is better” (e.g. Houde, 2008). Although much progress has been made in our understanding of different mortality processes such as starvation, predation and physical transport (Peck and Hufnagl, 2012), the relative impact of each process in establishing the cumulative mortality of specific cohorts and overall recruitment strength remains challenging to ascertain for most marine fish populations.

Numerous studies on marine and freshwater fish have considered larval growth, particularly the rapid gaining of length, to be decisive for survival and recruitment (Anderson, 1988; Houde, 1997). Studying larval foraging and growth is important for gaining a mechanistic understanding of processes governing marine fish recruitment and to make robust projections of the consequences of climate-driven shifts in direct (e.g. temperature) and indirect (prey abundance and type) factors. Field based observations of larval feeding are rare and linked to notorious methodological difficulties accompanied by a large uncertainty (Suthers et al., 2022). Diets and feeding preferences are poorly studied in larvae compared to juvenile and adult fish (Robert et al., 2014), and this lack of knowledge can potentially lead to biased estimates of the food-limited larval growth as well as starvation mortality. Field studies of diet preference are generally based on gut content analysis, which is associated with challenges including the identification of small and soft plankton prey (e.g. naked dinoflagellates or appendicularians) in the guts of fish larvae caught in the sea (e.g. Llopiz et al., 2011). Second, the zooplankton prey should be sampled simultaneously with fish larvae to accurately assess larval feeding environments (Pepin et al., 2015).

The ranges in sizes and taxonomic resolution of the sampled plankton should be broad enough to include all potential larval prey, which implies measuring and identifying a wide range of micro- to mesoplanktonic organisms (e.g. Llopiz and Cowen, 2009; Bils et al., 2016).

Temporal match between fish larvae and the spring “bloom” of their planktonic prey is considered a key factor determining larval survival and recruitment (Cushing, 1990; Peck et

al., 2012). Less is known about tropical fishes spawning in oligotrophic waters (Llopiz et al., 2011) and temperate fishes spawning in autumn or early winter. Larvae from the latter group encounter colder temperatures as well as shorter photoperiods and decreasing prey abundance as they develop into the winter (Hufnagl et al., 2015). Long-term climate variability affecting ecosystem productivity and phenology of various organisms, have caused past shifts in the spawning season of such fishes (ICES, 2005; Moyano et al., 2022) and the ongoing global warming could potentially drive the shifts in phenology (or prey requirements) beyond tolerable thresholds for the persistence of some populations in the future. Therefore, feeding processes and adaptation strategies are of great interest in such species. We describe here an example of Atlantic herring (*Clupea harengus*) in the North Sea to explore larval feeding conditions, starvation and growth using a combination of size-structured observations of the larval prey field and the individual-based physiological modelling.

North-Sea autumn spawning herring (NSASH), one of the most commercially important pelagic stocks in the region, is known to spawn between August and January in four main areas in the North Sea: Orkney-Shetland, Buchan, Banks and Downs (Dickey-Collas et al., 2010; Fig 1A). NSASH has a long history of exploitation, including a stock collapse caused by recruitment overfishing and subsequent recovery (Fig 1B; Payne et al., 2009; Geffen, 2009; Dickey-Collas et al., 2010). Since 2002, this stock has experienced a sustained period of low recruitment that has alarmed fisheries scientists and managers. The pre-recruitment life stages of NSASH have been extensively studied using field observations (e.g. Nash and Dickey-Collas, 2005; van Damme et al., 2009), laboratory experiments (e.g. Blaxter and Hempel, 1963; Kiørboe et al., 1987; Illing et al., 2018), as well as bioenergetic modeling (e.g. Heath et al., 1997; Hufnagl et al., 2015). A main conclusion from these studies is that elevated rates of larval mortality cause poor recruitment success, but whether North Sea herring larvae starve at the onset of exogenous feeding in agreement with the “critical period” hypothesis or over a longer period as they drift across the North Sea in winter is still debated. Hufnagl et al. (2015) highlighted the complexity of disentangling larval mortality due to starvation, predation and dispersion. Their model study pointed out some critical knowledge gaps such as the extremely sparse field observations of zooplankton abundance, size-structure and species composition during autumn and winter in the North Sea.

The main objective of this study was to investigate the feeding conditions that young herring larvae experience during their first month of life in the North Sea and whether these conditions differ among autumn- and winter-spawning sites. We used size- and taxa-resolved information on zooplankton collected simultaneously with herring larvae to describe the available prey field, including novel estimates of microplankton abundance. A physiological model simulating larval foraging and growth used these prey fields to test the hypothesis that recent, poor recruitment

of North Sea herring was linked to sub-optimal feeding conditions experienced during first feeding and that the available prey was insufficient to cover larval energy requirements. Furthermore, given a projected rise of water temperatures in the North Sea by the end of the 21st century (on average 2.0 °C, Schrum et al., 2016), we estimated how the zooplankton biomass and/or size composition would need to change to meet the increasing energy demand of herring larvae in a future climate.

Data and Methods

Data

Zoo- and phytoplankton, larval abundance and water temperature data were taken during the International Herring Larvae Survey (IHLS) in the North Sea between 2013 and 2019. In this study, we considered a merged Buchan and Banks area (further on Buchan/Banks) east of the British Isles (Fig.1A), where herring is known to spawn in September. The second area was the Downs area in the English Channel and Southern Bight, where spawning occurs in December-January (e.g. Dickey-Collas et al., 2010). Note that not all stations could be sampled every year due to a sampling failure or bad weather conditions (Table 4. 1).

Herring larvae and mesozooplankton were sampled using a Gulf VII high-speed sampler (280 µm mesh size, 0.2 m nose cone opening; Nash et al., 1998) and conducting double-oblique hauls from the surface to 5 m above the bottom. A PUP-net (55 µm mesh size) was attached to the Gulf VII and sampled microplankton. A detailed description of the zooplankton data analyses is available in Börner et al. (unpubl.) and briefly summarized in the supplements (S1 “Zooplankton data”). In this study, we included only planktonic organisms that were considered suitable for larval feeding based on their size, geometric form and previous studies identifying them as larval prey (Last, 1978; Pepin and Penney, 1997; Robert et al., 2014). The following 11 taxonomic groups were included: copepods, appendicularians, bivalve larvae, gastropod larvae, echinoderm larvae, ciliates, cladocerans, diatoms, dinoflagellates, foraminiferas, and silicoflagellates.

Herring larvae were preserved in formalin, total length of each individual was measured with the accuracy of 1 mm and abundance-at-length was calculated. Developmental stages of herring larvae (yolk-sac, pre-flexion, flexion, and post-flexion) per size class were documented. We refer the reader to Schmidt et al. (2009) for further technical and methodological details on the survey.

Data on water temperature were collected using a Seabird CTD (conductivity, temperature, depth) SBE 911 profiler mounted on the Gulf VII sampler. We calculated the mean temperature along the entire water column at each station to match depth-integrated plankton and larval samples.

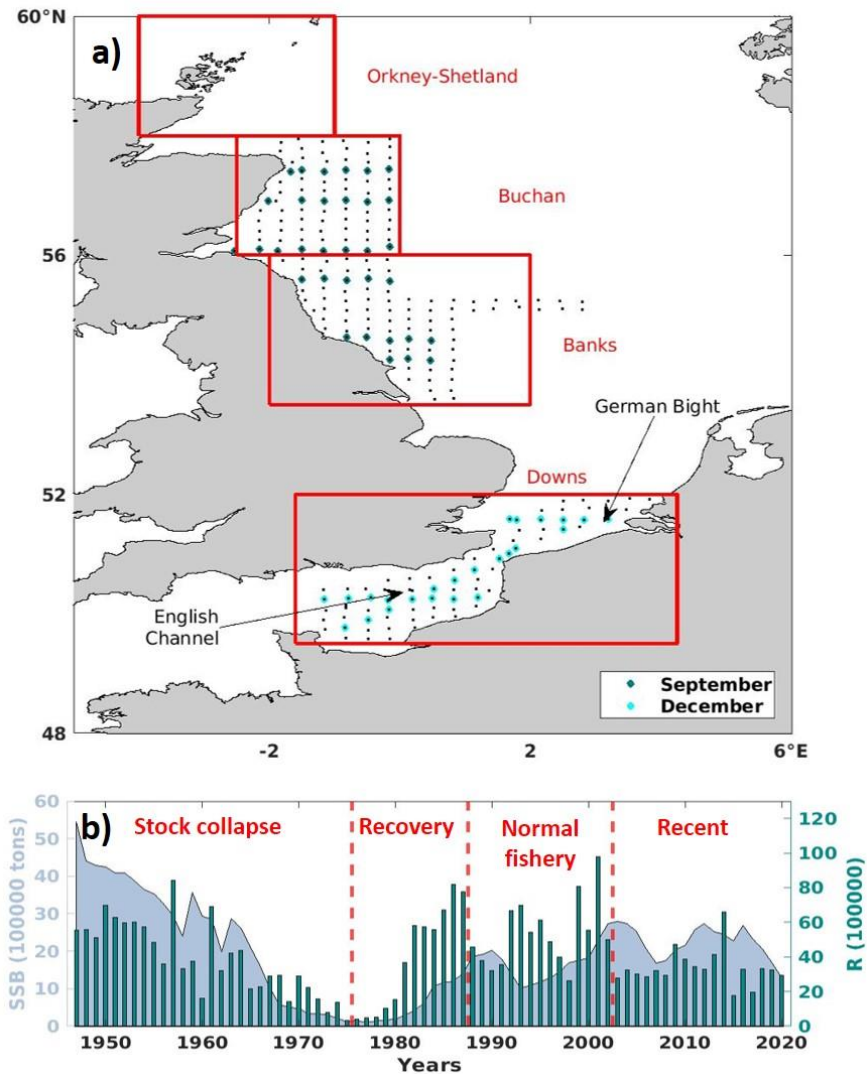


Figure 1. a) Study region in the western North Sea. Plankton samples taken in September (teal) and December (cyan dots) are shown together with a typical sampling grid of the Netherland's contribution to the International Herring Larvae Survey (black dots), where herring larvae were sampled. Known spawning locations (Orkney-Shetland, Buchan, Banks and Downs) of the North Sea Autumn Spawning Herring stock (NSASH) are identified. Arrows show two subareas in the Downs spawning area (English Channel and Southern Bight). b) Annual changes in spawning stock biomass (SSB, gray area) and recruitment (R, teal bars) of NSASH as obtained from the ICES stock assessment (<https://www.ices.dk/data/assessment-tools/Pages/stock-assessment-graphs.aspx>, accessed on June, 1st, 2022). Red dashed lines identify phases of herring stock history in agreement with Payne et al. (2009).

Table 1. The number of stations sampled during the IHLS from 2013 to 2019 and used in the study. No sampling was conducted in 2014 and 2015 in the Downs area due to bad weather conditions. September 2015 (Buchan/Banks) and December 2013 (Downs) were excluded due to a failure of the plankton sampling.

Year	Buchan/Banks areas (September)			Downs area (December)		
	CTD	Larvae	Zooplankton	CTD	Larvae	Zooplankton
2013	164	165	31	-	-	-
2014	144	145	27	-	-	-
2015	-	-	-	-	-	-
2016	162	162	35	79	77	24
2017	170	167	33	82	80	25
2018	156	155	35	34	26	14
2019	163	161	30	81	80	18

Methods

Observed larval prey fields and length-at-first-feeding

In situ estimates of plankton abundance and composition were used to provide the prey field for a larval foraging model. We calculated a normalized biomass size spectra (NBSS) based on the empirical paradigm of Sheldon's spectra (Sheldon et al., 1972; Blanco et al., 1994).

We first converted the equivalent spherical diameter (L_z , in μm) measured for each zooplankton organism to its individual dry weight w_z (in μg) using the equation of Huebert et al. (2018) (their Eq. A3), adapted to μm instead of mm originally used:

$$w_z = 4.43 \times 10^{-7} \cdot L_z^{2.5}, \quad (1)$$

Based on their dry weight w_z , planktonic organisms were grouped in size bins on the octave scale (with the interval of 2) and the bin-specific biomass was calculated by summing all

individual weights within each size bin. To obtain a normalized size spectrum β_z , we divided the bin-specific biomass by the width of the corresponding weight intervals Δw_z . We calculated β_z at each station and fitted a weighted linear regression to β_z on the log-log scale with the regression weights being proportional to the observed abundances within each size class. The normalized biomass spectrum β_z was then used to calculate the zooplankton biomass B_z in the size range between 20 and 2000 μm :

$$B_z = \int_{w_1}^{w_2} \beta_z dw_z \quad (2)$$

where w_1 and w_2 were dry weights of zooplankton of 20 and 2000 μm in size, respectively. Given the linear relationships between β_z and w_z on the log-log scale the Eq. 2 can be solved as:

$$B_z = \int_{w_1}^{w_2} \beta_z dw_z = \int_{w_1}^{w_2} a \cdot w_z^s dw_z = \begin{cases} a \cdot \ln w_z, & \text{if } s = 1 \\ a \cdot w_z^{s+1}, & \text{if } s \neq 1 \end{cases} \quad (3)$$

where s is the slope and a is the intercept of the linear regression fitted to β_z on the log-log scale. The biomass distribution in given size ranges was utilized in the optimal foraging routine of the bioenergetic model (see section “Bioenergetic model”).

We used length measurements and staging performed on captured herring larvae to obtain a field-based estimate of the larval length-at-first-feeding (LFF). The measured length of the formalin preserved larvae was converted to the length of fresh larvae (see S2 “Bias correction of larval length due to formalin preservation”). This resulted in a range in larval sizes between 5.3 and 26.2 mm. We split the Downs observations into two subareas (the English Channel area in the south-west and the Southern Bight area in the north-east; Fig. 1) and built the mean size-frequency distributions for yolk-sack and no-yolk-sac larvae for the Buchan/Banks and each subarea within Downs over the observed period 2013-2019.

Bioenergetic model

We used an physiological individual-based model of herring larvae originally developed by Hufnagl and Peck (2011) and advanced in follow-up studies (Hufnagl et al., 2015; Bils et al., 2016; Illing et al., 2018). This bioenergetic model keeps energy housekeeping of a herring larva based on the equation:

$$G = C \cdot AE \cdot (1 - SDA) - k \cdot R_s \quad (4)$$

where G is the energy available for somatic growth, C is the energy gain due to foraging, AE is the assimilation efficiency, SDA is specific dynamic action (i.e. metabolic costs of the digestion

of a meal) and R_s is the standard respiration rate. The parameter k is an activity multiplier. The energy gain C was modeled based on the optimal foraging approach (see S3 “Bioenergetic model” for more details). In this study, we applied three modifications to the model of Hufnagl and Peck (2011): i) a new parameterization of the standard respiration rate was used based on the recent measurements of Moyano et al. (2018); ii) a Boolean function was used for the dynamic energy allocation; iii) activity multiplier $k=2$ during the day and $k=1$ during the night. More details on these modifications and the full set of model equations can be found in the supplement S3 “Bioenergetic model”.

The model equations were iteratively solved for 24 hours (one day and one night) with hourly timestep in order to estimate the daily growth rates of herring larvae at the observed environmental and prey conditions. The photoperiod (length of daylight) was 12 h in September and 8 h in December, respectively. For each simulation, we used a spin up of 48 hours to achieve a realistic initial gut content in the beginning of our daily simulations. The modeled larval growth was converted to the daily specific growth rate (SGR, in percent dry weight per day, further on $\% \text{ dw} \cdot \text{d}^{-1}$) as:

$$\text{SGR} = 100 \cdot (w_{24} - w_0) \cdot 1/w_0 \quad (5)$$

where w_{24} and w_0 were larval weights at the beginning and at the end of the 24-hour simulation. Additionally, we calculated the ad-libitum larval growth or maximal growth capacity (SGR_{max}) at each station and for each larval length by keeping the NBSS slope fixed and gradually increasing the prey concentration until the modeled growth rate reached its maximum and stagnated. Herring larvae were considered to experience starvation if the predicted SGR was ≤ 0 , food-limited growth if $\text{SGR} > 0$ and $\text{SGR} < \text{SGR}_{\text{max}}$ and prey satiation, i.e. ad-libitum growth, if $\text{SGR} = \text{SGR}_{\text{max}}$.

Model simulations

We conducted three groups of model simulations: 1) diet preference scenarios, 2) growth predictions using in situ prey fields, and 3) optimal prey conditions. We performed simulations for the initial larval length varying between 5 and 27 mm with 0.1 mm length increment in order to cover the length distribution observed in the field. In the “diet preference” simulations, we tested two scenarios of larval feeding: i) “specialist”, where only copepods were included as a suitable prey, and ii) “generalist”, where all 11 taxonomic groups of plankton were considered as potential prey. For both scenarios, we used average NBSS obtained with corresponding zooplankton organisms. In these simulations, temperature was set to its area-specific mean values (calculated as the median of all observed temperatures within each area during the entire period): 12.3 °C for Buchan/Banks and 10.9 °C for Downs.

To predict larval growth at in situ prey fields, we simulated daily SGR of herring larvae at each station where zooplankton data were available (Fig. 1) using the station-specific water temperature, zooplankton NBSS slope and biomass that corresponded to the generalist feeding scenario. The simulated growth rate was expressed as a proportion of SGR_{max} in order to isolate effects of the prey limitation from the temperature- and size- dependency of larval growth. To clearly demonstrate the seasonal differences, we pooled all predicted growth rates for all stations within each season and calculated the proportion of larvae that were predicted to grow at a certain growth.

In the simulations of the “optimal prey conditions”, we further investigated the prey-predator relationships between plankton and herring larvae. We set water temperature to its area-specific mean value and estimated larval growth at a wider range of the size-spectra slope between -2 and 0 and a wider range of the zooplankton concentrations between 0.1 and 1000 mg/m³. For each larval length, we identified two values: i) the minimal prey biomass required for a positive larval growth (starvation point, B_{min}), and ii) an optimal NBSS slope that corresponds to the B_{min} .

Results

Observed prey fields and herring larvae

The total plankton biomass B_z of all eleven taxonomic groups in the range of sizes between 20 and 2000 μm was, on average, 3 times lower in winter in Downs (median of 3.4 mg·m⁻³ Fig. 2C) than in autumn in Buchan/Banks areas (median of 9.4 mg·m⁻³). The mean NBSS slope was significantly (t-test, $t(280)=9.64$, $p<0.01$) steeper in December (mean slope= -0.9; Fig. 2C) than in September (-0.73). Accordingly, the proportion of microplankton was higher in December in the Downs (40% of the total plankton biomass) than in September in Buchan and Banks areas (20 % of the total biomass).

Copepods were the most abundant taxa (between 73 and 100% of the biomass) of the mesozooplankton but their proportion decreased toward the low end of the size-spectra (i.e. $ESD<200 \mu\text{m}$). This caused a shallower NBSS slope in the copepod scenario in comparison to the generalist one (Fig. 2E and F compared to A and B). Furthermore, no copepods smaller than 40 μm were observed (Fig 2E and F and Figure 4. S5.1), therefore, all size-classes smaller than 40 μm were excluded from the NBSS used in the “specialist” scenario simulations (Fig 2B, gray bars).

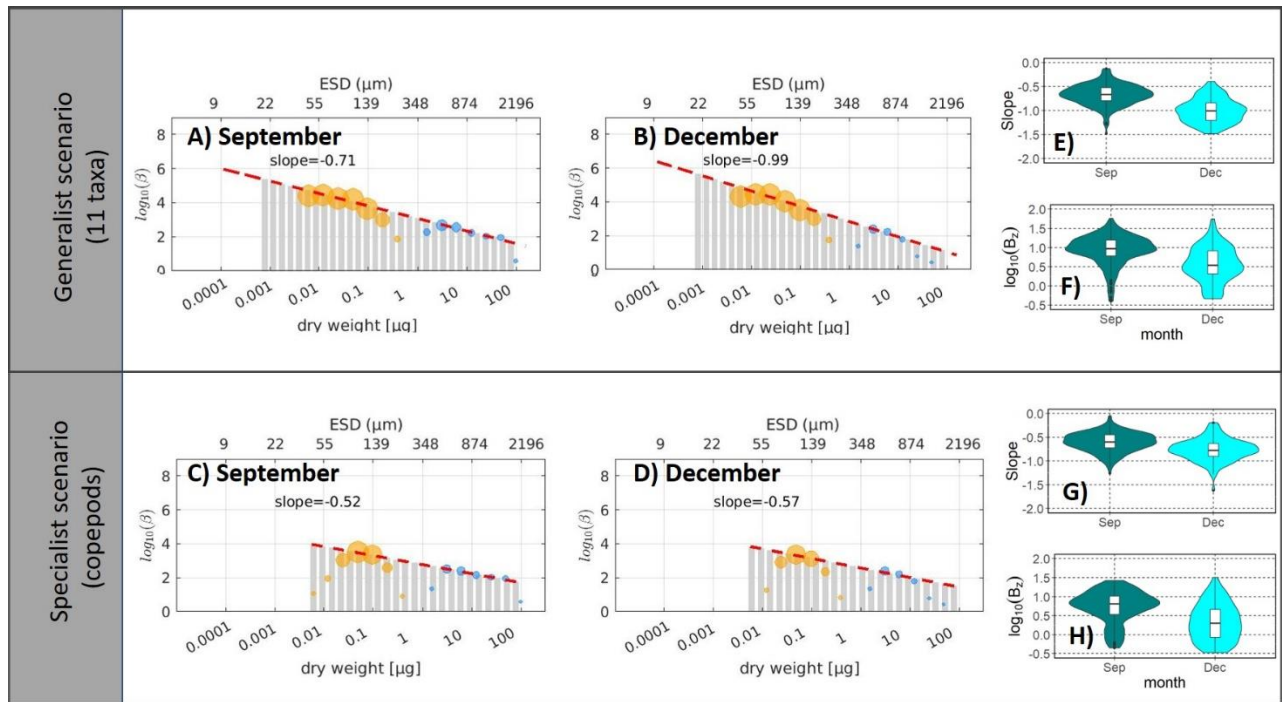


Figure 2: Mean normalized biomass size spectra (NBSS) obtained with 11 prey taxa (A – September, B – December), and with only copepods (C – September, D - December). Circles display the mean observed normalized biomass β_z averaged over all stations within the season/spawning area measured with a Flowcam (orange) and Zooscan (blue). The size of the circles is proportional to the log- abundance of the zooplankton organisms in corresponding size-bins. Red dashed lines indicate the weighted regression line fitted to the observed NBSS. Gray bars show the NBSS spectra used in the feeding scenarios. The distributions of the observed NBSS slope and the total zooplankton biomass with 11 prey taxa (E and F) and with only copepods (G and H) are shown for both seasons/spawning sites (teal - September (Buchan&Banks), cyan - December (Downs)). The zooplankton biomass B_z in F and H is in $\text{mg}\cdot\text{m}^{-3}$.

Larval length-frequency distributions as well as the proportion of the yolk-sac larvae differed among the spawning areas (Fig 3). In the Buchan/Banks area, herring larvae up to 26 mm were observed and the largest yolk-sac larvae were recorded in the 5th size-class (Fig 3A) corresponding to the length range between 9.7 and 10.8 mm. As for the Downs area, a larger proportion of smaller larvae was observed in the English Channel in comparison to the Southern Bight and the largest observed larvae were slightly smaller in the English Channel (21 mm) than in the Southern Bight (23 mm). The largest yolk-sac larvae were reported in the 7th length class (Fig 3B and C; length range between 11.9 and 13.0 mm) in both subareas of the Downs. We used the largest size of the observed yolk-sac larvae as a proxy for the largest length-at-first-feeding of herring larvae in both seasons.

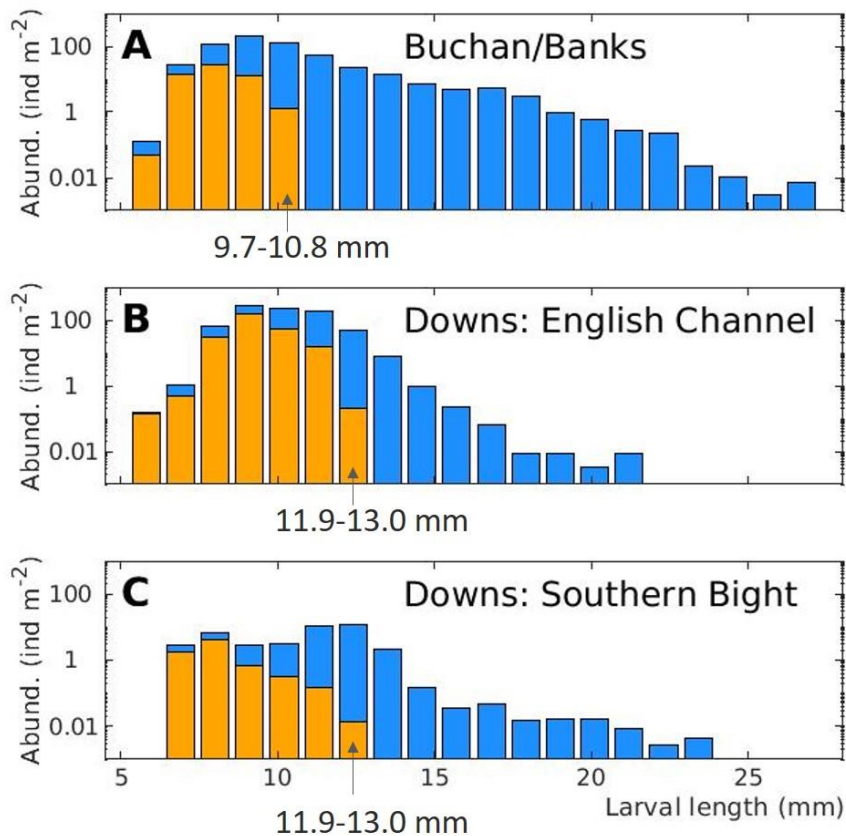


Figure 3. The mean length-frequency distributions of yolk-sac (orange) and post-yolk (blue) herring larvae observed the Buchan/Banks areas in September (A), in the English Channel (B) and the Southern Bight (C) in December. Larval length was corrected due to shrinkage occurring during the preservation. Larval abundances were averaged over the 2013-2019 period. Arrows indicate the largest size-classes of the observed yolk-sac larvae and the corresponding size-range is annotated.

Simulation 1 “Diet preference”: model sensitivity to the choice of the larval feeding scenario

Larval growth rates obtained in both dietary scenarios (specialist vs generalist) varied with larval length and differed among the spawning seasons/areas (Fig 4). In the specialist scenario, herring larvae smaller than 10.5 (12.5) mm in September (December) (orange curves in Fig. 4) were not able to consume enough prey to sustain their growth (predicted growth rates were negative). In the generalist scenario (blue curves in Fig 4), our model predicted a positive growth for smaller larvae in comparison to the specialist scenario in both spawning seasons (8.8 mm in September and 10.5 mm in December).

The maximal-growth capacity SGR_{max} (black dashed curves in Fig 4) changed with larvae size in a similar way in both seasons, but was reduced by almost half in December (between 7 and 13 % $dw \cdot d^{-1}$, Fig. 4B) compared to September (between 12 and 25 % $dw \cdot d^{-1}$, Fig. 4A) due to

a combined effect of a lower temperature and a shorter day length. At the mean prey concentrations, herring larvae were predicted to be food-limited in both feeding scenarios until they reached the length of 16.3 mm and 20.5 mm in September and December correspondingly. Independently of the season, the growth rate predicted in the specialist scenario was about 40% that in the generalist scenario (Fig. 4).

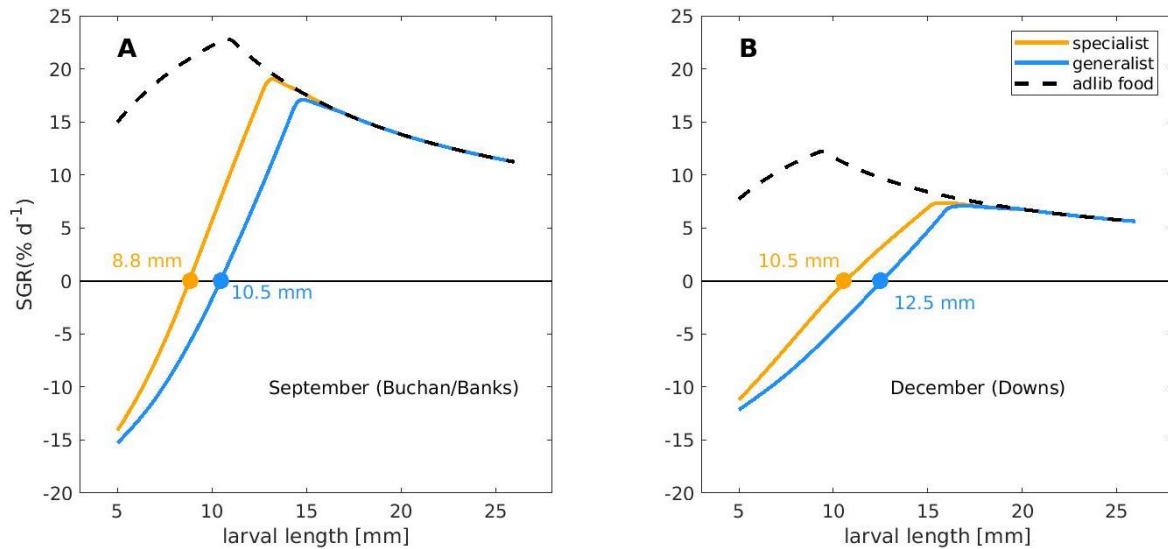


Figure 4. Simulated specific larval growth rate (SGR in % dw·d⁻¹), obtained with the mean NBSS for the generalist (orange) and specialist (blue) feeding scenarios in September (A) and December (B). Black dashed curves show the modeled “ab-libitum” feeding at corresponding environmental conditions (Buchan/Banks areas - T=12.3 °C, day length = 12 hours; Downs - T=10.9 °C, day length=8 hours). Black solid lines identify zero-growth. Orange and blue circles indicate minimal larval length at which modeled larvae were able to sustain a positive growth in corresponding feeding scenarios.

The generalist feeding scenario was further used to illustrate the role of microplankton in larval foraging at different prey biomass and larval length. The optimal foraging routine predicted that the optimal prey size increased with larval length and remained unchanged at different prey biomass (Fig 5, red dots). The foraging niche was found to broaden with increasing larval size and to narrow when the food availability increased. At two tested prey concentrations (0.3 and 6.3 mg·m⁻³), which correspond to the 2.5%- and 50%-percentiles of the observed biomass in both seasons, larvae of all size-classes were predicted to include microplankton prey in their diet (Fig 5). For example, 38% of the diet of an 8-mm larva consisted of microplankton and this proportion was found to decrease with larval size, as the optimal prey size increased. Although the contribution of microplankton decreased with increasing prey availability, only larger larvae (>18 mm) and only at the highest observed zooplankton biomass (90.9 mg·m⁻³) were predicted to have no microplankton in their diet.

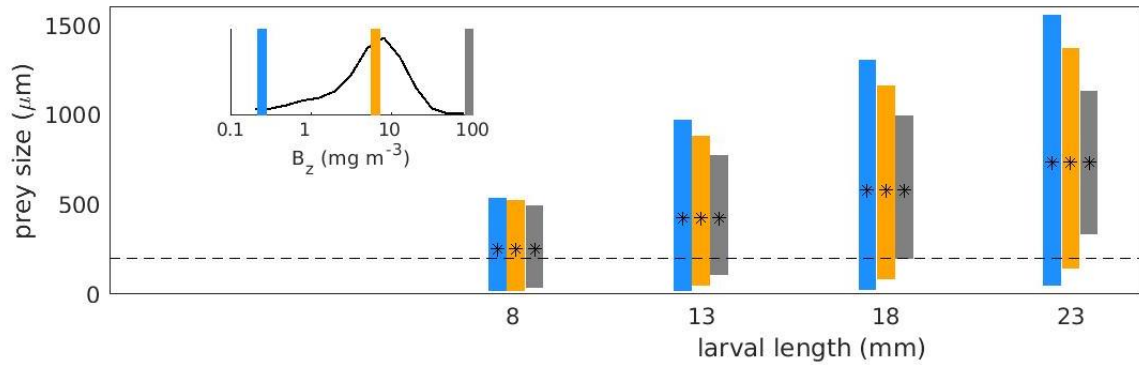


Figure 5. The width of the foraging niche of an 8-, 13-, 18 and 23-mm herring larva obtained in the model simulations with the minimal ($0.3 \text{ mg}\cdot\text{m}^{-3}$; blue), median ($6.3 \text{ mg}\cdot\text{m}^{-3}$; orange) and maximal ($90.9 \text{ mg}\cdot\text{m}^{-3}$; gray) observed prey biomass and a constant NBSS slope of -0.77 , which was the median of all observed slopes. Asterisks identify the optimal prey size of herring larvae and the black dashed line indicates $200 \mu\text{m}$ as a separation between micro- and meso- plankton. The inset shows the frequency distribution of the zooplankton biomass (B_z), observed in both spawning areas, and color bars show the corresponding prey biomasses used to calculate the foraging niches.

Simulation 2: predicted larval growth at the observed feeding conditions

The different feeding conditions herring larvae experienced in their spawning areas in September and in December (zooplankton biomass and size distribution, temperature and day length) resulted in different larval growth rates predicted with the bioenergetic model. The proportion of larvae with no growth decreased with increasing larval size and this decrease was faster in September (Fig. 6A) than in December (Fig. 6B). For example, 74% of the 8-mm larvae was predicted to starve in Buchan/Banks and this percentage decreased to 3% for 13-mm larvae (Fig. 6A). The vast majority (85%) of 18-mm larvae grew at ad-libitum rates. In Downs, 62% of 13-mm and 50% of the 18-mm larvae was predicted to starve, and only 26% of the 18-mm larvae grew at ad-libitum rates (Fig. 6B).

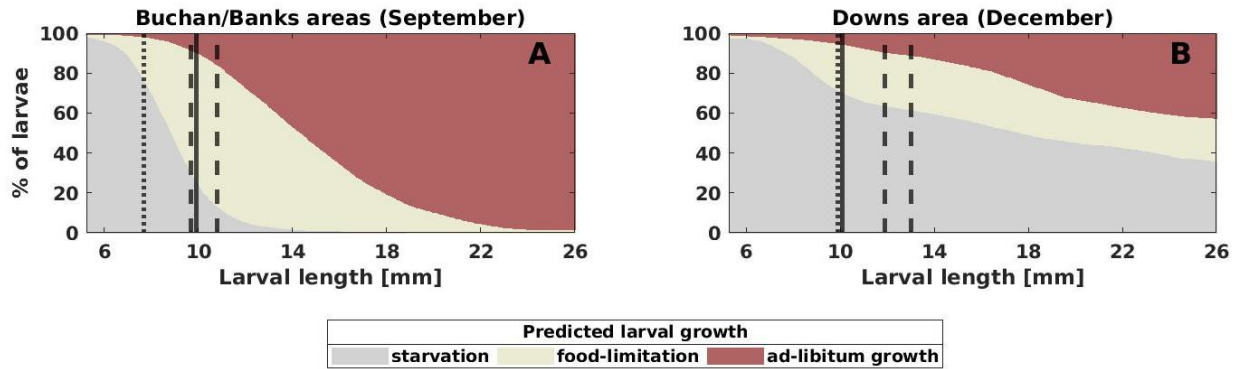


Figure 6 The fraction (in %) of all modeled larvae per size class that were predicted to experience starvation ($SGR \leq 0$, gray), food-limitation ($SGR > 0$ and $SGR < SGR_{max}$, beige) or to growth at their maximal temperature-, light- and size-dependent growth capacity ($SGR = SGR_{max}$, brown). The composites for Buchan/Banks areas in September (A) and Downs area in December (B) are shown. Dashed lines show the length range, where the largest yolk-sac larvae were observed in this study. Black solid lines show larval length-at-first-feeding (LFF) calculated after Hufnagl and Peck (2011) and dotted lines depict LFF reported by Blaxter and Hempel (1963).

To depict the spatial pattern in predicted larval growth we used three years with the full plankton data coverage (2016, 2017 and 2019; other years are shown in supplement S5 “The modelled larval growth in 2013, 2014 and 2018”). The observed prey concentrations in all three years had a similar spatial pattern with the highest prey concentration in the northern North Sea (in Buchan/Banks areas) and the lowest prey concentration in the English Channel (Fig 7, A, E and I). The zooplankton biomass observed in the Southern Bight was comparable with that in the Buchan/Banks areas in September. In all sampled years, prey biomass had a patchy structure with up to ten-fold differences in biomass in neighboring stations. This patchiness was reflected in the spatial distribution of predicted larval growth, which was particularly obvious for the smaller herring larvae (Fig. 7, B, F and J). In agreement with Fig 6, the observed plankton biomass at most of the stations did not support the growth of 8-mm larvae. A herring larva of 8 mm required zooplankton biomass $> 25 \text{ mg} \cdot \text{m}^{-3}$ to sustain its growth. Such high zooplankton biomass was observed only at about 7% of all stations broadly distributed across the sampling area (Fig 7). Larger larvae, as it is shown using an example of 13 mm (Fig 7c, g, and k) and 18 mm (d, h, and l) larvae, found enough food to grow almost at all observed stations, except those in the English Channel. The low zooplankton biomass ($< 2 \text{ mg} \cdot \text{m}^{-3}$) observed there in December caused a strong food deprivation of herring larvae of all tested sizes. Only a few stations had enough food to support larval growth.

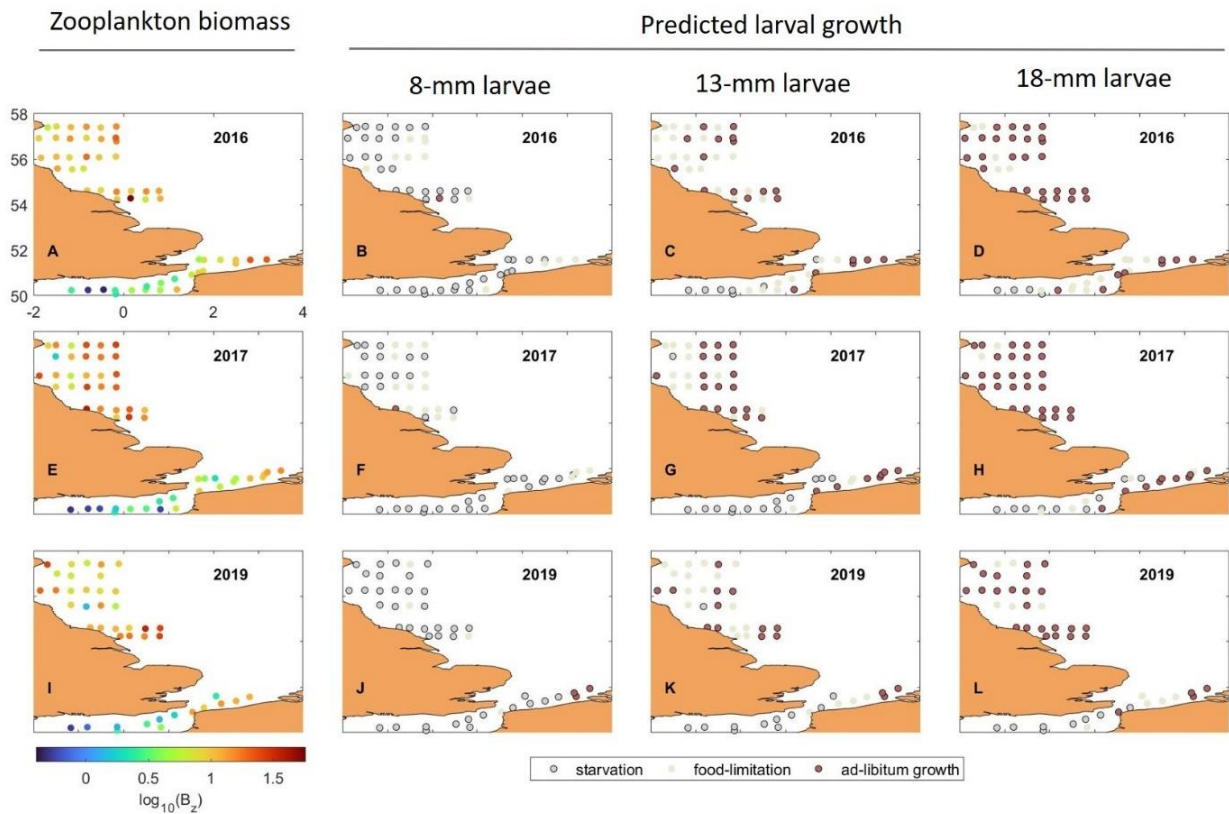


Figure 7: The observed plankton biomass (B_z) (in 2016 (A), 2017(E) and 2019(I)) and corresponding growth predicted for a 8-mm (B, F, J), 13-mm (C, G, K) and 18-mm herring larva (D, H, L). Colors correspond those of Fig. 6: gray - starvation ($SGR \leq 0$), beige - food-limitation ($SGR > 0$ and $SGR < SGR_{max}$) and brown – ad-libitum feeding ($SGR = SGR_{max}$). Please find the corresponding figure for the years 2013, 2014 and 2018 in supplemental materials (Figure 4. S5.1).

Simulation 3: optimal feeding conditions

The optimal feeding simulations showed that larval growth rate and the minimal zooplankton biomass required by a herring larva to sustain its growth vary not only with larval size, but also with slope of the zooplankton size-spectrum (Fig. 8). As we can see from the example of an 8-mm larva (Fig. 8A), the required biomass reached its absolute minimum (B_{min}) at slope of -0.93 (considered to be “optimal”) and was higher at the smaller and larger slopes. Similar patterns of B_{min} were obtained for larger herring larvae (see Fig. 8, B and C) as well, although an asymmetric distribution was observed with increasing larval size where a higher biomass was required at steeper slopes (those approaching -2) than at shallower ones (approaching 0). Interestingly, the observed prey slopes in the field (brown dots in Fig. 8) were dispersed around the NBSS slopes considered to be optimal in both seasons. The difference between the simulated B_{min} and the observed zooplankton biomass was larger in December (Fig. 8 D, E and F) than in September (Fig. 8 A, B and C).

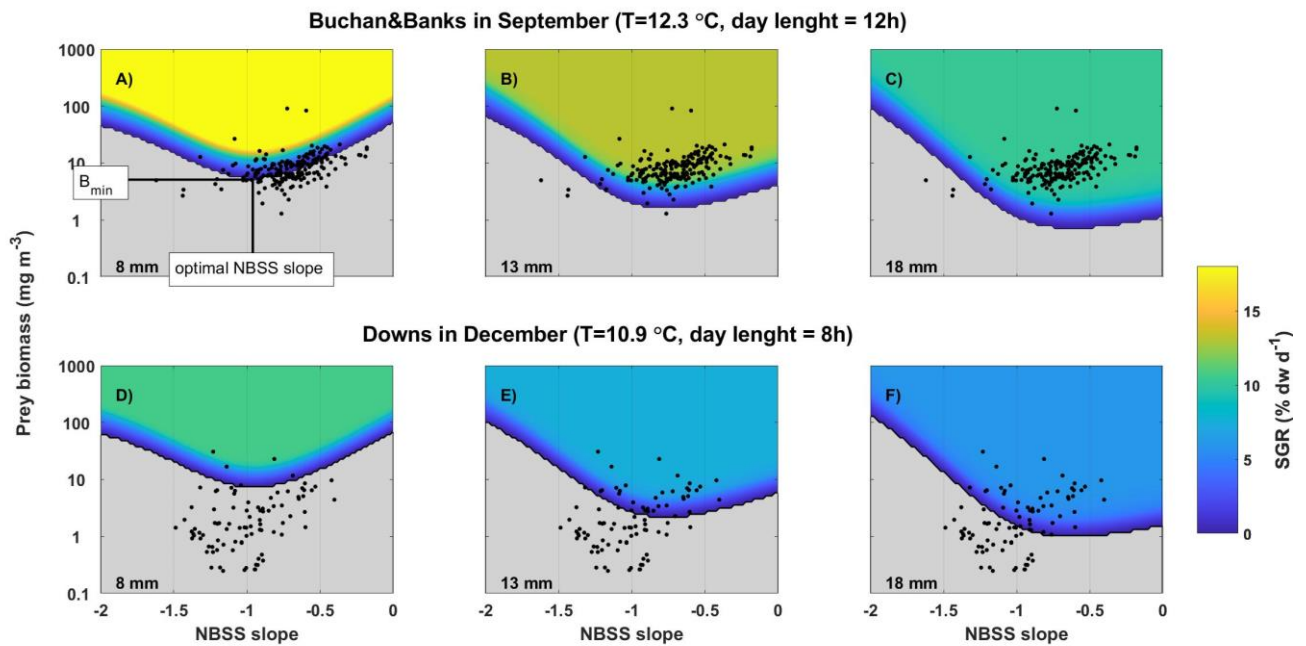


Figure 8. Modeled growth rate of herring larvae of 8 mm (A and D), 13 mm (B and E) and 18 mm (C and F) length foraging at different prey conditions (prey biomass and NBSS slope) in the Buchan/Banks in September (A, B and C) and in the Downs in December (D, E and F). Colors identify simulated specific growth rates (SGR in % dw·d⁻¹), gray color marks the area where predicted growth is negative (SGR<0), i.e. the larvae starved. The minimal biomass B_{min} required by a larva to sustain its growth and the corresponding optimal NBSS slope are marked in panel A. The larval growth was modeled at the mean observed temperatures and light conditions in corresponding spawning areas (Buchan/Banks areas - T=12.3 °C, day length = 12 hours; Downs - T=10.9 °C, day length=8 hours). Black dots indicate the observed prey fields (NBSS slope and biomass) in all sampled years and stations within corresponding spawning areas.

To further investigate the optimal feeding conditions, we calculated B_{min} and the optimal NBSS slope for each initial larval length and for both spawning seasons. The optimal NBSS slope increased with larval length from -1.1 to -0.6 for 5-mm to 27-mm larvae (Fig. 9A) and was similar in both spawning areas. The B_{min} exponentially decreased with the larval length (Fig. 9B): the smallest (5 mm) larvae required at least 67 mg·m³ to sustain their growth, whereas larger larvae (e.g. 20 mm) required ten-fold lower prey biomass (1.66 mg·m³). On average, the B_{min} was 19 % higher in December than in September.

The optimal NBSS slope did not change with increasing temperature as can be seen using a 13-mm larvae as an example (Fig. 9C). In contrast, the B_{min} increased with temperature in both areas (Fig. 9D). Given a projected 2 °C increase of the mean water temperature in the North Sea by the end of the 21st century, our model predicted that B_{min} for a 13-mm larva would increase from 5.6 to 7.6 mg·m³ (+35%) in the Downs and from 5.0 to 6.4 mg·m³ (+28%) in the Buchan/Banks.

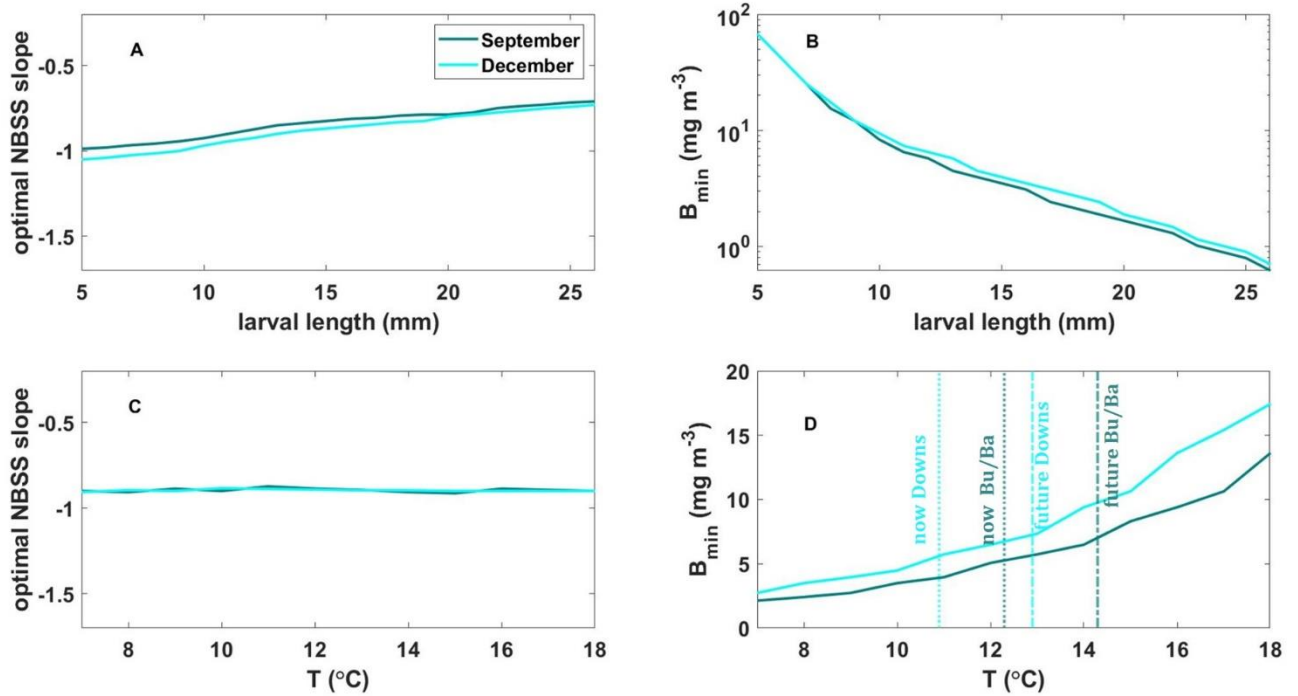


Figure 9. Optimal NBSS slope (A) and the corresponding minimal required biomass (B) modelled for a herring larva between 5 and 27 mm long and with the mean environmental conditions in September (teal, $T=12.3$ °C, day length = 12 hours) and December (cyan, $T=10.9$ °C, light=8 hours) for larval initial length between 5 and 26 mm. Please note the log-scale along the y-axis at the panel B. Optimal NBSS slope (C) and the minimal required biomass (D), predicted for a 13-mm herring larva in the model simulations with the day length of 12 hours (teal, corresponding to September conditions), and 8 hours (cyan, corresponding to December) but with water temperature varying between 7 °C and 18 °C. The vertical lines depict current (dotted) and projected (dashed) mean temperatures in the Buchan/Banks (teal) and the Downs (cyan) areas.

Discussion

To improve our understanding of biotic and abiotic factors effecting marine fish recruitment, there is a need to better resolve processes impacting larval growth and mortality, which is challenging in marine ecosystems (Pepin et al., 2015; Hinchliffe et al., 2021). Here, we addressed two major gaps in knowledge regarding feeding and growth of temperate larval fish: i) the difference in energetic needs between a specialist vs generalist feeding strategy, and ii) the probability of food limited growth and starvation during periods low secondary productivity (e.g. wintertime). Physiological individual-based models as one used in this study is a powerful tool to explore larval growth and its variability particularly in a food-limited environment. Estimates of larval growth from such models are sensitive to the methods used and assumptions made to construct larval prey fields. These prey fields can be generated using highly simplified theoretical consideration (Huebert and Peck, 2014), lower-trophic level models (Huebert et al., 2018) or based on measurements from field sampling campaigns (Kühn et al., 2008; Hufnagl et al., 2015). In contrast to the former two approaches, deriving prey fields

from in situ measurements provides the most accurate estimate of the spatiotemporal variability in the zooplankton biomass and size structure. We argue that covering a wide size-range of potential prey using automated identification and size measurement is necessary to not only understand the spatiotemporal dynamics of zooplankton in general but also to assess feeding conditions experienced by fish larvae. This automated approach is substantially less time-consuming compared to classical microscopy (Orenstein et al., 2022) and still provides sufficient information to accurately estimate larval growth by means of bioenergetics modelling. The approach taken here of combining simultaneous sampling of fish larvae and their planktonic prey and physiological modelling seems to be a plausible method to expand the existing larval monitoring programs providing estimates of larval abundance for the routine stock assessments toward more holistic ecosystem surveys.

In the following, we discuss our findings with respect to the feeding preference of herring larvae and compare larval feeding success between two spawning seasons and areas in the North Sea. We suggest that our growth estimates can be used not only to estimate the probability of larval mortality via starvation, but also provides indirect indices for other mortality processes given the tight link between larval size and predation risk (e.g. Bailey and Houde, 1989; Stige et al., 2019) or larval size and swimming ability influencing dispersion and drift (e.g. Woodson and McManus, 2007). We also discuss possible limitations of our modelling approach and point out critical knowledge gaps that hamper translating model-derived estimates of probability of starvation to cumulative larval mortality as a direct proxy of recruitment success.

Feeding modes of herring larvae and the role of microplankton

Previously reported field-based estimates of prey preference of herring larvae agree poorly. Some studies report that herring larvae have a clear preference for copepods, with a shift from smaller to larger stages or species of copepods with increasing larval size (e.g. Kiørboe et al., 1988; Wilson et al., 2018). More recent studies suggested that young herring larvae are generalist foragers, ingesting a wider range of proto- and microplankton organisms (de Figueiredo et al., 2005; Bils et al., 2016; Denis et al., 2016). While, no gut content analysis was included in this study, the results of our model scenarios provide some insight on a likely feeding strategy of larvae from the bioenergetic perspective.

Our results based on mean, observed feeding conditions suggest that “specialist” feeders (only copepods) needed to be, on average, 2-mm larger on the onset of the exogeneous feeding than “generalist” feeders to survive and sustain positive growth (Fig 3). The higher survival potential of small, potentially first-feeding, larvae in the generalist scenario was due to the broader range in microplankton prey species included in their diet. Moreover, if larvae survive this early period, the growth rates of larvae smaller than 16 mm (20 mm) in September

(December) were, on average, 40% lower in the “specialist” compared to the “generalist” scenario. Similar estimates of reduced growth were obtained by Bils et al. (2016) for herring larvae in the Irish Sea when microplankton was excluded from their feeding simulations. Such difference in growth may result in substantial reductions in larval survival since mortality rates are believed to decrease rapidly with increasing larval size (e.g. Houde, 2002). Payne et al. (2013) estimated that a 10% reduction in growth can result in a 60 to 80% reduction in the number of herring larvae surviving to metamorphosis.

A main reason for the differences in growth and survival of “specialist” and “generalist” feeders was that copepods formed on average only 20% of the observed biomass of microplankton (ESD 20-200 μm) (Fig. 2 and Fig. S5.1). The microzooplankton taxa with highest biomasses beside copepods were Dinoflagellates in September, and Bivalve larvae and Foraminifera in December. The optimal foraging theory used in this study predicted that small, in particular first-feeding, herring larvae include a substantial proportion of microplankton (also none copepods) in their diet (Fig 5). Our estimate of 38% of microzooplankton in the diet of an 8-mm larva agrees well with the estimated proportion of protozoa in the diet of herring larvae between 19 and 71 % obtained by de Figueiredo et al. (2005) in the Irish sea. Larger herring larvae, however, were predicted to be able to reach their maximal growth capacity by feeding only on copepods (Fig 5). This was in agreement with Denis et al. (2016) who reported a shift from the generalist feeding mode to a narrower specialist feeding as larvae grow. They showed that protists constituted a relevant part of the diet of Downs herring larvae smaller than 12 mm, whereas bigger larvae (between 13 and 15 mm) fed mainly on copepods and dinoflagellates. Given this growing body of literature on larval feeding on microplankton and our modelling results, we suggest that focusing only on copepods as a prey item of herring larvae, as for example in Kühn et al. (2008), Alvarez-Fernandez et al. (2015) or Hufnagl et al. (2015), could potentially lead to an underestimation of the larval growth and survival, particularly when early-feeding herring larvae are of concern.

Optimal, current and future prey fields of herring larvae

According to the seven years of observations used in this study, feeding conditions of herring larvae differed among herring spawning areas Buchan/Banks and Downs not only in terms of temperature and day length, but also in terms of available zooplankton biomass. This yielded different larval growth, as predicted with the bioenergetic model. Even in the most favorable “generalist” feeding scenario, food limitation was an important factor affecting small larvae in both areas. Larger larvae (>13 mm) were predicted to have food-limited growth during winter at Downs, but not in autumn at Buchan/Banks, where larvae approached their maximal growth temperature-specific growth capacity. These results compare well with previous field studies of Kjørboe et al. (1988) on Buchan herring larvae and Buckley and Durbin (2006) on Atlantic

cod (*Gadus morhua*) and haddock (*Melanogrammus aeglefinus*) on Georges Bank. Both studies showed a strong prey-limitation of young larvae, but not of larger larvae captured at the same stations.

Our findings for the Buchan/Banks areas are in line with the “critical period” hypothesis, which postulates that high larval mortality during the transition from yolk-sac to exogenous feeding is crucial for the year-class strength (Hjort, 1914). Some previous studies have argued for the importance of the critical period for the recruitment success of herring in the North Sea (Alvarez-Fernandez et al., 2015, Fässler et al., 2011). In contrast, we found the Downs larvae to have a subnational probability of starvation over a wider range of larval lengths and, therefore, well beyond the first-feeding period (Fig. 6). A closer inspection of the spatial distribution of zooplankton and predicted larval growth revealed that only the western part of the Downs (English Channel) was characterized by low zooplankton concentrations and, thus, a high proportion of starving larvae, whereas the feeding conditions in the eastern part (Southern Bight in the inner North Sea) were rather similar to those in September (Fig. 7). Given the prevailing direction of the water currents, herring larvae hatched in the English Channel would be transported to the Southern Bight (Hufnagl et al., 2015) where, according to our results, they would find more favorable feeding conditions. However, comparison of the larval length-frequency distributions in the English Channel and the Southern Bight revealed only a marginal shift towards larger larvae in the latter (Fig. 3C and D). This implies that herring larvae of all tested lengths between 5 and 27 mm are probably affected by starvation and/or food-limitation in winter in the English Channel. This suggests that the survival of winter herring larvae is not driven by a single, “critical” event but by continual losses due to starvation over the protracted overwintering period in agreement with Hufnagl et al. (2015). Our differentiation between larval growth conditions in the English Channel and Southern Bight will hopefully contribute to a better understanding of the larval survival in the Downs area. This spawning component is gaining increasing attention, because of its growing contribution to the overall NSASH recruitment, but has previously been shown to be challenging for modelling and process-understanding (Heath et al., 1997; Hufnagl et al., 2015).

The predicted rapid decrease in the probability of starvation with increasing larval size, particularly in September, suggests that larger first-feeding larvae have a better chance of surviving (finding enough food to support their growth) compared to their smaller siblings. The LFF parameterization of Hufnagl and Peck (2011) and temperature ranges in the spawning areas observed in this study yield LFF estimates of 9.9 ± 0.1 mm for larvae spawned in September, and 10.0 ± 0.1 mm for those spawned in December. The latter compares well with previously reported mean LFF of 9.9 mm for Downs larvae (Blaxter and Hempel, 1963), but is below the maximal LFF estimated in the present study based on the size of captured yolk-sac

larvae (Fig. 6B). As for the Buchan/Banks area, the LFF estimate of 9.9 of Hufnagl and Peck (2011) falls within the size range 9.7 to 10.8 mm, where the largest yolk-sac larvae were reported in this study, but is above LFF of 7.7 mm previously reported by Blaxter and Hempel (1963) for this area (Fig 6A). According to our results, these subtle differences in LFF result in substantially different probability of mortality due to starvation, particularly in September (see Table 4. 2). We further discuss LFF and its variability in the section „Uncertainties and critical gaps in knowledge” below.

Table 2. Length-at-first-feeding (LFF) of herring larvae as reported in previous studies and corresponding probability of starvation predicted in the “generalist” feeding scenario in both spawning areas/seasons (Fig 6). LFF estimates in this study were based on the size-range of the largest yolk-sac larvae observed in corresponding spawning areas between 2013 and 2019.

Spawning area/season	Reference	LFF estimate (mm)	Probability of starvation (in %)
Buchan/Banks (September)	Blaxter and Hempel, 1963	7.7	76
	Hufnagl and Peck (2011)	9.9	24
	This study	9.7 to 10.8	0.5 to 9
Downs (December)	Blaxter and Hempel, 1963	9.9	72
	Hufnagl and Peck (2011)	10.1	70
	This study	11.9 to 13.0	60 to 63

Further valuable conclusions can be drawn from the comparison of the observed prey fields (prey biomass and size-spectra) with the theoretical optimal feeding conditions of herring larval at different lengths and/or ages. Our model results suggest that the growth of herring larvae is sensitive to both plankton biomass and size structure (NBSS slope). Particularly young herring larvae were sensitive to changes in the NBSS (Fig 8), whereas larger larvae were found less sensitive to the less negative slopes (more larger prey items) because those larvae become more efficient in utilizing larger prey organisms. The importance of the zooplankton size structure for larval growth has been previously emphasized by modelling studies of Urtizberea and Fiksen (2013), David et al. (2022) and Huebert and Peck (2014), although the simulation results of the latter were somewhat different from ours (see more details in Supplement S6 “Model sensitivity to NBSS slope”).

To our knowledge, the role of the prey size-structure in the survival and growth of marine fish larvae has been rarely tested in the laboratory due to technical challenges related to offering

and maintaining a prey field characterized by a specific size-spectrum slope. However, given the known feeding behavior, prey preferences and gape limitation of fish larvae, one would expect the larval foraging success and growth to be dependent on the size structure of the prey field. Following seminal studies on size-spectrum theory in marine ecosystems (Sheldon et al., 1972; Hatton et al., 2021), the most recent study of Suthers et al. (2022) hypothesized a key role of NBSS slope in shaping growth and survival of fish larvae in marine ecosystems. Although, their conclusion is mainly based on a theoretical consideration, the dependency of larval growth and survival on zooplankton NBSS could provide a new context in quantifying or predicting fish recruitment.

The optimal slope of the zooplankton size spectrum, i.e. the slope at which larvae required the least biomass of prey for herring larvae to maintain their growth, was similar at Downs and Buchan/Banks and was well within the observed range of the NBSS slope calculated from field samples (Fig. 8). This may suggest that the larval foraging strategy is well adapted to the size-structure of the prey field encountered in the North Sea. The minimal prey biomass required for larval growth was, on average, 19% higher in December than in September. The reason for the higher prey requirements was a shorter day length in winter and, thus, a longer period of time when larvae pay for metabolic costs without energetic income. This finding points out that the energy savings afforded by decreased temperature in December does not fully compensate for the losses in foraging time due to the short, wintertime photoperiod. Projected warming will increase energetic costs and, therefore, be particularly challenging for larvae experiencing short day lengths. We estimated that a 13-mm herring larva will require 28% (35%) higher prey biomass in the Buchan/Banks (Downs) area to sustain their growth in the 2°C-warmer North Sea. It remains an open question whether the productivity of the North Sea will increase in the future, or Atlantic herring will adapt its spawning strategy, including phenology and/or distributional shift, to promote larval survival as it is known for various marine fish species (e.g. Bakun, 2006; Ottmann et al., 2021).

Uncertainties and critical knowledge gaps

Bioenergetic model

The model used in this study has been thoroughly validated and yielded a good comparison with laboratory and field studies of herring larvae (Hufnagl and Peck, 2011; Bils et al., 2016; Illing et al., 2018). Although we were not able to compare our modeled growth rates with in situ measurements based on the RNA:DNA or otolith microstructure analyses, we believe this model provided reliable estimates of growth and starvation of herring larvae. However, there are some important limitations to our modeling approach. First, although the optimal foraging routine used in our model represents an advancement in our mechanistic understanding of the

foraging process, this routine is still a simplified representation of the larval trophodynamics. It is solely based on the size-driven predator-prey interactions and does not take other potentially relevant aspects into account (e.g. prey visibility, species-specific energy content or escape behavior). Although size is likely an important factor in prey selection by larvae and the predicted prey niche breadth compares well with observed sizes of prey in larval guts (Hufnagl and Peck, 2011), we need to keep in mind that i) field-based analysis of larval gut content can be biased toward larger prey items, and ii) laboratory observations on predator-prey interactions are usually obtained using single prey species such as different life stages of a copepod (de Figueiredo et al., 2005; Robert et al., 2014). In our opinion, the main factor hindering the creation of more realistic foraging models is the availability of reliable field or laboratory data with taxonomical and size-resolved information on available versus consumed prey. We suggest that future feeding studies conducted in the laboratory or in mesocosms to employ more realistic prey fields and trophodynamic field studies to combine multiple approaches (such as visual gut content analysis, DNA metabarcoding and isotope analysis). Once such data are available, they can be easily integrated into the foraging routine of a bioenergetic model to account for the larval prey preferences.

Second, the metabolic rates used in this study (see Eq. S3.4 in supplements) were temperature- and size-dependent, and did not consider metabolic down-regulation as an adaptive strategy to poor feeding conditions. Illing et al. (2018) reported the metabolic rates of a starving larva being 8 to 34 % lower than those of a well-fed larva. A similar down-regulation was demonstrated herring larvae fed at low rations by Kiørboe et al. (1987). Such energy-saving mechanism is probably linked to the starvation resistance of herring larvae that allow them to survive at zero-growth rates whereas larvae of other species such as cod need to maintain a positive growth (e.g. 3% d⁻¹) to survive (Folkvord et al., 2015). However, the positive effects of this adaptation on larval survival remain questionable. Low or zero-growth increases a size-dependent predation pressure on larvae in agreement with the “bigger is better” and “stage duration” hypotheses (Anderson, 1988; Houde, 2008). Moreover, it is unclear for how long larvae can down-regulate their metabolism and still be able to successfully forage when they encounter favorable feeding conditions such as a patch of zooplankton. For example, Pedersen (1993) reported that larvae reared under low and high ration-cycles (5 and 10 days, respectively) grew slower during the high ration phase compared to conspecifics constantly fed high rations. A better understanding of a decreased performance of starved larvae and larval resilience to unfavorable feeding conditions (e.g. duration to point-of-no-return of yolk-sac and pre-flexion larvae) will be needed for different spawning components/seasons.

Prey field

Plankton concentration is known to vary at a wide range of spatial scales and its patchiness has been shown to be important for feeding dynamics of planktivorous predators, including fish larvae (Robinson et al., 2021). Although the simultaneous sampling of herring larvae and their planktonic prey used in this study was the best possible approach in these field campaigns, we need to be aware that the net sampling represents an “average” prey concentration across ~2 km at each station. Despite finding substantial variability in the distribution of zooplankton biomass at this scale (Fig 7, A, E, and I), prey patchiness relevant to larval foraging occurs at much smaller scales (10s of meter, Pepin et al., 2015). Previous studies suggested that prey patchiness at these small-scales and the random encounter of higher prey densities by individual larvae can enhance growth rates and sustain the survival of larvae within cohorts experiencing suboptimal feeding conditions (e.g. Davis et al., 1991; Pitchford and Brindley, 2001). Our ability to include prey patchiness in the individual-based model is limited by a lack of observations and process understanding of zooplankton patchiness. Alternative observational methods, for example, a Video Plankton Recorder (Davis et al., 2005; Lough and Broughton, 2006) or similar equipment could be used in the future to resolve the fine-scale patchiness in the distribution of fish larvae and their prey. This information is particularly valuable to better understand larval feeding success and survival in food-limited environments such as the winter North Sea.

Our modelling approach did not consider the impact of larval feeding on zooplankton and ability of herring larvae to overgraze its zooplankton prey. Pepin and Penney (2000) and Llopiz et al. (2010) found it rather unlikely that fish larvae can exert enough pressure to severely reduce zooplankton standing stocks. In contrast, Cushing (1983) suggested that lesser sandeel (*Ammodytes marinus*) larvae caused significant mortality on, and local depletion of, their zooplankton prey in the North Sea. Although larval prey consumption will likely have little impact if foraging occurs in a patch of high zooplankton biomass, intraguild competition and overgrazing may increase the risk of larval starvation when prey availability or productivity is low. To add more realism to larval foraging models, density-dependent effects and a feedback loop on the prey field need to be considered. Although larval fish consumption has been included as a mortality term in some low-trophic level models (i.e. Maar et al., 2014), to our knowledge, such feedback has been largely ignored in individual-based bioenergetic models of marine fish larvae.

Larval length at first feeding

Larval length is an important trait that determines various developmental attributes of fish larvae (e.g. swimming speed, capture success) and, thereby, controls larval feeding success and vulnerability to starvation during the first critical period of their life. Our results suggest that particularly young first feeding larvae are vulnerable to starvation and that a cohort-specific starvation mortality depends not only on the mean LFF, but on the length-frequency distribution of the first-feeding larvae within this cohort. Our literature review on herring spawning sub-components in the North Sea and herring stocks elsewhere revealed that the variability of larval length-at-hatch (LAH) has been well documented (e.g. Blaxter and Hempel, 1963; Peck et al., 2012), whereas less information is available on the variability of the LFF. To our knowledge, only two studies reported ranges of LFF for autumn-spawning herring larvae: i) Johannessen et al. (2000) estimated the standard deviation of LFF of 0.5 mm from laboratory experiments, and ii) Gamble et al. (1985) reported a LFF range of 0.8 mm in larvae reared in large, enclosed mesocosms. Due to a low number of parents used to produce offspring for laboratory/mesocosm experiments, we think that these LFF ranges underestimate the variability of LFF in the North Sea herring population. Field observations from the IHLS were not feasible to derive the range of LFF, because wild caught herring larvae rapidly lose their yolk-sac while being captured. Therefore, we only used these data to estimate the maximal size of yolk-sac larvae in the field as a proxy to the maximal LFF. The comparison of those LFF with previously reported ones, suggest the length range of first-feeding larvae of at least 2 mm. Our results underscore the need for up-to-date and quality assured estimates of herring larvae length-at-hatch and length-at-first feeding for different spawning components in the North Sea (and probably, elsewhere).

Temperature and parental factors (e.g. changes in stock age-structure due to climate change or exploitation) have often been reported as an important factor regulating egg size, LAH and LFF (Peck et al., 2012; Geffen, 2009, van Damme et al., 2009). It has been shown that egg size in herring populations differs not only among spawning seasons but between cohorts within the same spawning season due to seasonal difference in the size of females within spawning waves (Huang et al., 2022). Two-fold variation in egg size was reported by Blaxter and Hempel (1963) and dos Santos Schmidt et al. (2017) reported for the Downs and Buchan spawning areas. However, it is unclear how these differences in egg size translate into differences in LAH and LFF. As for temperature, Blaxter and Hempel (1963) questioned whether a uniform influence of incubation temperature on the hatching size of herring larvae exists for all Atlantic herring (sub)stocks. We suggest further laboratory and mesocosm investigations where mean and, even more importantly, ranges of larval LAH and LFF should be reported. Novel mobile mesocosm experimental setup with underwater video recordings

(e.g. Sswat et al., 2018) could produce new insights into trophodynamics of first-feeding herring larvae to overcome the problem that herring larvae often lose their yolk-sac if handled. Parental effects on LAH/LFF in North Sea herring can be studied using cross-fertilizations experiments (e.g. Berg et al., 2018) Furthermore, long-term monitoring of changes in LAH and LFF would be required to explore effects of temperature during incubation time and changes in the age(size)-structure and reproductive strategy of the parental NSASH stock.

Author Contributions

A.A., M.M and M.A.P. conceived the study. A.A. performed numerical simulations, statistical analyses and wrote the article. GB and CvD performed the field sampling. G.B. analyzed the zooplankton data. All authors discussed the results and contributed to the final manuscript. M.M. supervised the project.

Acknowledgements

This work has been partially funded by the German Research Foundation (THRESHOLDS, MO 867 2873/3-1) and by the German Federal Ministry of Education and Research (DAM-CoastalFutures, grant no 03F0911F). We would like to thank Eva Alvarez for her help with zooplankton NBSS, Björn Illing for providing length data on laboratory-reared larvae, Richard Nash and Audrey Geffen for their consulting on larval length-at-first feeding, Klaus Huebert and Marc Hufnagl for providing their model code, Ismael Nunez-Riboni and Tahereh Nakisa for their mathematical assistance, Andriy Martynenko for processing the CTD data, and Patrick Polte for his critical comments on early drafts of this manuscript. We would like to thank the crew of RV "Tridens" and staff of the Wageningen Marine Research for their support in data collection.

References

Akimova, A., M. Hufnagl and M. A. Peck (2019). "Spatiotemporal dynamics of predators and survival of marine fish early life stages: Atlantic cod (*Gadus morhua*) in the North Sea." *Progress in Oceanography* **176**: 102121.

Alvarez-Fernandez, S., P. Licandro, C. J. G. van Damme and M. Hufnagl (2015). "Effect of zooplankton on fish larval abundance and distribution: a long-term study on North Sea herring (*Clupea harengus*)." *ICES Journal of Marine Science* **72**(9): 2569-2577.

Anderson, J. T. (1988). "A review of size dependent survival during prerecruit stages of fishes in relation to recruitment." *Journal of Northwest Atlantic Fisheries Science* **8**: 55-56.

- Bailey, K. M. and E. D. Houde (1989). "Predation on eggs and larvae of marine fishes and the recruitment problem." *Advances in Marine Biology* **25**: 1-83.
- Bakun, A. (2006). "Wasp-waist populations and marine ecosystem dynamics: Navigating the "predator pit" topographies." *Progress in Oceanography* **68**(2): 271-288.
- Berg, F., O. W. Almeland, J. Skadal, A. Slotte, L. Andersson and A. Folkvord (2018). "Genetic factors have a major effect on growth, number of vertebrae and otolith shape in Atlantic herring (*Clupea harengus*)." *PLoS ONE* **13**(1): e0190995.
- Bils, F., M. Moyano, N. Aberle, M. Hufnagl, S. Alvarez-Fernandez and M. A. Peck (2016). "Exploring the microzooplankton–ichthyoplankton link: a combined field and modeling study of Atlantic herring (*Clupea harengus*) in the Irish Sea." *Journal of Plankton Research* **39**(1): 147-163.
- Blanco, J. M., F. Echevarría and C. García (1994). Dealing with size-spectra: some conceptual and mathematical problems.
- Blaxter, J. H. S. and G. Hempel (1963). "The Influence of Egg Size on Herring Larvae (*Clupea harengus* L.)." *ICES Journal of Marine Science* **28**(2): 211-240.
- Buckley, L. J. and E. G. Durbin (2006). "Seasonal and inter-annual trends in the zooplankton prey and growth rate of Atlantic cod (*Gadus morhua*) and haddock (*Melanogrammus aeglefinus*) larvae on Georges Bank." *Deep Sea Research Part II: Topical Studies in Oceanography* **53**(23): 2758-2770.
- Chambers, R. C. and E. A. Trippel, Eds. (1997). *Early Life History and Recruitment in Fish Populations*. Fish and Fisheries Series. London, Chapman & Hall.
- Cushing, D. H. (1983). "Are fish larvae too dilute to affect the density of their food organisms?" *Journal of Plankton Research* **5**(6): 847-854.
- Cushing, D. H. (1990). *Plankton Production and Year-class Strength in Fish Populations: an Update of the Match/Mismatch Hypothesis*. Advances in Marine Biology. J. H. S. Blaxter and A. J. Southward, Academic Press. **Volume 26**: 249-293.
- David, C. L., R. Ji, C. Bouchard, H. Hop and J. A. Hutchings (2022). "The interactive effects of temperature and food consumption on growth of larval Arctic cod (*Boreogadus saida*): A bioenergetic model." *Elementa: Science of the Anthropocene* **10**(1).
- Davis, C. S., G. R. Flierl, P. H. Wiebe and P. J. S. Franks (1991). "Micropatchiness, turbulence and recruitment in plankton." *Journal of Marine Research* **49**(1): 109-151.
- Davis, C. S., F. T. Thwaites, S. M. Gallagher and Q. Hu (2005). "A three-axis fast-tow digital Video Plankton Recorder for rapid surveys of plankton taxa and hydrography." *Limnology and Oceanography: Methods* **3**(2): 59-74.

de Figueiredo, G. M., R. D. M. Nash and D. J. S. Montagnes (2005). "The role of the generally unrecognised microprey source as food for larval fish in the Irish Sea." *Marine Biology* **148**(2): 395-404.

Denis, J., C. Vallet, L. Courcot, V. Lefebvre, J. Caboche, E. Antajan, P. Marchal and C. Loots (2016). "Feeding strategy of Downs herring larvae (*Clupea harengus* L.) in the English Channel and North Sea." *Journal of Sea Research* **115**: 33-46.

Dickey-Collas, M., R. D. M. Nash, T. Brunel, C. J. G. van Damme, C. T. Marshall, M. R. Payne, A. Corten, A. J. Geffen, M. A. Peck, E. M. C. Hatfield, N. T. Hintzen, K. Enberg, L. T. Kell and E. J. Simmonds (2010). "Lessons learned from stock collapse and recovery of North Sea herring: a review." *ICES Journal of Marine Science: Journal du Conseil* **67**(9): 1875-1886.

dos Santos Schmidt, T. C., A. Slotte, J. Kennedy, S. Sundby, A. Johannessen, G. J. Óskarsson, Y. Kurita, N. C. Stenseth and O. S. Kjesbu (2017). "Oogenesis and reproductive investment of Atlantic herring are functions of not only present but long-ago environmental influences as well." *Proceedings of the National Academy of Sciences* **114**(10): 2634-2639.

Fässler, S., M. Payne, T. Brunel and M. Dickey-Collas (2011). "Does larval mortality influence population dynamics? An analysis of North Sea herring (*Clupea harengus*) time series." *Fisheries Oceanography* **20**: 530-543.

Folkvord, A., K. W. Vollset and I. A. Catalán (2015). "Differences in growth and survival between cod *Gadus morhua* and herring *Clupea harengus* early stages co-reared at variable prey concentrations." **87**(5): 1176-1190.

Fuiman, L. A. and R. G. e. Werner (2002). *Fishery Science: The unique contributions of early life stages*. Bodwin, Cornwall, Blackwell Science Ltd.

Gamble, J. C., P. MacLachlan and D. D. Seaton (1985). "Comparative growth and development of autumn and spring spawned Atlantic herring larvae reared in large enclosed ecosystems." *Marine Ecology Progress Series* **26**: 19-33.

Geffen, A. J. (2009). "Advances in herring biology: from simple to complex, coping with plasticity and adaptability." *ICES Journal of Marine Science* **66**(8): 1688-1695.

Hatton, I. A., R. F. Heneghan, Y. M. Bar-On and E. D. Galbraith (2021). "The global ocean size spectrum from bacteria to whales." *Science Advances* **7**(46): eabh3732.

Heath, M., B. Scott and A. D. Bryant (1997). "Modelling the growth of herring from four different stocks in the North Sea." *Journal of Sea Research* **38**(3-4): 413-436.

- Hinchliffe, C., P. Pepin, I. M. Suthers and D. S. Falster (2021). "A novel approach for estimating growth and mortality of fish larvae." *ICES Journal of Marine Science* **78**(8): 2684-2699.
- Hjort, J. (1914). "Fluctuations in the Great Fisheries of Northern Europe." *Rapports et Procès-Verbaux des Réunions* **20**: 1-228.
- Houde, E. D. (1997). "Patterns and trends in larval-stage growth and mortality of teleost fish." *Journal of Fish Biology* **51**: 52-83.
- Houde, E. D. (2002). Mortality. *Fishery Science. The 268 Unique Contributions of Early Life Stages*. L. A. Fuiman, Werner, R.G. (Eds.), Blackwell Publishing, Oxford: 64-87.
- Houde, E. D. (2008). "Emerging from Hjort's Shadow." *J. Northw. Atl. Fish. Sci* **41**: 53-70.
- Huang, A. T., K. Alter, P. Polte and M. A. Peck (2022). "Disentangling seasonal from maternal effects on egg characteristics in western Baltic spring-spawning herring *Clupea harengus*." *Journal of Fish Biology* **n/a**(n/a).
- Huebert, K. B., J. Pätsch, M. Hufnagl, M. Kreuz and M. A. Peck (2018). "Modeled larval fish prey fields and growth rates help predict recruitment success of cod and anchovy in the North Sea." *Marine Ecology Progress Series* **600**: 111-126.
- Huebert, K. B. and M. A. Peck (2014). "A Day in the Life of Fish Larvae: Modeling Foraging and Growth Using Quirks." *PLoS ONE* **9**(6): e98205.
- Hufnagl, M. and M. A. Peck (2011). "Physiological individual-based modelling of larval Atlantic herring (*Clupea harengus*) foraging and growth: insights on climate-driven life-history scheduling." *ICES Journal of Marine Science* **68**(6): 1170-1188.
- Hufnagl, M., M. A. Peck, R. D. M. Nash and M. Dickey-Collas (2015). "Unravelling the Gordian knot! Key processes impacting overwintering larval survival and growth: A North Sea herring case study." *Progress in Oceanography* **138, Part B**: 486-503.
- ICES (2005). Spawning and life history information for North Atlantic cod stocks. ICES Cooperative Research Report. K. M. E. Brander. ICES, Copenhagen: 152
- Illing, B., M. Moyano, J. Berg, M. Hufnagl and M. A. Peck (2018). "Behavioral and physiological responses to prey match-mismatch in larval herring." *Estuarine, Coastal and Shelf Science* **201**: 82-94.
- Johannessen, A., G. Blom and A. Folkvord (2000). "Differences in growth pattern between spring and autumn spawned herring (*Clupea harengus* L.) larvae." *Sarsia* **85**(5-6): 461-466.
- Kjørboe, T., P. Munk and K. Richardson (1987). "Respiration and growth of larval herring *Clupea harengus*: Relation between specific dynamic action and growth efficiency." *Marine Ecology-progress Series - MAR ECOL-PROGR SER* **40**: 1-10.

Kjørboe, T., P. Munk, K. Richardson, V. Christensen and H. Paulsen (1988). "Plankton dynamics and larval herring growth, drift and survival in a frontal area." *Marine Ecology-progress Series - MAR ECOL-PROGR SER* **44**: 205-219.

Kühn, W., M. A. Peck, H.-H. Hinrichsen, U. Daewel, A. Moll, T. Pohlmann, C. Stegert and S. Tamm (2008). "Defining habitats suitable for larval fish in the German Bight (southern North Sea): An IBM approach using spatially- and temporally-resolved, size-structured prey fields." *Journal of Marine Systems* **74**(1): 329-342.

Last, J. M. (1978). "The food of four species of pleuronectiform larvae in the eastern English Channel and southern North Sea." *Marine Biology* **45**(4): 359-368.

Llopiz, J. and R. Cowen (2009). "Variability in the trophic role of coral reef fish larvae in the oceanic plankton." *Marine Ecology-progress Series - MAR ECOL-PROGR SER* **381**: 259-272.

Llopiz, J. K., D. E. Richardson, A. Shiroza, S. L. Smith and R. K. Cowen (2010). "Distinctions in the diets and distributions of larval tunas and the important role of appendicularians." *Limnology and Oceanography* **55**(3): 983-996.

Lough, R. G. and E. A. Broughton (2006). "Development of micro-scale frequency distributions of plankton for inclusion in foraging models of larval fish, results from a Video Plankton Recorder." *Journal of Plankton Research* **29**(1): 7-17.

Maar, M., A. Rindorf, E. F. Møller, A. Christensen, K. S. Madsen and M. van Deurs (2014). "Zooplankton mortality in 3D ecosystem modelling considering variable spatial-temporal fish consumptions in the North Sea." *Progress in Oceanography* **124**(0): 78-91.

Moyano, M., B. Illing, L. Christiansen and M. A. Peck (2018). "Linking rates of metabolism and growth in marine fish larvae." *Marine Biology* **165**(1): 5.

Nash, R. D. M. and M. Dickey-Collas (2005). "The influence of life history dynamics and environment on the determination of year class strength in North Sea herring (*Clupea harengus* L.)." *Fisheries Oceanography* **14**(4): 279-291.

Nash, R. D. M., M. Dickey-Collas and S. P. Milligan (1998). "Descriptions of the Gulf VH/PRO-NET and MAFF/Guildline unencased high-speed plankton samplers." *Journal of Plankton Research* **20**(10): 1915-1926.

Orenstein, E. C., S.-D. Ayata, F. Maps, É. C. Becker, F. Benedetti, T. Biard, T. de Garidel-Thoron, J. S. Ellen, F. Ferrario, S. L. C. Giering, T. Guy-Haim, L. Hoebeke, M. H. Iversen, T. Kjørboe, J.-F. Lalonde, A. Lana, M. Laviale, F. Lombard, T. Lorimer, S. Martini, A. Meyer, K. O. Möller, B. Niehoff, M. D. Ohman, C. Pradaliere, J.-B. Romagnan, S.-M. Schröder, V. Sonnet, H. M. Sosik, L. S. Stemmann, M. Stock, T. Terbiyik-Kurt, N. Valcárcel-Pérez, L. Vilgrain, G. Wacquet, A. M. Waite and J.-O. Irisson (2022). "Machine learning techniques to characterize functional traits of plankton from image data." *Limnology and Oceanography* **67**(8): 1647-1669.

Ottmann, D., Ø. Fiksen, M. Martín, F. Alemany, L. Prieto, D. Álvarez-Berastegui and P. Reglero (2021). "Spawning site distribution of a bluefin tuna reduces jellyfish predation on early life stages." *Limnology and Oceanography* **66**(10): 3669-3681.

Payne, M., S. Ross, L. Worsøe Clausen, P. Munk, H. Mosegaard and R. D. M. Nash (2013). "Recruitment decline in North Sea herring is accompanied by reduced larval growth rates." *Marine Ecology Progress Series* **489**: 197-211.

Payne, M. R., E. M. C. Hatfield, M. Dickey-Collas, T. Falkenhaus, A. Gallego, J. Gröger, P. Licandro, M. Llope, P. Munk, C. Röckmann, J. O. Schmidt and R. D. M. Nash (2009). "Recruitment in a changing environment: the 2000s North Sea herring recruitment failure." *ICES Journal of Marine Science: Journal du Conseil* **66**(2): 272-277.

Peck, M. A., K. B. Huebert and J. K. Llopiz (2012). "Intrinsic and extrinsic factors driving match-mismatch dynamics during the early life history of marine fishes." *Advances in Ecological Research* **47**: 177-302.

Peck, M. A. and M. Hufnagl (2012). "Can IBMs tell us why most larvae die in the sea? Model sensitivities and scenarios reveal research needs." *Journal of Marine Systems* **93**(0): 77-93.

58 Peck, M. A., P. Kanstinger, L. Holste and M. Martin (2012). "Thermal windows supporting survival of the earliest life stages of Baltic herring (*Clupea harengus*)." *ICES Journal of Marine Science* **69**(4): 529-536.

Pedersen, B. H. (1993). "Growth and mortality in young larval herring (*Clupea harengus*); effects of repetitive changes in food availability." *Marine Biology* **117**(4): 547-550.

Pepin, P. and R. Penney (2000). "Feeding by a larval fish community: Impact on zooplankton." *Marine Ecology Progress Series* **204**: 199-212.

Pepin, P. and R. W. Penney (1997). "Patterns of prey size and taxonomic composition in larval fish: are there general size-dependent models?" *Journal of Fish Biology* **51**(sA): 84-100.

Pepin, P., D. Robert, C. Bouchard, J. F. Dower, M. Falardeau, L. Fortier, G. P. Jenkins, V. Leclerc, K. Levesque, J. K. Llopiz, M. G. Meekan, H. M. Murphy, M. Ringuette, P. Sirois and S. Sponaugle (2015). "Once upon a larva: revisiting the relationship between feeding success and growth in fish larvae." *ICES Journal of Marine Science* **72**(2): 359-373.

Petrik, C. M., R. Ji and C. S. Davis (2014). "Interannual differences in larval haddock survival: hypothesis testing with a 3D biophysical model of Georges Bank." *Fisheries Oceanography* **23**(6): 521-553.

Pitchford, W. J. and J. Brindley (2001). "Prey Patchiness, Predator Survival and Fish Recruitment." *Bulletin of Mathematical Biology* **63**(3): 527-546.

- Robert, D., H. M. Murphy, G. P. Jenkins and L. Fortier (2014). "Poor taxonomical knowledge of larval fish prey preference is impeding our ability to assess the existence of a "critical period" driving year-class strength." *ICES Journal of Marine Science: Journal du Conseil* **71**(8): 2042-2052.
- Robinson, K. L., S. Sponaugle, J. Y. Luo, M. R. Gleiber and R. K. Cowen (2021). "Big or small, patchy all: Resolution of marine plankton patch structure at micro- to submesoscales for 36 taxa." *Science Advances* **7**(47): eabk2904.
- Schmidt, J., C. van Damme, C. Röckmann and M. Dickey-Collas (2009). "Recolonisation of spawning grounds in a recovering fish stock: Recent changes in North Sea herring." *SCIENTIA MARINA* **73**: 153-157.
- Schrum, C., J. Lowe, H. E. M. Meier, I. Grabemann, J. Holt, M. Mathis, T. Pohlmann, M. D. Skogen, A. Sterl and S. Wakelin (2016). *Projected Change—North Sea. North Sea Region Climate Change Assessment*. M. Quante and F. Colijn. Cham, Springer International Publishing: 175-217.
- Sheldon, R. W., A. Prakash and W. H. Sutcliffe Jr. (1972). "The size distribution of particles in the ocean." *Limnology and Oceanography* **17**(3): 327-340.
- Sswat, M., M. H. Stiasny, J. Taucher, M. Algueró-Muñiz, L. T. Bach, F. Jutfelt, U. Riebesell and C. Clemmesen (2018). "Food web changes under ocean acidification promote herring larvae survival." *Nature Ecology & Evolution* **2**(5): 836-840.
- Stige, L. C., L. A. Rogers, A. B. Neuheimer, M. E. Hunsicker, N. A. Yaragina, G. Ottersen, L. Ciannelli, Ø. Langangen and J. M. Durant (2019). "Density- and size-dependent mortality in fish early life stages." *Fish and Fisheries* **20**(5): 962-976.
- Suthers, I. M., Z. White, C. Hinchliffe, D. S. Falster, A. J. Richardson and J. D. Everett (2022). "The Mortality/Growth ratio of larval fish and the slope of the zooplankton size-spectrum." *Fish and Fisheries* **23**(3): 750-757.
- Urtizberea, A. and Ø. Fiksen (2013). "Effects of prey size structure and turbulence on feeding and growth of anchovy larvae." *Environmental Biology of Fishes* **96**(9): 1045-1063.
- van Damme, C., M. Dickey-Collas, A. Rijnsdorp and O. Kjesbu (2009). "Fecundity, atresia, and spawning strategies of Atlantic herring (*Clupea harengus*)." *Canadian Journal of Fisheries and Aquatic Sciences* **66**: 2130-2141.
- van Damme, C. J. G., M. R. Dickey-Collas, Adriaan D. and O. S. Kjesbu (2009). "Fecundity, atresia, and spawning strategies of Atlantic herring (*Clupea harengus*)." *Canadian Journal of Fisheries and Aquatic Sciences* **66**(12): 2130-2141.
- Wilson, C. J., H. M. Murphy, C. Bourne, P. Pepin and D. Robert (2018). "Feeding ecology of autumn-spawned Atlantic herring (*Clupea harengus*) larvae in Trinity Bay, Newfoundland: Is recruitment linked to main prey availability?" *Journal of Plankton Research* **40**(3): 255-268.

Woodson, C. B. and M. A. McManus (2007). "Foraging behavior can influence dispersal of marine organisms." *Limnology and Oceanography* **52**(6): 2701-2709

General Discussion



Drawings by Justine Courboulès

The lack of knowledge about plankton dynamics and environmental drivers in the North Sea limits our understanding of long-term trends in biomass and biodiversity in the region. Previous studies from various parts of the North Sea may provide some insight into long-term changes of key species and functional groups (e.g. Widdicombe et al. 2010, Löder et al. 2011, Bresnan et al. 2015). However, the North Sea is highly heterogeneous and changes observed in other areas may not always be consistent or may even contradict those reported (Capuzzo et al. 2015, 2018) and, therefore extrapolations should be done with caution. Additionally, few datasets include the small size fractions of the plankton community hampering our full understanding of plankton dynamics at large spatial and temporal scales.

In my thesis, we conducted a comprehensive assessment of plankton dynamics in the North Sea during times of low productivity, covering the entire region and two main spawning grounds of herring. Through this thesis, we generated a unique dataset that provided more accurate mesozoo-, novel microzoo-, and PZP estimates. By analyzing and comparing the prey fields of the two spawning grounds and seasons in the North Sea in Chapter 3, we demonstrated the impact of prey availability and size on larval condition and growth, emphasizing the importance of PZP for herring larvae, especially in Downs, as discussed in Chapter 4. This study adds to our understanding of plankton dynamics during the winter, their interactions with the environment, and their potential impact on overwinter growth and survival of larval herring and, therefore, recruitment dynamics. In this general discussion, I will synthesize the findings of the different chapters, expand on topics that go beyond the scope of each individual chapter, explore broader implications, and suggest future perspectives.

The plankton community in winter

The results reported in this thesis show that the plankton standing stock biomass in the North Sea, during winter, ranged between 4.7 and 23.8 and between 21.4 and 195.6 $\mu\text{g C m}^{-3}$ for the MZP and MesoZP communities, respectively. This is a critical ecological information, since the plankton stocks surviving the winter are the baseline for the plankton succession in spring and determine the stock of secondary production (Sommer et al. 2007). Moreover, based on the winter stock data as provided by this thesis, the production rate of the plankton biomass can be estimated and predictions that are more reliable can be made. Changes in primary production can be driven by various factors including nutrient and light availability, temperature, and grazing (Cadée & Hegeman 2002, Behrenfeld et al. 2006, Cloern et al. 2014) with a cascading effect on higher trophic levels, especially during times of low productivity and biomass (Sommer et al. 2007). Due to a lack of reliable data of plankton standing stocks at the lower trophic levels, it is still unclear whether the recent marked temperature increase during winter can influence the long-term local and broad scale system productivity and which other drivers are important. Ultimately, this might have important implications since this productivity

can have drastic effects on the secondary production, for instance nauplii, which are an important component of the winter zooplankton community and a critical food source for herring larvae (main biomass source, even in generalist scenario) (chapter 4).

During times of low productivity, the microbial loop is mainly responsible for carbon cycling and energy transfer towards higher trophic levels (Levinsen & Nielsen 2002). The observed dominance of small taxa such as *Heterocapsa* spp. in winter (Chapter 1), which is known to increase its bacterial ingestion rate during the times of low irradiation (Millette et al. 2017), is a strong indicator of an enhanced microbial activity and energy transfer during this time of the year. Furthermore, the here reported higher nauplii abundance compared to other studies (www-wgze.net) (Chapter 3,4) underlines the strength and importance of the microbial loop in winter, since they primarily feed on heterotrophic protists, rather than on phytoplankton (Turner 2004). Indeed, higher biomass of nauplii were observed in the southern German Bight than in the English Channel, which coincided with the peak of abundance of Ciliates and partially of dinoflagellates (Chapter 1 and 3). However, the structure of microbial food webs was found to be significantly altered by changing inter-annual climatic conditions, which can be induced by climate change. Warming in general was found to promote the relationships among smaller groups, taxa or species, while diminishing the role of large phytoplankton and ciliates which may result in a potential alteration of energy circulation through the microbial food web (Trombetta et al. 2020).

Differences in PZP community composition were typically reported at smaller spatial scales (Montagnes & Lessard 1999), where different water masses congregate (Yang et al. 2021). Here we report a slight shift in the community composition nearby the transition zone between the North Sea and the Atlantic Ocean both in the northern (through the Orkney-Shetland passage) and southern (English Channel) areas. When combining MZP and MesoZP data, we confirmed the previously indicated community change and found a clear transition in community composition along classical water mass characteristics such as temperature and salinity in the Buchan/Banks and Downs areas. This community shift along clear environmental drivers was not shown in the PZP community only. This indicates that relying solely on the highly variable PZP dynamics will make it hard to distinguish between large-scale processes and locally induced variability patterns.

Plankton dynamics and fisheries

When the lower trophic levels control the abundance and productivity of higher trophic levels, the system is bottom up controlled. Bottom up control can be seasonal or initiated by the effect of environmental stressors (Lynam et al. 2017). In shelf seas, such as the North Sea, variability in zooplankton production was found to exert a pronounced bottom up effect on fish production

(Heath 2005). Under ongoing climate change, the bottom up effect, especially on planktivory fish such as Herring may be more distinct as they react directly on changes in plankton production (Lynam et al. 2017). On early life stages of fish, the bottom up effect is more pronounced during first feeding, when fish larvae require a sufficient amount of prey in terms of abundance and size (“critical period”, Hjort 1914) and the amount of prey needed is expected to increase under climate change as a response to increasing temperatures (chapter 4). Investigation of the factors that affect feeding success during the larval stage is, thus, an essential research area that assists in our understanding of the recruitment variability among marine fish populations (Hjort 1914, Hunter 1980, Houde 2008). In chapter 4, we investigated the feeding conditions of herring larvae in their spawning grounds and found significant differences in the feeding conditions, which I will discuss in the following.

In Buchan/Banks, the in situ prey field was not adequate to support the growth of larvae < 10 mm in length, whereas bigger larvae were able to reach their maximal temperature-dependent growth capacity due to a sufficient amount of larger prey. These differences in growth potential between larval sizes is linked to the mouth gape of larvae, which limits their prey spectra. Therefore, smaller larvae are more dependent on smaller prey like PZP, while larger larvae are able to feed on larger mesozooplankton, if sufficiently available. Indeed, here I show that the plankton community in this area was composed by higher relative abundances of larger zooplankton, expressed by the less negative slopes of the community size spectra, with relatively high contribution of larger mesozooplankton taxa as also reflected as positive scores by the RDA (Chapter 3).

In the Downs compartment, larvae experienced higher and longer starvation-probability at all sizes (from 6 to 26 mm). However, the main limitation here appears to be food availability, since this system is biomass-restricted to sustain growth. This contrast with Buchan/Banks area where larvae seem to be more impacted by the community composition and size structure than by limited availability of prey items as larger larvae were not at risk to starvation. Indeed, the overall biomass of zooplankton in Downs was lower than in Buchan/Banks (Chapter 3), and composed by lower relative abundance of small prey organisms, expressed by the steeper size spectra slopes (Chapter 3). However, in both spawning grounds and seasons, larvae showed better growth performance when MZP was included in their diet (chapter 4), which agrees with previous studies that suggested that Downs’s larvae might rely more on PZP than MZP (Denis et al. 2016, Bils et al. 2022). Hence, despite the appropriate size community structure to support the larval growth in Downs, the lower zooplanktonic biomass appeared to be a crucial factor affecting the growth and survival of herring larvae and thus their recruitment. However, we cannot exclude the likely methodological bias affecting these results. Indeed, the underrepresentation of PZP in Downs may be attributed to the use of formalin as a fixation

method to obtain biomass for the models. In Chapter 1, ciliates were found to be abundant in the English Channel, with lugol preserved samples showing over 600 individuals, compared to only 0.18 individuals per liter in Chapter 3. This disparity may have influenced the predicted food limitation in the English Channel. The theory of the "critical period" (Hjort 1914) suggests that the first feeding larvae are the most susceptible to food limitation. Our findings, however, indicate that larval survival in Downs is not confined to a single critical period, but rather, their elevated vulnerability to starvation persists throughout larval development. This could have significant implications since, even if PZP is underestimated due to the fixation method, the absence of larger prey will affect the larvae at later stages when their metabolic demands increase. Although food limitation for herring larvae in the Downs spawning ground has been demonstrated, previous research has indicated that the proportion of newly hatched larvae from Downs contributing to the total larvae has been increasing since the 1990s (Schmidt et al. 2009). The observation may suggest that the Downs larvae are drifting into the southern North Sea early enough, where they might be able to find more favorable food conditions during later developmental stages.

The North Sea is home to a diverse array of marine organisms besides Herring (*Clupea harengus*) that are economically and culturally important to the region, such as Plaice (*Pleuronectes platessa*) or Cod (*Gadus morhua*). Plankton, as the base of the marine food web, plays a crucial role in supporting these organisms. Examine how plankton populations change during the winter is needed to predict food availability and recruitment patterns, not only for winter spawners, which in turn is important for managing and conserving fish populations in general. The dependence of fish production on plankton production is evident as highest fisheries production overlaps with seasons and areas of highest plankton production (e.g. (Nielsen & Richardson 1989, Heath 2005). Hufnagl et al. (2015) suggested a combination of field, laboratory and field studies to successfully unravel the key processes of fish recruitment. Including in situ prey fields of simultaneously sampled herring larvae into a bioenergetics model revealed some important patterns but given the number of processes affecting recruitment, there is a need to develop end-to-end models including physical and biochemical changes, nutrient dynamics, primary and secondary production (Brander 2010, Pörtner et al. 2014) to make reliable predictions on marine production, including fish. Therefore, to better manage fish stocks, there is a need for a general understanding of baseline processes such as seasonal effect on the phytoplankton-zooplankton dynamics.

Environmental drivers of plankton dynamics and possible scenarios under climate change

Although we could not find a clear link between distribution pattern and the environment of the PZP community, growth and reproduction of zooplankton is generally highly temperature sensitive (Mauchline 1998). With their short generation times, biomass and community structure is often tightly coupled with climate and environmental stresses (Hays et al. 2005, Chiba et al. 2018). Due to this fact, they are minimally effected by multi-year carryover effect such as higher trophic levels (e.g. fish) meaning that their population size closely tracks seasonal-to inter-annual environmental condition changes (Mackas & Beaugrand 2010). Ongoing ocean warming impacts seasonal cycles and inter-annual trends in the ocean. These impacts are best measureable in the smaller than the larger organism. While climate change is often discussed on a global scale, some regions are experiencing higher impact rates and more local extreme events than the whole planet, such as the North Sea (Quante & Colijn 2016).

Linking the prominence of the microbial loop during these times with the climate related changes over the past two centuries; we can assume that PZP will have a more significant impact in a warmer future (Aberle et al. 2007). This is due to several reasons: 1) an increase in sea temperature will result in higher growth rates for PZP, 2) more stratified waters will enhance the rate at which PZP encounter their prey, and 3) a reduction in phytoplankton cell size is expected, which will be favorable for PZP as they are adapted to consuming smaller cells. In this manner, more energy will flow through a thriving PZP community, rather than sinking to deeper waters or being directed straight to larger metazoan grazers like small copepods (Caron & Hutchins 2013). As phytoplankton size becomes biased towards smaller cells, PZP will serve as an important link in the trophic chain between small-sized phytoplankton and metazoans (Figueiredo et al. 2009). These changes may lead to an increased recycling of nutrients in the pelagic. The general temperature increase is accelerating heterotrophic processes faster, which may cause a mismatch between predator and prey with significant impacts on the whole ecosystem stability and its season-adapted processes (Wiltshire & Manly 2004).

We showed that under ongoing climate change, the minimum biomass needs for larval herring will increase in both spawning grounds, but more distinct in Downs (+35%), where current feeding conditions already do not supply efficient growth (Chapter 4). With the observed increase in abundance and the predicted increase in the face of climate change in the North Sea during winter, it may be beneficial for the smaller herring larvae, potentially improving their nutrition and survival. On the other hand, the consequences for larger herring larvae that have

to rely on small food due to the higher abundance of very small organisms may include slower growth rates and reduced survival. While small organisms such as PZP can still provide nutrition, larger larvae require more energy and larger prey to sustain their growth and development. If their diet is limited to small food, it may not provide enough energy for them to grow, especially if increased temperatures during winter leads to increased metabolic demands, which could ultimately affect their survival at later development stages.

To address the impacts of ongoing climate change, it is important to focus on organisms and seasons that are more prone to changes, starting at the bottom of the food web (Kreyling et al. 2019). However, distinguishing natural variability, especially in small planktonic organisms, is a challenging task, and fragmented studies make it even more difficult. The same drivers affecting seasonal growth and production, such as temperature and nutrients, may cause local-induced and inter-annual variation, resulting in a carryover effect on different temporal scales (into the following year, season, trophic level, etc.). Extreme events can also severely influence year-year plankton biomass and abundance on both local and broader scales. Short or incomplete time series have the issue that unusual years, even delayed due to carryover effects, can have a large and flawed impact on the observed trends (Widdicombe et al. 2010), making it difficult to separate cyclical and non-cyclical, locally induced, seasonal, and inter-annual variations. To reduce the local effect of variations and incorporate short datasets in large time series with different resolutions to match broad scale patterns, Scott et al. (2023) suggest changing the spatial resolution to mask small spatial changes and emphasize large-scale patterns, or vice versa. Currently, there is a general lack of understanding of multi-driver impacts in the face of climate change, with the impact of single drivers being studied more intensively (Richardson 2009). An integrative approach, combining the study of individual and simultaneous factors along with different organizational levels (individual, population, and community), should be the aimed approach, which will be discussed below.

Ecosystem approach and bioindicators

The North Sea, as well as other European seas, has and is undergoing significant ecosystem changes in recent decades (Beaugrand 2004, Alheit et al. 2005). Given that these transformations have occurred across all trophic levels (Beaugrand et al. 2003, Alvarez-Fernandez et al. 2012), the goal of fisheries management has been to apply an ecosystem-based approach (Folke et al. 2004). Assessing the states of ecosystems and projecting their future under different scenarios has become a critical requirement for ecosystem management (Jørgensen 2002).

However, the most comprehensive approach to understand larval growth and survival related to zooplankton biomass and size structure over time and space, is the combination of modeling

and field measurements, as noted by Hufnagl et al. (2015). Using individual-based physiological models, such as in Chapter 4 of this thesis, can be an effective way to study larval growth and variation when food is limited. The generated size spectra slopes based on the plankton data was used to improve an IBM for growth and survival of early life stages of herring. With this parameterization, the IBM indicated food-limited areas for the different larval size classes in the respective spawning areas. By adding taxonomic information to the approach, we revealed the influence of the general community composition on zooplankton biomass, particularly the lack of larger, biomass-rich prey items such as nauplii. The approach used in this study, is based on broad taxonomic sorting, which has advantages such as the exclusion of non-prey organisms before generating the size spectra. It also allows for more realistic predator-prey interactions and the calculation of species-averaged predator: prey-mass ratios (PPMR). For instance, the abundance of chaetognatha in some areas may also indicate processes such as predation on larvae and food competition. In that sense, the traditional size spectra approach has its limitations, as it is based on the assumption that larger organisms feed on smaller ones and would not reveal predator-prey interactions between taxa of similar sizes. Thus, a certain amount of taxonomic identification is necessary.

Long and broad-scale data on winter plankton dynamics will be helpful to improve these kind of models by providing baseline information on the availability and dynamics of prey for fish during the winter, which can help predict the carrying capacity of the ecosystem and the carrying capacity of fish populations. The data presented here can be also used to improve ecosystem model estimates. Ecosystem models are able to predict interactions between different components of an ecosystem, such as plankton, fish, and other organisms as well as abiotic parameters. Data on winter plankton dynamics is needed to parameterize and validate these models, allowing to better understand the functioning of the North Sea ecosystem and predict how it may respond to changes in the future (for a review see Moll & Radach 2003). Pollution models, which are used to predict how pollutants such as agricultural related nutrients move through the environment and how they will affect different organisms will also profit from knowledge on winter plankton dynamics (e.g. James 2002). Ultimately, climate change models can be also parameterized to improve the accuracy by providing estimates on how plankton populations are likely to respond to changes in temperature, precipitation, and other environmental factors (see Schrum et al. 2016). In summary, data on winter plankton dynamics can be useful for numerous modelling approaches by providing important information on how the ecosystem, climate and fish populations respond to the changes in the environment and pollutants. It allows to have a better understanding of the functioning of the ecosystem and to predict how it may be impacted by the future changes, which can help inform management decisions and policy-making.

Nevertheless, monitoring all trophic levels is a complicated and time-consuming task. Therefore, a major research objective has been to identify suitable environmental indicators for assessing the "good environmental state" which are straightforward to monitor and are responsive to changes in the ecosystem (Rees et al. 2008). The "good environmental state" (GES) is a term used in marine management to describe the ideal condition of a marine ecosystem. It is a benchmark against which the status of an ecosystem can be measured, and is defined as the environmental status that would be achieved if pressures on the marine environment were reduced to levels that enable the ecosystem to function in a healthy and sustainable way (Dickey-Collas et al. 2017). In the process of monitoring changes in the state of ecosystems and trophic relationships, the use of bioindicators is an essential tool. To observe changes in the good environmental status of the world's oceans, for example, as a result of climate change and overfishing, bioindicators are needed that can rapidly detect change, are easy to apply, and simple to monitor.

PZP is often considered as indicator for conservation purposes (e.g. Bils et al. 2019). However, observing changes in the PZP community requires extensive effort and highly skilled observers who can differentiate between plankton species and the difficulties in preservation such as the loss of organisms due to inappropriate preservation or shelf life of the samples remain. Moreover, the quick reaction time of PZP may be more obstructive than expedient. Ciliates for instance, may respond rigorous to small-scale, local changes rather than to broad scale changes. These quick responses makes it hard to discern between cyclical variability of several factors, the local conditions, the communities natural variability due to other factors such as production or predation. Therefore, using only PZP as bioindicators would require certain data prerequisites, including an appropriate length and spatial scale of the data. In summary, although the PZP community has some valuable characteristics to serve as bioindicators, a more holistic approach across a broader size range of plankton offers more reliable and robust results reflecting impacts of both, local- and broad- as well as short- and long-term changes. Difficulties with sampling, preservation and the challenging nature of processing the data may be one of the contributing factors to the scarcity of these holistic approaches.

Plankton sampling and Methodologies

There is a general underrepresentation of small taxa in plankton studies due to the traditional use of nets $>200\ \mu\text{m}$ which causes underestimations of zooplankton abundances and biomass and subsequently hinders the understanding of ecosystem processes, especially when studying times of low productivity. The presented method of combining different meshed nets offers a better enumeration and catchability, although no plankton sampling system is able to provide true estimates of abundance for the different plankton components equally (Owens et al. 2013). With the here presented dataset we improved the estimation of Mesozooplankton

abundance and biomass and also provided inexistent estimates of broad scale Microzooplankton community abundance and biomass in the autumn and winter. Although we cannot assume that the estimates are complete, it can be used as a baseline. Baseline estimates about the general primary production in the North Sea, are scarce due to two main factors. First, traditional methods of measuring primary production is time and labor extensive and second, satellite remote sensing data, which became a valuable tool to obtain insight in spatial and temporal patterns of primary production, particularly at the global scale (see Westberry et al. 2008) is limited due to the thick cloud cover during winter time. This lack of data for the low productive season results in poor model estimates, already at the baseline. This might help to explain the discrepancy between zooplankton model results and field samples (Everett et al. 2017).

The presented DOC pipeline (Chapter 2) demonstrates that continuous adaptation is necessary and significantly enhances classification performance compared to limited or no adaptation. Despite working with abundant and diverse taxonomic plankton groups, the pipeline maintained high performance levels in the face of changes of the plankton community, making it a useful tool for research questions that focus on broad groups for instance. Our DOC is a powerful tool for adapting a classifier model to work with plankton communities that change over space and time, and offers high accuracy, adaptability, versatility, and ease of use. The pipeline's user-friendly interface also makes it accessible to non-experts.

The development of plankton image classification systems has been strongly influenced by the desire to reduce sampling processing times. Plankton imaging can be broadly divided into two parts, the imaging of preserved samples (e.g. FlowCAM, ZooSCAN) and the in-situ imaging (e.g. VPR, ROV). The imaging of physical samples has the advantage that imaging can be an additional tool next to other analysis techniques (e.g. biochemical or molecular analysis) and the results of the imaging can be physically checked. However, the time-consuming sampling device application, the addressed problems in preserving samples and the delay in sample processing (unless the device is applicable on board) remains. *In situ* plankton devices have the advantage that sample preservation and storage problems disappear. However, with *in situ* devices, no physical evidence rather than the stored image exists and the main limitations are the limits in resolution or orientation of the imaged particle. Distinct morphological features may not be visible. These devices are usually costly due to a proper camera to ensure a certain image quality and the size limitations of the imaged organisms are usually narrow due to focus depth (for a comprehensive review see Lombard et al. 2019). More recent devices focus on the application via the survey ships clean water inlets. This ensures a condition independent and unlimited application on the entire survey area and time (e.g. Plankton Image Analyser (PI); Scott et al. 2021). The main limitations here are mainly the fixed sampling depth, the loss

of delicate organisms through the pumping process and the collection rate and subsequent storage of the data. Whichever device used, the combination of imaging devices (e.g. PI, Zooscan, FlowCAM) and machine learning techniques (e.g. ZooProcess, Plankton Identifier, EcoTaxa) to identify and classify different types of plankton based on digital images changed the game. These tools are designed to support and accelerate the analysis process as the number of samples taken, physically or digital, supersedes their processing. They are trained using a dataset of labeled/ human-identified plankton images, and can then be used to automatically identify and classify new plankton images. The disadvantage of such automated classifier algorithms is the essential precondition of a labelled training set.

Outlook

The growing threat of anthropogenic impacts, such as overfishing, pollution, and climate change highlight the urgent need for a deeper understanding of the marine ecosystems. Only by enhancing our knowledge of ecosystem functioning, we can develop effective strategies to mitigate the detrimental effects of human activities on marine habitats, and ensure their preservation for future generations. The primary findings of my thesis underscore the urgent requirement for detailed and extensive short- and long-term spatially-resolved data on the abundance and biomass of PZP, MZP and MesoZP as well as their specific and broad-scale dynamics. These estimates are critical for developing precise models of, for instance, energy transfer and nutrient recycling in marine ecosystems, given their crucial role as a key component of the carbon cycle. The number of steps involved in energy transfer determines the amount of carbon/energy that is available for fish and their offspring, therefore affecting recruitment dynamics. This essential aspect must be taken into account when making decisions related to the management of marine ecosystems.

The future of plankton sampling will involve continued advancements in sampling devices and techniques, with a focus on improving efficiency, accuracy, and applicability. Automation is becoming increasingly common in the form of autonomous underwater vehicles (AUVs), which can collect large amounts of data quickly and accurately, even in harsh or inaccessible environments (e.g. EXOCETUS, Harvey & Ryan 2012). Advances in DNA sequencing technologies are also allowing researchers to analyze plankton samples more thoroughly and accurately than ever before, providing a detailed picture of the diversity and abundance of plankton populations and identifying changes in community structure over time (Sildever et al. 2021). Satellite-based remote sensing is already and will continue to provide valuable information on the distribution and abundance of phytoplankton populations over large spatial scales, which can help to identify areas of high biological productivity and environmental stress. To achieve a more comprehensive picture of plankton populations and their ecology, multiple sampling techniques are increasingly being integrated, such as the combination of net tows,

optical plankton counters, and high-throughput sequencing. The integration of data from multiple sources will help to overcome the limitations of individual sampling techniques and improve our understanding of plankton dynamics. Overall, the future of plankton sampling will continue to focus on technological innovation and the integration of multiple sampling techniques, which will provide a more detailed and accurate understanding of the ecology and dynamics of plankton populations in the ocean.

As the volume of data from plankton samples continues to increase, the need for efficient and accurate plankton classification technology becomes ever more pressing. While traditional methods rely on manual identification and counting, these approaches are time-consuming and require highly trained personnel. The development of user-friendly AI-based classification technologies has the potential to revolutionize the way we analyze plankton data. By leveraging deep learning algorithms, AI-based systems can rapidly and accurately classify plankton species from digital images, reducing the need for manual identification and allowing for the processing of large amounts of data in a fraction of the time. Furthermore, user-friendly interfaces such as the DOC (Chapter 3) can enable even non-experts to use these technologies, making them accessible to a wider range of researchers. Overall, the development of user-friendly AI-based plankton classification technology is essential for improving our ability to promptly process the vast amounts of data produced in order to monitor and understand plankton dynamics, which are critical for predicting and managing the health of marine ecosystems.

This thesis has contributed significantly to our understanding of the plankton dynamics in the North Sea during the low productive seasons and its potential impact on the growth and survival of herring larvae. However, there are still uncertainties and knowledge gaps that require further research. First, the complexity of the link between MZP and MesoZP goes beyond the information that can be derived from size spectra approaches, and the predator-prey interactions are generally not well understood. As a result, studying these interactions directly in the field is a challenging task. In addition, the potential consequences of an enhanced microbial loop on higher trophic levels and the costs associated with the extra step in energy transfer efficiency remain to be investigated across multiple trophic levels. Although this thesis has shed light on the optimal prey size for different larval sizes, it is still unclear what costs feeding on suboptimal prey has on larval growth, metabolism, and condition at different temperatures. Understanding the costs of feeding on suboptimal prey for larval fish, including the reduction in growth and condition, and the underlying physiological changes such as metabolism and activity, will improve our knowledge of food limitation in the field during a critical life stage for many species. Additionally, this information may help predict how fish larvae can cope with the change towards smaller prey species due to climate change.

Researching the uncertainties and knowledge gaps mentioned above is not an easy task. Mesocosm experiments provide a promising opportunity to study the intricate interactions between MZP, MesoZP, and higher trophic levels in semi *in-situ* conditions. Additionally, innovative in situ observational techniques can be applied within mesocosms to advance our understanding of plankton dynamics. Hence, it is imperative to conduct further research on predator-prey interactions, including the abiotic effects with the help of mesocosms and novel observational techniques, to develop effective ecosystem-based management strategies for sustainable fisheries in the North Sea.

In conclusion, to improve the accuracy of modeling methods and advance ecosystem-based management in fisheries, there is an urgent need for a more comprehensive and widespread dataset of a broader range of plankton components. Therefore, the continuation of the here established time series of abundance, biomass, distribution, and size composition of the broad plankton community throughout the winter season is crucial. The ongoing collection of this data will be critical in gaining a comprehensive understanding of the North Sea ecosystem over time, promoting the sustainable use of its natural resources.

References

- Aberle N, Lengfellner K, Sommer U (2007) Spring bloom succession, grazing impact and herbivore selectivity of ciliate communities in response to winter warming. *Oecologia* 150:668–681.
- Alheit J, Möllmann C, Dutz J, Kornilovs G, Loewe P, Mohrholz V, Wasmund N (2005) Synchronous ecological regime shifts in the central Baltic and the North Sea in the late 1980s. *ICES J Mar Sci* 62:1205–1215.
- Alvarez-Fernandez S, Lindeboom H, Meesters E (2012) Temporal changes in plankton of the North Sea: Community shifts and environmental drivers. *Mar Ecol Prog Ser* 462:21–38.
- Beaugrand G (2004) The North Sea regime shift: Evidence, causes, mechanisms and consequences. *Prog Oceanogr* 60:245–262.
- Beaugrand G, Brander KM, Lindley JA, Souissi S, Reid PC (2003) Plankton effect on cod recruitment in the North Sea. *Nature* 426:661–664.
- Behrenfeld MJ, O'Malley RT, Siegel DA, McClain CR, Sarmiento JL, Feldman GC, Milligan AJ, Falkowski PG, Letelier RM, Boss ES (2006) Climate-driven trends in contemporary ocean productivity. *Nature* 444:752–755.

- Bils F, Aberle N, van Damme CJG, Peck MA, Moyano M (2022) Role of protozooplankton in the diet of North Sea autumn spawning herring (*Clupea harengus*) larvae. *Mar Biol* 169:1–16.
- Bils F, Moyano M, Aberle N, van Damme CJG, Nash RDM, Kloppmann M, Loots C, Peck MA (2019) Broad-scale distribution of the winter protozooplankton community in the North Sea. *J Sea Res* 144:112–121.
- Brander K (2010) Impacts of climate change on fisheries. *J Mar Syst* 79:389–402.
- Bresnan E, Cook KB, Hughes SL, Hay SJ, Smith K, Walsham P, Webster L (2015) Seasonality of the plankton community at an east and west coast monitoring site in Scottish waters. *J Sea Res* 105:16–29.
- Cadée GC, Hegeman J (2002) Phytoplankton in the Marsdiep at the end of the 20th century; 30 years monitoring biomass, primary production, and *Phaeocystis* blooms. *J Sea Res* 48:97–110.
- Capuzzo E, Lynam CP, Barry J, Stephens D, Forster RM, Greenwood N, McQuatters-Gollop A, Silva T, van Leeuwen SM, Engelhard GH (2018) A decline in primary production in the North Sea over 25 years, associated with reductions in zooplankton abundance and fish stock recruitment. *Glob Chang Biol* 24:e352–e364.
- Capuzzo E, Stephens D, Silva T, Barry J, Forster RM (2015) Decrease in water clarity of the southern and central North Sea during the 20th century. *Glob Chang Biol* 21:2206–2214.
- Caron DA, Hutchins DA (2013) The effects of changing climate on microzooplankton grazing and community structure: Drivers, predictions and knowledge gaps. *J Plankton Res* 35:235–252.
- Chiba S, Batten S, Martin CS, Ivory S, Miloslavich P, Weatherdon L V. (2018) Zooplankton monitoring to contribute towards addressing global biodiversity conservation challenges. *J Plankton Res* 40:509–518.
- Cloern JE, Foster SQ, Kleckner AE (2014) Phytoplankton primary production in the world's estuarine-coastal ecosystems. *Biogeosciences* 11:2477–2501.
- Denis J, Vallet C, Courcot L, Lefebvre V, Caboche J, Antajan E, Marchal P, Loots C (2016) Feeding strategy of Downs herring larvae (*Clupea harengus* L.) in the English Channel and North Sea. *J Sea Res* 115:33–46.
- Dickey-Collas M, McQuatters-Gollop A, Bresnan E, Kraberg AC, Manderson JP, Nash RDM, Otto SA, Sell AF, Tweddle JF, Trenkel VM (2017) Pelagic habitat: Exploring the concept of good environmental status. *ICES J Mar Sci* 74:2333–2341.

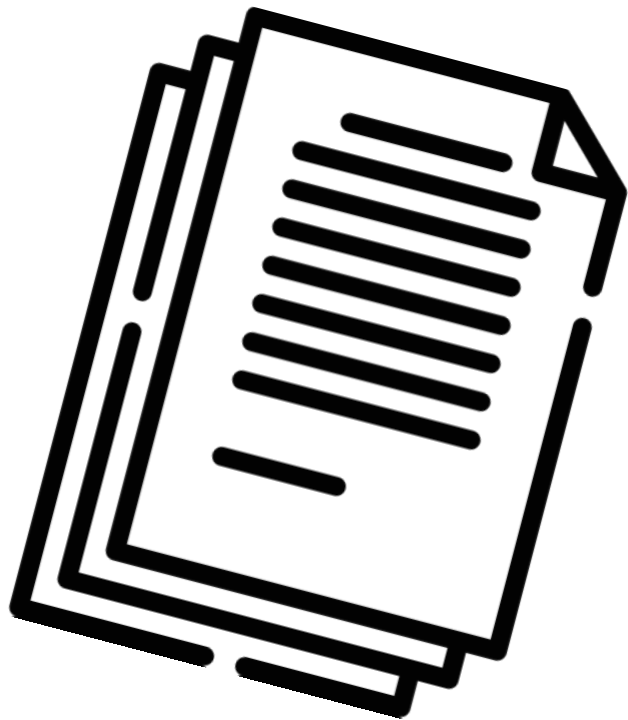
- Everett JD, Baird ME, Buchanan P, Bulman C, Davies C, Downie R, Griffiths C, Heneghan R, Kloser RJ, Laiolo L, Lara-Lopez A, Lozano-Montes H, Matear RJ, McEnnulty F, Robson B, Rochester W, Skerratt J, Smith JA, Strzelecki J, Suthers IM, Swadling KM, van Ruth P, Richardson AJ (2017) Modeling what we sample and sampling what we model: Challenges for zooplankton model assessment. *Front Mar Sci* 4:1–19.
- Figueiredo GM, Montagnes DJS, Nash RDM (2009) The importance of protozooplankton as prey for copepods in the coastal areas of the central Irish Sea. *Hydrobiologia* 628:227–239.
- Folke C, Carpenter S, Walker B, Scheffer M, Elmqvist T, Gunderson L, Holling CS (2004) Regime shifts, resilience, and biodiversity in ecosystem management. *Annu Rev Ecol Evol Syst* 35:557–581.
- Harvey, J. B., Ryan, J. P., Marin III, R., Preston, C. M., Alvarado, N., Scholin, C. A., & Vrijenhoek, R. C. (2012). Robotic sampling, in situ monitoring and molecular detection of marine zooplankton. *Journal of Experimental Marine Biology and Ecology*, 413, 60-70.
- Hays GC, Richardson AJ, Robinson C (2005) Climate change and marine plankton. *Trends Ecol Evol* 20:337–344.
- Heath MR (2005) Regional variability in the trophic requirements of shelf sea fisheries in the Northeast Atlantic, 1973-2000. *ICES J Mar Sci* 62:1233–1244.
- Hjort J (1914) Fluctuations in the great fisheries of Northern Europe. *Rapp Procés-Verbaux* 20:1–228.
- Houde ED (2008) Emerging from Hjort's shadow. *J Northwest Atl Fish Sci* 41:53–70.
- Hufnagl M, Peck MA, Nash RDM, Dickey-Collas M (2015) Unravelling the Gordian knot! Key processes impacting overwintering larval survival and growth: A North Sea herring case study. *Prog Oceanogr* 138:486–503.
- Hunter JR (1980) Feeding Ecology and Predation of Marine Fish Larvae.
- James ID (2002) Modelling pollution dispersion, the ecosystem and water quality in coastal waters: a review. *Environ Model Softw* 17:363–385.
- Jørgensen SE (2002) Ecosystem management and ecological modeling. *ScientificWorldJournal* 2:107–121.

- Kreyling J, Grant K, Hammerl V, Arfin-Khan MAS, Malyshev A V., Peñuelas J, Pritsch K, Sardans J, Schloter M, Schuerings J, Jentsch A, Beierkuhnlein C (2019) Winter warming is ecologically more relevant than summer warming in a cool-temperate grassland. *Sci Rep* 9:1–9.
- Levinsen H, Nielsen TG (2002) The trophic role of marine pelagic ciliates and heterotrophic dinoflagellates in arctic and temperate coastal ecosystems: A cross-latitude comparison. *Limnol Oceanogr* 47:427–439.
- Löder MGJ, Meunier C, Wiltshire KH, Boersma M, Aberle N (2011) The role of ciliates, heterotrophic dinoflagellates and copepods in structuring spring plankton communities at Helgoland Roads, North Sea. *Mar Biol* 158:1551–1580.
- Lombard F, Boss E, Waite AM, Uitz J, Stemmann L, Sosik HM, Schulz J, Romagnan JB, Picheral M, Pearlman J, Ohman MD, Niehoff B, Möller KO, Miloslavich P, Lara-Lopez A, Kudela RM, Lopes RM, Karp-Boss L, Kiko R, Jaffe JS, Iversen MH, Irisson JO, Hauss H, Guidi L, Gorsky G, Giering SLC, Gaube P, Gallager S, Dubelaar G, Cowen RK, Carlotti F, Briseño-Avena C, Berline L, Benoit-Bird KJ, Bax NJ, Batten SD, Ayata SD, Appeltans W (2019) Globally consistent quantitative observations of planktonic ecosystems. *Front Mar Sci* 6.
- Lynam CP, Llope M, Möllmann C, Helaouët P, Bayliss-Brown GA, Stenseth NC (2017) Interaction between top-down and bottom-up control in marine food webs. *Proc Natl Acad Sci U S A* 114:1952–1957.
- Mackas DL, Beaugrand G (2010) Comparisons of zooplankton time series. *J Mar Syst* 79:286–304.
- Mauchline J (1998) *Adv. Mar. Biol.* 33: The biology of calanoid copepods.
- Millette NC, Pierson JJ, Aceves A, Stoecker DK (2017) Mixotrophy in *Heterocapsa rotundata*: A mechanism for dominating the winter phytoplankton. *Limnol Oceanogr* 62:836–845.
- Moll A, Radach G (2003) Review of three-dimensional ecological modelling related to the North Sea shelf system. *Prog Oceanogr* 57:175–217.
- Montagnes DJS, Lessard EJ (1999) Population dynamics of the marine planktonic ciliate *Strombidinopsis multiauris*: its potential to control phytoplankton blooms. *Aquat Microb Ecol* 20:167–181.
- Nielsen T, Richardson K (1989) Food chain structure of the North Sea plankton communities: seasonal variations of the role of the microbial loop. *Mar Ecol Prog Ser* 56:75–87.

- Owens NJP, Hosie GW, Batten SD, Edwards M, Johns DG, Beaugrand G (2013) All plankton sampling systems underestimate abundance: Response to 'Continuous plankton recorder underestimates zooplankton abundance' by J.W. Dippner and M. Krause. *J Mar Syst* 128:240–242.
- Pörtner H-O, Karl DM, Boyd PW, Cheung W, Lluch-Cota SE, Nojiri Y, Schmidt DN, Zavialov PO, Alheit J, Aristegui J (2014) Ocean systems. In: *Climate change 2014: impacts, adaptation, and vulnerability. Part A: global and sectoral aspects. contribution of working group II to the fifth assessment report of the intergovernmental panel on climate change*. Cambridge University Press, p 411–484
- Quante M, Colijin F (2016) North Sea Region Climate Assessment (NOSCCA).
- Rees HL, Hyland JL, Hylland K, Mercer Clarke CSL, Roff JC, Ware S (2008) Environmental indicators: Utility in meeting regulatory needs. An overview. *ICES J Mar Sci* 65:1381–1386.
- Richardson AJ (2009) Plankton and Climate. In: *Encyclopedia of Ocean Sciences*. Elsevier, p 455–464
- Schmidt JO, Van Damme CJG, Röckmann C, Dickey-Collas M (2009) Recolonisation of spawning grounds in a recovering fish stock: recent changes in North Sea herring. *Sci Mar* 73:153–157.
- Schrum C, Lowe J, Meier HEM, Grabemann I, Holt J, Mathis M, Pohlmann T, Skogen MD, Sterl A, Wakelin S (2016) Projected change—North sea. *North Sea Reg Clim Chang Assess*:175–217.
- Scott J, Pitois S, Close H, Almeida N, Culverhouse P, Tilbury J, Malin G (2021) In situ automated imaging, using the Plankton Imager, captures temporal variations in mesozooplankton using the Celtic Sea as a case study. *J Plankton Res* 43:300–313.
- Scott J, Pitois S, Creach V, Malin G, Culverhouse P, Tilbury J (2023) Resolution changes relationships: Optimizing sampling design using small scale zooplankton data. *Prog Oceanogr* 210:102946.
- Sildever S, Laas P, Kolesova N, Lips I, Lips U, Nagai S (2021) Plankton biodiversity and species co-occurrence based on environmental DNA – a multiple marker study. *Metabarcoding and Metagenomics* 5:175–197.

- Sommer U, Aberle N, Engel A, Hansen T, Lengfellner K, Sandow M, Wohlers J, Zöllner E, Riebesell U (2007) An indoor mesocosm system to study the effect of climate change on the late winter and spring succession of Baltic Sea phyto- and zooplankton. *Oecologia* 150:655–667.
- Trombetta T, Vidussi F, Roques C, Scotti M, Mostajir B (2020) Marine Microbial Food Web Networks During Phytoplankton Bloom and Non-bloom Periods: Warming Favors Smaller Organism Interactions and Intensifies Trophic Cascade. *Front Microbiol* 11:1–19.
- Turner JT (2004) The importance of small planktonic copepods and their roles in pelagic marine food webs. *Zool Stud* 43:255–266.
- Westberry T, Behrenfeld MJ, Siegel DA, Boss E (2008) Carbon-based primary productivity modeling with vertically resolved photoacclimation. *Global Biogeochem Cycles* 22.
- Widdicombe CE, Eloire D, Harbour D, Harris RP, Somerfield PJ (2010) Long-term phytoplankton community dynamics in the Western English Channel. *J Plankton Res* 32:643–655.
- Wiltshire KH, Manly BFJ (2004) The warming trend at Helgoland Roads, North Sea: Phytoplankton response. *Helgol Mar Res* 58:269–273.
- Yang J, Chen Z, Chen D, Xu D (2021) Spatial distribution of the microzooplankton communities in the northern South China Sea: Insights into their function in microbial food webs. *Mar Pollut Bull* 162:111898.

Supplements



Supplements: Chapter 1

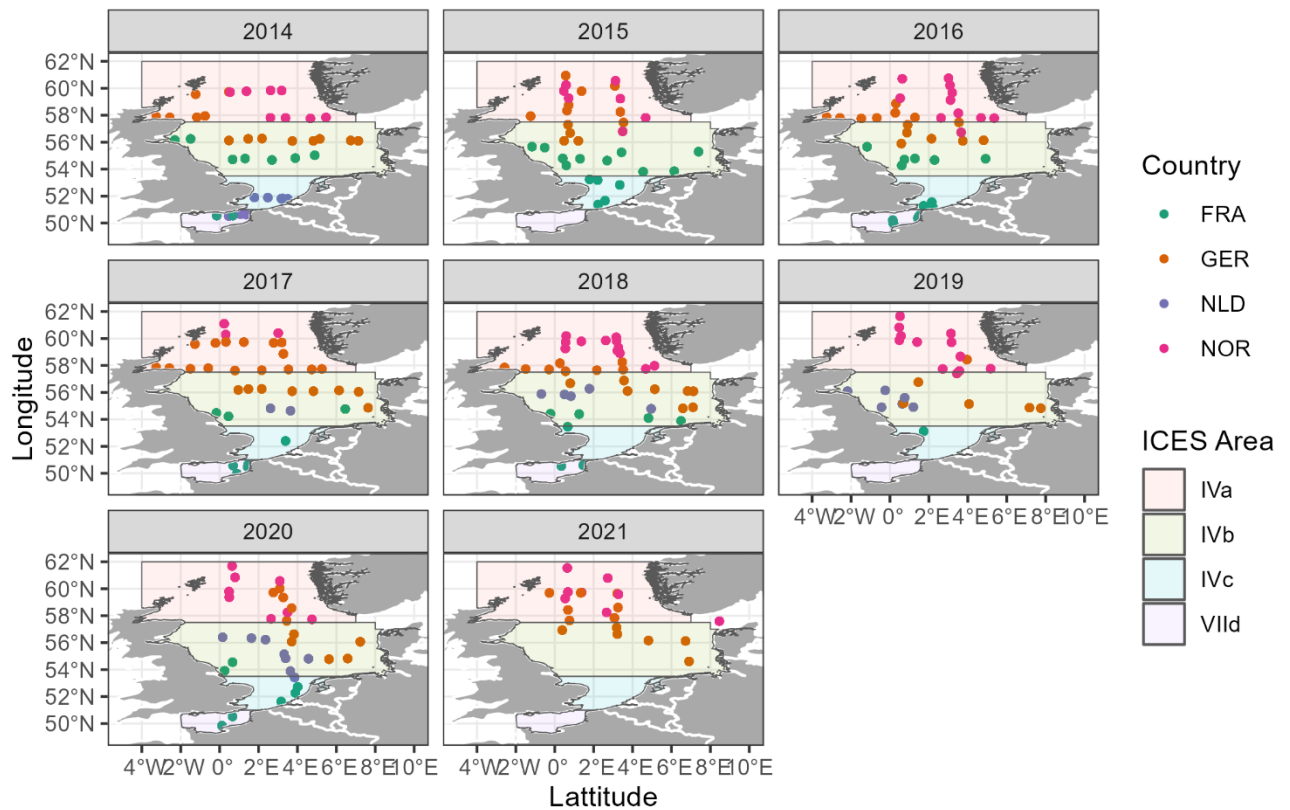


Fig. S1 spatial coverage per year of the Protozooplankton sampling stations in the North Sea during the International Bottom Trawl Survey Q1 from 2014-2021. The ICES areas are depicted by the background color (red= IVa, green= IVb, blue=IVc, and purple= VIIId) and the stations are colour-coded according to the IBTS leading country (FRA=France, GER=Germany, NLD=The Netherlands, NOR=Norway).

Table S1. Survey period of the IBTS Q1 per respective country and year

Country	Year	Start date	End date
France	2014	15.01	13.02
France	2015	21.01	09.02
France	2016	22.01	13.02
France	2017	20.01	08.02
France	2018	25.01	06.02
France	2019	25.01	05.02
France	2020	11.01	24.01
Germany	2014	26.01	20.02
Germany	2015	29.01	18.02
Germany	2016	05.02	19.02
Germany	2017	24.01	19.02
Germany	2018	26.01	19.02
Germany	2019	04.01	18.02
Germany	2020	12.01	29.01
Germany	2021	27.01	12.02
Netherlands	2014	27.01	31.01
Netherlands	2017	24.01	26.01
Netherlands	2018	02.02	08.02
Netherlands	2019	29.01	04.02
Netherlands	2020	21.01	31.01
Norway	2014	16.01	18.02
Norway	2015	17.01	09.02
Norway	2016	13.01	27.01
Norway	2017	22.01	15.02
Norway	2018	13.02	26.02
Norway	2019	09.02	28.02
Norway	2020	12.02	02.03
Norway	2021	19.01	08.02

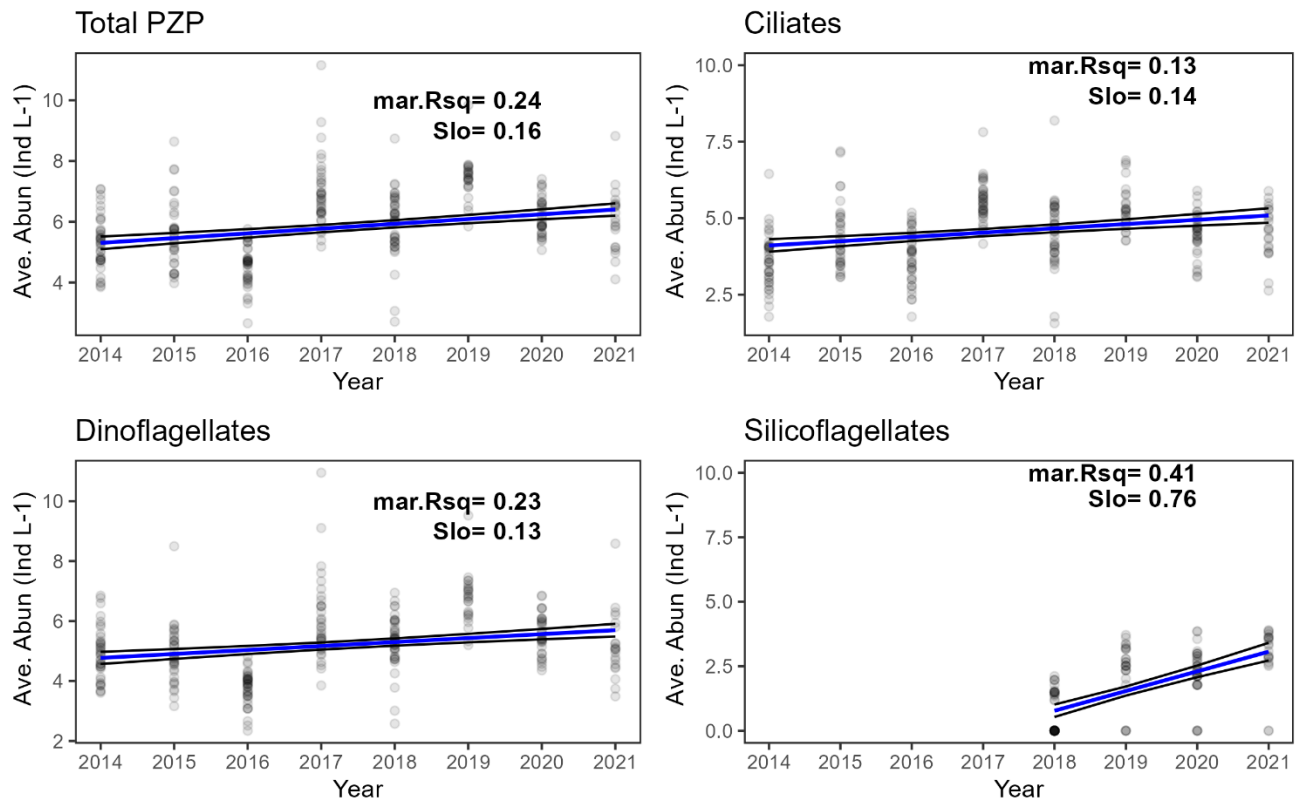


Fig.S2 : Mean 4th-root transformed abundance trend averaged across all stations for (A) the whole PZP community, (B) Ciliates, (C) Dinoflagellates, (D) Silicoflagellates. All three groups increased significantly in abundances over the last seven years. The variance of the fixed effects (year) (marginal R² (mar.Rsq)) and Slope (Slo) are displayed for total PZP and each main group.

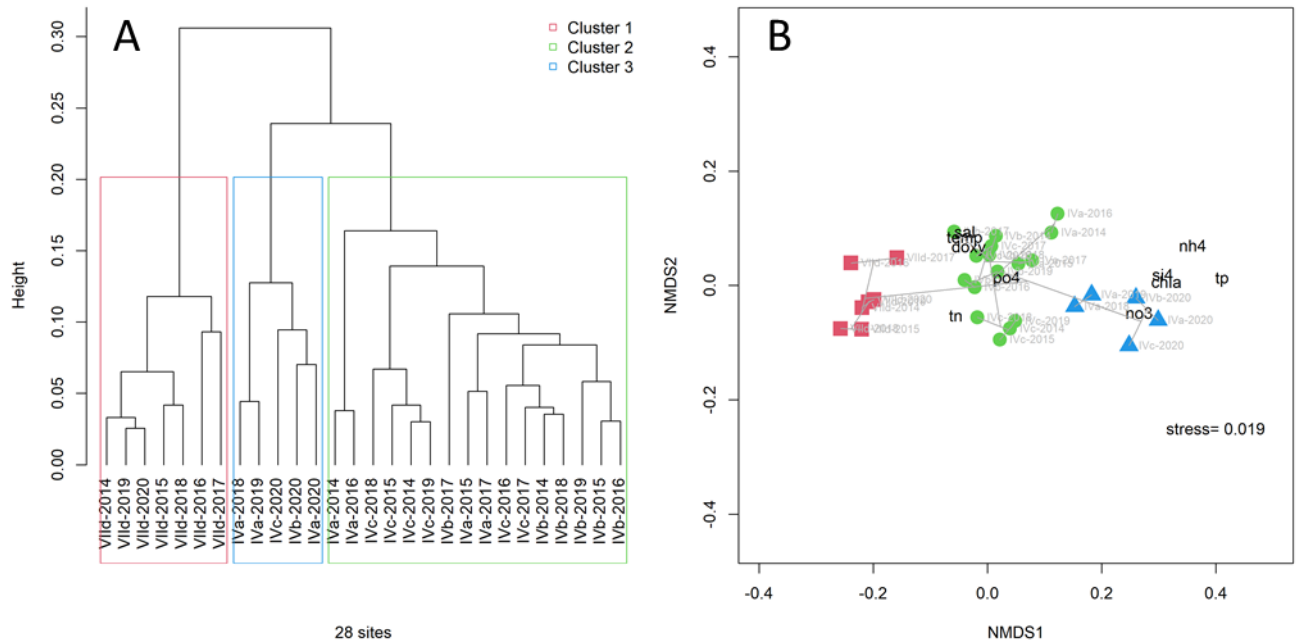


Figure S3: (A) Dendrogram obtained for the four ICES areas per each year based on the environment and nutrients. (B) NMDS plot of the environmental variables for the four ICES areas and the different years. Colors represent the different clusters from the dendrogram. Sites are clearly separated by the key environmental variables temperature (TEMP), salinity (SAL), oxygen (DOXY) and nutrients (NH4 – ammonia, NO3 – Nitrogen, SI4 – Silicates, TN – total nitrogen) with an excellent goodness of fit (stress <0.05).

Table S2. Taxa-specific coefficients used for estimating biomass B of individual zooplankters as a function of their biovolume BV : $\log_{10} B = a + b \cdot \log_{10} BV$. Note that a and b were adjusted to the units of $B[\mu\text{gC}]$ and $BV[\mu\text{m}^3]$ used in this study.

Biovolume [μm^3]	$= \frac{\pi}{6} * d^2 * w$	d=diameter h = width	Oleynia et al., (2016)
Log pgC cell ⁻¹	$= \log a + b * \log V (\mu\text{m}^3)$	a = -0.665 b = 0.939 V = biovolume	Menden-Deuer & Lessard (2000)

Supplements Chapter 2

Instruction manual for the DOC application

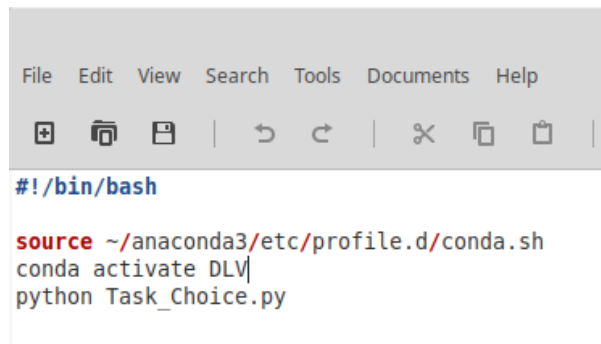
Preface

The following steps require that the basic foundations of a computer capable of Deep Learning have been set up. These include the fulfillment of all hardware requirements as lined out in SI II and the installation of a Linux operating system (the DOC application was tested successfully under Ubuntu 18.04 and Linux Mint 19.1). Furthermore, required drivers (CUDA) of the Nvidia® (Santa Clara, CA / US) Graphics card and Python 3 (via the Anaconda (Anaconda Software Distribution, 2016) distribution) have to be installed (SI III), and a Conda environment containing the packages listed in SI III (in the correct version) has to be created.

Preparatory work

In these steps the path to the Anaconda environment of your computer is set in the start script of the application. They require knowing the location of this environment, and the modification of one line of code. Any IT technician familiar with Linux computers should be able to execute these steps

1. Change path to the location of your anaconda installation (“source ...”), and change the name from “DLV” to the name of your Anaconda environment in the bash script “Start_Here.sh” (fig. 1).



```
File Edit View Search Tools Documents Help
+ | | | | | | | |
#!/bin/bash
source ~/anaconda3/etc/profile.d/conda.sh
conda activate DLV
python Task_Choice.py
```

Fig. 1: Bash script “Start_Here.sh” in text-editor view

2. Set “Start_Here.sh” to “executable” (right-click, check box) (fig. 2). Check whether the Python scripts (featuring the “.py” suffix) are set to executable, and if not, set them to executable as before.

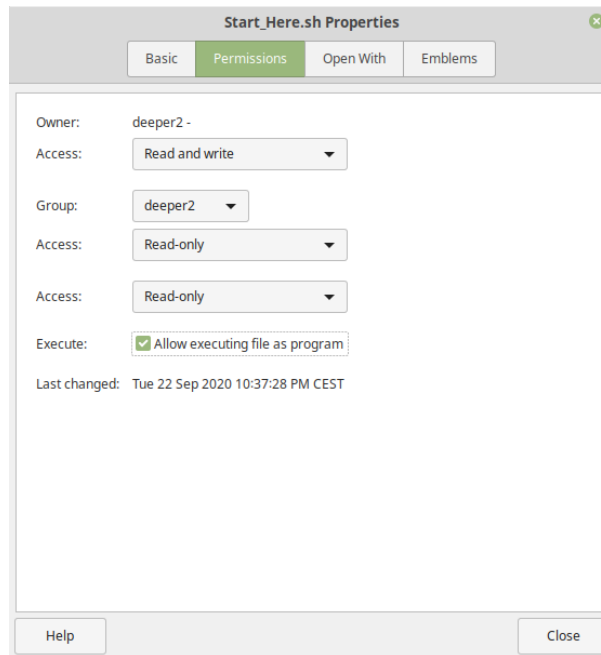


Fig. 2: Properties manager of script “Start_Here.sh”

General remarks

During the process, the file “Start_Here.sh” will be called multiple times. Depending on your operating-system settings, a window will prompt when double-clicking on the file, asking you how to proceed (fig. 3). It is recommendable to choose the option “run in terminal”, which means that the file is run in executable mode, and that program output like progress bars will be visible in a terminal window that opens automatically and closes automatically once a process is finished.

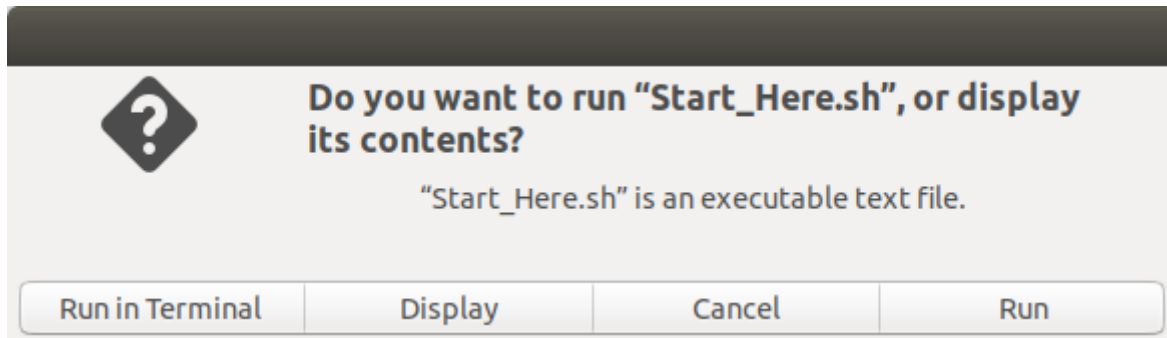


Fig. 3: Options manager for executing script “Start_Here.sh”.

In some parts of the graphical user interface, it is necessary to write input into an orange-colored input field and confirm the input by clicking a button. For programming reasons, this field is still visible and accessible after confirmation, but should not be modified at that point in any way. Only enter input into an input field when the program dialogue asks for it (negative example in 4).

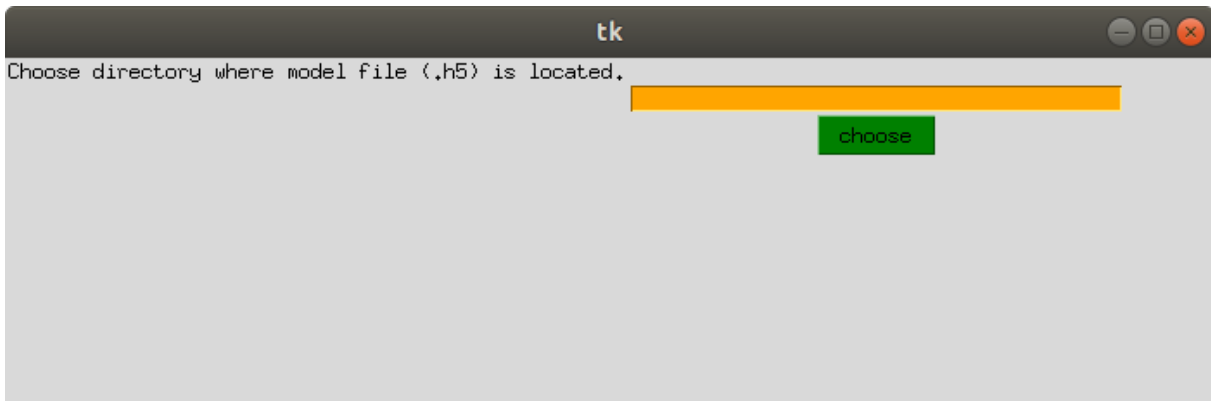


Fig. 4: User interface with input line that should not be modified in the current step

If you have made an error in your input or selection of an option, it is advisable to close the application, and to then restart it. Do not attempt to make a correction after you have clicked on a “confirm” button.

At several points, you will be asked to provide the location of a target folder. This location is chosen via a file-browser window that opens automatically. When asked for the location, navigate through the folder structure until you see the target folder listed in the window (fig. 5). Do not enter this folder before confirming the target location.

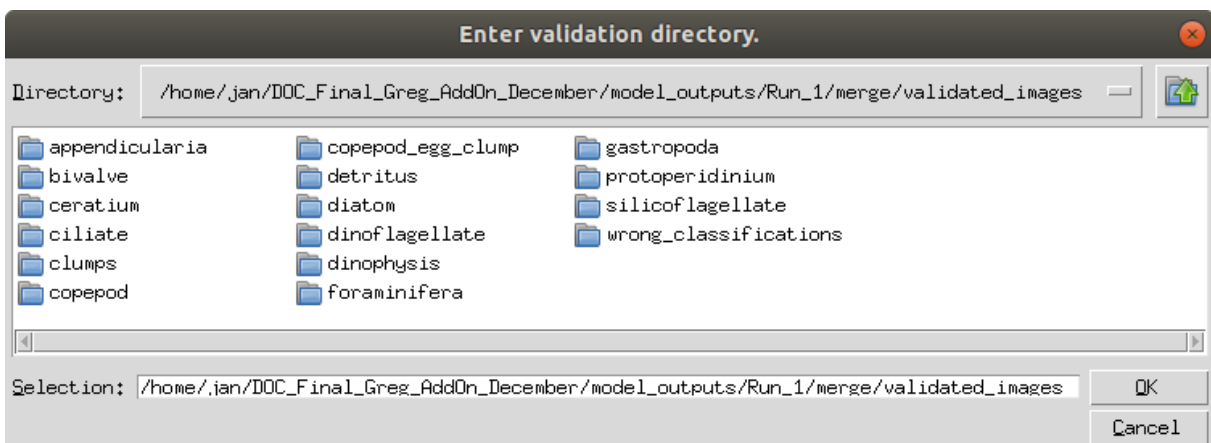


Fig. 5: File-browser window of the user application. The folder “wrong_classifications” is the target folder that is being asked for in the current user dialogue. The next step would be to click the “OK” button

Some scripts in the application will create temporary files and folders that are deleted after process completion. Do not mingle with or delete these files or folders!

It is a good idea not to execute other memory-intensive processes on the Deep-Learning computer during image classification and model training.

1. Classify images of one survey station

Double-click on “Start_Here.sh”, and choose the option “classify_images (single folder)” (fig. 6). You need to provide the name of your station folder (this folder should only contain images; no other files or directories!), the location of this folder, the location of the model file (“Final_Classifier.h5”) and the location of the “Model_Executable” script (figs. 7-11). Make sure

that the image folder does not contain “broken” files (these are sometimes created in copying processes that are not successfully completed).

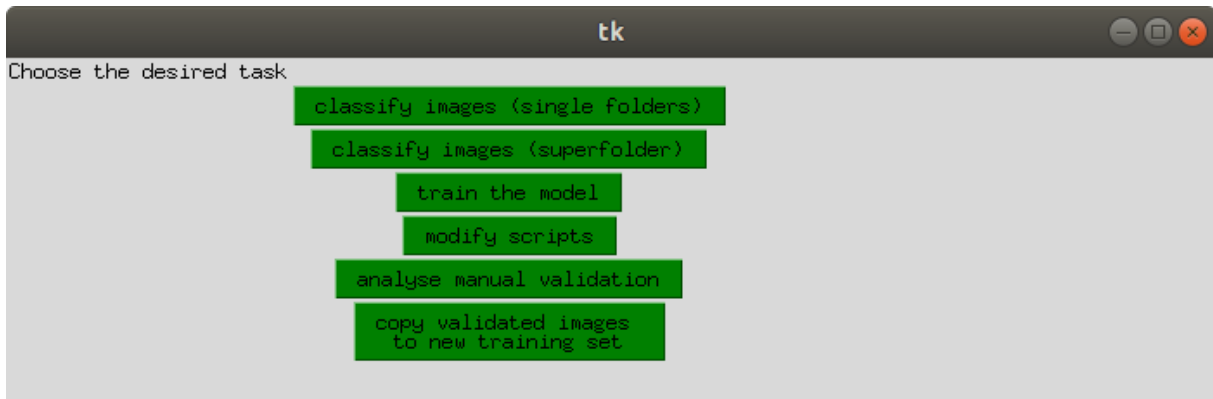


Fig. 6: Task menu that appears upon opening “Start_Here.sh”

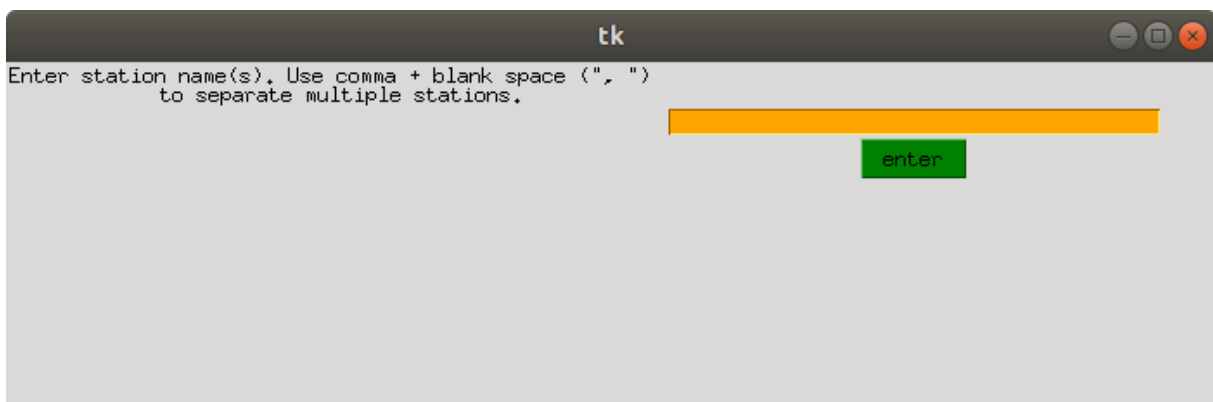


Fig. 7: First step in the “classify images (single folder)” task: The name of a folder of unsorted plankton images should be entered into the input field

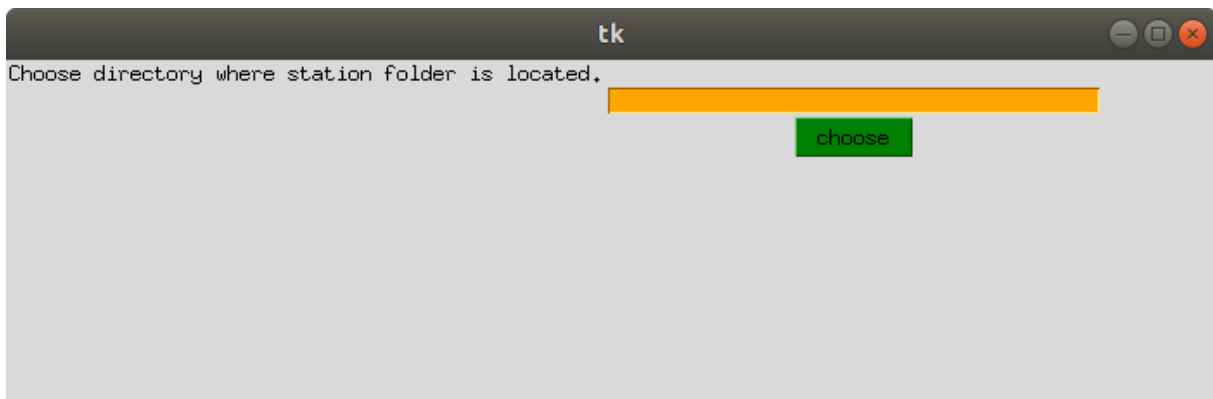


Fig. 8: Second step in the “classify images (single folder)” task: The path to the folder of images to be classified should be provided by clicking on “choose”. This will open a file-browser window for locating the folder (see also fig. 5). After path selection, a “confirm” button must be clicked (not pictured)

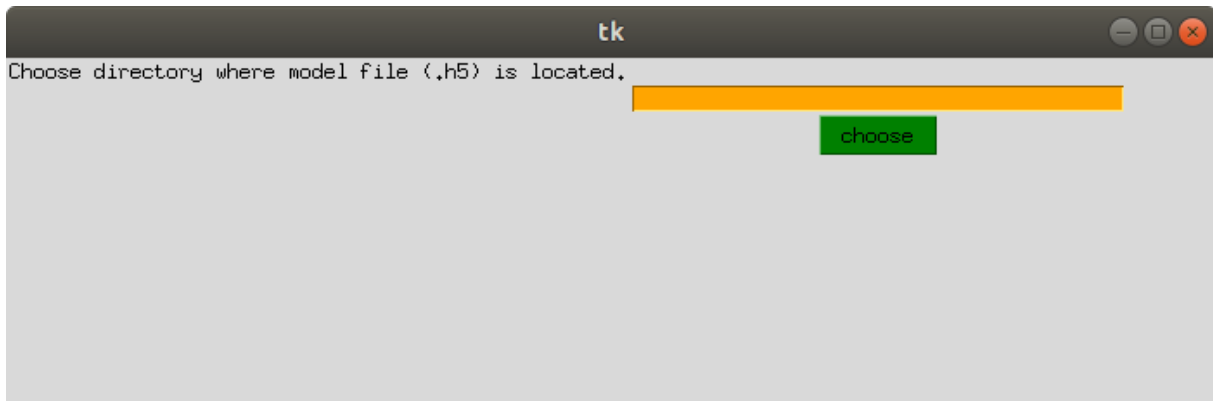


Fig. 9: Third step in the “classify images (single folder)” task: The path to the classifier-model file (“Final_Classifier_Model.h5”) should be provided by clicking on “choose”. This will open a file-browser window for locating the folder. After path selection, a “confirm” button must be clicked to proceed (not pictured)

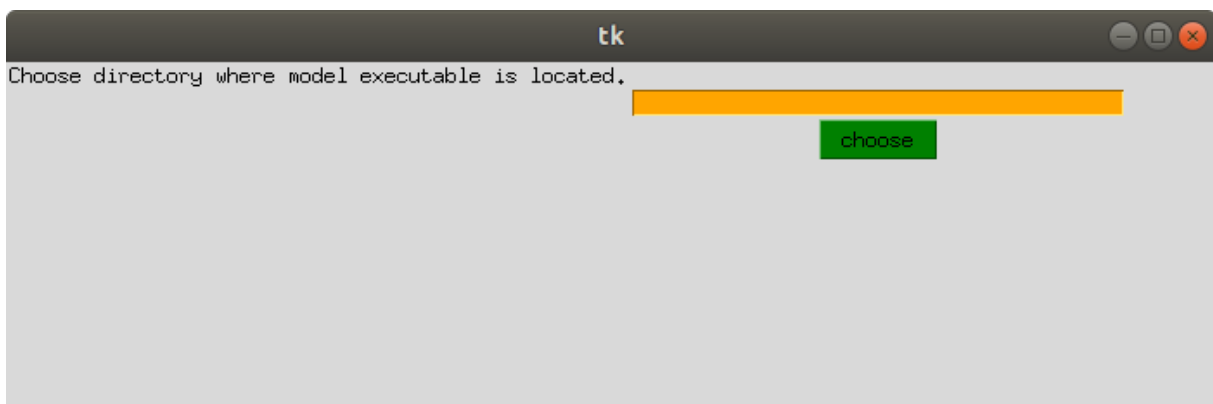


Fig. 10: Fourth step in the “classify images (single folder)” task: The path to the classification script (“Model_Executable_CNN_NoDataAugmentation4GUI.py”) should be provided by clicking on “choose”. This will open a file-browser window for locating the folder. After path selection, a “confirm” button must be clicked to proceed (not pictured)

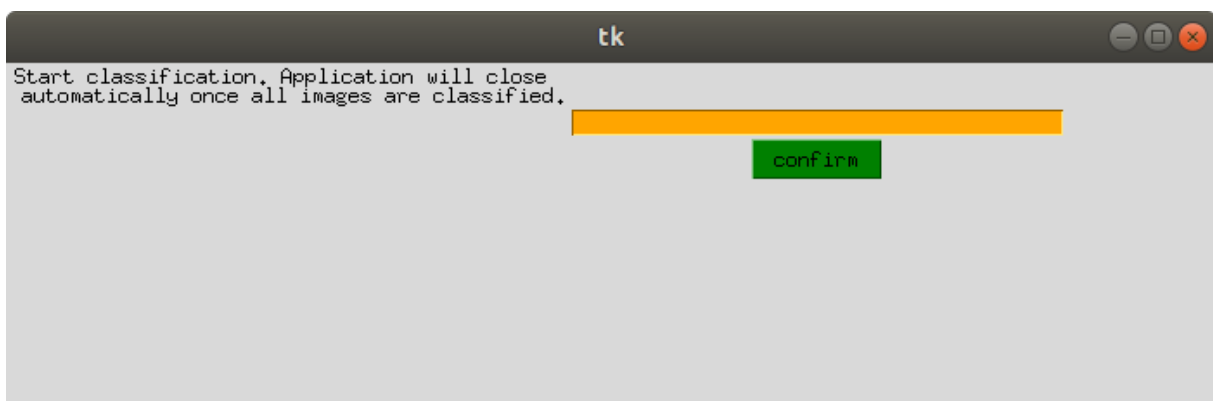


Fig. 11: Final step in the “classify images (single folder)” task: Final confirmation to start classification is given by clicking the “confirm” button

2. Validate classification

Perform a manual validation of the model output, i.e. make a copy of the model-output folder and move wrongly-classified images into the correct .class folders; if necessary, create new class folders.

Be aware that it may not be a good idea to create new folders for new classes that were very rarely encountered during validation. Training a model (see below) on these few images will very likely not lead to good classification results.

In the end, you should have one folder that is the original model output (i.e., the folder “classified_images”, automatically created by the classifier script), and one folder containing your validated classification. Both folders should have the same structure, and of course contain identical (and the identical amount of) images!

You do not need to do any changes to the “uncertain_classifications” folder in the original model output – just leave it as it is.

If you encountered new classes during manual re-analysis, be sure to name the folders in a manner that is consistent with the naming of the other class folders. In particular, avoid capital letters, underscores, dots and numbers. This is necessary to maintain the “alpha-numerical order” of classes in the classification scripts!

In order to implement the DOC concept, it is wise to classify a few samples, i.e. two to three, and to then merge all model-output folders and all corrected folders. This is convenient in order to get more images to stock the training set up with.

To start the comparison between model classification and expert validation, double-click on “Start_Here.sh”, and choose “analyze manual validation”. The program will compare the location of each image between the class folders of the original model output and your manual correction, and thus infers miss-classification rates. The program dialogue will ask you for the names and locations of the two folders, as well as for the location of the script “Manual_Validation_Analysis4GUI.py”, and will then start the comparison (figs. 12-15). It will fail if the number and file names of the images are not exactly the same for the two folders, so make sure copy processes are successfully completed if you need to transfer image folders between multiple computers for manual validation.

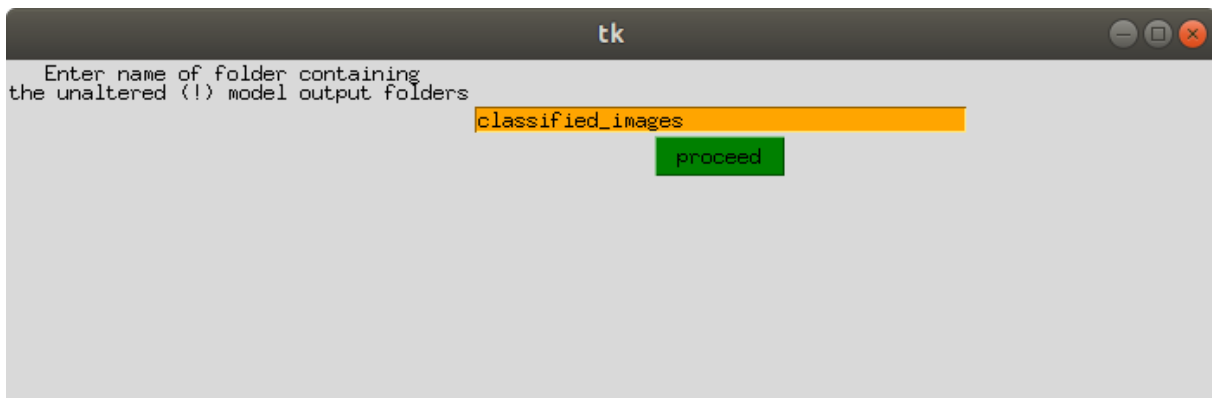


Fig. 12: First step in the “analyze manual validation” task: The name of the folder containing the automatic-classification output (class folders) should be entered into the input field.

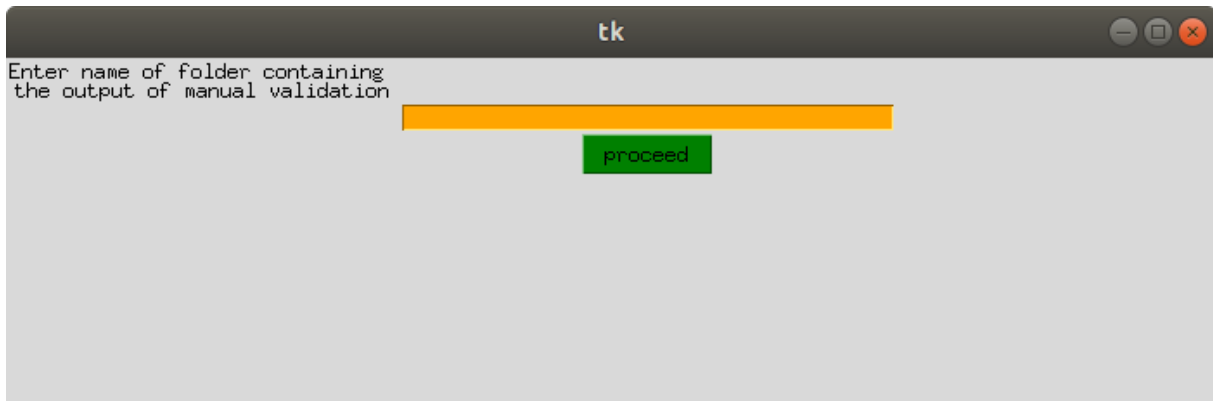


Fig. 13: Second step in the “analyse manual validation” task: The folder containing the expert-validated classification (class folders) should be given by clicking “proceed”, which opens a file-browser window. After navigating to the folder location, a confirmation by clicking a “confirm” button (not shown) is required.

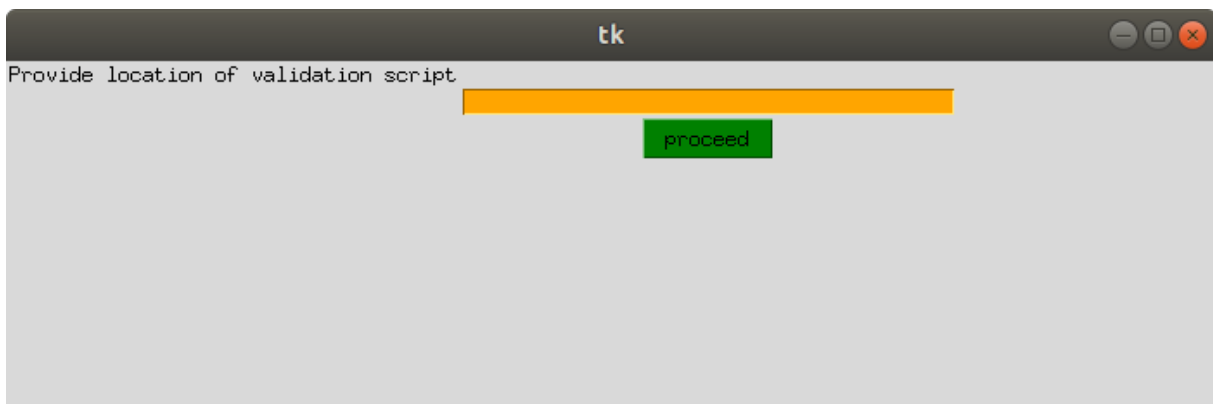


Fig. 14: Third step in the “analyse manual validation” task: The folder containing the script for comparing automatic and expert-validated classification (“Manual_Validation_Analysis4GUI.py”) should be given by clicking “proceed”, which opens a file-browser window. After navigating to the folder location, a confirmation by clicking a “confirm” button (not shown) is required.

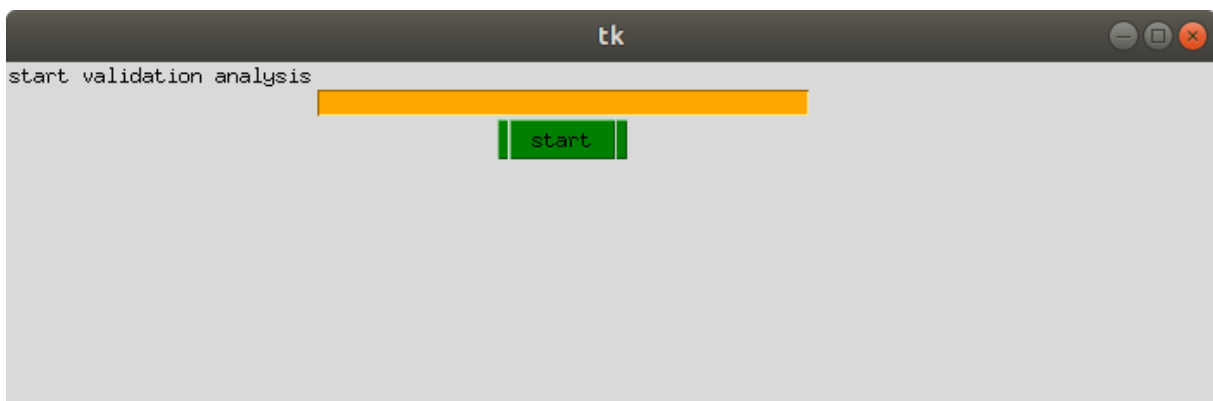


Fig. 15: Final step in the “analyse manual validation” task: Final confirmation to start the comparison between automatic and expert-validated classification is given by clicking the “start” button.

The application will create two scripts that are of further importance within the “Scripts” directory: “Image_Stockup_Recommendation.csv” and “Thresholds.csv”.

Within the folder containing the manually corrected class folders, a new folder has been created called “wrong_classifications”. This contains all images that you reassigned to other class folders during the manual validation.

3. Stock up the training data-set with new images

Create a duplicate of the folder containing the training-images class-folders. If you do not care about keeping a copy of the prior training set, no duplication is needed, and the original training folder will be modified.

If you encountered new classes during manual re-classification, be sure to add respective empty folders in the new training-set folder! Furthermore, if not all classes that were part of the prior training set are included in the “wrong_classifications” folder, be sure to add respective empty folders here, as well!

Double-click on “Start_Here.sh”, and choose “copy validated images to new training set”. The program dialogue will ask you for the name and location of the folder that provides the images for the new, extended training set. This is the aforementioned “wrong_classifications” folder (fig. 16).

Also, you are asked to provide the location of the training folder, which should be the copy of the original folder just created (“Training_2”) (fig. 17).

You are then asked to provide the names of the class folders in the source folder and those of the target folders (fig. 18). These names should be identical (this this input demand will be removed in a future version due to redundancy). Names should be given in alphabetical order.

You are further asked to provide the relative number of images to be added to the new training set (values between 0 and 1). Take these from the file “Image_Stockup_Recommendation.csv”, which was created in the prior step. Note that the sequence of classes in the .csv file is not alphabetical, but that the sequence of stock-up ratios must be provided in the same sequences as the class names!

Set “NA” values to 0. If you encountered new classes during manual re-analysis, be sure to set the stock-up values to “1”! (These values are originally set to 0 in the “Image_Stockup_Recommendation.csv” file). Also be sure to add the new class names in the respective input lines, in the correct alphabetical position in the sequence of class names!

The aforementioned inputs should be provided with comma-space separation (“, “). It is a good idea to keep these in a Word file for later use – it can speed up the process of typing.

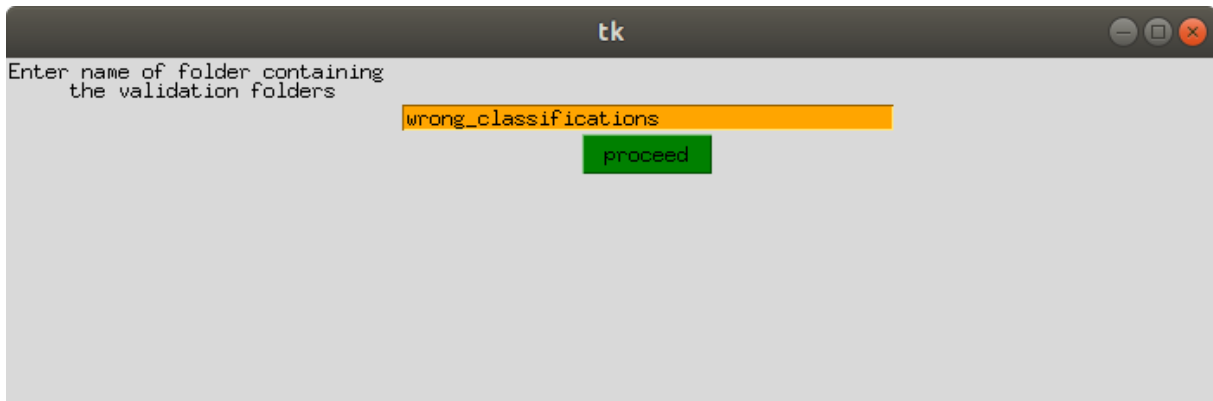


Fig. 16: First step in the “copy validated images to new training set” task: The name of the folder containing the wrongly classified images (arranged in class folders, as per the expert validation) should be entered into the input field

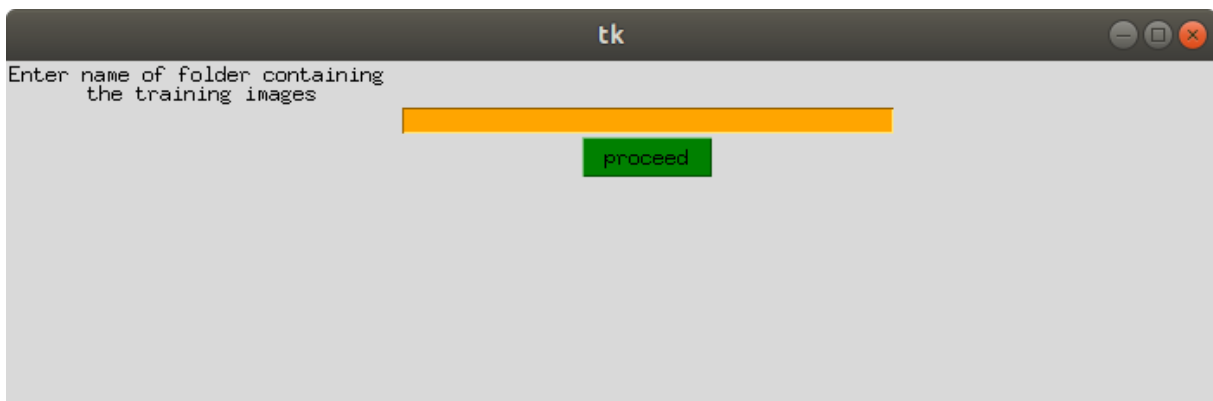


Fig. 17: Second step in the “copy validated images to new training set” task: The name of the training folder to be stocked up with new images should be entered into the input field.

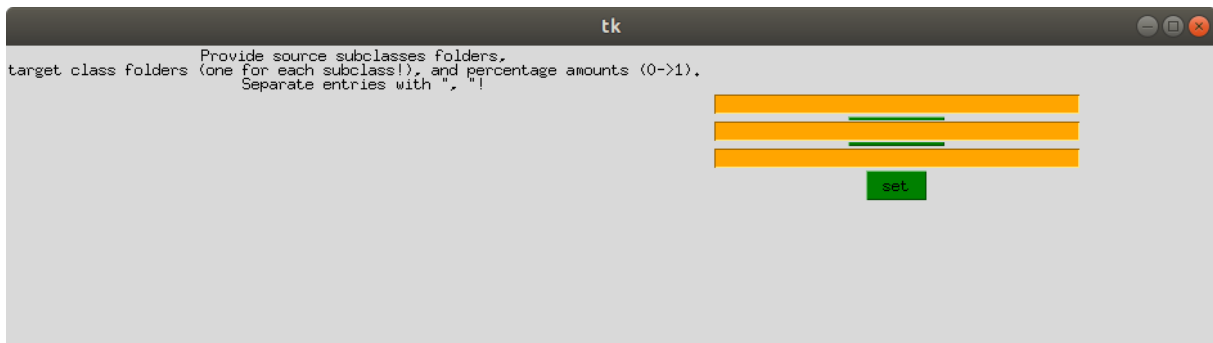


Fig. 18: Final step in the “copy validated images to new training set” task: The names of classes should be entered into the upper two input fields. The relative values for image stock-up should be entered into the lower-most input field. Copying of the images is started by clicking “set”.

4. Train a new model

Make a copy of the scripts folder (name it e.g. “Scripts_2”). You can delete all the newly-created .csv files – except for “Thresholds.csv”, which will be required later.

From now on, work in this folder only!

Double-click on “Start_Here.sh”, and choose “train the model”. You are then asked to provide the name and location of the updated training set (“Training_2”), as well as the location of the “Train4GUI_EX” scripts (“X” indicating numbers 1 to 8). You can then start the training (figs. 19-22), which may take a while depending on the number and size of the training images, and

on your computer and GPU specifications (it takes about 50 minutes for about 50 k training images on the authors' computer).

The new model is then saved as "Final_Classifier_Model.h5" in the current scripts folder. This means that the baseline model of the same name is over-written.

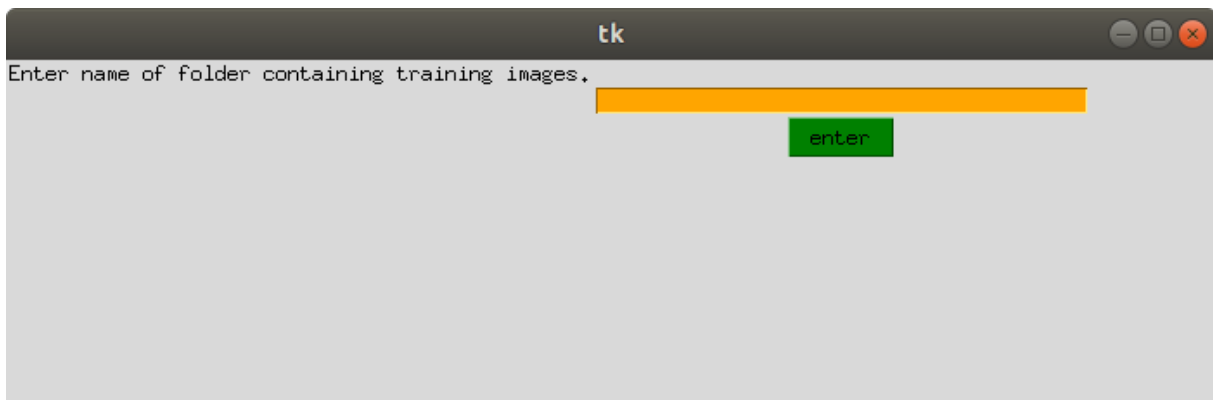


Fig. 19: First step in the "train the model" task: The name of the folder containing the training images should be entered into the input field.

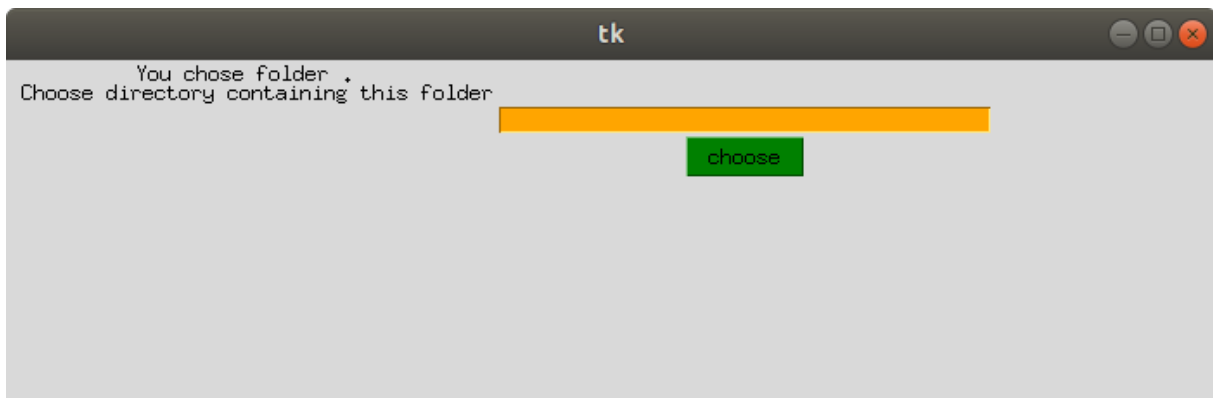


Fig. 20: Second step in the "train the model" task: The folder containing the training set should be given by clicking "proceed", which opens a file-browser window. After navigating to the folder location, a confirmation by clicking a "confirm" button (not shown) is required.

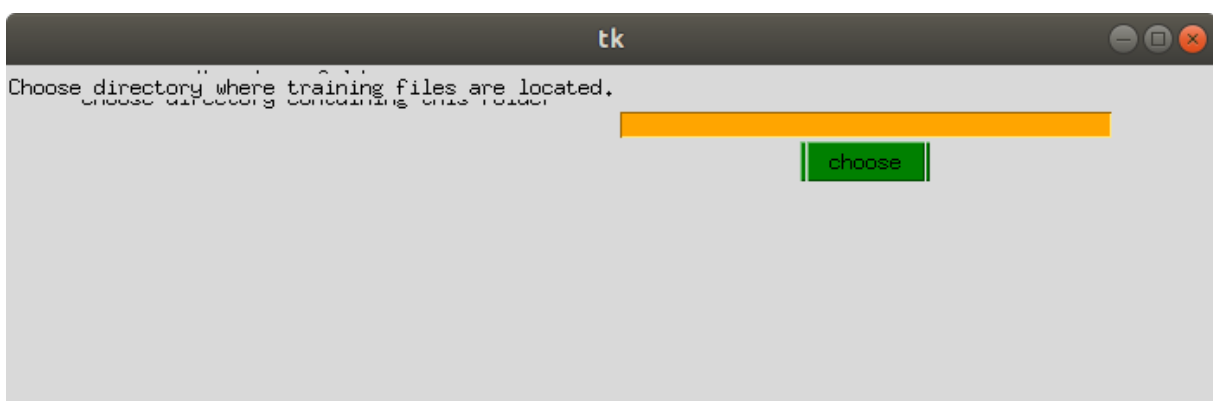


Fig. 21: Third step in the "train the model" task: The folder containing the training scripts ("Train4GUI_E1.py" and so on) should be given by clicking "proceed", which opens a file-browser window. After navigating to the folder location, a confirmation by clicking a "confirm" button (not shown) is required.

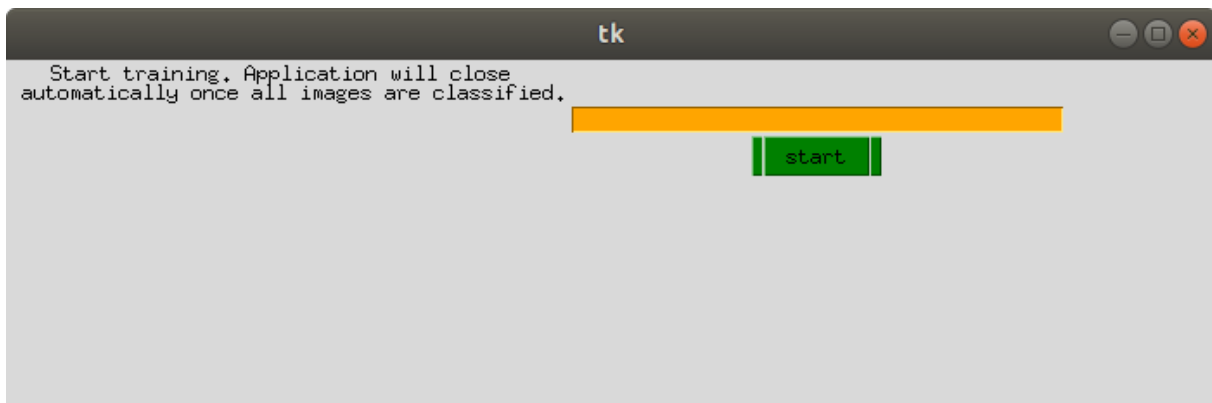


Fig. 22: Final step in the “train the model” task: Final confirmation to start the training is given by clicking the “start” button.

5. Incorporate new thresholds

The script that performs the classification must now be updated with the thresholds generated in step #3.

Double-click on “Start_Here.sh” and choose “modify scripts”. Then choose the option “change classes” (fig. 23). You are asked for the location of the script “Model_Executable_CNN_NoDataAugmentation4GUI.py”, which is located in the scripts folder (fig. 24).

You are then asked to provide the class names. As in step #3, provide the names in alphabetical order (fig. 25). Finally, you are asked to provide the new threshold values (fig. 26). These are contained in the file “Thresholds.csv” that was generated in step #3 (if you accidentally deleted it, you can copy it from the previous scripts folder). Note that while class names are not provided in this file, the sequence of values is already correct, so you can maintain it as it is. Note that the top “0” is not a number, but a column header.

If you encountered new classes during manual re-analysis: Make sure to also provide the new class names, and to provide threshold values for these new classes. These values are not included in “Thresholds.csv”, and should initially be set to 0.6. Make sure to add class names and threshold values at the correct alphabetical position in the sequence of class names and values, respectively. This position can be derived from the sequence of folders in your new training-set folder (if you kept class naming consistent).

As in step #3, make sure to separate the values with comma-space (“, “). After confirmation (fig. 27), the aforementioned script is over-written, while a copy of the previous version is maintained (bearing the suffix “_old”). This can be deleted or kept for future reference.

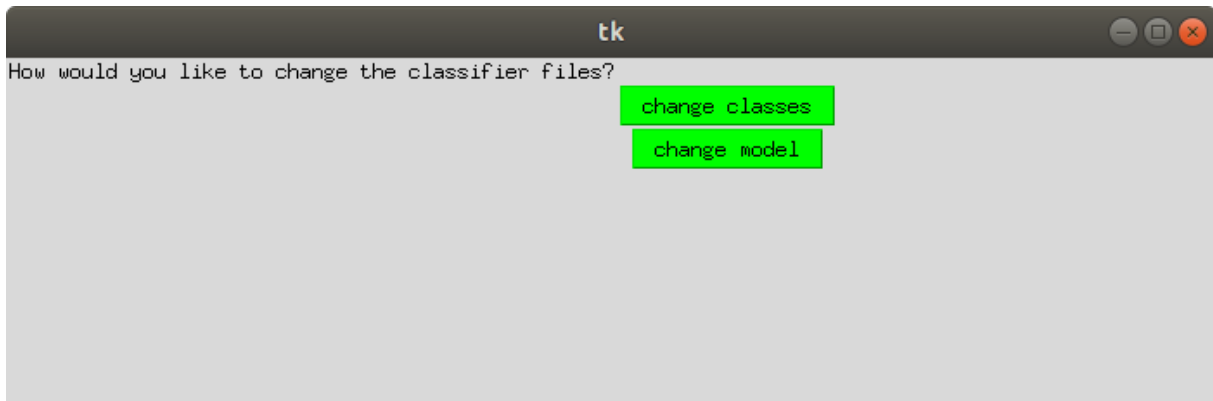


Fig. 23: First step in the “modify scripts” task: Select the “change classes” option.

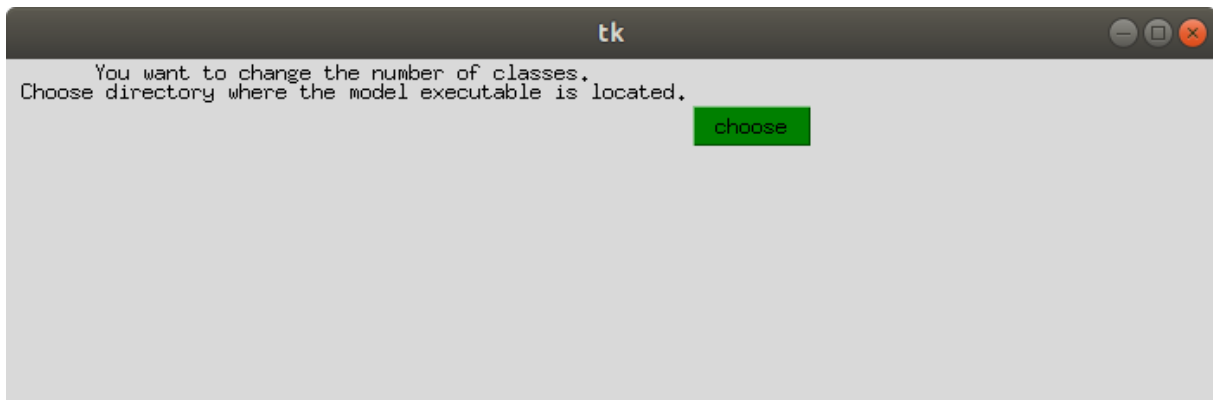


Fig. 24: Second step in the “modify scripts” task: The folder containing the classification script (“Model_Executable_CNN_NoDataAugmentation.py”) should be given by clicking “proceed”, which opens a file-browser window. After navigating to the folder location, a confirmation by clicking a “confirm” button (not shown) is required.

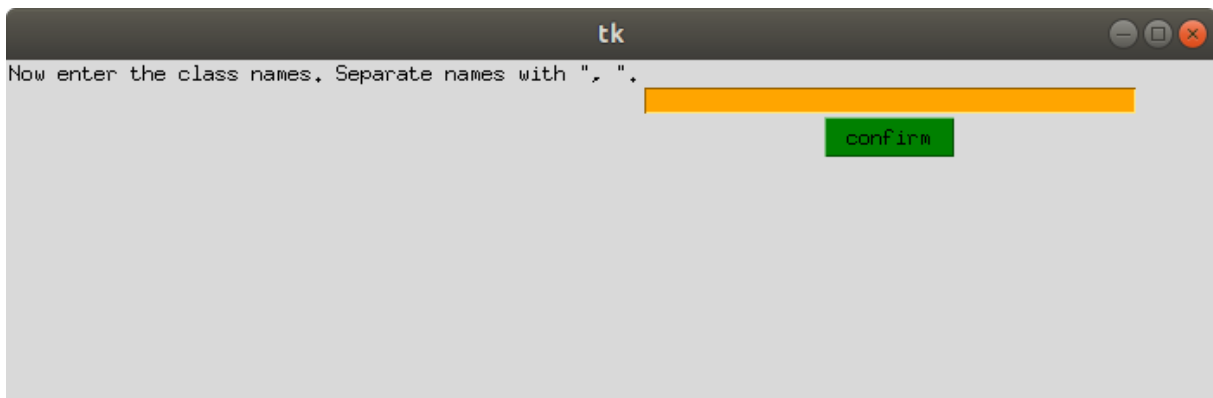


Fig. 25: Third step in the “modify scripts” task: The class names of all classes in the current training set should be typed into the input line.

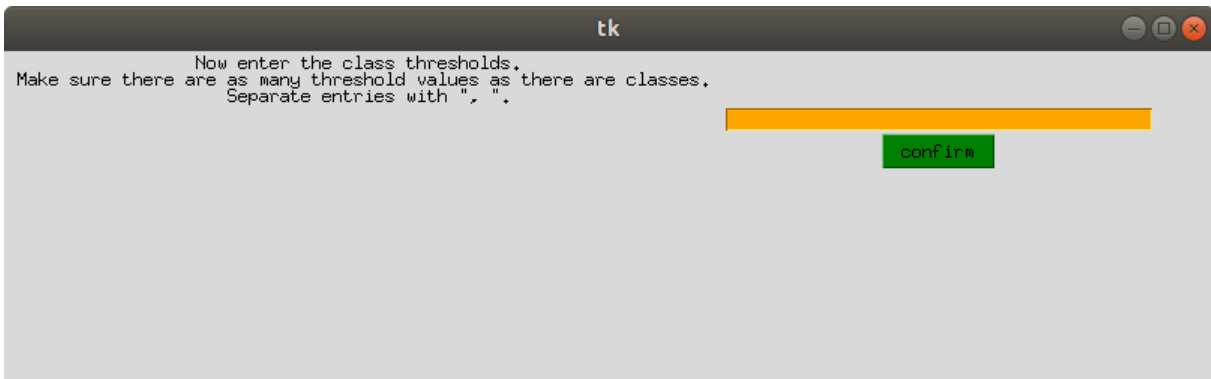


Fig. 26: Fourth step in the “modify scripts” task: The new classification thresholds – as given by the “Thresholds.csv” file – should be typed into the input line, their sequence corresponding to the sequence of class names in the previous step.

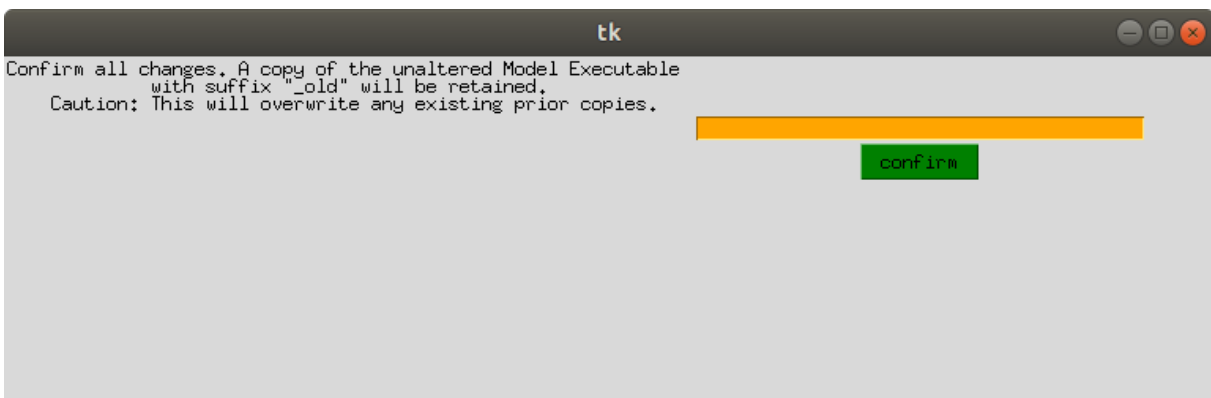


Fig. 27: Final step in the “modify scripts” task: A confirmation for over-writing the existing thresholds in the classification script (“Model_Executable_CNN_NoDataAugmentation.py”) is required, which is given by clicking “confirm”.

6. Start the cycle anew

You can now proceed from step #1 again. Make sure to always create a copy of the scripts folder; to avoid confusion regarding different versions of models and scripts.

You can also choose the option “classify super-folder” when opening “Start_Here.sh” and provide a folder containing several image folders, or you type the names of several image folders in a row (separated with comma-space) in the basic “classify images” option. This way, a batch of image folders can be classified.

Technical prerequisites – hardware

Tab. SI II / 1: Hardware required for operating the DOC application. Two working systems are presented

Component	Computer #1	Computer #2
Computer	Dell Precision 5530 notebook	Dell Optiplex 790 work station
CPU	Intel Core i7	Intel Core i5

GPU	Nvidia Quadro P2000	Nvidia Quadro P2000
Hard drive	SSD, 512 GB	SSD Toshiba, 240 GB
RAM	32 GiB	8 GB

Technical prerequisites – software

Tab. SI III / 1: Software required for operating the DOC application

Operating system / program / package	Version
Linux Ubuntu	18.04.4 LTS
Linux Mint	19.1
CUDA	10.0.130
Python	3.6.8
CUDNN	7.2.1
Dplython	0.0.7
Keras	2.2.4
NumPy	1.17.4
Pandas	0.23.4
Pillow	5.4.1
SciPy	1.1.0
Tensorflow	1.12.0
TkInter	8.6

Hyperparameter settings of the classifier model

Tab. SI IV / 1: Hyper-parameter settings of the CNN used in the DOC pipeline

Parameter	Setting
learning rate	0.0001
learning-rate decay rate	0.001
optimizer	Adam (Kingma & Ba, 2014)
loss function	categorical cross-entropy
batch size	20
image size	120 x 120 pixels
distribution for initial CNN-parameter values	Glorot uniform (Glorot & Bengio, 2010)
VGG16 initial parameter values	ImageNet weights

Tab. SI V / 2: Details on the CNN architecture (nomenclature follows that used in the Keras API (Chollet, 2015)).

layer type	units	kernel_size	strides	activation
pre-trained base (VGG16)	-	-	-	-
Conv2D	1000	1 x 1	1	relu
Flatten	-	-	-	-
Dense	number of classes * 30	-	-	relu
Dense	number of classes	-	-	softmax


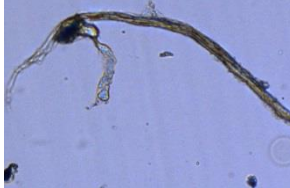


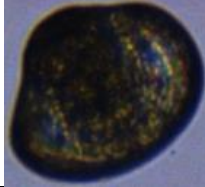



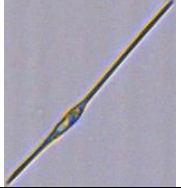

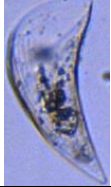


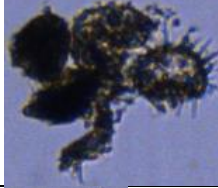




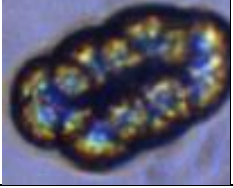
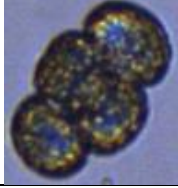

Unfreezing scheme and model architecture

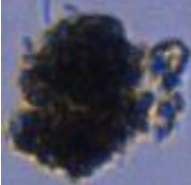
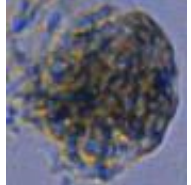
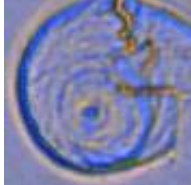


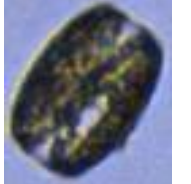
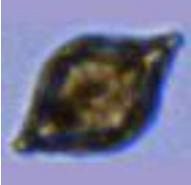

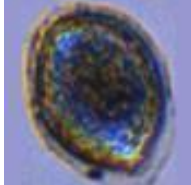
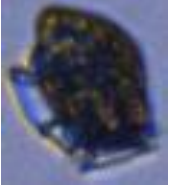

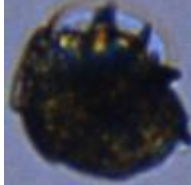

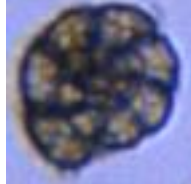
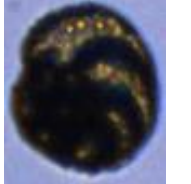
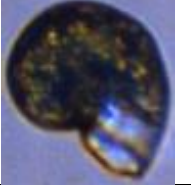
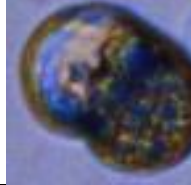
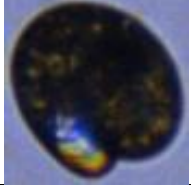

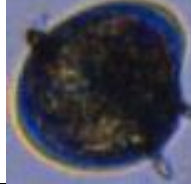
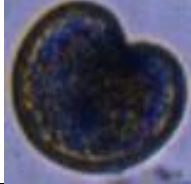



Tab. SI V / 1: Unfreezing scheme of the CNN layers used in the DOC pipeline. Blue = frozen layer, red = unfrozen layer.

Layer	Epoch 1	Epoch 2	Epoch 3	Epoch 4	Epoch 5	Epoch 6	Epoch 7	Epoch 8
block1-conv1	Blue	Blue	Blue	Blue	Blue	Blue	Blue	Blue
block1-conv2	Blue	Blue	Blue	Blue	Blue	Blue	Blue	Blue
block2-conv1	Blue	Blue	Blue	Blue	Blue	Blue	Blue	Blue
block2-conv2	Blue	Blue	Blue	Blue	Blue	Blue	Blue	Green
block3-conv1	Blue	Blue	Blue	Blue	Blue	Green	Blue	Green
block3-conv2	Blue	Blue	Blue	Blue	Green	Green	Blue	Green
block3-conv3	Blue	Blue	Blue	Green	Green	Green	Blue	Green
block4-conv1	Blue	Blue	Green	Green	Green	Green	Blue	Green
block4-conv2	Blue	Green	Green	Green	Green	Green	Blue	Green
block4-conv3	Green	Green	Green	Green	Green	Green	Blue	Green
block5-conv1	Green	Green	Green	Green	Green	Green	Blue	Green
block5-conv2	Green	Green	Green	Green	Green	Green	Blue	Green
block5-conv3	Green	Green	Green	Green	Green	Green	Blue	Green
convolutional layer	Green	Green	Green	Green	Green	Green	Green	Green
dense layer #1	Green	Green	Green	Green	Green	Green	Green	Green
dense layer #2	Green	Green	Green	Green	Green	Green	Green	Green

Properties of the training images

Tab. SI VI / 1: Properties of the baseline training dataset used to train the baseline model in the DOC pipeline

Class	Number of images ¹	Number of training images	Example image	Example image	Example image
Appendicularians	200	160			
Bivalves	500	400			
<i>Ceratium</i> spp.	1500	1200			
Ciliates	1000	800			
Clumps	2000	1600			
Copepods	4000	3200			
Copepod egg clumps	200	160			

Detritus	9000	7200			
Diatoms	4500	3600			
Other dinoflagellates	500	400			
<i>Dinopysis</i> spp.	500	400			
Foraminifera	500	400			
Gastropods	2000	1600			
<i>Protoperdinium</i> spp.	1000	800			
Silicoflagellates	500	400			

¹before setting aside validation and test images

Training-performance trajectories of baseline model

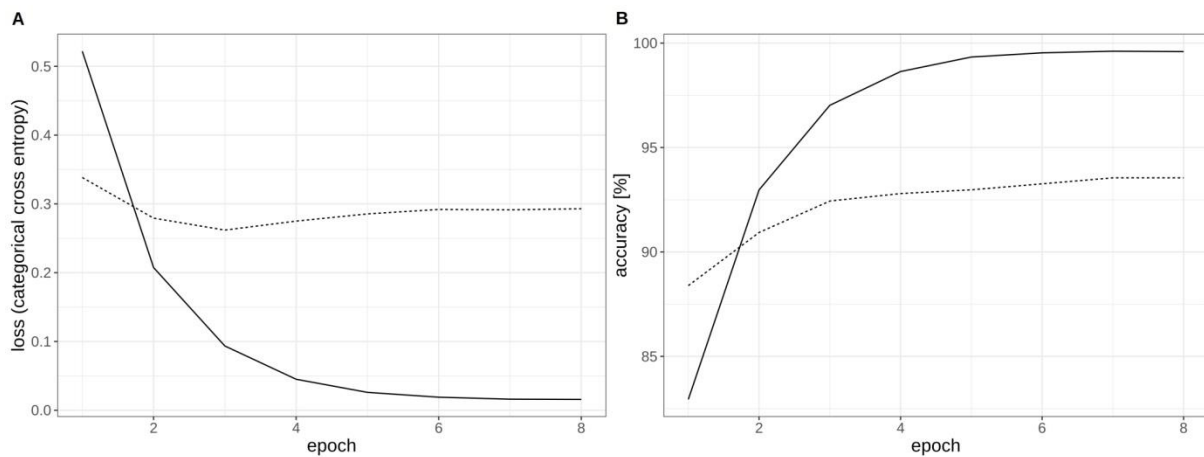


Fig. SI VII / 1: Loss trajectories (a) and accuracy trajectories (b) for the baseline model while being trained and validated on the respective baseline image data sets. Solid line indicates training loss / accuracy, dotted line indicates validation loss / accuracy.

SI VIII Observed and predicted class-specific relative abundances with baseline model

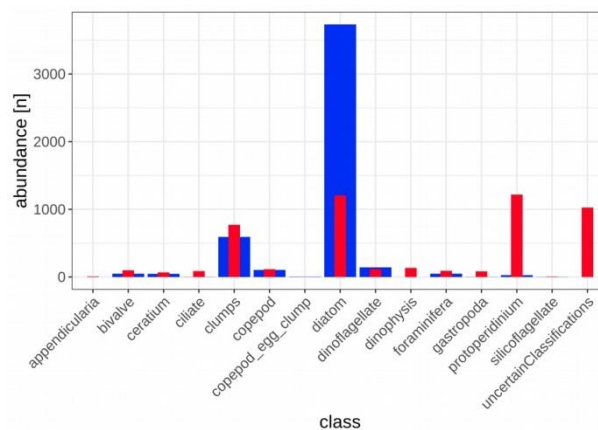


Fig. SI VIII / 1: Observed (blue) and predicted (red) abundances of plankton taxa in the first two stations of the December survey. Predictions done with the baseline classifier model.

Comparison of exclusive training-set adaptation and exclusive threshold adaptation

In order to analyze the effects of training-set updates (and training new classification models on the updated training sets) and reduction of classification thresholds in isolation, we performed two separate classification runs for the September-survey plankton samples. In the first, we updated the training set based on class-specific miss-classification rates and trained a new classification model on the updated set, but did not change the classification thresholds (thus, they remained at 0.6 for each class over all adaptation steps). In the second classification run, we updated the classification thresholds as described in the Materials & Methods section, but did not update the training set; in effect, we used the baseline model together with changing classification thresholds for all survey samples. Weighted-mean recall and weighted-mean precision (see Material & Methods section for a description of the averaging procedure) were calculated for each pair of plankton samples for both classification runs. The resulting performance trajectories were compared to the fully-adaptive (where both

the training set and thresholds were constantly updated) and to the non-adaptive classification run (where neither the training set nor the thresholds were adapted).

Analysis of the four trajectories showed that solely updating the training set yielded higher precision, and that solely updating the thresholds yielded higher recall (in some samples), than the combined approach (fig. SI IX / 1). However, recall was lower in the former approach, while precision was lower in the latter approach, compared to the combination of updating the training set and updating the thresholds.

We concluded that the combined approach yields the best trade-off between maintaining relatively high recall and maintaining relatively high precision, and therefore incorporated it into the DOC pipeline.

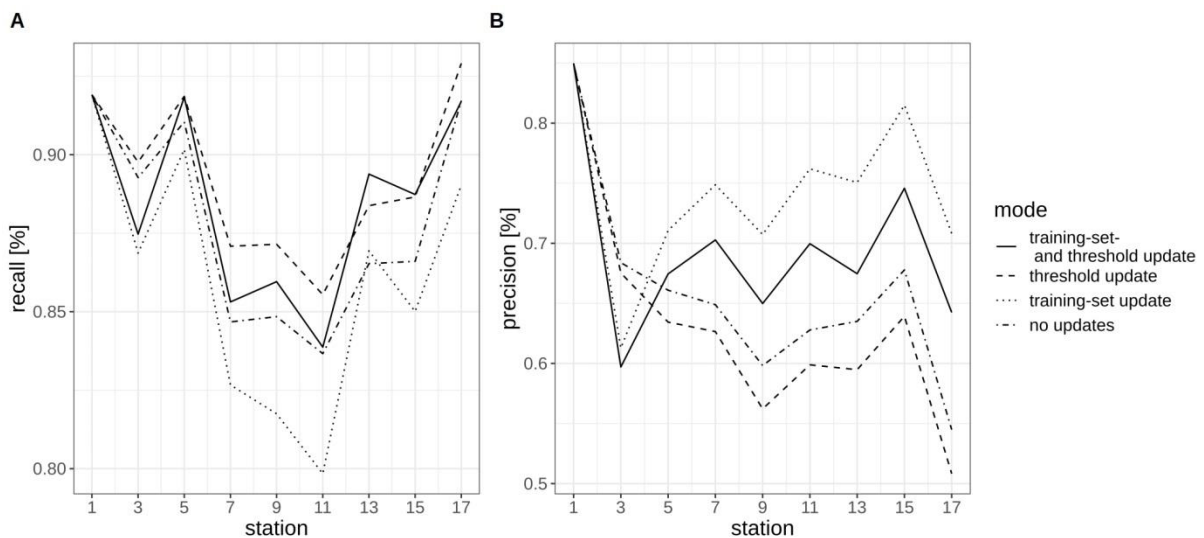


Fig. SI IX / 1: Recall (**A**) and precision (**B**) trajectories for different combinations of training-set updates and threshold updates.

Extended plots of classification performance

The following figures show performance trajectories for all nine differently adapted models over all 18 survey samples, whereas the figures in the main text only show a selection of models.

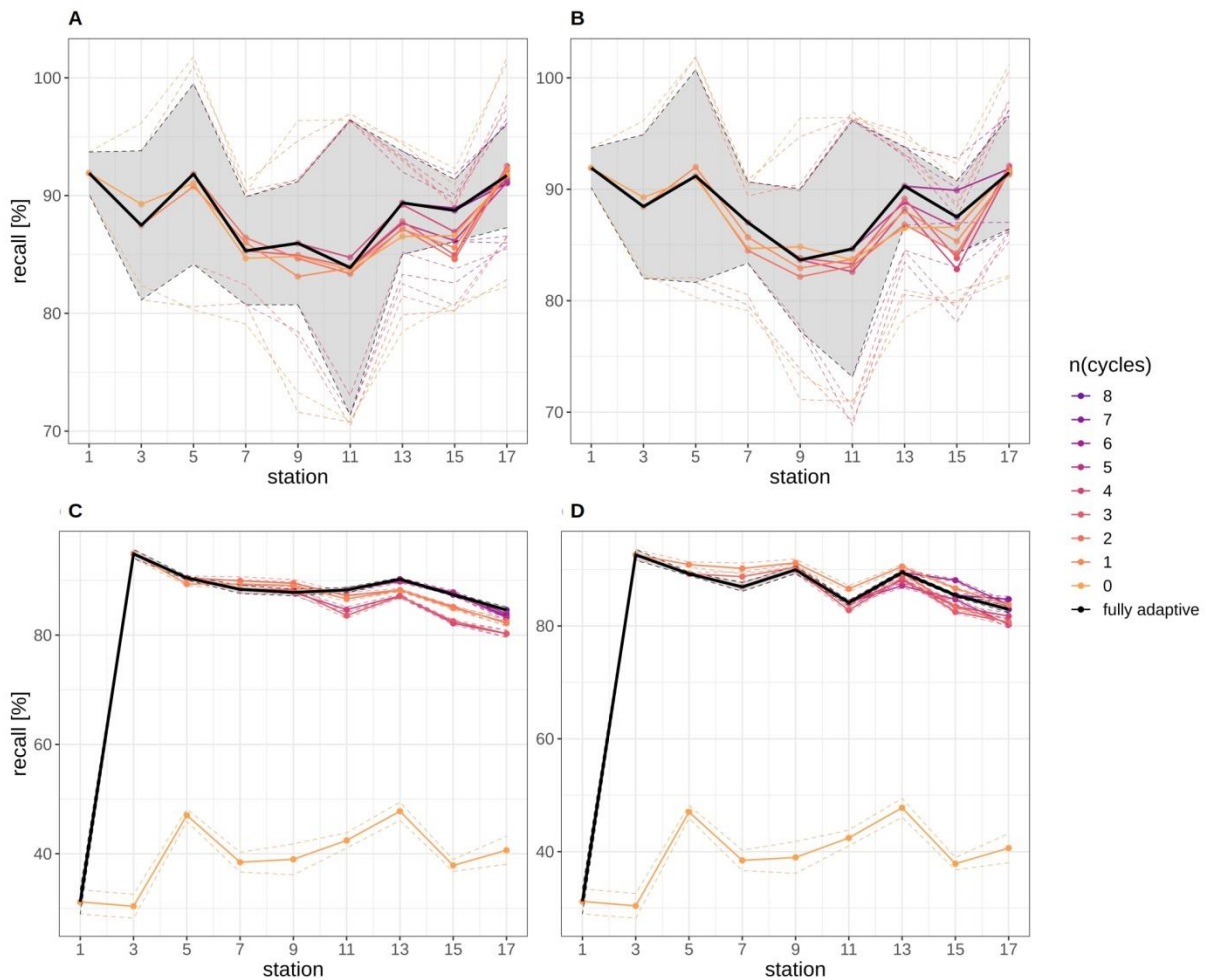


Fig. SI X / 1: Recall trajectories for different modes of adaptation using the DOC. Solid black line represents weighted mean of the fully-adaptive implementation, grey area denotes the corresponding weighted standard deviation. Colored solid and dashed lines represent weighted mean and weighted standard deviation of less-adaptive implementations (denoted by the number of adaptation cycles). (**A**, **B**): September survey; (**C**, **D**): December survey. Results for two replicates are shown for each survey. Note that weighted standard deviation for the fully-adaptive implementation in the December survey was not omitted, but is very small compared to that in the September survey.

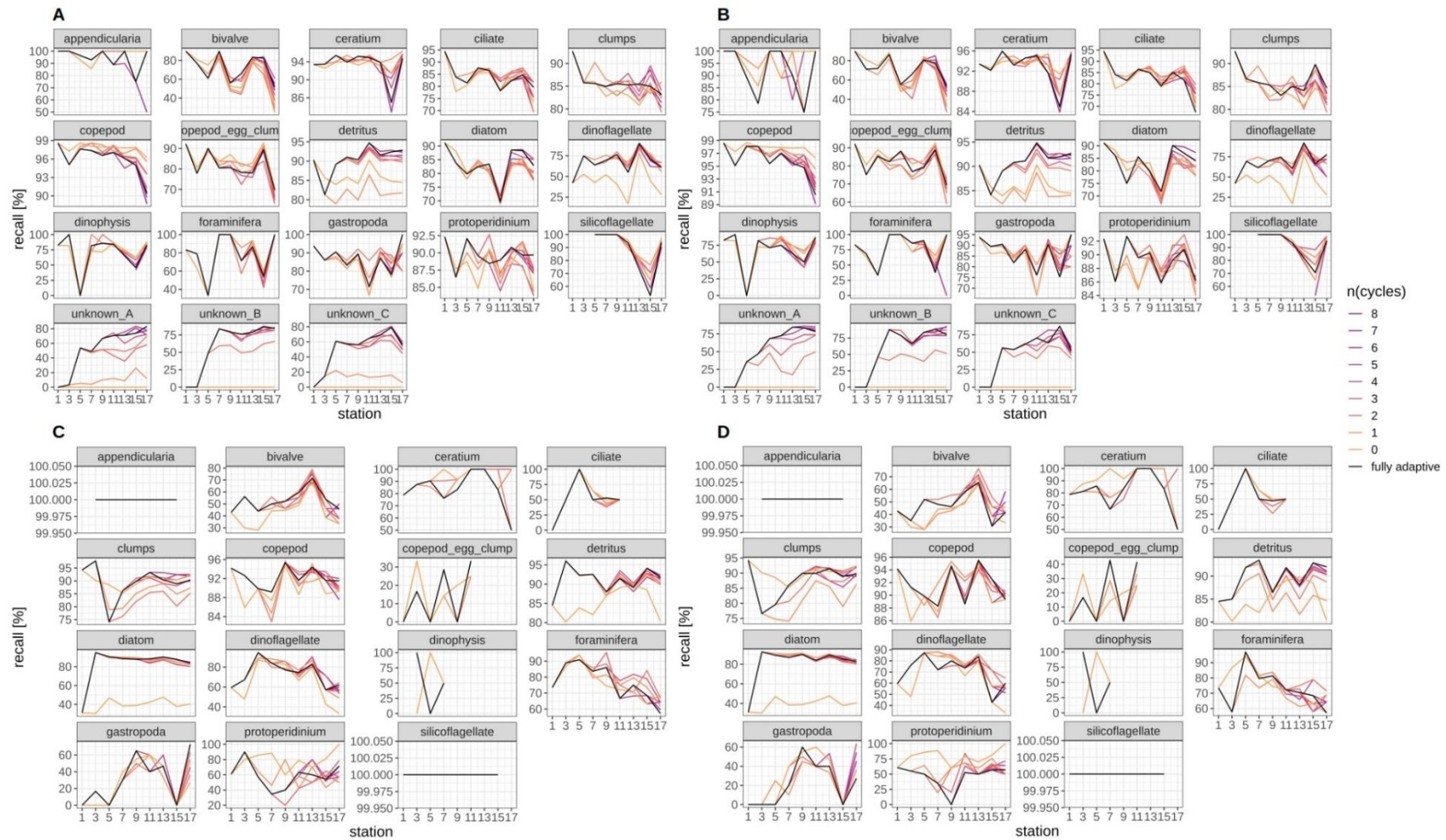


Fig. SI X / 2: Class-specific recall for the September (**A**, **B**) and December (**C**, **D**) surveys. Results for two replicates are shown for each survey. Black line represents fully adaptive DOC implementation (training-set update every second station); colored lines represent less-adaptive implementations (denoted by the number of adaptation cycles).

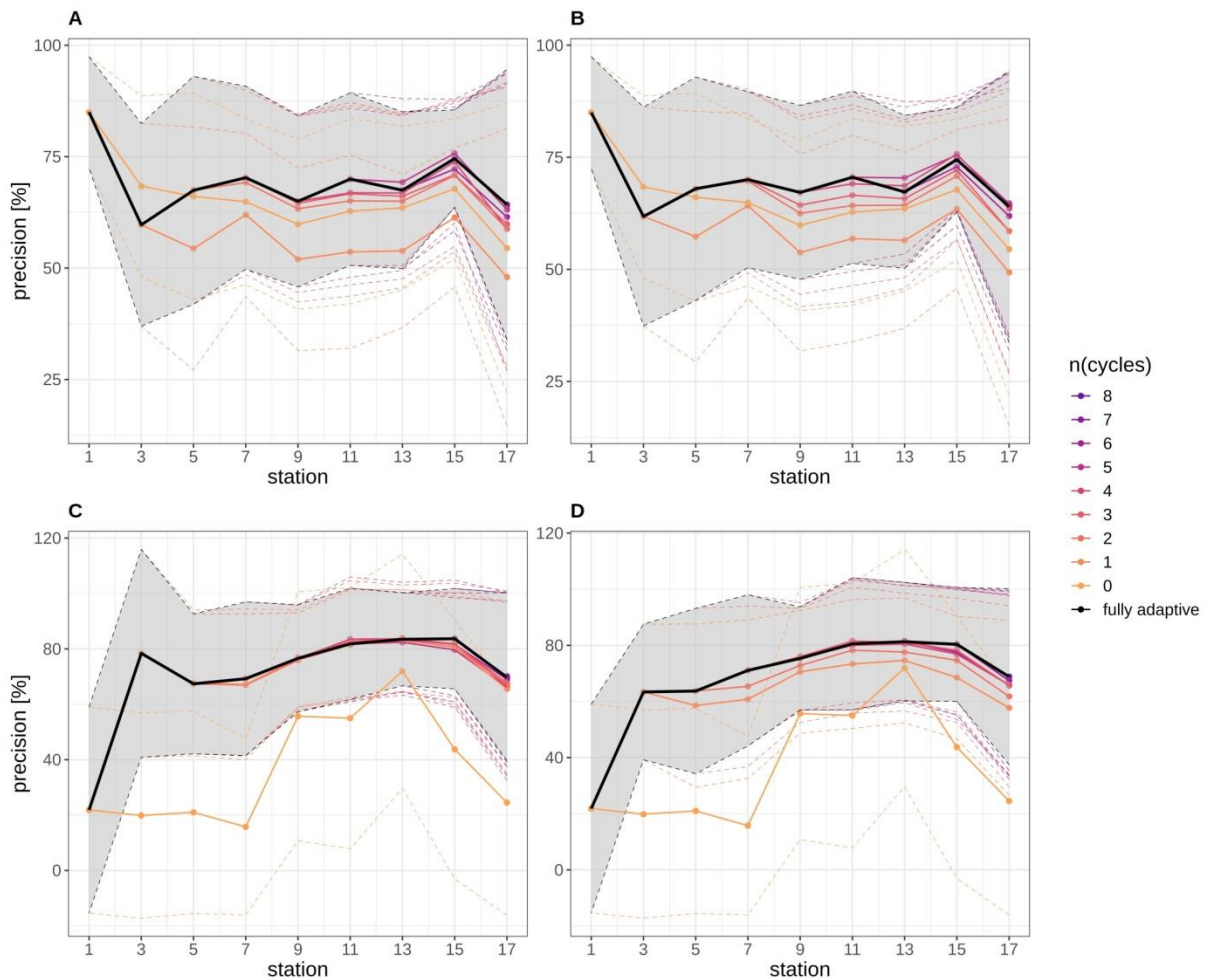


Fig. SI X / 3: Precision trajectories for different modes of adaptation using the DOC. Solid black line represents weighted mean of the fully-adaptive implementation, grey area denotes the corresponding weighted standard deviation. Colored solid and dashed lines represent weighted mean and weighted standard deviation of less-adaptive implementations (denoted by the number of adaptation cycles). (A, B): September survey; (C, D): December survey. Results for two replicates are shown for each survey.

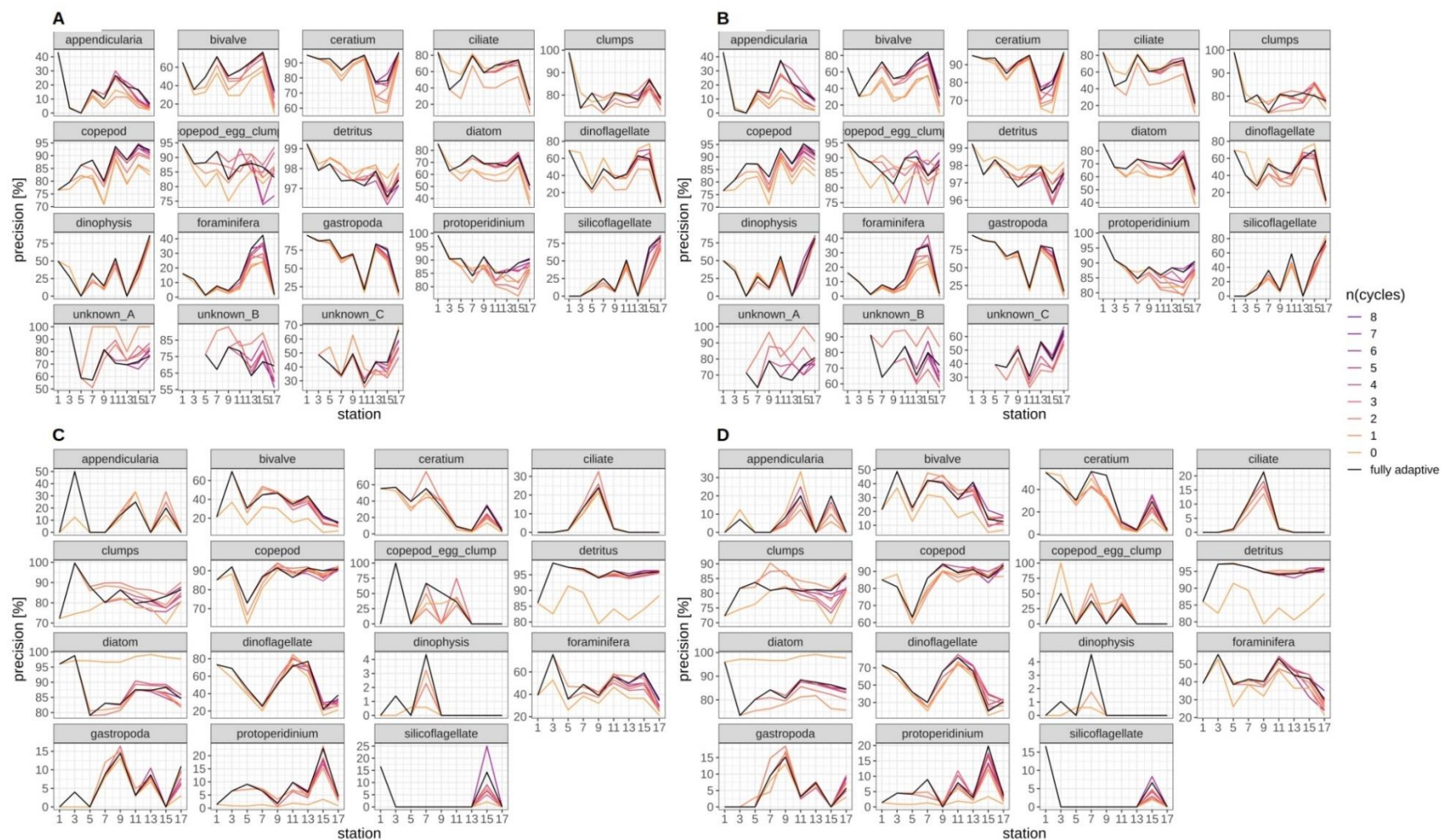


Fig. SI X / 4: Class-specific precision for the September (**A, B**) and December (**C, D**) surveys. Results for two replicates are shown for each survey. Black line represents fully adaptive DOC implementation (training-set update every second station); colored lines represent less-adaptive implementations (denoted by the number of adaptation cycles). Results for two replicates are shown for each survey.

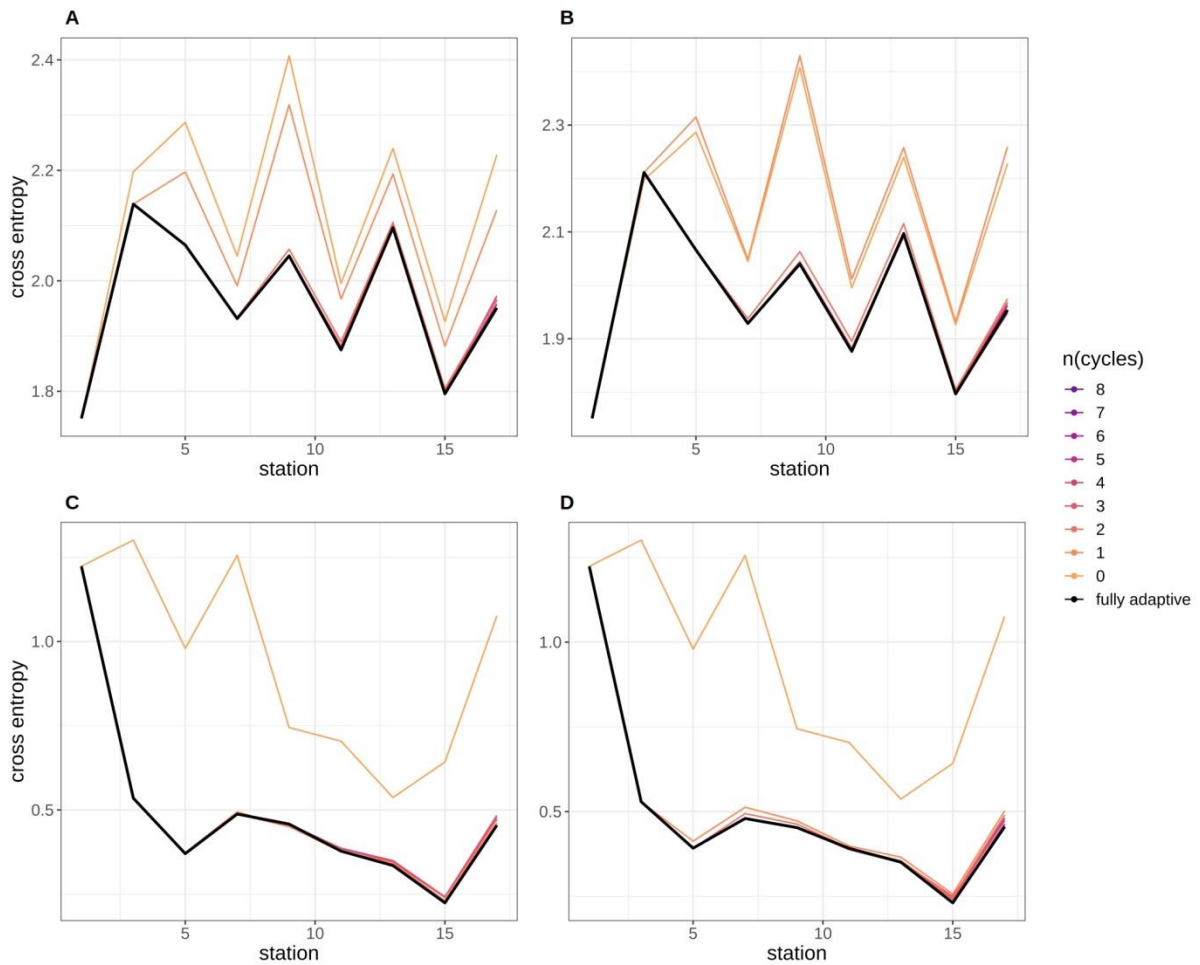


Fig. SI X / 5: Cross-entropy trajectories for different modes of adaptation using the DOC. Solid black line represents weighted mean of the fully-adaptive implementation, grey area denotes the corresponding weighted standard deviation. Colored solid and dashed lines represent weighted mean and weighted standard deviation of less-adaptive implementations (denoted by the number of adaptation cycles). (A, B): September survey; (C, D): December survey. Results for two replicates are shown for each survey.

Supplements Chapter 3

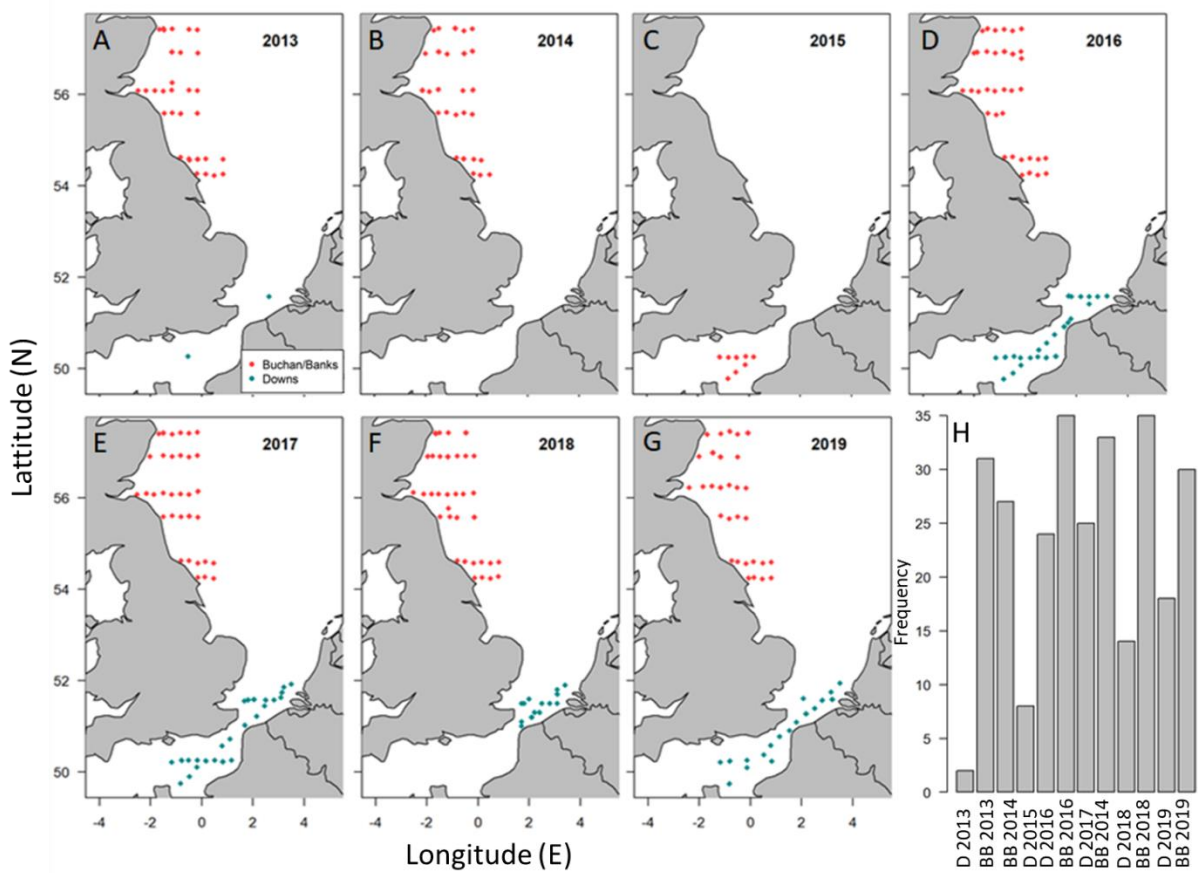


Fig. S1. Map of stations per year (panels A-G) from the International Herring Larval Survey in the Buchan/Banks (September, red dots) and Downs spawning grounds (December, cyan dots) analyzed in this study. H) shows the number of stations per spawning ground (BB= Buchan/Banks, D= Downs) and year. Note that there was no data available for Downs in 2014 and in Buchan/Banks in 2015.

Table S1. Taxa-specific coefficients used for estimating biomass B of individual zooplankters as a function of their biovolume BV: $\log_{10}B = a + b \cdot \log_{10}BV$. Note that a and b were adjusted to the units of B[μgC] and BV[μm^3] used in this study.

Taxa	a	b	Reference
Diatoms (<3000 μm)	-6.54	0.811	Menden-Deuer & Lessard (2000)
Diatoms ($\geq 3000 \mu\text{m}$), phytoplankton	-6.93	0.811	
ciliate tripos dinoflagellate protoperidinium dinophysis silicoflagellate foraminifera	-6.29	0.88	Kiørboe (2013)
copepods	-6.48	0.95	
cladocera malacostraca	-5.85	0.92	
appendicularia chaetognatha polychaeta	-8.49	1.08	
bivalves gastropods	-5.64	0.83	
jellies	-7.22	0.98	
echinodermata	-6.42	0.94	

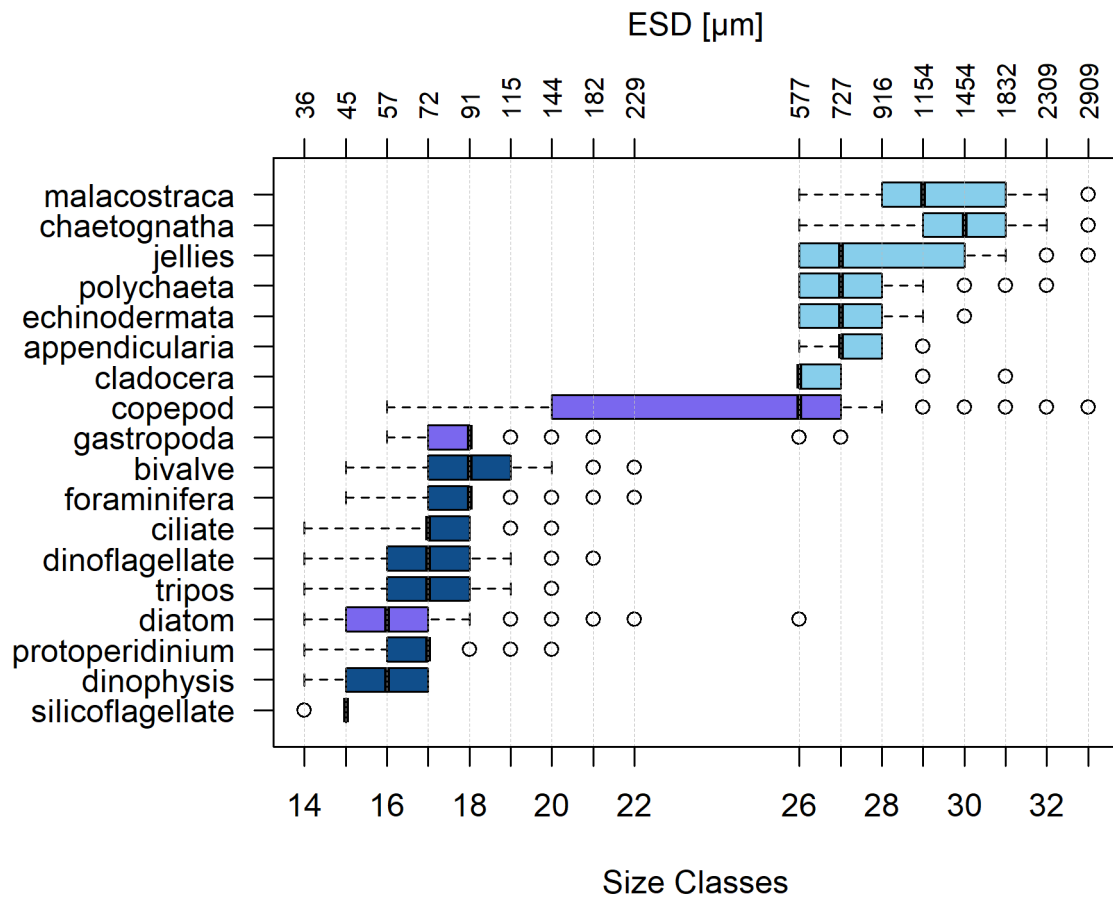


Fig. S2. Size classes for the different taxa analyzed using the FlowCAM (dark blue), the ZooSCAN (light blue) or both (purple) in descending order. Sizes classes are based on the biovolume, using an octave scale with the top y-axis representing the size as equivalent spherical diameter (ESD). The box represents the inter-quartile ranges (IQR), the circles are the outliers, detected as higher or below quartiles $\pm 1.5 \times \text{IQR}$, and the dashed lines shows the maximum/minimum values without outliers.

Table S2. SIMilarity PERcentage (SIMPER) results for Downs and Buchan/Banks plankton communities, showing the most important taxa sets contributing to the dissimilarities between both groups. Reported results include Taxa sets average contribution to overall dissimilarity (average), standard deviation of contribution (sd), Average to sd ratio (ratio), Average abundances per group (ava, avb), ordered cumulative contribution (cumsum), taxa sets contribution in to overall abundance (contrib%) with the statistical significance ($p = 0$ '****' 0.001 '***' 0.01 '**' 0.05 '.' 0.1 " 1).

	Average	Contribution SD	Ratio Average/SD	Average abund. Downs	Average abund. Buchan/Banks	Cumulative contribution	Contribution to overall abundance (%)
tripos	0.03	0.02	1.90	2.23	5.05	0.13	12.94**
dinophysis	0.03	0.01	2.00	1.56	4.29	0.25	12.47**
silicoflagellate	0.03	0.01	2.20	0.52	3.16	0.37	11.86**
ciliate	0.02	0.01	1.84	1.77	3.86	0.47	9.69**
protopteridium	0.02	0.01	2.17	3.06	4.74	0.55	7.71**
gastropoda	0.02	0.01	2.63	2.35	4.00	0.62	7.54**
cladocera	0.01	0.01	1.32	1.18	2.13	0.67	4.55**
diatom	0.01	0.01	1.31	5.45	5.55	0.71	3.96
jellies	0.01	0.00	2.30	1.47	2.32	0.75	3.85**
copepod	0.01	0.01	1.38	3.71	4.51	0.78	3.77**
echinodermata	0.01	0.01	1.37	1.16	1.97	0.82	3.71**
malacostraca	0.01	0.00	2.57	1.62	2.40	0.86	3.56**
appendicularia	0.01	0.01	0.94	1.29	1.86	0.89	3.02*
foraminifera	0.01	0.00	1.68	2.95	2.28	0.92	2.99**
polychaeta	0.01	0.00	2.03	1.06	1.64	0.94	2.54**
chaetognatha	0.01	0.00	1.34	1.88	2.36	0.96	2.24**
dinoflagellate	0.00	0.00	1.05	3.07	3.34	0.98	1.91
bivalve	0.00	0.00	1.03	3.09	3.26	1.00	1.69
Permutation: free		Number of permutations: 999	overall: 0.227				

Water temperature in the Buchan/Banks area varied between 10 and 15 °C and was generally higher close to the coast than at more offshore stations. As for the Downs area, the warmest water ($T > 12$ °C) was observed in the southwestern stations and temperature decreased to 7-9 °C toward northeast (Fig. S4A). Salinity above 35 was observed at the northern offshore stations and gradually decreased to 34.4 to the south and toward the coast (Fig. S4B). Salinity in Downs varied between 33 and 35.5 and the strongest differences in salinity were observed between off- and inshore stations (Fig. S4B). An exceptionally low salinity < 34.6 was observed everywhere in this area in September 2016. Highest turbidity was found in the northern coastal stations with a decrease towards offshore and the south (Fig. S4C). Maximum larval herring abundances were comparable across both spawning grounds (206.7 Ind m^{-3} in Buchan/Banks vs 193.4 Ind m^{-3} in Downs), although average larval abundances were generally higher in September (Fig. S4D).

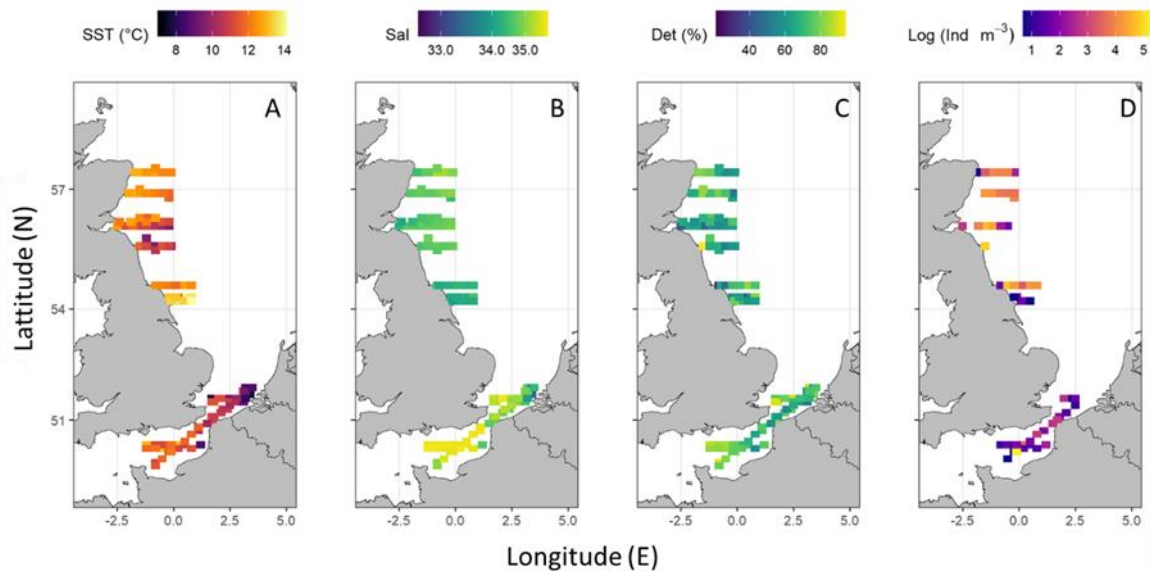


Fig. S3. Mean variability of the environmental variables across the sampling period (2013-2019) in the Buchan/Banks area (September) and Downs (December). (A) mean temperature (SST (°C)), (B) mean salinity (Sal), (C) relative turbidity (%) and (D) logarithmic larval herring abundance (Log (Ind m^{-3})).

Table S3: Plankton abundance (Ind x10² m⁻³) per year as total mesozoo (MesoZP) and microplankton (MicroZP) and by taxa in Buchan/Banks (BB) as minimum (min), maximum (max), average values (mean) as well as the overall average and the relative abundance (%).

taxa	BB 2013 Ind x10 ² m ⁻³			BB 2014 Ind x10 ² m ⁻³			BB 2016 Ind x10 ² m ⁻³			BB 2017 Ind x10 ² m ⁻³			BB 2018 Ind x10 ² m ⁻³			BB 2019 Ind x10 ² m ⁻³			Overall Ind x10 ² m ⁻³	
	min	max	mean	min	max	mean	min	max	mean	min	max	mean	min	max	mean	min	max	mean	mean	%
tripos	1.604	879.728	306.738	0.443	574.087	266.405	52.426	6092.999	603.918	13.347	3821.122	826.395	3.175	363.461	132.135	2.563	326.172	149.271	380.810	25.664
ciliate	0.636	114.102	38.820	1.060	111.856	48.535	0.237	181.919	78.125	0.795	19.461	11.136	0.402	57.440	21.227	0.327	142.763	57.523	42.561	3.859
diatom	0.017	499.915	178.483	5.654	107.273	47.135	16.656	6407.280	1066.146	19.943	729.860	169.547	8.051	1436.507	552.772	10.605	1878.529	393.493	401.263	36.379
dinoflagellate	0.330	79.081	18.823	0.186	9.487	4.546	0.922	35.343	14.407	0.421	16.554	6.018	0.084	32.185	8.374	0.189	18.898	5.031	9.533	0.864
dinophysis	0.155	27.147	11.148	2.191	2805.928	714.064	13.952	2919.773	390.431	0.146	193.086	119.690	0.166	218.720	110.660	0.077	59.922	27.177	228.862	20.749
foraminifera	0.082	2.797	0.823	0.030	0.379	0.173	0.237	3.315	1.590	0.092	1.579	0.798	0.075	0.800	0.369	0.036	9.827	3.878	1.272	0.115
protoperidinium	1.584	122.162	34.940	6.998	683.836	265.745	8.850	952.982	263.183	26.560	1102.321	190.225	1.361	128.444	74.756	5.341	138.371	63.067	148.653	13.477
silicoflagellate	0.120	15.026	7.784	0.040	1.884	0.821	0.459	2463.559	849.515	0.108	13.633	5.812	0.052	11.762	3.802	0.031	14.062	3.209	145.157	13.160
bivalve	0.164	13.692	8.207	0.079	32.265	10.914	0.437	30.414	5.100	0.826	36.263	13.597	0.254	12.759	6.412	0.218	15.118	5.737	8.328	0.755
copepod all	10.885	129.801	58.771	7.725	125.973	41.410	13.736	340.826	49.381	17.773	338.698	90.293	9.448	142.357	60.115	16.715	228.490	54.296	59.044	
copepods	1.330	1.210	5.770	0.420	29.330	3.170	1.790	97.510	8.810	0.780	16.030	8.070	0.460	20.340	7.370	0.780	16.030	7.900	6.848	0.621
nauplii	9.002	127.474	59.474	5.334	125.156	44.767	8.831	243.314	41.266	15.595	323.296	83.833	8.005	122.014	53.595	4.674	214.234	47.174	55.018	4.988
gastropoda	0.211	49.016	18.183	0.667	166.561	36.730	0.023	89.452	39.053	0.289	263.202	127.507	2.078	98.628	53.671	0.207	75.444	42.118	52.877	4.794
appendicularia	0.006	0.227	0.117	0.006	0.051	0.031	0.019	1.566	0.225	0.057	0.493	0.231	0.025	0.406	0.176	0.011	0.569	0.264	0.174	0.016
chaetognatha	0.026	0.912	0.371	0.005	2.949	0.470	0.041	2.350	0.422	0.057	1.168	0.533	0.052	1.703	0.644	0.045	0.904	0.513	0.492	0.045
cladocera	0.006	0.152	0.097	0.003	0.155	0.055	0.009	2.350	0.813	0.033	1.851	0.510	0.025	0.992	0.508	0.006	0.650	0.241	0.371	0.034
echinodermata	0.004	0.225	0.073	0.004	0.155	0.027	0.022	1.072	0.305	0.020	0.212	0.084	0.025	1.503	0.626	0.013	0.125	0.094	0.202	0.018
jellies	0.011	1.433	0.616	0.004	0.569	0.289	0.027	5.091	1.044	0.025	0.543	0.292	0.029	1.173	0.631	0.006	0.824	0.456	0.555	0.050
malacostraca	0.034	1.478	0.553	0.008	3.104	0.432	0.036	3.916	0.429	0.033	0.617	0.321	0.103	6.291	2.147	0.040	2.074	0.710	0.765	0.069
polychaeta	0.006	0.094	0.045	0.002	0.013	0.007	0.012	0.268	0.141	0.020	0.209	0.095	0.028	0.109	0.060	0.011	0.100	0.062	0.068	0.006
Total	64.592	1360.076	355.815	36.517	3900.380	863.677	124.786	19273.796	1769.658	142.587	5589.444	902.573	73.445	1609.013	544.307	70.304	2312.206	402.071	806.350	100.000
MesoZP	2.019	13.943	7.610	0.793	37.816	4.229	3.441	112.784	10.598	1.144	19.863	10.172	2.534	29.104	12.617	1.043	16.013	8.901	9.021	1.102
MicroZP	58.625	1354.473	373.685	35.103	3897.262	893.376	118.128	19161.011	1754.796	136.944	5571.008	901.230	61.548	1600.171	539.057	57.569	2296.194	396.351	809.749	98.898

Table S4: Plankton abundance (Ind x10² m⁻³) per year as total mesozoo (MesoZP) and microplankton (MicroZP) and by taxa in Downs (Dow) as minimum (min), maximum (max), average values (mean) as well as the overall average and the relative abundance (%).

taxa	DOW 2013 Ind x10 ² m ⁻³			DOW 2015 Ind x10 ² m ⁻³			DOW 2016 Ind x10 ² m ⁻³			DOW 2017 Ind x10 ² m ⁻³			DOW 2018 Ind x10 ² m ⁻³			DOW 2019 Ind x10 ² m ⁻³			Overall Ind x10 ² m ⁻³	
	min	max	mean	min	max	mean	min	max	mean	min	max	mean	min	max	mean	min	max	mean	mean	%
tripos	0.000	0.000	0.000	1.542	28.171	18.243	0.055	1.940	0.818	0.221	1.448	0.752	0.098	98.295	53.854	0.298	6.159	3.082	12.792	1.435
ciliate	0.000	0.000	0.000	0.567	0.729	0.675	0.113	0.405	0.259	0.118	2.070	1.038	0.102	9.215	4.690	0.115	5.643	4.246	1.818	0.204
diatom	331.802	658.078	474.114	231.327	1030.379	692.146	58.461	1367.317	485.295	28.267	1137.300	312.299	56.989	3158.959	1207.245	78.177	8045.778	1540.732	785.305	88.119
dinoflagellate	1.446	8.025	5.948	3.822	18.781	9.924	0.051	19.638	7.590	0.118	12.935	5.593	0.186	23.617	8.591	1.382	157.027	24.104	10.292	1.155
dinophysis	0.000	0.000	0.000	0.671	3.426	1.960	0.069	0.130	0.096	0.074	0.781	0.507	0.098	0.512	0.325	0.079	0.684	0.382	0.545	0.061
foraminifera	3.132	12.964	9.205	0.849	12.073	5.942	0.720	13.665	4.749	0.265	13.417	3.525	0.116	10.262	3.446	1.422	74.775	15.479	7.058	0.792
protoperidinium	3.704	3.704	3.704	1.082	24.146	13.219	0.257	13.092	6.103	0.106	70.684	23.848	0.279	56.315	17.627	0.145	52.268	17.875	13.729	1.541
silicoflagellate	0.000	0.000	0.000	0.000	0.000	0.000	0.055	0.214	0.135	0.106	0.414	0.311	0.000	0.000	0.000	0.000	0.000	0.000	0.074	0.008
bivalve	0.964	10.495	8.679	0.425	11.403	6.910	0.626	59.009	19.954	0.132	19.609	5.896	1.217	41.980	14.824	1.012	49.655	14.350	11.769	1.321
copepod all	7.329	43.870	28.073	12.525	22.621	17.045	2.774	102.816	47.755	2.445	92.272	37.949	0.285	89.805	19.874	1.895	411.930	72.793	37.248	
copepods	0.340	3.120	1.900	0.090	0.260	0.190	0.270	18.540	6.480	0.010	11.690	5.980	0.280	4.020	2.330	0.060	24.880	3.850	3.455	0.388
nauplii	6.988	40.744	30.440	12.316	22.352	16.535	2.490	95.346	44.916	2.322	81.751	33.590	2.839	86.008	23.125	1.827	403.784	79.744	38.058	4.271
gastropoda	0.723	1.235	0.928	0.018	2.835	1.919	0.012	33.173	24.829	0.006	3.104	1.402	0.003	1.024	0.209	0.145	29.957	5.942	5.871	0.659
appendicularia	0.000	0.000	0.000	0.012	0.028	0.021	0.005	0.155	0.094	0.008	0.058	0.025	0.005	0.116	0.051	0.003	0.175	0.026	0.036	0.004
chaetognatha	0.034	0.042	0.041	0.057	0.377	0.203	0.014	0.603	0.249	0.021	0.490	0.165	0.012	0.798	0.263	0.011	0.719	0.124	0.174	0.020
cladocera	0.000	0.000	0.000	0.011	0.056	0.030	0.006	0.472	0.106	0.058	0.058	0.058	0.001	0.005	0.003	0.004	0.140	0.074	0.045	0.005
echinodermata	0.014	0.014	0.014	0.000	0.000	0.000	0.015	0.044	0.029	0.006	0.050	0.027	0.001	0.037	0.015	0.004	0.005	0.004	0.015	0.002
jellies	0.014	0.014	0.014	0.009	0.098	0.048	0.007	0.314	0.095	0.002	0.122	0.057	0.003	0.032	0.016	0.003	0.047	0.014	0.041	0.005
malacostraca	0.001	0.103	0.097	0.009	0.050	0.025	0.011	0.744	0.248	0.002	0.151	0.059	0.002	0.122	0.048	0.003	0.233	0.056	0.089	0.010
polychaeta	0.072	0.072	0.072	0.005	0.005	0.005	0.024	0.024	0.024	0.002	0.023	0.008	0.005	0.012	0.010	0.001	0.001	0.001	0.020	0.002
Total	345.439	738.608	539.080	299.163	1072.556	720.760	65.275	1438.825	515.564	38.497	1209.195	322.990	63.316	3299.240	1161.280	90.778	8810.034	1664.070	820.624	100.000
MesoZP	0.380	3.360	2.020	0.210	0.770	0.460	0.410	19.590	6.560	0.160	11.800	5.880	0.430	5.090	2.540	0.160	25.690	3.850	3.552	0.423
MicroZP	345.050	735.250	522.220	298.800	1072.350	721.490	64.790	1436.230	518.480	37.960	1208.740	337.320	60.570	3294.150	1261.120	90.570	8801.000	1654.400	835.838	99.577

Table S5: Plankton biomass ($\mu\text{gC} \times 10^5 \text{ m}^{-3}$) per year as total mesozoo (MesoZP) and microplankton (MicroZP) and by taxa in Buchan/Banks (BB) as minimum (min), maximum (max), average values (mean) as well as the overall average and the relative biomass (%).

taxa	BB 2013 biomass x 10 ⁵ [$\mu\text{gC} \text{ m}^{-3}$]			BB 2015 biomass x 10 ⁵ [$\mu\text{gC} \text{ m}^{-3}$]			BB 2016 biomass x 10 ⁵ [$\mu\text{gC} \text{ m}^{-3}$]			BB 2017 biomass x 10 ⁵ [$\mu\text{gC} \text{ m}^{-3}$]			BB 2018 biomass x 10 ⁵ [$\mu\text{gC} \text{ m}^{-3}$]			BB 2019 biomass x 10 ⁵ [$\mu\text{gC} \text{ m}^{-3}$]			Overall biomass x10 ⁵ [$\mu\text{gC} \text{ m}^{-3}$]	
	min	max	mean	min	max	mean	min	max	mean	min	max	mean	min	max	mean	min	max	mean	mean	%
ceratium	0.066	5.731	2.800	0.021	11.679	6.477	1.311	69.075	13.650	0.696	140.989	31.429	0.157	12.640	5.855	0.157	5.738	3.018	10.538	1.836
ciliate	0.008	1.548	0.623	0.011	2.405	1.022	0.002	2.982	1.147	0.017	0.669	0.280	0.004	1.288	0.466	0.003	1.834	1.035	0.762	0.133
diatom	0.077	2.180	0.931	0.059	0.779	0.340	0.074	8.026	1.650	0.148	2.078	1.029	0.131	4.438	1.840	0.080	6.708	1.372	1.194	0.208
dinoflagellate	0.002	1.593	0.369	0.002	0.165	0.079	0.019	0.609	0.314	0.017	0.708	0.235	0.001	1.053	0.308	0.003	0.600	0.153	0.243	0.042
dinophysis	0.001	0.271	0.124	0.022	35.074	8.418	0.142	31.276	4.027	0.003	1.976	1.244	0.003	2.222	1.146	0.001	0.703	0.354	2.552	0.445
foraminifera	0.006	0.253	0.063	0.001	0.017	0.008	0.013	0.311	0.147	0.008	0.200	0.101	0.004	0.152	0.054	0.001	0.593	0.248	0.103	0.018
protoperidinium	0.052	2.619	0.941	0.140	15.288	5.669	0.164	29.415	7.669	0.924	23.770	4.941	0.074	6.111	3.298	0.124	5.678	1.900	4.069	0.709
silicoflagellate	0.001	0.077	0.040	0.000	0.009	0.004	0.002	11.729	4.342	0.000	0.065	0.029	0.000	0.054	0.020	0.000	0.071	0.015	0.742	0.129
copepod	110.105	960.274	447.300	88.058	6352.755	497.588	88.183	3087.109	301.596	75.031	792.192	399.639	45.070	1217.366	418.005	52.675	629.873	347.875	402.001	70.048
nauplii	0.960	13.984	6.760	0.767	11.849	4.831	1.100	21.289	5.120	3.071	41.956	13.728	0.863	15.668	8.375	0.735	35.158	7.843	7.776	1.355
appendicularia	0.017	2.853	1.259	0.012	0.438	0.223	0.039	4.058	0.676	0.098	1.526	0.839	0.067	3.588	0.838	0.017	2.936	1.316	0.859	0.150
bivalve	0.009	1.078	0.729	0.019	5.086	2.099	0.011	2.294	0.912	0.155	6.549	3.542	0.138	5.052	2.630	0.033	4.733	1.359	1.878	0.327
chaetognatha	1.827	124.054	23.297	0.298	309.454	49.582	1.316	97.328	18.369	1.889	64.270	23.828	0.750	71.183	28.083	1.521	58.520	24.849	28.001	4.879
cladocera	0.651	13.283	7.680	0.255	10.892	4.288	0.451	154.386	42.938	1.322	88.506	26.023	0.674	52.221	24.518	0.191	34.351	13.742	19.865	3.461
echinodermata	0.039	3.497	1.177	0.044	5.597	1.281	0.251	22.731	6.835	0.290	5.724	1.528	0.244	19.107	7.854	0.139	1.590	1.191	3.311	0.577
gastropoda	2.669	114.962	61.806	0.251	46.411	15.301	0.340	67.482	27.143	0.042	84.885	45.699	2.271	164.790	67.342	0.087	57.816	22.596	39.981	6.967
jellies	0.248	115.236	53.049	0.229	85.849	41.696	0.525	322.749	61.634	0.092	102.782	27.346	0.321	184.972	67.513	0.233	93.755	48.859	50.016	8.715
malacostraca	4.295	1140.332	375.982	9.457	2388.914	286.823	6.994	1198.953	155.940	8.501	466.972	170.315	12.558	560.630	274.665	14.523	728.707	265.081	254.801	44.399
polychaeta	0.131	10.606	4.393	0.038	3.625	0.848	0.189	33.244	9.614	0.049	10.489	2.631	0.176	2.230	0.919	0.027	8.362	3.124	3.588	0.625
Total	293.727	1428.495	634.930	212.820	9183.152	714.039	157.451	5001.189	535.238	125.625	1261.100	630.217	133.308	1522.093	684.771	145.271	1029.727	522.069	620.211	100.000
MesoZP	283.745	1417.307	671.586	190.603	9176.340	799.427	147.898	4843.293	519.487	103.965	1201.827	555.921	124.444	1503.394	699.219	141.529	1020.754	515.486	626.854	96.177
MicroZP	1.751	29.021	11.374	1.819	65.208	21.469	3.580	157.895	29.297	12.337	211.157	48.728	5.349	41.037	22.383	2.916	50.375	16.233	24.914	3.823

Table S6: Plankton biomass ($\mu\text{gC} \times 10^5 \text{ m}^{-3}$) per year as total mesozoo (MesoZP) and microplankton (MicroZP) by taxa in Downs (Dow) as minimum (min), maximum (max), average values (mean) as well as the overall average and the relative biomass (%).

taxa	Dow 2013			Dow 2015			Dow 2016			Dow 2017			Dow 2018			Dow 2019			Overall			
	biomass $\times 10^5$ [$\mu\text{gC} \text{ m}^{-3}$]			biomass $\times 10^5$ [$\mu\text{gC} \text{ m}^{-3}$]			biomass $\times 10^5$ [$\mu\text{gC} \text{ m}^{-3}$]			biomass $\times 10^5$ [$\mu\text{gC} \text{ m}^{-3}$]			biomass $\times 10^5$ [$\mu\text{gC} \text{ m}^{-3}$]			biomass $\times 10^5$ [$\mu\text{gC} \text{ m}^{-3}$]			biomass $\times 10^5$ [$\mu\text{gC} \text{ m}^{-3}$]			
	min	max	mean	min	max	mean	min	max	mean	min	max	mean	min	max	mean	min	max	mean	min	max	mean	mean
ceratium	0.000	0.000	0.000	0.034	0.690	0.413	0.002	0.049	0.021	0.003	0.022	0.016	0.001	3.387	1.731	0.007	0.135	0.072	0.375	0.234		
ciliate	0.000	0.000	0.000	0.002	0.013	0.009	0.003	0.003	0.003	0.001	0.046	0.029	0.001	0.243	0.126	0.001	0.219	0.162	0.055	0.034		
dinophysis	0.000	0.000	0.000	0.008	0.061	0.029	0.001	0.002	0.001	0.001	0.010	0.006	0.001	0.008	0.004	0.001	0.006	0.004	0.007	0.005		
silicoflagellate	0.000	0.000	0.000	0.000	0.000	0.000	0.000	0.001	0.001	0.000	0.003	0.002	0.000	0.000	0.000	0.000	0.000	0.000	0.000	0.000		
protoperidinium	0.055	0.055	0.055	0.024	0.619	0.333	0.004	0.221	0.094	0.001	1.765	0.549	0.003	1.829	0.459	0.002	1.008	0.350	0.307	0.191		
dinoflagellate	0.014	0.125	0.090	0.120	0.503	0.311	0.001	0.704	0.298	0.003	0.369	0.148	0.009	0.559	0.200	0.037	5.777	0.702	0.291	0.181		
foraminifera	0.074	0.327	0.231	0.026	0.532	0.213	0.024	0.673	0.199	0.004	0.578	0.157	0.004	0.313	0.115	0.201	7.938	1.629	0.424	0.264		
bivalve	0.164	0.829	0.703	0.036	1.234	0.787	0.134	8.092	2.765	0.020	2.906	0.929	0.113	7.307	2.063	0.148	9.458	2.079	1.554	0.967		
diatom	0.945	2.422	1.589	0.977	3.282	2.419	0.156	5.376	2.052	0.140	4.397	1.621	0.237	10.506	4.585	0.472	57.347	9.420	3.614	2.249		
gastropoda	0.070	0.102	0.083	0.014	0.344	0.242	0.030	2.922	2.209	0.013	0.245	0.144	0.025	0.275	0.148	0.009	3.354	0.679	0.584	0.363		
copepod	7.611	67.624	41.680	4.128	9.232	6.260	5.612	409.641	142.965	2.393	302.708	147.944	9.366	224.708	96.920	2.278	687.327	109.899	90.945	56.596		
nauplii	0.796	3.947	2.985	1.144	3.200	1.838	0.271	13.102	4.867	0.260	10.540	4.205	0.269	14.068	3.302	0.151	76.378	13.177	5.063	3.150		
appendicularia	0.000	0.000	0.000	0.025	0.070	0.050	0.009	1.004	0.429	0.016	0.206	0.085	0.017	0.342	0.154	0.007	0.419	0.087	0.134	0.084		
cladocera	0.000	0.000	0.000	0.266	2.928	1.238	0.269	45.977	6.602	3.803	3.803	3.803	0.030	0.157	0.123	0.094	4.545	2.378	2.357	1.467		
polychaeta	0.238	0.238	0.238	0.008	0.008	0.008	0.040	0.040	0.040	0.004	0.935	0.325	0.017	1.147	0.404	0.016	0.016	0.016	0.172	0.107		
echinodermata	0.415	0.415	0.415	0.000	0.000	0.000	0.271	1.119	0.702	0.106	1.596	0.594	0.047	0.957	0.462	0.404	0.472	0.438	0.435	0.271		
chaetognatha	1.054	1.949	1.857	1.494	7.367	5.144	0.226	31.198	10.609	0.396	14.959	5.602	0.661	30.023	10.557	0.203	37.208	4.186	6.326	3.937		
jellies	2.842	2.842	2.842	0.043	0.793	0.388	0.056	32.714	7.991	0.024	16.368	5.772	0.022	0.409	0.167	0.019	17.709	4.760	3.653	2.274		
malacostraca	1.663	26.896	25.318	2.387	24.875	12.238	0.484	417.046	123.733	0.226	230.418	73.543	0.458	50.373	19.294	1.491	25.931	12.228	44.392	27.626		
Total	12.490	102.929	57.032	18.929	37.903	26.357	19.108	845.942	137.836	7.296	485.217	134.862	24.555	255.310	137.275	10.027	755.302	112.977	101.057	100.000		
MesoZP	10.430	95.122	56.927	13.094	33.815	21.421	17.627	835.662	195.621	6.246	482.677	193.709	18.300	232.038	106.432	2.797	707.839	109.431	113.923	50.714		
MicroZP	2.060	7.807	4.670	3.032	6.651	5.276	0.810	25.031	6.906	0.857	14.614	5.504	0.308	35.626	11.790	1.219	156.761	23.810	9.659	4.300		

Table S7: Compilation of abundance and biomass estimates of different broad zooplankton groups over the North Sea and other temperate shelf seas.

Group	Taxa	Type	Estimates	Unit	Method, Mesh Size	Location	Area	Season	Reference	
Microplankton	Diatoms	Abundance	80000.0	Ind L ⁻¹	water sample	Stonehaven	North Sea	Autumn	Bresnan et al., 2015	
	Diatoms	Abundance	129390.0	Ind L ⁻¹	Time Series	Helgoland Roads	North Sea	Autumn	Yang et al., 2021	
	Diatoms	Abundance	69767.0	Ind L ⁻¹	water sample	Stonehaven	North Sea	Autumn	ICES, 2013	
	Diatoms	Abundance	11628.0	Ind L ⁻¹	water sample	Stonehaven	North Sea	winter	ICES, 2013	
	Dinoflagellates	Abundance	950.0	Ind m ³	PUP net, 55µm	Buchan/Banks	North Sea	Autumn	This study	
	Dinoflagellates	Abundance	2000.0	Ind L	Water sample	Stonehaven	North Sea	Autumn	Bresnan et al., 2015	
	Dinoflagellates	Abundance	200000.0	Ind L	Time Series	Helgoland Roads	North Sea	Autumn	Yang et al., 2021	
	Dinoflagellates	Abundance	1030.0	Ind m ³	PUP net, 55µm	Downs	North Sea	Winter	This study	
	Dinoflagellates	Abundance	1123.8	Ind m ³	Water sample	Stonehaven	North Sea	Winter	Bresnan et al., 2015	
	Tripos	Abundance	38080.0	Ind m ³	PUP net, 55µm	Buchan/Banks	North Sea	Autumn	This study	
	Tripos	Abundance	1280.0	Ind m ³	PUP net, 55µm	Downs	North Sea	Autumn	This study	
	Tripos	Abundance	600.0	Ind L	Time Series	Helgoland Roads	North Sea	Autumn	Yang et al., 2021	
	Tintinnid	Abundance	4.2	Ind L ⁻¹	PUP net, 55µm	Buchan/Banks	North Sea	Autumn	This study	
	Tintinnid	Abundance	0.2	Ind L ⁻¹	PUP net, 55µm	Downs	North Sea	Winter	This study	
	Tintinnid	Abundance	4.6	Ind L ⁻¹	Water sample	North Sea	North Sea	Winter	Bils et al., 2019	
	Copepod nauplii	Abundance	5.5	Ind L	PUP net, 55µm	Buchan/Banks	North Sea	Autumn	This study	
	Copepod nauplii	Abundance	4.0 - 20.0	Ind L ⁻¹	Ring Net, 65 µm	Dove Station	North Sea	Autumn	Pitois et al., 2009	
	Copepod nauplii	Abundance	3.8	Ind L ⁻¹	PUP net, 55µm	Downs	North Sea	Winter	This study	
	Copepod nauplii	Abundance	15.0 - 43.0	Ind L ⁻¹	Ring Net, 65 µm	Dove Station	North Sea	Winter	Pitois et al., 2009	
	Copepod nauplii	Biomass	0.8	mg C m ³	PUP net, 55µm	Buchan/Banks	North Sea	Autumn	This study	
	Copepod nauplii	Biomass	0.6	mg C m ³	water sample	L4	North Sea	Autumn	Djehri et al., 2018	
	Copepod nauplii	Biomass	0.5	mg C m ³	PUP net, 55µm	Downs	North Sea	Winter	This study	
	Copepod nauplii	Biomass	0.1	mg C m ³	water sample	L4	North Sea	Winter	Djehri et al., 2018	
	Total	Abundance	809.8	Ind L ⁻¹	water sample	Buchan/Banks	North Sea	Autumn	This study	
	Total	Abundance	64865.0	Ind L ⁻¹	water sample	L4	North Sea	Autumn	ICES, 2013	
	Total	Abundance	835.8	Ind L ⁻¹	water sample	Downs	North Sea	winter	This study	
	Total	Abundance	16216.0	Ind L ⁻¹	water sample	L4	North Sea	winter	ICES, 2013	
	Mesozooplankton	Copepods	Abundance	685.0	Ind m ³	GULF V, 280 µm	Buchan/Banks	North Sea	Autumn	This study
		Copepods	Abundance	1831.1	Ind m ³	WP2, 200 µm	Stonehaven	North Sea	Autumn	ICES, 2013
		Copepods	Abundance	1143.0	Ind m ³	WP2, 200 µm	L4	North Sea	Autumn	Djehri et al., 2018
		Copepods	Abundance	1098.3	Ind m ³	Bongo, 333 µm	Georges Bank	N Atlantic	Autumn	Morse et al., 2017
		Copepods	Abundance	346.0	Ind m ³	GULF V, 280 µm	Downs	North Sea	Winter	This study
		Copepods	Abundance	1500.0	Ind m ³	WP2, 200 µm	L4	North Sea	Winter	Eloire et al., 2010
		Copepods	Abundance	661.0	Ind m ³	WP2, 200 µm	L4	North Sea	Winter	Djehri et al., 2018
		Copepods	Abundance	1500.0	Ind m ³	WP2, 200 µm	Belgium Coast	North Sea	annual ave.	Mortelmans et al., 2021
		Copepods	Abundance	281.4	Ind m ³	WP2, 200 µm	Stonehaven	North Sea	Winter	ICES, 2013
		Appendicularia	Abundance	17.4	Ind m ³	GULF V, 280 µm	Buchan/Banks	North Sea	Autumn	This study
		Appendicularia	Abundance	3.6	Ind m ³	GULF V, 280 µm	Downs	North Sea	Winter	This study
		Appendicularia	Abundance	24.9	Ind m ³	Bongo, 333 µm	Georges Bank	N Atlantic	annual mean	Kane, 2007
		Chaetognatha	Abundance	49.2	Ind m ³	GULF V, 280 µm	Buchan/Banks	North Sea	Autumn	This study
		Chaetognatha	Abundance	17.4	Ind m ³	GULF V, 280 µm	Downs	North Sea	Winter	This study
		Chaetognatha	Abundance	68.6	Ind m ³	WP2, 200 µm	Stonehaven	North Sea	Autumn	ICES, 2013
		Chaetognatha	Abundance	19.7	Ind m ³	WP2, 200 µm	L4	North Sea	winter	ICES, 2013
		Chaetognatha	Abundance	5.6	Ind m ³	Bongo, 333 µm	Georges Bank	N Atlantic	Autumn	Morse et al., 2017
Chaetognatha		Abundance	29.7	Ind m ³	Bongo, 333 µm	Georges Bank	N Atlantic	annual mean	Kane, 2007	
Echinodermata larvae		Abundance	20.2	Ind m ³	GULF V, 280 µm	Buchan/Banks	North Sea	Autumn	This study	
Echinodermata larvae		Abundance	1.5	Ind m ³	GULF V, 280 µm	Downs	North Sea	Winter	This study	
Echinodermata larvae		Abundance	118.9	Ind m ³	WP2, 200 µm	L4	North Sea	Autumn	ICES, 2013	
Echinodermata larvae		Abundance	4.0	Ind m ³	WP2, 200 µm	L4	North Sea	Winter	ICES, 2013	
Echinodermata larvae		Abundance	5.3	Ind m ³	Bongo, 333 µm	Georges Bank	N Atlantic	Autumn	Morse et al., 2017	
Echinodermata larvae		Abundance	28.7	Ind m ³	Bongo, 333 µm	Georges Bank	N Atlantic	annual mean	Kane, 2007	
Gastropoda larvae		Abundance	5287.7	Ind m ³	GULF V, 280 µm	Buchan/Banks	North Sea	Autumn	This study	
Gastropoda larvae		Abundance	587.1	Ind m ³	GULF V, 280 µm	Downs	North Sea	Winter	This study	
Gastropoda larvae		Abundance	113.2	Ind m ³	WP2, 200 µm	L4	North Sea	Autumn	ICES, 2013	
Gastropoda larvae		Abundance	6.4	Ind m ³	WP2, 200 µm	L4	North Sea	Winter	ICES, 2013	
Gastropoda larvae		Abundance	2.6	Ind m ³	Bongo, 333 µm	Georges Bank	N Atlantic	Autumn	Morse et al., 2017	
Polychaeta		Abundance	6.8	Ind m ³	GULF V, 280 µm	Buchan/Banks	North Sea	Autumn	This study	
Polychaeta		Abundance	2.0	Ind m ³	GULF V, 280 µm	Downs	North Sea	Winter	This study	
Polychaeta		Abundance	0.8	Ind m ³	Bongo, 333 µm	Georges Bank	N Atlantic	Autumn	Morse et al., 2017	
Total		Abundance	902.0	Ind m ³	GULF VII, 280 µm	Buchan/Banks	North Sea	Autumn	This study	
Total		Abundance	4172.9	Ind m ³	WP2, 200 µm	L4	North Sea	Autumn	Eloire et al., 2010	
Total		Abundance	4800.0	Ind m ³	WP2, 200 µm	English Channel	North Sea	Autumn	ICES, 2013	
Total		Abundance	1239.0	Ind m ³	Bongo, 333 µm	Georges Bank	N Atlantic	Autumn	Morse et al., 2017	
Total		Abundance	354.9	Ind m ³	GULF VII, 280 µm	English Channel	North Sea	Winter	This study	
Total		Abundance	1500.0	Ind m ³	WP2, 200 µm	L4	North Sea	Winter	Eloire et al., 2010	
Total		Abundance	266.6	Ind m ³	GULF VII, 280	English Channel	North Sea	Winter	Dudeck et al., 2021	

References

- Bils F, Moyano M, Aberle N, van Damme CJG, Nash RDM, Kloppmann M, Loots C, Peck MA (2019) Broad-scale distribution of the winter protozooplankton community in the North Sea. *J Sea Res* 144:112–121.
- Bresnan E, Cook KB, Hughes SL, Hay SJ, Smith K, Walsham P, Webster L (2015) Seasonality of the plankton community at an east and west coast monitoring site in Scottish waters. *J Sea Res* 105:16–29.
- Djeghri N, Atkinson A, Fileman ES, Harmer RA, Widdicombe CE, McEvoy AJ, Cornwell L, Mayor DJ (2018) High prey-predator size ratios and unselective feeding in copepods: A seasonal comparison of five species with contrasting feeding modes. *Prog Oceanogr* 165:63–74.
- Dudeck T, Rohlf N, Möllmann C, Hufnagl M (2021) Winter zooplankton dynamics in the English Channel and southern North Sea: Trends and drivers from 1991 to 2013. *J Plankton Res* 43:244–256.
- Kane J (2007) Zooplankton abundance trends on Georges Bank, 1977-2004. *ICES J Mar Sci* 64:909–919.
- Kjørboe T (2013) Zooplankton body composition. *Limnol Oceanogr* 58:1843–1850.
- Menden-Deuer S, Lessard EJ (2000) Carbon to volume relationships for dinoflagellates, diatoms, and other protist plankton. *Limnol Oceanogr* 45:569–579.
- Morse RE, Friedland KD, Tommasi D, Stock C, Nye J (2017) Distinct zooplankton regime shift patterns across ecoregions of the U.S. Northeast continental shelf Large Marine Ecosystem. *J Mar Syst* 165:77–91.
- Mortelmans J, Aubert A, Reubens J, Otero V, Deneudt K, Mees J (2021) Copepods (Crustacea: Copepoda) in the Belgian part of the North Sea: Trends, dynamics and anomalies. *J Mar Syst* 220:103558.
- Pitois SG, Shaw M, Fox CJ, Frid CLJ (2009) A new fine-mesh zooplankton time series from the Dove sampling station (North Sea). *J Plankton Res* 31:337–343.
- Saccà A (2016) A simple yet accurate method for the estimation of the biovolume of planktonic microorganisms. *PLoS One* 11.
- O'Brien, T. D., Wiebe, P.H., and Falkenhaus, T. (Eds). 2013. ICES Zooplankton Status Report 2010/2011. ICES Cooperative Research Report No. 318. 208 pp.
- Yang J, Löder MGJ, Wiltshire KH, Montagnes DJS (2021) Comparing the Trophic Impact of Microzooplankton during the Spring and Autumn Blooms in Temperate Waters. *Estuaries and Coasts* 44:189–198.

Supplements Chapter 4

S1. Zooplankton data

Collected plankton samples from both the PUPnet (55 μm mesh) and Gulf VII (280 μm mesh) were stored onboard in 4% buffered formalin following the approach of Bils et al. (2022). The microplankton samples were then sieved through a 300- μm mesh and the fraction smaller than 300 μm was diluted in 50-500 ml distilled water depending on the zooplankton density. The diluted samples were analyzed using the Flowcam image analysis system (Christian et al., 1998), which counted particles, made a digital image and measured the size of each particle. The Flowcam was instructed to measure approx. 10000 particles per sample, containing at least 10% of living organisms. Obtained images of microplankton organism were classified using a machine-learning dynamic optimization cycle (Conradt et al., 2022), followed by a final manual validation step.

Mesozooplankton samples were subsampled using a fractionation factor between 1/16 and 1/1024 depending on the original sampled material following Motoda (1967). To identify and measure zooplankton organisms, we used ImageJ software (v. 1.41o) with ZooProcess (v.7.19) and the Plankton Identifier software (v.1.3.4). The automatic identification of the organisms was manually validated.

After the micro- and mezoplankton datasets were merged, organisms smaller or bigger than the effective size-range of the PUP (<55 μm) and Gulf VII nets (>3000 μm) were excluded from the dataset. All organisms were then classified in 15 taxonomic sets, including species, genus or families, with class as the lowest taxonomic resolution (Fig. S1). As it is mentioned in the main text, 11 taxonomic sets were identified as potential herring larval prey and included in this study.

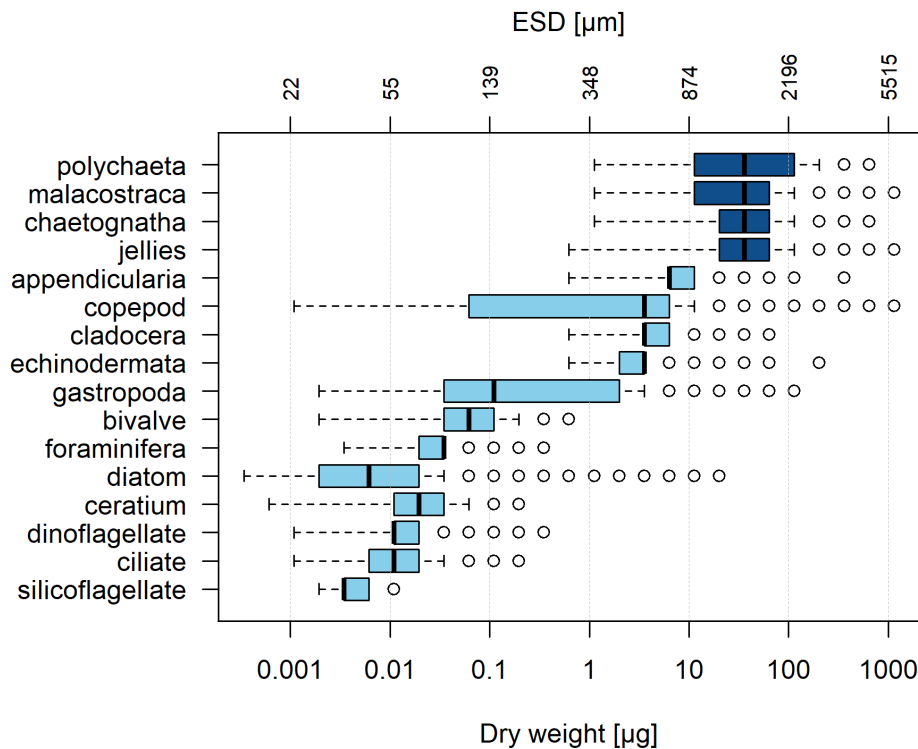


Figure S1. Boxplot of the 15 taxonomic groups identified in the plankton samples. Lower and upper box boundaries are the 25th and 75th percentiles, respectively, line inside box is the median. Upper (lower) error lines are the largest (smallest) values within 1.5 times interquartile range above 75th (below 25th) percentile. Open circles mark outside data, i.e. data >1.5 and <3 times interquartile range beyond either end of the box. Light blue color marks the planktonic organisms considered as larval prey in the “generalist” feeding scenario. The taxonomic groups not included in the larval diet are shown in dark blue. ESD is an equivalent spherical distance. Dinoflagellates taxonomic group includes *Dinophysis* spp., *Proto-peridinium* spp., and *Ceratium* spp.

S2. Bias correction of larval length due to formalin preservation

Fish larvae stored in 4% formalin are known to shrink in their total length (Fox, 1996). We recalculated the length of a herring larva prior storage l_1 from the length measurements of the formalin-preserved larvae l_p , using a correction equation provided by M. Moyano and B. Illing based on their laboratory experiments (Fig. S2.1):

$$l_1 = 1.10 \cdot l_p - 0.25 \quad (\text{S2.1})$$

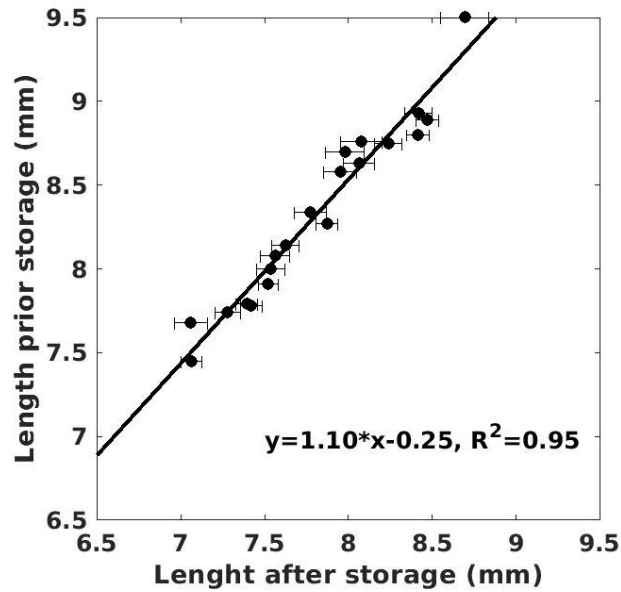


Figure S2.1 Lengths of a herring larva prior 4% formalin-storage against stored lengths. The line shows the best linear fit.

S3. Bioenergetic model

Table S3.1 contains the full set of the parameters and equations of the bioenergetic model of herring larvae used in this study. This model utilized an optimal foraging routine to calculate the amount of food a larva forages per time unit (Letcher et al., 1996, Daewel et al., 2011, Kühn et al., 2008). The optimal foraging approach first ranks the prey size classes accordingly to the ratio Q :

$$Q_i = \frac{w_{z_i} \cdot CS_i}{HT_i}, \quad (\text{S3.1})$$

where w_{z_i} is the zooplankton dry weight, CS_i is the capture success and HT_i is the handling time (see Table S3.1).

Once the prey size classes are ranked, a profitability P_j is assigned to each ranked prey class j :

$$P_j = \frac{\sum_j w_{z_j} \cdot ER_j \cdot CS_j}{1 + \sum_j ER_j \cdot HT_j} \quad (\text{S3.2})$$

where ER_j is the encounter rate (see Table S3.1). Prey size classes were included in the larval diet sequentially on the basis of their ranks until the profitability P_j began to decrease (Letcher et al., 1996).

The amount of the foraged food F ($\mu\text{g} \cdot \text{s}^{-1}$) was then found as the maximum of P_j :

$$F = \max(P_j) \quad (\text{S3.3})$$

The energy gain C (Eq. 4 in the main text) was then calculated from F under consideration of the size-dependent maximal gut content (GC_{\max}) and gut evacuation rate (GER, Table S3.1).

The majority of the equations was directly adopted from Hufnagl and Peck (2011), other have been arithmetically simplified in comparison to their original form. Furthermore, we applied three modifications to the original model:

1) We used the standard respiration rate R_s from Moyano et al. (2018) instead of the one used in Hufnagl and Peck (2011) and Hufnagl et al. (2015):

$$R_s = 0.02 \cdot (w_l^{0.886}) \cdot e^{0.105 \cdot T} \quad (\text{S3.4})$$

where w_l was the dry weight of a herring larva (in μg) and T ($^{\circ}\text{C}$) is temperature. This allowed us to reproduce the ad-libitum growth rates of herring larvae reported by Moyano et al. (2018)

2) Dynamic growth allocation scheme was replaced by a Boolean function following Huebert and Peck (2014). The proportion p of the energy G available for growth allocated to the length growth was:

$$p = 1, \text{ if } w_l > w_{\text{ref}} \text{ and } p = 0, \text{ if } w_l \leq w_{\text{ref}}, \quad (\text{S3.5})$$

where w_{ref} was the reference larval weight (see Table S3.1). We are convinced that the Boolean function is more suitable to describe energy allocation than the function used in Hufnagl and Peck (2011) (their Eq.22), because the later exceeded 1 if $w_l > 1.04 \cdot w_{\text{ref}}$ or drops below 0 if $w_l < 0.96 \cdot w_{\text{ref}}$ (Figure S3.1)

3) Since the herring larvae are visual feeders and thus only feed during the day, the activity multiplier k was taken $k_{\text{day}}=2$ and $k_{\text{night}}=1$, following the approach of Huebert and Peck (2014) to differentiate between active feeding and passive phase during the night. No dependency on prey concentrations or gut fullness was included in our study.

Table S3.1: Summary of all variables, parameters and equations of the bioenergetic model simulating larval foraging and growth at observed zooplankton prey fields and temperatures. HP2011 stays for Hufnagl and Peck (2011), HP2014 – for Huebert and Peck (2014)

Description	Value/Equation	Unit	Comments
Variables			
Larval length	L_l	mm	
Larval dry weight	w_l	μg	
Zooplankton total biomass	B_z	$\mu\text{g}/\text{m}^3$	Eq. 3 in main text
Zooplankton size class index	i		
Zooplankton dry weight in class i	$w_{z,i}$	μm	
Prey biomass in the size class i	B_i	$\mu\text{g}/\text{m}^3$	
Temperature	T	$^{\circ}\text{C}$	
Prey field			
Zooplankton size in class i	$L_{z,i} = 2.25 \cdot 10^6 \cdot w_i^{0.4}$	μg	Adapted from HP2014

Prey abundance in the size class i	$A_i = B_i/w_i$	number of individuals	
Maximal prey size	$L_{z \max} = \frac{2200}{1 + \left(\frac{L_1}{14}\right)^{-2}}$	μm	Simplified HP2011
The optimal foraging routine			
Handling Time	$HT_i = e^{0.264 \cdot 10^d}$, where $d = 20 \frac{L_{z i}}{L_1}$	s	HP2011
Capture Success	$CS_i = 1.1 - \left(1.1 \cdot \frac{L_{z i}}{L_{z \max}}\right)$	s^{-1}	HP2011
Encounter Rate	$ER_i = \left(\frac{2}{3} \cdot \pi \cdot RD_i^3 \cdot \frac{A_i}{1000} \cdot PF\right) + \left(\pi \cdot RD_i^2 \cdot \frac{A_i}{1000} \cdot PF \cdot PD \cdot \sqrt{V_l^2 + V_i^2 + \varepsilon^2}\right)$	# s	Corrected HP2011
Angle of visual acuity	$\alpha = 0.0167 \cdot e^b$, where $b = 9.14 - 2.4 \cdot \ln(L_1) + 0.229 \cdot (\ln(L_1))^2$,	degree	HP2011
Reactive Distance	$RD_i = \frac{L_{z i}}{2 \cdot \tan\left(\frac{\alpha}{2}\right)}$	mm	HP2011
Pause frequency	$PF = 0.35$	1/s	HP2011
Pause duration	$PD = 0.35$	s	HP2011
Larval swimming speed	$V_l = 6.7 + \frac{127.21}{1 + 4.1 \cdot 10^3 \cdot e^{-0.27 \cdot L_1}}$	mm/s	Corrected and simplified HP2011
Zooplankton swimming speed	$V_i = 0.003 \cdot L_{z i}$	mm/s	HP2011
Turbulent velocity	$\varepsilon = 1.3$	mm/s	HP2011
Energy budget and growth			
Activity Multiplier	$k = 2.5$ during the day $k = 1$ during the night	unitless	HP2014
Standard Respiration	$R_s = 0.02 \cdot (w_l^{0.886}) \cdot e^{0.105 \cdot T}$	$\mu\text{g dw} \cdot \text{h}^{-1}$	Moyano et al., 2018
Reference larval weight	$w_{\text{ref}} = 0.019 \cdot L_1^{3.603e^{0.0067 \cdot T}}$	μg	HP2011
Larval dry weight at hatch	$W_{\text{min}} = 0.019 \cdot (11 - 0.09 \cdot T)^f$ where $f = 3.614 \cdot e^{0.0063 \cdot T}$	μg	HP2011
Assimilation Efficiency	$\beta = 0.6 \cdot (1 - 0.3 \cdot e^c)$ where $c = -0.003 \cdot (w_l - W_{\text{min}})$	unitless	Corrected HP2011
Specific dynamic action	$SDA = 0.10$	unitless	HP2011
Maximal gut content	$GC_{\text{max}} = 0.045 \cdot w_{\text{ref}}^{1.02}$	μg	Corrected and simplified HP2011
Gut evacuation rate	$GER = 100 * 0.59 \cdot L_1^{-0.83} \cdot 1.097^T$	% / h	Simplified HP2011

Proportion Allocated Length Growth to	$p = \begin{cases} 1, & \text{if } w_1 > w_{\text{ref}} \\ 0, & \text{if } w_1 \leq w_{\text{ref}} \end{cases}$	unitless	This study
---------------------------------------	---	----------	------------

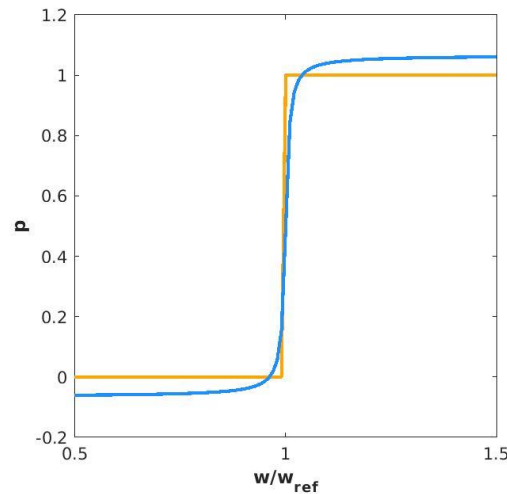


Figure S3.1. The proportion p of the available energy a herring larva allocates to growth in length as a function of the larval conditional index expressed as a ratio of an actual larval weight w_1 to the reference larval weight w_{ref} (Table S3.1). Orange line depicts the approach used in this study and in Huebert and Peck (2014), the blue line depicts the approach of Hufnagl and Peck (2011) .

S4. The proportion of copepods in different size-classes of the plankton samples

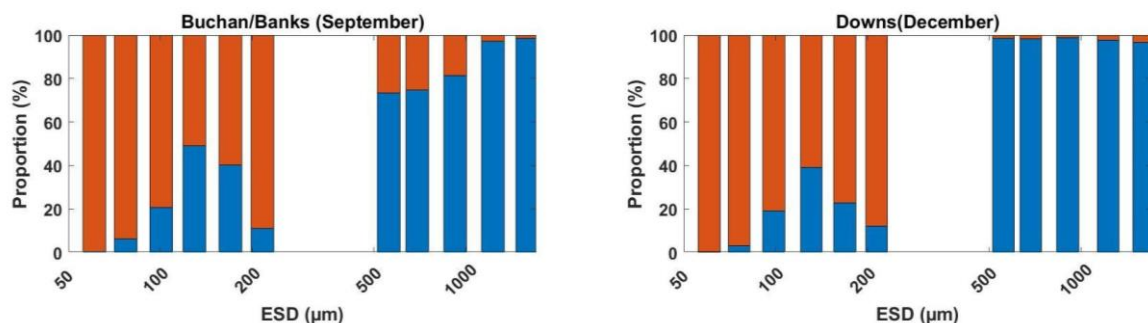


Figure S4.1. Relative proportion (% of the biomass) of copepods in size-classes of the plankton samples in the Buchan/Banks areas in September (left panel) and in the Downs area in December (right panel).

S5. The modelled larval growth in 2013, 2014 and 2018

The spatial distribution of the plankton biomass and the modelled larval growth rates obtained using the observed biomasses and the station-specific temperatures in 2013, 2014, and 2018 is shown in Fig S4. In these years, none or only few stations were sampled in Downs due to bad weather conditions.

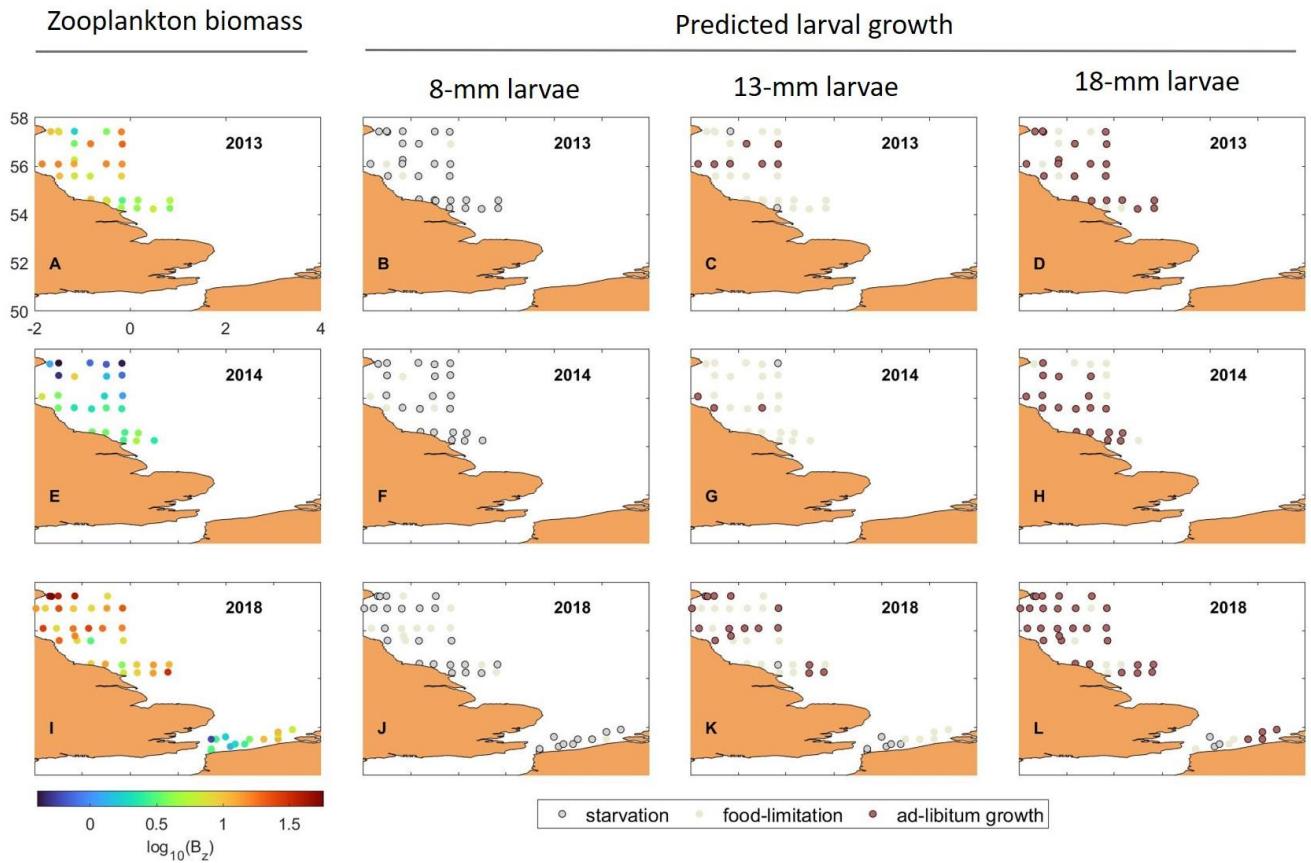


Figure S5.1. The observed plankton concentrations (in 2013(A), 2014 (E) and 2018(I)) and corresponding growth predicted for a herring larva of the initial length of 8 mm (B, F, J), 13 mm (C, G, K) and 18 mm (D, H, L). Colors correspond to: gray - starvation ($SGR \leq 0$), beige - food-limitation ($SGR > 0$ and $SGR < SGR_{max}$) and brown – ad-libitum feeding ($SGR = SGR_{max}$). Please find the corresponding figure for the years 2016, 2017 and 2019 in the main text (Figure 7).

S6. Model sensitivity to the NBSS slope

Fig 9 in the main text shows the sensitivity of the modelled larval growth to the zooplankton biomass and size-spectra slope for herring larvae of 8-mm, 13-mm and 18-mm length. The comparison of the results for a 13-mm larva revealed some discrepancies in the shape of starvation ($SGR = 0$) and satiation ($SGR=SGR_{max}$) curves reported by Huebert and Peck (2014) (their Fig. 4). Furthermore, the optimal NBSS slope in our study (-0.9) was somewhat less steep than the optimal slope of -1.4 obtained by Huebert and Peck (2014). The detailed analyses of both models showed that the different parameterizations of the handling time HT was main reason for this discrepancy: the HT used in this study as well as in Hufnagl and Peck (2011) increased with the increasing prey size (see Table S3.1), whereas HT considered to be constant in Huebert and Peck (2014). To demonstrate this, we simulated the larval growth using the same set of equations (Table 3.1), but different HT (Fig. S6.1) and plotted the results the same way as in Huebert and Peck (2014). The model simulation with the constant HT (Fig. 6.1b) reproduced well the shape of the starvation and satiation curves reported in Huebert and Peck (2014).

To our opinion the increase of the handling time with the prey size is more realistic than the approach used by Huebert and Peck (2014). However, a detailed comparison of both models remains beyond the scope of this paper.

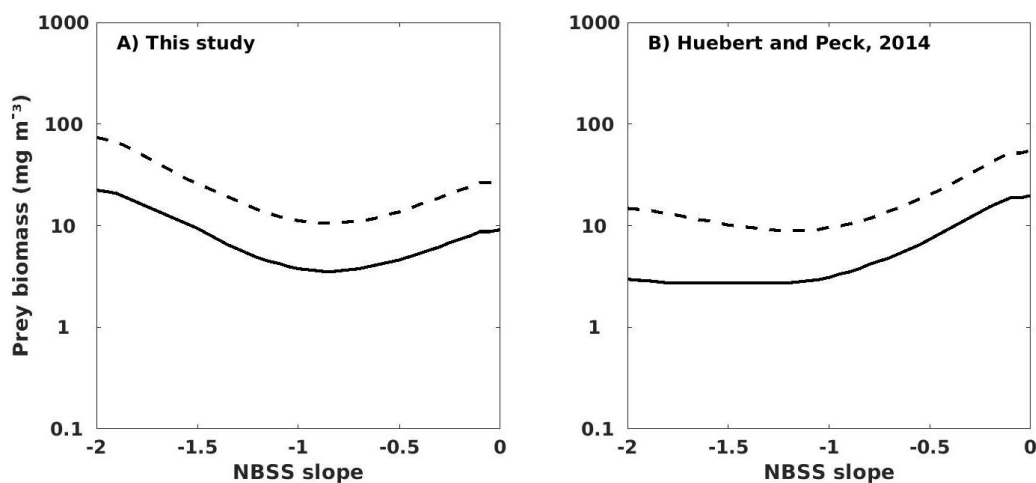


Figure S6.1. Starvation (solid lines) and satiation (dashed lines) points predicted for a 13-mm herring larva feeding at different prey conditions (prey biomass and NBSS slope). A) the results obtained with the handling time parameterization used in this study, B) the results obtained with the constant handling time in agreement with Huebert and Peck (2014)

References:

- Bils, F., N. Aberle, C. J. G. van Damme, M. A. Peck and M. Moyano (2022). "Role of protozooplankton in the diet of North Sea autumn spawning herring (*Clupea harengus*) larvae." *Marine Biology* 169(7): 90.
- Christian, K. S., E. S. Michael and S. Y. Charles (1998). "An imaging-in-flow system for automated analysis of marine microplankton." *Marine Ecology Progress Series* 168: 285-296.
- Conradt, J., G. Börner, Á. López-Urrutia, C. Möllmann and M. Moyano (2022). "Automated Plankton Classification With a Dynamic Optimization and Adaptation Cycle." *Frontiers in Marine Science* 9.
- Daewel, U., M. A. Peck and C. Schrum (2011). "Life history strategy and impacts of environmental variability on early life stages of two marine fishes in the North Sea: an individual-based modelling approach." *Canadian Journal of Fisheries and Aquatic Sciences* 68(3): 426-443.
- Fox, C. J. (1996). "Length changes in herring (*Clupea harengus*) larvae: effects of capture and storage in formaldehyde and alcohol." *Journal of Plankton Research* 18(4): 483-493.
- Huebert, K. B. and M. A. Peck (2014). "A Day in the Life of Fish Larvae: Modeling Foraging and Growth Using Quirks." *PLoS ONE* 9(6): e98205.
- Hufnagl, M. and M. A. Peck (2011). "Physiological individual-based modelling of larval Atlantic herring (*Clupea harengus*) foraging and growth: insights on climate-driven life-history scheduling." *ICES Journal of Marine Science* 68(6): 1170-1188.
- Hufnagl, M., M. A. Peck, R. D. M. Nash and M. Dickey-Collas (2015). "Unravelling the Gordian knot! Key processes impacting overwintering larval survival and growth: A North Sea herring case study." *Progress in Oceanography* 138, Part B: 486-503.
- Kühn, W., M. A. Peck, H.-H. Hinrichsen, U. Daewel, A. Moll, T. Pohlmann, C. Stegert and S. Tamm (2008). "Defining habitats suitable for larval fish in the German Bight (southern North Sea): An IBM approach using spatially- and temporally-resolved, size-structured prey fields." *Journal of Marine Systems* 74(1): 329-342.
- Letcher, B. H., J. A. Rice, L. B. Crowder and K. A. Rose (1996). "Variability in survival of larval fish: disentangling components with a generalized individual-based model." *Canadian Journal of Fisheries and Aquatic Sciences* 53(4): 787-801.
- Motoda, S. (1967). *Devices of Simple Plankton Apparatus III*.
- Moyano, M., B. Illing, L. Christiansen and M. A. Peck (2018). "Linking rates of metabolism and growth in marine fish larvae." *Marine Biology* 165(1): 5.

List of Publications

Published Articles

Conradt, J., **Börner, G.**, Lopez-Urrutia, A., Möllmann, C., & Moyano, M. (2022). Automated Plankton Classification With a Dynamic Optimization and Adaptation Cycle.

Moullec, F., Asselot, R., Auch, D., Blöcker, A. M., **Börner, G.**, Färber, L., ... & Pellerin, F. (2021). Identifying and addressing the anthropogenic drivers of global change in the North Sea: a systematic map protocol. *Environmental Evidence*, 10(1), 1-11.

Moyano, M., Illing, B., Akimova, A., Alter, K., Bartolino, V., **Börner, G.**, ... & Polte, P. (2022). Caught in the middle: bottom-up and top-down processes impacting recruitment in a small pelagic fish. *Reviews in Fish Biology and Fisheries*, 1-30.

In review or submitted

Akimova A, **Börner G**, Peck MA, van Damme C, Moyano M (2022). Combining modeling with novel field observations yields new insights into food limitation of wintertime larval fish [Manuscript submitted for publication].

In Preparation

Börner G, Frelat R, Akimova A, van Damme C, Peck MA, Moyano M (2023). Plankton community composition and size structure in the North Sea in autumn and winter from 2013-2019

Börner G, Otto S, Aberle N, Harmer R, Bils F, van Damme C, Kloppmann M, Nash RDM, Möllmann C, Moyano M (2023) Spatio-temporal distribution of the North Sea winter protozooplankton community between 2014 and 2021

Eidesstattliche Versicherung

Hiermit erkläre ich an Eides statt, dass ich die vorliegende Dissertationsschrift selbst verfasst und keine anderen als die angegebenen Quellen und Hilfsmittel benutzt habe. |

I hereby declare upon oath that I have written the present dissertation independently and have not used further resources and aids than those stated in the dissertation.

Ort, den | City, date

Hamburg, 21/02/2023

Unterschrift | Signature

A handwritten signature in black ink, appearing to be 'J. Müller', written in a cursive style.

Funding

I was funded by the German Research Foundation (DFG) under project THRESHOLDS (Disentangling the effects of climate-driven processes on North Sea herring recruitment through physiological thresholds, MO 2873-3-1)

The results of this publication reflect only the author's view and the commission is not responsible for any use that may be made of the information it contains.

